การศึกษาระบบพอลิเมอร์ผสมระหว่างพอลิเอทิลีนความหนาแน่นสูง และพอลิบิวทิลีนซัคซิเนท

นางสาวอัจฉราพร อ้นที

วิทยานิพนธ์นี้เป็นส่วนหนึ่งของการศึกษาตามหลักสูตรปริญญาวิศวกรรมศาสตรมหาบัณฑิต
สาขาวิชาวิศวกรรมพอลิเมอร์
มหาวิทยาลัยเทคโนโลยีสุรนารี
ปีการศึกษา 2556

THE STUDY OF POLYMER BLEND SYSTEM BETWEEN HIGH DENSITY POLYETHYLENE AND POLY (BUTYLENE SUCCINATE)

Ajcharaporn Aontee

A Thesis Submitted in Partial Fulfillment of the Requirements for the

Degree of Master of Engineering in Polymer Engineering

Suranaree University of Technology

Academic Year 2013

THE STUDY OF POLYMER BLEND SYSTEM BETWEEN HIGH DENSITY POLYETHYLENE AND POLY (BUTYLENE SUCCINATE)

Suranaree University of Technology has approved this thesis submitted in partial fulfillment of the requirements for a Master's Degree.

Thesis Examining Committee

_____

(Assoc. Prof. Dr. Yupaporn Ruksakulpiwat)

Chairperson

_____

(Asst. Prof. Dr. Wimonlak Sutapun)

Member (Thesis Advisor)

_____

(Asst. Prof. Dr. Chantima Deeprasertkul)

Member

_____

(Asst. Prof. Dr. Kasama Jarukumjorn)

Member

_____ _____

(Prof. Dr. Sukit Limpijumnong) (Assoc. Prof. Flt. Lt. Dr. Kontorn Chamniprasart)

Vice Rector for Academic Affairs and Innovation

Dean of Institute of Engineering

อัจฉราพร อ้นที : การศึกษาระบบพอลิเมอร์ผสมระหว่างพอลิเอทิลีนความหนาแน่นสูงและพอลิบิวทิลีนซัคซิเนท (THE STUDY OF POLYMER BLEND SYSTEM BETWEEN HIGH DENSITY POLYETHYLENE AND POLY (BUTYLENE SUCCINATE) อาจารย์ที่ปรึกษา : ผู้ช่วยศาสตราจารย์ ดร.วิมลลักษณ์ สุตะพันธ์, 263 หน้า.

วิทยานิพนธ์นี้ศึกษาผลของสัดส่วนของการผสมและความเข้ากันได้ต่อสมบัติทางกายภาพของพอลิเมอร์ผสมระหว่างพอลิเอทิลีนความหนาแน่นสูงและพอลิบิวทิลีนซัคซิเนท สมบัติทางกายภาพที่ตรวจสอบ ได้แก่ สมบัติทางกล สมบัติทางความร้อน พฤติกรรมการหลอมและการตกผลึก การดูดน้ำและการย่อยสลายทางชีวภาพ รวมถึงการตรวจสอบสัณฐานวิทยาของพอลิเมอร์ผสม พอลิเมอร์ผสมถูกเตรียมที่สัดส่วนของพอลิบิวทิลีนซัคซิเนทตั้งแต่ร้อยละ 20 ถึง 80 โดยน้ำหนัก พอลิเอทิลีนความหนาแน่นสูงกราฟต์ด้วยมาเลอิกแอนไฮไดรด์ (HDPE-g-MAH) และเอทิลีน-โพรพิลีนรับเบอร์กราฟต์ด้วยมาเลอิกแอนไฮไดรด์ (EPR-g-MAH) ถูกใช้เป็นสารช่วยเพิ่มความเข้ากันได้ที่ปริมาณ 2, 4, 6 และ 8 ส่วนในร้อยส่วนของพอลิเมอร์ผสม

สัณฐานวิทยาของพอลิเมอร์ผสมชนิดไม่เข้ากันระหว่างพอลิเอทิลีนความหนาแน่นสูงและพอลิบิวทิลีนซัคซิเนทประกอบด้วยวัฏภาคกระจายมีลักษณะเป็นทรงกลม มีลักษณะยืดออก และมีลักษณะเป็นเส้นใย เมื่อปริมาณของวัฏภาคกระจายเป็นร้อยละ 20, 30 และ 40 โดยน้ำหนักตามลำดับ สัณฐานแบบต่อเนื่องทั้งสองเฟสเกิดขึ้นเมื่อปริมาณของวัฏภาคกระจายโดยประมาณเท่ากับร้อยละ 50 โดยน้ำหนัก

สำหรับพอลิเมอร์ผสมพอลิเอทิลีนความหนาแน่นสูงที่ปริมาณพอลิบิวทิลีนซัคซิเนทเป็นร้อยละ 20 ถึง 50 โดยน้ำหนักนั้น ยังก์มอดุลัสและเปอร์เซ็นการยืด ณ จุดขาดลดลง ความทนทานต่อแรงดึง ณ จุดขาดเพิ่มขึ้นและความทนทานต่อแรงดึง ณ จุดครากของพอลิเมอร์ผสมเปลี่ยนแปลงอย่างไม่มีนัยสำคัญเมื่อเพิ่มปริมาณพอลิบิวทิลีนซัคซิเนท พอลิบิวทิลีนซัคซิเนทมีผลเล็กน้อยต่อเสถียรภาพทางความร้อน พฤติกรรมการหลอมและการตกผลึก ในขณะที่การดูดน้ำและการย่อยสลายทางชีวภาพของพอลิเมอร์ผสมเพิ่มขึ้น การปรับปรุงความเข้ากันได้ของพอลิเมอร์ผสมด้วยสารช่วยเพิ่มความเข้ากันได้ทั้งสองชนิดทำให้วัฏภาคของพอลิบิวทิลีนซัคซิเนทมีความสม่ำเสมอมากขึ้น พอลิเอทิลีนความหนาแน่นสูงกราฟต์ด้วยมาเลอิกแอนไฮไดรด์ปรับปรุงความทนทานต่อแรงกระแทก เปอร์เซ็นต์การยืด ณ จุดขาดและความทนทานต่อแรงดึงของพอลิเมอร์ผสมให้ดีขึ้น ในขณะที่มีผลเล็กน้อยต่อยังก์มอดุลัสของพอลิเมอร์ผสม เสถียรภาพทางความร้อนของพอลิเมอร์ผสมได้รับผลกระทบเล็กน้อยจากการเติมสารช่วยเพิ่มความเข้ากันได้ทั้งสองชนิด สารช่วยเพิ่มความเข้ากันได้ทั้งสองชนิดมีผลต่อพฤติกรรมการหลอมและการตกผลึกของพอลิเมอร์ผสม การดูดน้ำ

และการย่อยสลายทางชีวภาพของพอลิเมอร์ผสม ถึงแม้ว่า เอทิลีน-โพรพิลีนรับเบอร์กราฟต์ด้วยมาเลอิกแอนไฮไดรด์ส่งผลเชิงลบต่อความแข็งของพอลิเมอร์ผสมแต่ช่วยปรับปรุงความทนทานต่อแรงกระแทกของพอลิเมอร์ผสม การดูดน้ำของพอลิเมอร์ผสมลดลงเล็กน้อยในขณะที่และการย่อยสลายทางชีวภาพของพอลิเมอร์ผสมได้รับการปรับรุงให้ดีขึ้นตามปริมาณเอทิลีน-โพรพิลีนรับเบอร์กราฟต์ด้วยมาเลอิกแอนไฮไดรด์ที่มากขึ้น ในเชิงเปรียบเทียบ พอลิเอทิลีนความหนาแน่นสูงกราฟต์ด้วยมาเลอิกแอนไฮไดรด์มีประสิทธิภาพในการปรับปรุงสมบัติเชิงกลของพอลิเมอร์ผสมพอลิเอทิลีนความหนาแน่นสูง โดยที่ปริมาณที่เหมาะสมของพอลิเอทิลีนความหนาแน่นสูงกราฟต์ด้วยมาเลอิกแอนไฮไดรด์คือ 2 ส่วนในร้อยส่วนของพอลิเมอร์ผสม

สำหรับพอลิเมอร์ผสมพอลิบิวทิลีนซัคซิเนทที่ปริมาณพอลิเอทิลีนความหนาแน่นสูงร้อยละ 20 ถึง 50 โดยน้ำหนักนั้น ยังก์มอดุลัสเพิ่มขึ้น เปอร์เซ็นต์การยืด ณ จุดขาด ความทนทานต่อแรงดึง ณ จุดคราก และความทนทานแรงดึง ณ จุดขาดของพอลิเมอร์ผสมลดลงเมื่อเพิ่มปริมาณของพอลิ-เอทิลีนความหนาแน่นสูง พอลิเอทิลีนความหนาแน่นสูงไม่มีผลอย่างมีนัยสำคัญต่อเสถียรภาพทางความร้อน พฤติกรรมการหลอมและการตกผลึกของพอลิเมอร์ผสม แต่มีผลกระทบต่อการดูดน้ำและการย่อยสลายทางชีวภาพของพอลิเมอร์ผสม

การปรับปรุงความเข้ากันได้ของพอลิเมอร์ผสมพอลิบิวทิลีนซัคซิเนทด้วยสารช่วยเพิ่มความเข้ากันได้ทั้งสองชนิดมีผลทำให้สัณฐานวิทยาของพอลิเมอร์ผสมมีความสม่ำเสมอมากขึ้น พอลิเอทิลีนความหนาแน่นสูงกราฟต์ด้วยมาเลอิกแอนไฮไดรด์ปรับปรุงเปอร์เซ็นต์การยืด ณ จุดขาดและความทนต่อแรงกระแทกของพอลิเมอร์ผสมให้ดีขึ้น ในขณะที่พอลิเอทิลีนความหนาแน่นสูงกราฟต์ด้วยมาเลอิกแอนไฮไดรด์มีผลเล็กน้อยต่อยังก์มอดุลัสและความทนทานต่อแรงดึงของพอลิเมอร์ผสม เสถียรภาพทางความร้อน พฤติกรรมการหลอมและการตกผลึกของพอลิเมอร์ผสม การดูดน้ำและการย่อยสลายทางชีวภาพของพอลิเมอร์ผสมได้รับอิทธิพลเล็กน้อยจากการเติมพอลิเอทิลีนความหนาแน่นสูงกราฟต์ด้วยมาเลอิกแอนไฮไดรด์ ถึงแม้ว่าเอทิลีน-โพรพิลีนรับเบอร์กราฟต์ด้วยมาเลอิกแอนไฮไดรด์จะส่งผลกระทบเชิงลบต่อความแข็งของพอลิเมอร์ผสมแต่ช่วยปรับปรุงความความเหนียวของพอลิเมอร์ผสม เอทิลีน-โพรพิลีนรับเบอร์กราฟต์ด้วยมาเลอิกแอนไฮไดรด์ยังส่งผลกระทบต่อเสถียรภาพทางความร้อน พฤติกรรมการหลอมและการตกผลึก การดูดน้ำและการย่อยสลายทางชีวภาพของพอลิเมอร์ผสมอีกด้วย พอลิเอทิลีนความหนาแน่นสูงกราฟต์ด้วยมาเลอิกแอนไฮไดรด์ช่วยในการปรับปรุงสมบัติเชิงกลของพอลิเมอร์ผสมพอลิบิวทิลีนซัคซิเนท โดยที่ปริมาณที่เหมาะสมคือ 6 ส่วนในร้อยส่วนของพอลิเมอร์ผสม

สาขาวิชา วิศวกรรมพอลิเมอร์ ลายมือชื่อนักศึกษา_____

ปีการศึกษา 2556 ลายมือชื่ออาจารย์ที่ปรึกษา_____

AJCHARAPORN AONTEE : THE STUDY OF POLYMER BLEND SYSTEM BETWEEN HIGH DENSITY POLYETHYLENE AND POLY (BUTYLENE SUCCINATE). THESIS ADVISOR : ASST. PROF. WIMONLAK SUTAPUN, Ph.D., 263 PP.

HDPE/PBS/COMPATIBILIZATION/HDPE BLEND/PBS BLEND

This thesis was to study effect of blend composition and compatibilization on physical properties of HDPE and PBS blend. The physical properties included mechanical and thermal properties, melting and crystallization behavior, water absorption, and biodegradability. Phase morphology of the blends was also investigated. The blends were prepared at PBS compositions of 20 – 80 wt.%. HDPE-g-MAH and EPR-g-MAH were used as compatibilizer at 2, 4, 6, and 8 phr.

Immiscible phase morphology of HDPE and PBS blend contained sphere, elongated, and fibrillar domains when the dispersed phase composition was 20, 30 and 40 wt.%, respectively. Co-continuous morphology was obtained at the blend weight ratio about 50/50.

For PBS/HDPE blend at 20 – 50 wt.% PBS, Young's modulus and elongation at break decreased, stress at break increased, and yield strength insignificantly changed with increasing PBS content. PBS slightly affected thermal stability, and melting and crystallization behavior whereas water absorption increased and biodegradability improved with adding PBS. Compatibilized blend with HDPE-g-MAH and EPR-g-MAH led to more uniform PBS domains. HDPE-g-MAH made improvement in impact strength, elongation at break and tensile strength of the blend

whereas it slightly affected Young's modulus. Thermal stability of the blend was slightly affectec by adding either HDPE-g-MAH or EPR-g-MAH. HDPE-g-MAH and EPR-g-MAH both affected melting and crystallization behavior, water absorption, and biodegradability of the blend. Even though, EPR-g-MAH had negative effect on stiffness, it helped improve impact strength of the blend. Water absorption slightly decreased whereas biodegradability of the blend got better with adding EPR-g-MAH. HDPE-g-MAH was more effective than EPR-g-MAH for improving mechanical properties of the blend with HDPE-g-MAH optimum content of 2 phr.

For HDPE/PBS blend at 20 - 50 wt.% HDPE, Young's modulus increased; and elongation at break, yield strength, and stress at break decreased as increasing HDPE content. HDPE insignificantly affected thermal stability, melting and crystallization behavior but it affected water absorption and biodegradability of the blend. Compatibilized blend with HDPE-g-MAH and EPR-g-MAH resulted in more homogeneity of phase morphologies. HDPE-g-MAH made improvement in elongation at break and impact strength of the blend whereas it slightly affected Young's modulus and tensile strength. Thermal stability, melting and crystallization behavior, water absorption and biodegradability of the blend were slight influence by adding HDPE-g-MAH. Even though, compatibilizing blend with EPR-g-MAH had negative effect on stiffness, this was enhancement in toughness of the blend. EPR-g-MAH affected thermal stability, melting and crystallization behavior, water absorption and biodegradability of the blend. HDPE-g-MAH was effective for improving mechanical properties of PBS blend with optimum content of 6 phr.

School of Polymer Engineering Student's Signature _____

Academic Year 2013 Advisor's Signature _____

ACKNOWLEDGEMENTS

I wish to acknowledge the research and scholarship (OROG) funding from Suranaree University of Technology (SUT). The grateful thanks and appreciation are given to the thesis advisor, Asst. Prof. Wimonlak Sutapun (Ph.D.) for her consistent thesis supervision and thoughtfully comment on several drafts and advice towards the completion of this study. I would not have achieved this far and this thesis would not been completed without all of supporting that I have always received from her. Besides my advisor, I would like to thank the rest of my thesis committee: Assoc. Prof. Dr. Yupaporn Ruksakulpiwat, Asst. Prof. Kasama Jarukumjorn (Ph.D.) and Asst. Prof. Chantima Deeprasertkul (Ph.D.) for their insightful comments and hard questions.

I wish to thank Chemical Innovation, Co., Ltd. for kindly supplying HDPE-g-MAH (Fusabond® MB 100D, Dupont™).

A special thanks to my family. Words cannot express how grateful I am to my grandmother and grandfather, my mother and father, my elder brother and younger sister for all of the goodwill that you've offered to me. I would also like to thank all of my friends who spent time together throughout 4 years at SUT and supported me in writing. I would like to thanks my brother Panuwat Pakdeechote who taught me how to get happier at work. At the end I would like express appreciation to my beloved friend Adisorn Sridej who incented me to strive towards my goal and heartened me in when I felt down.

Ajcharaporn Aontee

TABLE OF CONTENTS

Page

TABLE OF CONTENTS (Continued)

Page

TABLE OF CONTENTS (Continued)

Page

TABLE OF CONTENTS (Continued)

Page

TABLE OF CONTENTS (Continued)

Page

TABLE OF CONTENTS (Continued)

Page

TABLE OF CONTENTS (Continued)

Page

TABLE OF CONTENTS (Continued)

Page

LIST OF TABLES

Table **Page**

LIST OF TABLES (Continued)

Table **Page**

LIST OF TABLES (Continued)

Table **Page**

LIST OF TABLES (Continued)

Table **Page**

LIST OF FIGURES

Figure **Page**

LIST OF FIGURES (Continued)

Figure **Page**

LIST OF FIGURES (Continued)

Figure **Page**

LIST OF FIGURES (Continued)

Figure **Page**

LIST OF FIGURES (Continued)

Figure **Page**

LIST OF FIGURES (Continued)

Figure **Page**

LIST OF FIGURES (Continued)

Figure **Page**

LIST OF FIGURES (Continued)

Figure **Page**

LIST OF FIGURES (Continued)

Figure **Page**

SYMBOLS AND ABBREVIATIONS

HDPE	=	High density polyethylene
PBS	=	Poly (butylene succinate)
HDPE-g-MAH	=	High density polyethylene grafted with maleic anhydride
EPR-g-MAH	=	Ethylene-propylene rubber grafted with maleic anhydride

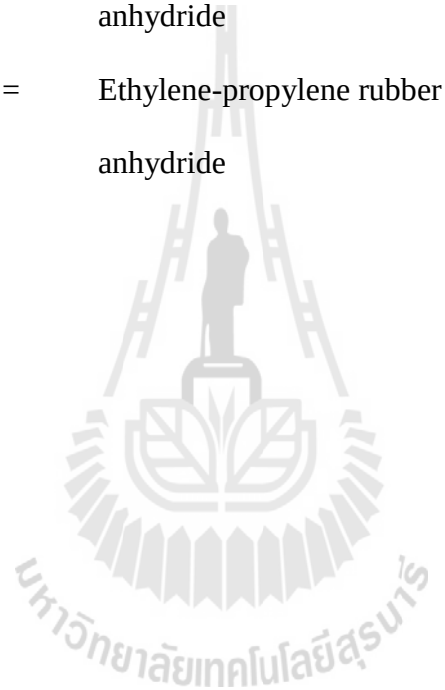

CHAPTER I

INTRODUCTION

1.1 Background

Nowadays, plastic materials play an important role in daily life as packaging, bottles, toys, potable pipe, electronic parts, and housewares. High density polyethylene (HDPE) is one of the most widely used plastic materials. It is the world's third-largest commodity plastic resin after polyvinyl chloride (PVC) and polypropylene (PP) (Liu, Yu, Cheng and Qu, 2009). The global forecasting consumption for HDPE is 92.1 million in 2015 with an annual growth rate of 5.6 wt.% (Rappaport, 2011) HDPE is used in many applications such as packaging and household goods. The HDPE packagings include sterile packaging, pharmaceutical packaging and milk bottles. The household goods consists of fences, picnic tables, pipes, floor tiles, buckets, crates, flower pots and recycling bins. In addition, HDPE is emerged as an ideal polymer for automobile parts as plastic joint connector, car handle, gear box and fuel tank cap (Chanda and Roy, 2006). It is widely used because of moderate cost, light weight, low thermal conductivity, high abrasion resistance, high corrosion resistance, high specific strength, and inert to most chemicals (Kim, Park, Kim and Suh, 2000)

According to a vastly increase of production and consumption of HDPE, more plastic waste is increasingly discarded in environment, by which it becomes a major impact on global pollution. As predicted in the next 5 year, approximately 10 million

tons of HDPE waste will be gathered in nature for a long period of time due to its poor biodegradability causing much environmental pollution.

There are several methods for handling plastic waste such as a landfill, an incineration, depolymerization, and recycling. For a landfill method, HDPE plastic waste is still the major environmental problem because HDPE plastics decompose hardly in natural environment since HDPE is a non-polar material, as shown in HDPE chemical structure shown in figure 1.1(a). An average time for a HDPE bottle to fully biodegrade is approximately 1,000 years on land and 450 years in water. However, time also varies with size of the product (Source: Headwaters Cooperative Recycling, Inc, 2012). The chemical modification of HDPE, use of photo-oxidation additive, and blending HDPE with a biodegradable polymer are the efficient method to obtain the biodegradable material from HDPE (Singh, Bhunia, Rajor and Choudhary, 2010). However, the disadvantage of HDPE chemical modification is time consuming and use of some chemical reactants in the process of modification. Likewise, the use of photo-oxidation additive is convenient but it is not effective for buried HDPE waste because it does not directly exposure with UV light. Another comfortable method for improving biodegradability of HDPE is blending HDPE with a biodegradable polymer. It has been previously reported that the material from non-biodegradable polymer blended with a biodegradable polymer degraded more easily after discarding in the environment. According to Łabużek, Nowak and Pająk's studied (2003), it was found that the film of polyethylene blended with 60 wt% PBS (Bionolle) in dimension of 40 mm x 40 mm squares was degraded within 90 days by fungi which encounter in a dump.

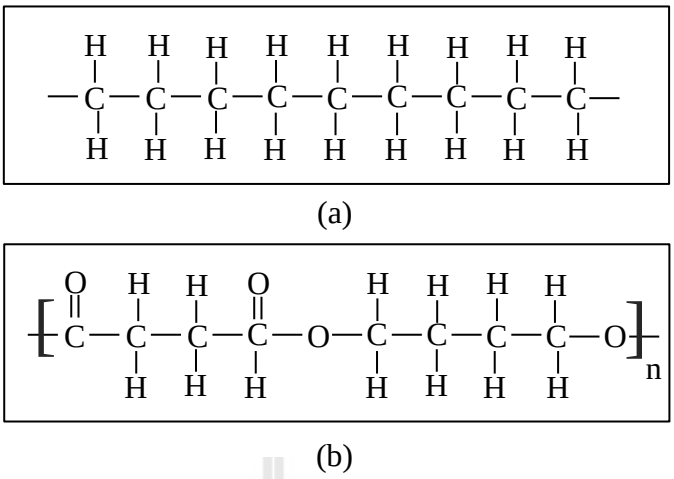

(a)

(b)

Figure 1.1 Chemical structures of (a) HDPE and (b) PBS

Nowadays, there is a great interest in replacing non-biodegradable plastics with biodegradable plastics. Poly (butylene succinate) (PBS) is a biodegradable polymer with some physical and mechanical properties quite similar to commercial non-biodegradable polymer such as HDPE, LDPE, and PP,. In comparison, PBS exhibits a melting point slightly lower than those of HDPE. Its tensile strength, tensile stress at break and flexural strength are moderately higher than that of HDPE. Furthermore, it can be processed using the same processing machine which employed to process those conventional polymers, as well. (Ray, Bandyopadhyay, and Bousmina, 2007). Some physical and mechanical properties of PBS and HDPE are comparatively shown in Table 1.1.

Table 1.1 Comparison of physical and mechanical properties of PBS and HDPE

Properties	Polymers		Units
	HDPE*	PBS**	
Glass transition temperature	-60	-24	^{o}C
Melting temperature	131	110	^{o}C
Crystallinity	71	53	%
Flexural modulus	1,225	530	MPa
Flexural strength	25	34	MPa
Tensile strength	27.5	37	MPa
Tensile stress at break	17.6	37	MPa
Elongation at break	620	300	%
Izod impact strength	3	8.2	kJ/m^2
Heat deflection temperature (HDT)	75	84	^{o}C
Price	740-1700[a]	4500-5000[b]	US $/ton

*Source: *SCG Technical Datasheet*, 2009. **GS Pla properties sheet*, 2011.

[a]Source: *Worldscrap Co.,Ltd.*, 2012.

[b]Source: *Shanghai Pangtai Industry Co., Ltd.*, 2012.

PBS is able to process in the field of textiles, melt blown, multifilament, monofilament, flat and split yarn. In the field of general plastics, it is injected into molded products. Thus, it is a promising biodegradable plastic for several applications (Ray, Bandyopadhyay, and Bousmina, 2007). It has been reported previously that the bottle product derived from PBS (Bionolle#1000) was fragmented within 1week and had almost completely disappeared after 4 weeks in hot compost. In addition, this bottle product had lost about 25% in weight after 16 weeks of soil burial during the summer (Moore and Saunders, 1998). The fast degradation of PBS is a consequence of its polarity as shown in PBS chemical structure in Figure 1.1(b). However, PBS has the significant disadvantage in term of cost; it is much more expensive than

conventional synthesis thermoplastic such as HDPE and PP about 3-6 times as comparatively shown in Table 1.1.

Presently, PBS market is expected to grow as increasing demand of biodegradable plastics. Mitsubishi Chemical Corporation currently produces and markets PBS at 3,000 ton/year in Japan. The forecasting demand of PBS market will grow to 50,000 ton/year in the next 4 years and up to 100,000 ton/year in 10 years. In addition, Mitsubishi Chemical Corporation of Japan and PTT Public Company Limited of Thailand have formed a joint venture as PTT MCC Biochem Company (PMBC). PMBC is established to develop and produce PBS using sugar derived succinic acid as a raw material. The plant site is expected to locate in Map Ta Phut Industrial Estate, Rayong, Thailand. It is expected to start up in 2015 for a capacity of 20,000 ton/year. (Source: ICIS Chemical Business, 2011).

According to high price of PBS, it is not economically feasible to be used alone without diluting with cheaper plastics or compounding with low price functional fillers. The blending PBS with cheaper commodity plastics such as HDPE, LDPE and PP is a selective way to reduce the material cost of PBS-derived product. Among various low price commercial plastics, HDPE is the most suitable to dilute material cost of PBS-derived product since it has comparable mechanical properties to those of PBS. Therefore, it was expected that blending HDPE with PBS will improve biodegradability of consumer products derived from HDPE, and also dilutes the material cost of PBS-derived product.

1.1.1 Polymer blending

Polymer blending is a convenient method for developing new polymeric materials. It combines properties of both blend components to improve

some certain properties such as impact strength, rigidity, ductility, chemical-solvent resistance and flammability. Polymer blending also benefits the manufacturer by improving processability, scrap reduction, and high productivity (Groeninckx, Vanneste and Everaert, 2003). However, properties of polymer blends are controlled by two main parameters; material and processing parameters. The material parameters affecting polymer blend properties are viscosity ratio, blend composition, elasticity and interfacial properties (Chareunkvun, 2007). On the other hand, processing parameters affecting polymer blend properties are barrel temperature, screw geometry, mixing and processing temperature, residence time of mixing and shear rate (Ambrósio and Junior, 2011).

Although, the parameters affecting blend properties are controlled, most cases, polymer blend remains immiscible resulting in poor mechanical properties of their blended materials (Mbarek, Jaziri, Chalamet and Carrot, 2010). Likewise, the blend of HDPE and PBS is an immiscible blend. This is due to HDPE is nonpolar whereas PBS is polar material. As a result, mechanical properties of the blend especially tensile and impact strength become worsen. Accordingly, there is a strong need to enhance compatibility of polymer blends. The use of a compatibilizer is the capable way to improve compatibility of polymer blends. Boutevin, Lusinchi, Pietrasanta, and Robin (1996) found that the adding of HDPE-g-MAH into PET/HDPE blend led to an increase of stress at break and elongation at break of the blend up to 60% and 150%, respectively. This improvement was a consequence of HDPE-g-MAH enhanced compatibility between PET and HDPE.

1.2 Statement of motivation

High density polyethylene (HDPE) is widely used due to their good mechanical properties, low cost, easy processability, high corrosion resistance and high biological attack resistance. However, much concern has been placed on plastic waste pollution, since HDPE waste will accumulate in the environment each year, leading to long-term environmental and waste management problems. HDPE waste will be gathered in nature approximately 10 million tons in the next 5 year and takes almost 1,000 years for degradation in nature (Source: Energy Information Administration, 2007). Therefore, the biodegradability of HDPE-derived product has to be enhanced in order to make it faster degraded in nature. Since,

On the contrary, PBS, a biodegradable polymer, has gain attention from industries and scientists as a tentative replacement for HDPE but its use is not wide spread yet due to its limitation from high price as mentioned previously.

Accordingly, the main objective of this research is distinguished into two aspects. The first aspect is to enhance biodegradability of HDPE by blending with biodegradability polymer, like PBS. The second aspect is to reduce the cost of biodegradable products from PBS by diluting with a cheaper polymer, like HDPE. However, blending HDPE and PBS is immiscible blends because HDPE is nonpolar whereas PBS is a polar material. For this reason, the HDPE-g-MAH and EPR-g-MAH were used as compatibilizers for enhancement of interfacial compatibility between HDPE and PBS phases. Two main factors affecting the blend properties are blend composition and compatibility. Therefore, in this review, effect of blend composition and compatibilization enhancement has been focused.

1.3 Research objectives

The main purposes of blending HDPE and PBS in this research are as follows:

(i) To investigate the effect of blend composition on flow and thermal properties, mechanical properties, degree of crystallinity, water absorption, morphological properties and biodegradability of HDPE and PBS blends.

(ii) To investigate the effect of compatibilizer on flow and thermal properties, mechanical properties, degree of crystallinity, water absorption, morphological properties and biodegradability of HDPE and PBS blends.

1.4 Scope and limitation of the research

In this study, the blend of HDPE and PBS at various compositions was prepared. The injection grade of HDPE and PBS having close flow and mechanical properties were used. To study the compatibilizing effect, HDPE-g-MAH and EPR-g-MAH were employed at a content of 2, 4, 6 and 8 phr of the blend.

The test specimens were prepared via an injection machine. The flow properties and thermal properties were investigated. The mechanical properties including tensile, flexural and impact were tested using universal testing machine. In addition, the fractured surface of the blend was examined. Furthermore, the water absorption and biodegradability of the blends during natural soil burial were also monitored via weight reduction.

CHAPTER II

LITERATURE REVIEW

2.1 Melting behavior of Poly (butylene succinate)

Yoo and Im (1999) observed the melting behavior of PBS. It was found that PBS exhibited two endotherms during DSC heating. The two endotherms could be explained by the recrystallization phenomenon. It was fact that polymers crystallized as metastable lamellae, therefore, this was a reason why recrystallization or reorganization is possible during an elevating temperature scan. The metastable lamellae had their melting point depressed because of their large surface or volume ratios. Partly of crystals melted and then recrystallized prior to completely melted at higher temperature.

Qiu, Komura, Ikehara and Nishi (2003) observed the melting behavior of PBS. It was found that PBS exhibited two melting endotherms in the DSC traces upon heating to the melt. This occurrence was caused by the melting and recrystallization mechanism. The first melting at low temperature corresponded to the melting of the crystallites with low thermal stability. The final melting endotherm was ascribed to the melting of the crystallites formed through the reorganization of the crystallites with high thermal stability.

Yasuniwa, Tsubakihara, Satou and Iura (2005) studied the melting behavior of PBS. It was observed that the double melting peaks of PBS appeared evidently in the DSC curve. The mechanism of double melting peaks was explained by the melt-

recrystallization model. The melt-recrystallization model meant that small or imperfect crystals or both change successively to more stable crystals through melting and recrystallization. Also, it was suggested that melting and recrystallization were competitive in the heating process. An endothermic peak appeared when the rate of melting overwhelmed that of the recrystallization. On the contrary, an exothermic peak appeared when the rate of recrystallization overwhelmed that of melting.

Liu, Li, Zhang and Xiao (2006) investigated melting behavior of PBS. It was found that PBS exhibited multiple melting peaks. It was suggested that the melting peak at lower temperature associated with the fusion of the crystals grown by normal primary crystallization and the melting peak at higher temperature was the melting of the most perfect crystals after reorganization during the heating process in DSC measurement.

Xu and Guo (2010). It was report that PBS had two spherulitic forms, α form and β form The spherulite of α form melted at higher temperature than spherulite of β form. However, the melting endotherm of β spherulite might or might not be observed from a DSC thermogram depending on heating rate, cooling rate and thermal history.

2.2 Biodegradability of Poly (butylene succinate) and Poly (butylene succinate) Blend

2.2.1 Poly (butylene succinate)

Fujimaki (1998) studied the biodegradability of biodegradable aliphatic polyesters, trademarked ‘BIONOLLE’ such as Poly (butylene succinate) (#l000 series) and Poly (butylene succinate adipate copolymer) (#3000 series). It was observed that biodegradability of BIONOLLE very much depended on polymer

structure. However, crystalline aliphatic polymers, both of #l000 series and #3000 series, was biodegraded in compost, in moist soil, in fresh water with activated sludge and in sea water. In addition, pure powder of BIONOLLE #l000 and #3000 were composted rapidly in hot compost.

Zhao *et al.* (2005) studied the biodegradation of poly (butylene succinate) (PBS) under controlled composting conditions. Three forms of PBS, namely, granule, powder, and film, were used in their study and four strains were isolated from the compost and identified as *Aspergillus*, *Penicillium*, *Bacillus*, and *Thermopolyspora*. It was reported thatt PBS with the form of powder showed the best biodegradability under controlled composting conditions. The biodegradation rate was influenced by the sample form. The powder formed sample showed the fastest degradation because of its largest specific surface area, then followed by film-formed and granule formed PBS in sequence. The biodegradation process of PBS exhibited three phases with different degradation speed. The biodegradation in the first phase was slow, got accelerated in the second phase, and leveled off in the third phase. After composting, the molecular weight of PBS film decreased distinctly and the polymer surface was badly eroded. They concluded that *Aspergillus* was the best PBS degrading microorganism. The biodegradation curves of PBS samples with different forms are shown in Figure 2.1.

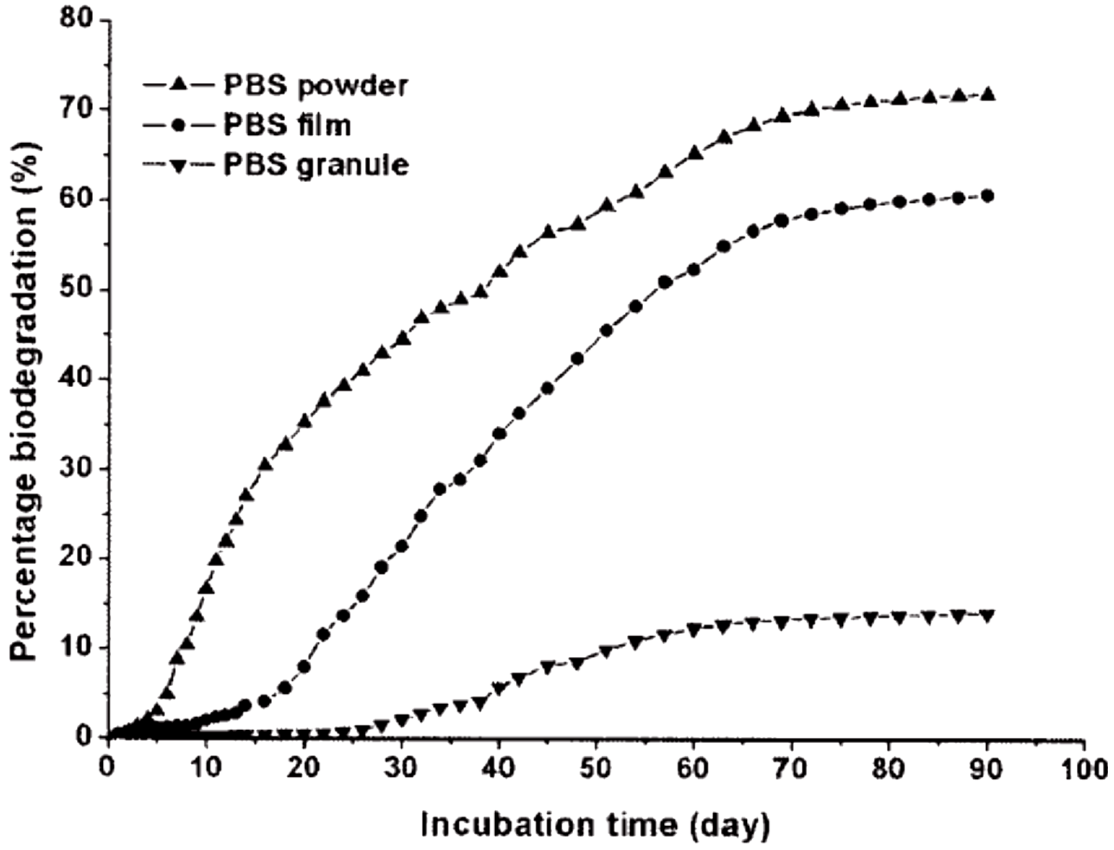

Figure 2.1 Biodegradation of PBS samples with different forms under controlled composting conditions (Zhao *et al.*, 2005).

2.2.2 Poly (butylene succinate) and low density polyethylene blend

Łabużek *et al.* (2003) investigated the biodegradation of low-density polyethylene (LDPE) film modified with PBS (Bionolle) by fungi. Two strains of fungi *Aspergillus niger* and *Penicillium funiculosum* were used in their study. The LDPE film modified with PBS was prepared at blend compositions of LDPE/PBS was 40/60 wt.%. Then, LDPE/PBS film was cut into strips (ca. 40 mm x 10 mm) prior to incubate with fungi. It was found that *Aspergillus niger* and *Penicillium*

funiculosum fungi were capable of degrading LDPE film modified with PBS. The LDPE/PBS film could be degraded within 90 days.

Nowak, Pająk, Bratkowicz and Rymarz (2011) studied the degree of biodegradation of LDPE and LDPE film modified with PBS (PBS/LDPE). The LDPE film modified with PBS was prepared at blend compositions of PBS/LDPE was 30/70 wt.%. PBS/LDPE film was cut into 40 mm x 40 mm squares. After the incubation, it was observed that the PBS/LDPE film degraded faster than conventional LDPE in all environmental conditions tested: waste coal soil, forest soil and soil from an extinct volcano crater. It was also investigated that the film would be easily colonized by microorganisms inhabiting each of the soils. They concluded that bacteria belonging to the genus, *Bacillus*, and the fungi, *Gliocladium viride*, *Aspergillus awamori* and *Mortierella subtilissima*, were able to colonize both LLDPE and LDPE film modified with PBS. The percentage of weight loss of the films after soil incubation is displayed in Table 2.1.

Table 2.1 The percentage of weight loss of the films after biodegradation (Nowak, Pająk, Bratkowicz and Rymarz, 2011).

Location of soil sampling	**Time (days)**	**Weight loss (%)**		
		LDPE film	**PBS/LDPE film**	**PBS film**
Waste coal	75	0.03	0.18	2.49
	150	0.15	0.34	4.35
	225	0.26	0.5	5.76
Forest	75	0.03	0.22	0.91
	150	0.05	0.4	1.97
	225	0.13	0.52	2.02
Crater	75	0.03	0.28	7.53
	150	0.21	0.56	13.54
	225	0.28	0.62	17.03

2.3 Physical properties of PET/HDPE blend

2.3.1 Effect of blend composition

2.3.1.1 Tensile properties

Pietrasanta, Robin, Torres, and Boutevin (1999) studied the effect of blend composition on tensile properties of PET/HDPE blends. The blends of PET/HDPE were prepared at a composition of 0/100, 10/90, 20/80, 30/70, 40/60 and 100/0 wt.%. It was found that the Young's modulus of the blend gradually increased as increasing PET content, due to the fact that PET had a higher modulus comparing to HDPE. It was also revealed that adding 10 wt.% to 40 wt.% PET made the elongation at break of the blend decreased.

Maksimov, Meri, Kalnin and Zicans (2003) investigated the effect of blend composition on tensile properties of PET/HDPE blends. The PET/HDPE blend was prepared at compositions of 0/100, 10/90, 30/70, 50/50 and 100/0 wt.%. It was revealed that Young's modulus of the blend increased as increasing PET content. This was due to the Young's modulus of PET was considerably higher than that of HDPE. For elongation at break, it was found that the elongation at break of the blend decreased as increasing PET content. In addition, it was observed the yield stress of PET/HDPE blends increased as increasing content of PET, according to the higher yield stress of PET as compared with HDPE. Also, it was found that stress at break of the blend decreased as increasing PET content from 10 to 30 wt.%. Noticeably, at 50 wt.% PET, the stress at break of the blend slightly increased.

Chareunkvun (2007) observed the effect of blend composition on tensile properties of HDPE/PET blend. The PET/HDPE blend was prepared at composition of 0/100, 20/80, 40/60 and 100/0 wt.%. The elongation at break of PET

was 4.42% whereas HDPE did not break within tensile testing condition. Adding PET into HDPE matrix led to a decrease of elongation at break the blend. In addition, the elongation at break the blend decreased with adding more PET. However, adding PET into HDPE matrix did insignificant affect the tensile strength of the blend.

2.3.1.2 Impact property

Chareunkvun (2007) studied the impact strength of PET/HDPE blends at various blend compositions. The PET/HDPE blends were prepared at compositions of 0/100, 20/80, 40/60 and 100/0 wt.%. The impact strength of HDPE and PET was 20.24 kJ/m^2 and 1.43 kJ/m^2, respectively. It was revealed that the impact strength of the blend gradually decreased as increasing PET content.

2.3.2 Effect of compatibilization

2.3.2.1 Tensile properties

Boutevin, Lusinchi, Pietrasanta and Robin (1996) studied the influence of compatibilizer on PET/HDPE at the blend composition of 40/60 wt.%. The HDPE-g-GMA was used as a compatibilizer. It was found that adding 5 wt.% HDPE-g-GMA into PET/HDPE blend resulted in an improvement of elongation at break of the blend about 150%. In addition, the stress at break of the blend could be improved about 60% comparing to uncompatibilized blend.

Laurienzo, Immirzi and Malinconico (2001) studied the effect of compatibilizer on Young's modulus and elongation at break of PET/HDPE (30/70 wt.%) blend. It was found that addition 10 wt % of poly (ethylene terephthalate)-co-(ε-caprolactone) into PET/HDPE resulted in the decreasing Young's modulus of the compatibilized blend. In addition, the elongation at break of compatibilized blend was not improved. The elongation at break of the blend strongly depended on the blend

component and interfacial adhesion between two phases. The results implied that the poly (ethylene terephthalate)-co-(ε-caprolactone) was not able to increase the interpenetration between the phases of HDPE and PET. The researchers suggested that there were others parameters of which affected the elongation at break of compatibilized blend such as the blend composition, molecular weight and also the content of compatibilizer.

Lusinchi, Boutevin, Torres, and Robin (2001) studied the compatibilization of PET/HDPE (40/60) blend using HDPE-g-MAH as a compatibilizer. It was observed that the addition of a small content of HDPE-g-MAH directly to HDPE/PET blends improved mechanical properties including stress at break and elongation at break of the blend. This was a consequence of interaction between reactive functional groups of compatibilizer and functional end groups of PET, incorporated with the compatible of HDPE matrix and compatibilizer.

Torres, Robin and Boutevin (2001) studied the compatibilization of PET/HDPE (30/70 wt.%) blend by adding grafted copolymers (HDPE-g-GMA) . The effect of the compatibilizer was obtained by studying tensile properties of PET/HDPE blend. It can be seen that HDPE-g-GMA was an effective compatibilizer for PET/HDPE blend. The significant improvement of elongation at break of compatibilezed blend was found. These result showed that interaction had been created between HDPE matrix and PET domain in presence of HDPE-g-GMA compatibilizer.

Fasce, Seltzer and Frontini (2005) studied the effect of compatibilizer on tensile properties of PET/HDPE of uncompatibilized and compatiblized PET/HDPE blend. The PET/HDPE blend was prepared at 50 wt%

HDPE and 50 wt.% PET. The ethylene/methacrylate acid copolymer (EMA) was used as a compatibilizer at a content of 1 wt.%. It was reported that the tensile strength of the blend improved after adding small amount (1 wt.%) of EMA. The improvement of tensile strength was associated with chemical reactions between PET and ethylene-methacrylate acid copolymer, as proposed in Figure 2.2.

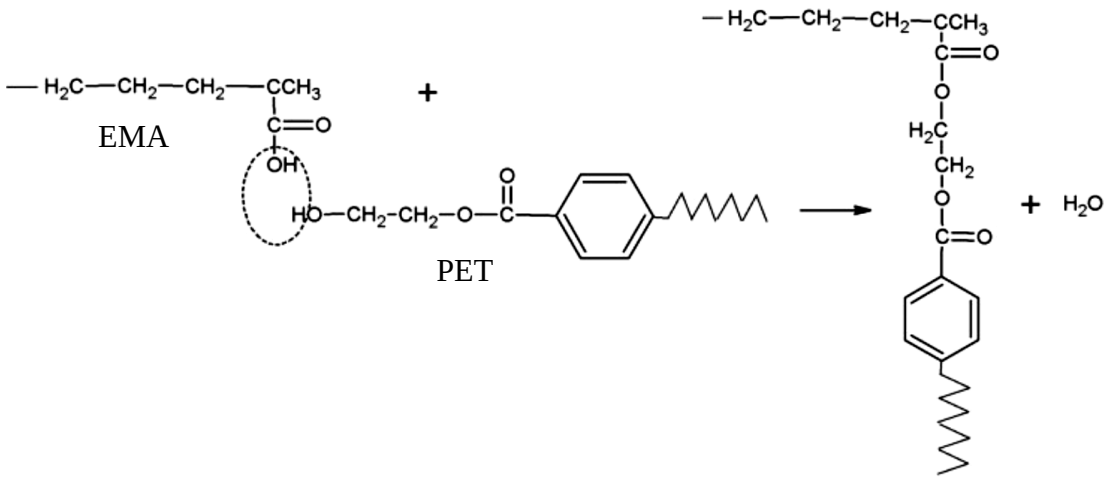

Figure 2.2 Schematic of chemical reaction between PET and EMA (Fasce, Seltzer and Frontini, 2005)

Mbarek, Jaziri, Chalamet and Carrot (2010) investigated the effect of two types of compatibilizers on the tensile properties of PET/HDPE blends. The blend of PET/HDPE was in weight compositions of 7.5/90 and 15/80 wt.% Ethylene-glycidyl methacrylate copolymer (E-GMA) and ethylene acrylic ester-glycidyl methacrylate (E-EA-GMA) terpolymer were used as compatibilizers. The results showed that addition of 2.5 wt% and 15 wt% of E-GMA and E-EA-GMA into PET/HDPE blend did not affect Young's modulus of PET/HDPE blend. However, E-GMA copolymer provides a tenfold increase of the elongation at break of the blend

while E-EA-GMA copolymer made the elongation at break increased by a threefold comparing to uncompatibilized blend.

2.3.2.2 Impact property

Pietrasanta, Robin, Torres, and Boutevin (1999) investigated the effect of HDPE-g-GMA on impact property of PET/HDPE blends. The blend composition of PET/HDPE was 20/80 and 40/60 wt.%. It was observed that the impact strength for all compositions of PET/HDPE blends improved after adding 5 wt% of HDPE-g-GMA. This improvement was a consequence of chemical reaction between glycidyl methacrylate and end group of PET.

Mbarek, Jaziri, Chalamet and Carrot (2010) investigated the effect of two types of compatibilizers on the impact strength of PET/HDPE blends. The blend of PET/HDPE was in weight compositions of 7.5/90 and 15/80 wt.% Ethylene-glycidyl methacrylate copolymer (E-GMA) and ethylene acrylic ester-glycidyl methacrylate (E-EA-GMA) terpolymer were used as compatibilizers. It was revealed that both E-GMA and E-EA-GMA were effective compatibilizers for improving impact strength of PET/HDPE blend. In comparison, at the same content of compatibilizer, E-GMA was more effective than E-EA-GMA.

2.4 Physical properties of HDPE/PET blend

2.4.1 Effect of blend composition

2.4.1.1 Tensile properties

Boutevin, Lusinchi, Pietrasanta and Robin (1996) studied the influence of blend composition on stress at break of HDPE/PET blend. The HDPE content was varied from 10 wt.% to 50 wt.%. It was observed that the stress at break

of the blend decreased as increasing HDPE content. They suggested that this was due to the surface tension between two phases was high, and resulted in poor mechanical performance.

Kim, Park, Kim, and Suh (2000) observed the influence of blend composition on tensile properties including elongation at break and yield strength of HDPE/PET blend. The HDPE content was varied from 10 wt.% to 50 wt.%. It was revealed that adding 10 wt.% to 50 wt.% HDPE made the elongation at break of the blend decreased. They suggested that elongation at break was very sensitive to the adhesion strength. Therefore, the decrease in elongation at break of the blend was probably due to there was no adhesion between HDPE and PET phase. For the tensile strength, it was observed that the tensile strength of the blend decreased with adding 10 wt.% to 50 wt.% HDPE. It was suggested that was due to the lower strength of HDPE comparing to PET. Also, they suggested that might be due to an incompatible of HDPE and PET phase.

Pietrasanta, Robin, Torres, and Boutevin (1999) studied the effect of blend composition on tensile properties of HDPE/PET blends. The blends of HDPE/PET in weight compositions of 0/100, 20/80, 40/60 and 100/0 were prepared. It was found that the Young's modulus of the blend gradually decreased as increasing HDPE content, due to the fact that HDPE had a lower modulus comparing to PET. It was also revealed that adding 20 wt.% and 40 wt.% HDPE into PET matrix made the elongation at break of the blend decreased.

Maksimov, Meri, Kalnin and Zicans (2003) investigated the effect of blend composition on tensile properties of HDPE/PET blends. The HDPE/PET blends contained 0, 10, 30 and 50 wt.% HDPE. It was found that Young's

modulus of the blend decreased as increasing HDPE content. This was due to the Young's modulus of HDPE was considerably smaller than that of PET. For elongation at break, it was observed that the elongation at break of the blend decreased as increasing HDPE content from 10 wt.% to 50 wt.%. It was suggested that the blends lost their ability for deformational after adding HDPE. It was also observed the yield stress and stress at break of HDPE/PET blends slightly decreased as increasing content of HDPE, according to the lower yield stress and stress at break of HDPE as compared with PET.

Chareunkvun (2007) observed the effect of blend composition on tensile properties of HDPE/PET blend. The HDPE/PET blend was prepared at 0 wt.%, 20 wt.%, 40 wt.%, 100 wt.% HDPE. It was found that adding 20 wt.% and 40 wt.% HDPE made the elongation at break of the blend decreased. Furthermore, it was found that the tensile strength of HDPE/PET blend decreased as increasing HDPE.

Mbarek, Jaziri, Chalamet and Carrot (2010) investigated the effect of blend composition on tensile properties of HDPE/PET blend. The HDPE/PET composition was 5/95, 10/90, 15/85 and 20/80 wt.%. It was revealed that increasing HDPE content from 5 wt.% to 20 wt.% did not affect the elongation at break of the blend. The elongation at break of the blend remained very low as compared to neat HDPE. In addition, it was found that the stress at break of the blend slightly decreased with adding 5 wt.% to 20 wt.% HDPE into PET matrix. This was due to the lack of adhesion between HDPE and PET phase leading to an incompatible between the two phases.

2.4.1.2 Impact property

Mbarek, Jaziri, Chalamet and Carrot (2010) studied impact strength of HDPE/PET blends at HDPE content of 5 wt.%, 10 wt.%, 15 wt.% and 20 wt%. It was observed that the impact strength of the blend slightly improved with adding HDPE.

Chareunkvun (2007) investigated the impact strength of HDPE/PET blends at various blend compositions. The HDPE content was 0, 20, 40 and 100 wt%. The impact strength of the blend depended on the blend composition. It was revealed that the impact strength of the blend increased as increasing HDPE content.

2.4.1.3 Thermal degradation temperature

Lei, Wu, Clemons and Guo (2009) investigated the effect of blend composition on thermal degradation temperature of HDPE/PET blend. The HDPE content in the blend was 30 wt.% to 50 wt.%. It was observed that HDPE degraded at a temperature of 442ºC. Adding HDPE into PET matrix did insignificantly affect thermal degradation of both PET phase and HDPE phase itself.

2.4.2 Effect of compatibilization

2.4.2.1 Tensile properties

Jabarin and Bhakkad (1995) studied ternary blends of PET, HDPE, and maleic anhydride grafted polyethylene resin (PE-g-MAH). The HDPE/PET/PE-g-MAH ternary blends were prepared at blend composition of 5/80/15, 10/80/10 and 15/80/5 wt.%. It was revealed that the improvement of adhesion between PE-g-MAH chains and the PET matrix made PET matrix toughen, leading to a decrease in the Young's modulus of the compatibilized blend.

Kalfoglou, Skafidas, and Kallitsis (1995) investigated the effect of compatibilizer types on tensile properties of HDPE and PET blends. The compatibilizers were ethylene-glycidyl methacrylate copolymer (E-GMA), an ethylene ethylacrylate glycidyl methacrylate terpolymer (E-EA-GMA), a hydrogenated styrene butadiene-styrene copolymer grafted with maleic anhydride (SEBS-g-MA), and MA-modified ethylene-methyl acrylate copolymer (E-MeA-g-MA). The blends were prepared with 20/70/10 weight ratio of HDPE/PET/compatibilizer. They had found that the compatibilizing effectiveness decreased in a sequence like this: E-GMA>E-EA-GMA>SEBS-g-MA>E-MeA-g-MA. The different reactivities of the compatibilizers depended on the type of functionality in the compatibilizers. In the case of GMA-containing compatibilizers, the dispersed phase of HDPE was more efficiently stabilized due to high reactivity of GMA. GMA might react with both carboxyl and hydroxyl terminal group of the polyester but MA might only react with the hydroxyl moieties. The result indicated that the ultimate strength and elongation at break of the blend depended on adhesion between the PET and HDPE phase in the compatibilized blend.

Dimitrova *et. al.*, (2000) investigated the effect of using SEBS-g-MAH as a compaitibilizer in HDPE/PET blend. The blend composition of HDPE/PET was 20/80 wt.%. The SEBS-g-MAH elastomer was used at a content of 5 wt.% of the blend. It was reported that SEBS-g-MAH greatly improved elongation at break of the compatibilized. The improvement of the elongation at break could be attributed to the compatibilization raised by the intrinsic high value of elongation at break of SEBE-g-MAH elastomer However, the yield strength and Young's modulus

of the compatibilized almost unchanged as compared to those of uncompatibilized blend.

Guerrero, Lozano, Gonzalez, and Arroyo (2001) reported the effect of a compatibilizer on the tensile properties of HDPE/PET blends. The composition of HDPE/PET blend was 25/75 wt.%. The compatibilizer was a copolymer of ethylene and methacrylic acid partially neutralized with zinc (E-MAA) (Surlyn). Addition of 7.5% of Surlyn in HDPE/PET (25/75 wt%) improved the elongation at break from 2.6 to 41.5% which was double of neat PET value due to an increase of interfacial adhesion between PET and HDPE phase. The olefinic part of Surlyn was compatible with HDPE, whereas the carboxylic end groups would form strong hydrogen bonds with carbonyl group of PET.

Pracella, Rolla, Chionna and Galeski (2002) studied the effect of compatibilizer on tensile properties of HDPE/PET blend. The blend composition was 25/75. The ethylene-co-glycidyl methacrylate copolymer (E-GMA) was used as a compatibilizer at a content of 1-5 phr of the blend. It was found that the addition of compatibilizer caused a marked improvement of the tensile behavior of the blend. A large increase of elongation at break (from 110% to about 370%) together with higher stress at break (from 19 to 23 MPa) was found with increasing E-GMA content in the range of 2-4 phr. Higher content of compatibilizer did not give rise to further improvement of elongation at break and stress at break of the blend. However, the Young's modulus and yield strength of the compatibilized blend decreased slightly in the same composition range. The compatibilization efficiency of E-GMA was derived by the presence of grafting reactions between the epoxy groups of E-GMA and the carboxyl/hydroxyl groups of PET.

2.4.2.2 Impact property

Pietrasanta, Robin, Torres, and Boutevin (1999) investigated the effect of HDPE-g-GMA on impact property of HDPE/PET blends. The blend composition of HDPE/PET was 20/80 and 40/60 wt.%. It was observed that the impact strength for all compositions of HDPE/PET blends improved after adding 5 wt% of HDPE-g-GMA. This improvement was a consequence of chemical reaction between glycidyl methacrylate and end group of PET.

2.5 Physical properties of other blends of polyolefins and polyester

2.5.1 Effect of blend composition

2.5.1.1 Tensile properties

Tsai and Chang (1996) studied the effect of blend composition on tensile properties of PP/PBT blend. The PP content was 30 wt%, 50 wt.% and 70 wt%. It was observed that the elongation at break of the blend slightly increased with increasing PP content. On the other hand, the yield strength of the blend slightly decreased with an increase in PP content.

Kang *et al.* (1999) observed the effect of blend composition on yield strength of LLDPE/PBT blend at 20 wt.% to 80 wt.% LLDPE. It was found that the yield strength of the blends decreased with increasing LLDPE. It was expected as a result of a weaker of yield strength of the LLDPE in comparison with PBT.

Kim, Kim, Shin, Choi and Jhon (2001) studied the influence of blend composition on tensile properties of LLDPE/BDP (biodegradable aliphatic polyester) blend. The LLDPE/BDP composition was 10/90, 30/70, 50/50, 70/30 and 90/10, respectively. It was observed that the Young's modulus and yield strength of

the blend decreased as increasing LLDPE content, following the additivity rule with respect to the blending ratios.

Qi, Nie, Zhou, Mao and Zhang (2006) studied the effect of blend composition on yield strength of HDPE/PBT blend. The HDPE content was in range of 5 wt.% to 20 wt.%. It was observed that the yield strength of the blend decreased with an increase in HDPE. This was a consequence of an incompatible between HDPE and PBT phase.

2.5.1.2 Impact property

Kang *et al.* (1999) observed the effect of blend composition on impact strength of LLDPE/PBT blend. The LLDPE/PBT composition was 20/80, 40/60, 60/40 and 80/20, respectively. It was found that the impact strength of the blend slightly increased with increasing LLDPE compositions at a lower concentration of LLDPE but was remarkably increased with increasing LLDPE compositions above concentration of 60 wt.%. The rapid increase of impact strength was due to the presence of LLDPE could be easily inferred from the phase change morphology, as shown in Figure 2.3. Although LLDPE acts as the toughening material for PBT at lower concentrations of LLDPE, the larger LLDPE particles dispersed in PBT could not act as a good toughening material due to the immiscibility with PBT.

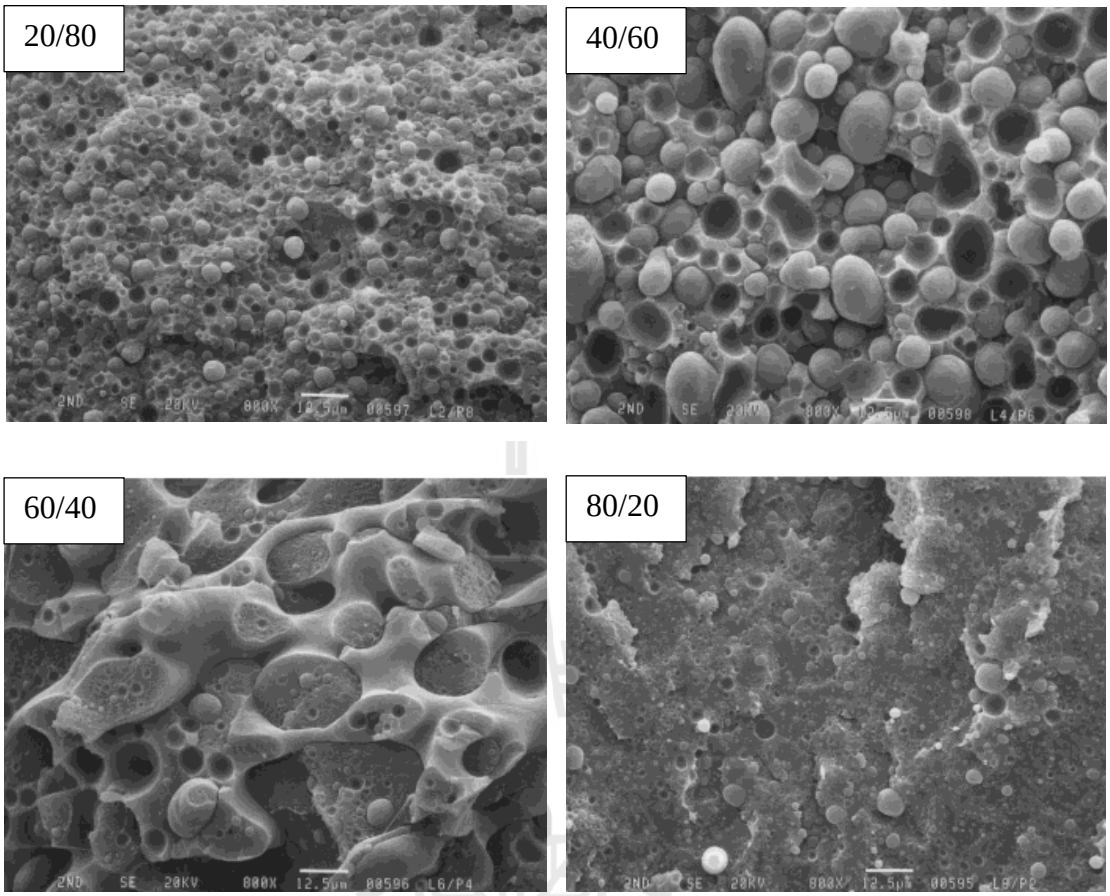

Figure 2.3 SEM micrographs of LLDPE/PBT blend (Kang *et al.*, 1999).

Kim, Kim, Shin, Choi and Jhon (2001) studied the influence of blend composition on impact strength of the blend between biodegradable aliphatic polyester and linear low density polyethylene (BDP/LLDPE). The BDP/LLDPE composition was 10/90, 30/70, 50/50, 70/30 and 90/10, respectively. The impact strength of pure LLDPE and BDP was 60 and 3.3 kg.cm/cm^2. For the blend, it was observed that the impact strength of the blend increased as increasing LLDPE content, following the additivity rule.

2.5.1.3 Thermal degradation temperature

Pang *et. al.*, (2008) studied the effect of blend composition on thermal degradation temperature of poly (propylene carbonate) (PPC) and poly (butylene succinate (PBS) blend. The blend composition of PPC/PBS was 10/90, 30/70, 50/50, 30/70 and 90/10 wt.%. They found that thermal stability of PCC could be greatly improved by the incorporation of a small amount of PBS. However, thermal stability of PBS did not improve after adding PCC.

2.5.1.4 Melting and crystallization behavior

Kang *et al*. (1999) studied crystallization behavior of PBT/LLDPE blend. It was found that the double melting peaks of PBT occurred according to the recrystallization phenomenon. However, the double melting peaks of PBT in the blends did not appreciably change with its content. Also, the melting temperature of LLDPE was not appreciably changed. The results might be due to the fact that PBT was immiscible with LLDPE over all the blend concentration.

Qi, Nie, Zhou, Mao and Zhang (2006) investigated the effect of blend composition on crystallization behavior of PBT/HDPE blend. It was found that the double melting peaks of PBT occurred. However, adding more PBT did insignificantly affected the double melting peaks of PBT. Similarly, adding more PBT into the blend slightly affected the melting temperature of HDPE. On the other hand, adding PBT into PBT/HDPE blend resulted in a decrease of X_c of HDPE whereas the X_c of PBT itself slightly changed. It was suggested that the crystallization of HDPE molecular chains was prohibited because of the addition of PBT.

2.5.2 Effect of compatibilization

2.5.2.1 Tensile properties

Zainuddin, Sudradjat, Razzak, Yoshii and Makuuchi (1999) studied the compatibilization effect of polypropylene-grafted maleic anhydride (PP-g-MAH) (Modic) on polypropylene-co-ethylene (CPP) and PBS (Bionolle) blended. The blend composition of CPP/ PBS was prepared at 25/75, 50/50 and 75/25 wt.%. The PP-g-MAH content was 5, 10 and 15 wt.% of the blend. It was found that all compositions of the compatibilized blend showed significant improvement on the tensile strength and elongation at break as compared to uncompatibilized blend. The compatibilization mechanism based on interfacial reaction and in situ formation of the compatibilizer should here be envisaged. Indeed, because CPP contained few ethylene units, it could be assume to be miscible with PP-g-MAH. Also, it was possible that part of PP-g-MAH migrated to the interface, where the maleic anhydride groups attached to it react with end groups or ester groups of backbone of PBS.

Kim, Park, Kim, and Suh (2000) studied the compatibilization of HDPE/PET blends. High-density polyethylene grafted with the blocked isocyanate group (HDPE-g-BHI) was used as a reactive compatibilizer for an immiscible HDPE/PET blend. The blend ratios of either HDPE-g-BHI/PET or HDPE/PET were 90/10, 70/30, 50/50, 30/70, and 10/90 by weight. It was found that the tensile strength and elongation at break of reactive compatibilized blends were higher than those of uncompatibilized blends. This was due to during the melt blending in an internal mixer, the chemical reaction occurred between the isocyanate group and carboxyl or hydroxyl end groups of PET resulting in a reduction of interfacial tension and increased interfacial adhesion between those two phases.

Wang and Hillmyer (2001) studied the effect of polyethylene-poly (L-lactide) diblock copolymer (PE-b-PLLA) on tensile properties of LDPE/PLLA (20/80) blends. PE-b-PLLA was used at a content of 2, 5 and 10 wt.%. It was observed that the tensile stress and modulus of the LDPE/PLLA blend with PE-b-PLLA decreased slightly with adding more PE-b-PLLA while the elongation at break significantly increased. These results indicated that PE-b-PLLA was a good compatibilizer for LDPE/PLLA blends. They proposed that interfacial adhesion in ternary blends came not only from the chain entanglement but also from the co-crystallization between the segments of the block copolymer.

Qi, Nie, Zhou, Mao and Zhang (2006) investigated the influence of high density polyethylene-g-maleic anhydride (HDPE-g-MAH) on tensile properties of HDPE/PBT blends. They prepared HDPE/PBT and HDPE-g-MAH/PBT blends by the reactive extrusion approach. The HDPE and HDPE-g MAH content was 5, 10, 20, 25 and 30 wt%. They found that the tensile strength of HDPE-g-MAH/PBT blend was higher than those of the HDPE/PBT blends. It was likely that the addition of HDPE-g-MAH yielded a finer dispersion of the dispersed HDPE phase and stronger adhesion between PBT and HDPE phases, contributing to the improvement of the tensile properties of the compatibilized blends.

Singh, Bhunia, Rajor and Choudhary (2011) investigated the effect of compatibilizer on mechanical properties of PLLA/LLDPE blends. The blend composition of PLLA/LLDPE was 20/80 by weight. Maleic anhydride grafted low density polyethylene (LDPE-g-MAH) was used as a compatibilizer at a content of 2, 4, 6, 8 and 10 phr. It was found that the addition of compatibilizer decreased the tensile strength as well as elongation at break of blends. This was due to high melt

flow index and polymeric nature of LDPE-g-MAH. LDPE-g-MAH also acted as a plasticizer which increase or decrease the elongation at break. It had been observed that the uncompatibilized blend had better retention of tensile properties than compatibilized blend. However, it was suggested that the blend compatibilized with 4 phr LDPE-g-MAH showed optimum tensile properties.

2.5.2.2 Impact property

Tsai and Chang (1996) studied the effect of compatibilizer on impact strength of PBT/PP blend. The blend composition of PBT/PP blend was 70/30 wt.%. The ethylene-co-glycidyl methacrylate copolymer (E-GMA) with 12 wt.% GMA was used as a compatibilizer. It was observed that the presence of EG in the blend could improve 137% in impact strength of the compatibilized blend comparing to uncompatibilized blend.

Kang *et. al.*, (1999) investigated the effect of compatibilizer on impact strength of PBT/LLDPE (70/30) blend. EVA-g-LLDPE was used as a compatibilizer at a content of 1, 3, 5, 7 and 10 wt.%. They found that the impact strength of the compatibilized blend was improved. In addition, the impact strength of the blend was markedly improved with adding more EVA-g-LLDPE. It was suggested that improvement was a consequence of interaction between maleic anhydride functional groups in EVA-*g*-MAH with the hydroxyl ends of PBT.

2.6 Factor affecting phase morphology of blend between HDPE and PET

2.6.1 PET/HDPE blend

2.6.1.1 Effect of blend composition

Iñiguez, Michel, Romero and Nuñez (2000) studied the effect of blend composition on phase morphology of PET/HDPE blends. The PET/HDPE blend composition was prepared at 10/90, 20/80 and 30/70 by volume. SEM micrographs showed that the morphologies PET/HDPE blend were typical of immiscible blends. In addition, the particle size of PET dispersed almost linearly with the concentration of PET, as shown in Figure 2. 4.

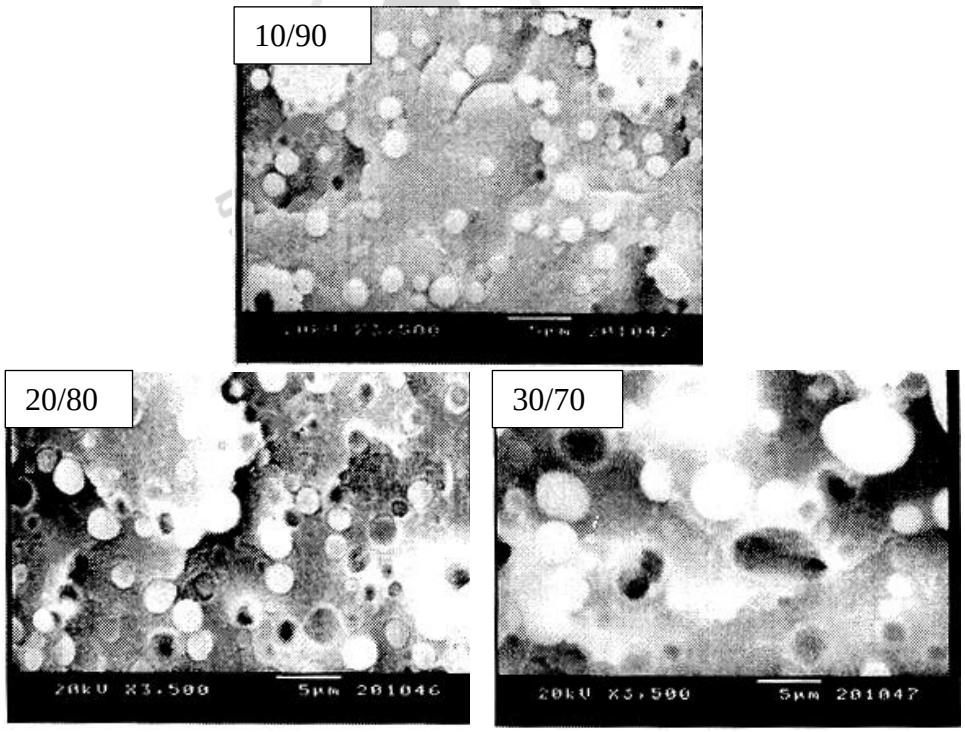

Figure 2.4 SEM micrographs of PET/HDPE blend at various blend compositions (Iñiguez, Michel, Romero and Nuñez, 2000).

2.6.1.2 Effect of viscosity ratio

Iñiguez, Michel, Romero and Nuñez (2000) studied the viscosity ratio affecting phase morphology of PET/HDPE blends. The PET/HDPE blend composition was prepared at 10/90, 20/80, 30/70, 40/60, 50/59, 60/40, 70/30, 80/20 and 90/10 by volume. They explained that if they take into account that the viscosity ratio (η_d/η_m) was low (0.25), when PET was the dispersed phase and particle disintegration was the process that governs the particle size blends. On the other hand, at higher viscosity ratios (4.0), when HDPE was the dispersed phase, the droplet breakup process becomes much slower and consequently starts to dominate droplet size. Under such conditions, the droplet size increases with viscosity ratio and changes only slightly with concentration.

Laurienzo, Immirzi and Malinconico (2001) investigated the effect viscosity ratio on PET/HDPE blend. They prepared PET/HDPE blends at a composition of 30/70 wt%. They found that the phase structure of 30/70 (PET/HDPE) blend showed a characteristic of immiscible blend. The PET phase was dispersed into the HDPE matrix as continuous phase. Obviously, average diameter of the PET domains was rather small, about 2 μm. The quite fine of PET particles inside the HDPE matrix was related to the lower viscosity of PET compared to HDPE resulting in low viscosity ratio.

2.6.1.3 Effect of compatibilization

Boutevin, Lusinchi, Pietrasanta and Robin (1996) investigated the effect of compatibilizer on phase morphology of PET/HDPE (40/60) blend. The PET/HDPE blend was prepared without and with 5 wt.% HDPE-g-MAH. SEM micrograph revealed the large particles including elongated and spherical of PET

domain. Adding 5 wt.% HDPE-g-MAH led to a decrease in size and gave rise to more uniform of PET domain. These results were a consequence of decreasing interfacial tension between PET and HDPE phase leading to breakup of the droplet. The SEM micrograph of uncompatibilized and compatibilized PET/HDPE blend was comparatively shown in Figure 2.5.

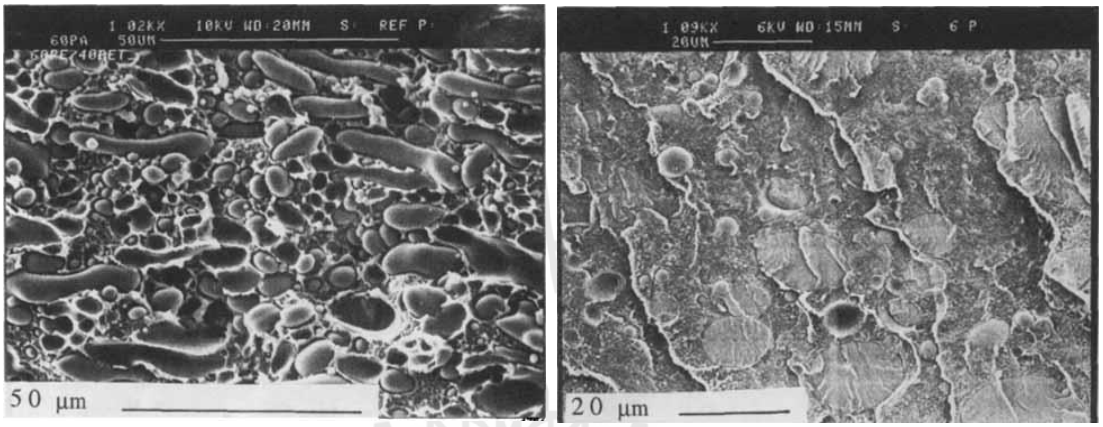

Uncompatibilized PET/HDPE Compatibilized PET/HDPE

Figure 2.5 SEM micrograph of uncompatibilized blend and compatibilized blend with 5 wt.% HDPE-g-MAH (Boutevin, Lusinchi, Pietrasanta and Robin, 1996).

Iñiguez, Michel, Romero and Nuñez (2000) studied the effect of compatibilizer on phase morphology of PET/HDPE blends. The PET/HDPE blend composition was prepared at 10/90, 20/80 and 30/70 by volume. The compatibilizer agent used in their studies was Kraton G-1652, which was a SEBS triblock copolymer containing 70 %w of a random copolymer of hydrogenated ethylene-butene, and 30 %w of styrene. The compatibilizer content was 10 wt.% of PET. It was observed that SEM micrographs of the blend, illustrated in Figure 2.6 showed that PET spherical

particles dispersed in HDPE matrix and a decrease of the particle size for compatibilized blend. The addition of the compatibilizer agent decreased the droplet size by 45% for average number diameter (D_n) and by 35% for average volume diameter (D_v). These results implied that interphase tension between PET and HDPE diminished with the presence of the triblock copolymer. The reduction of interfacial tension promoted the droplet breakup by the presence of repulsive forces between particles, which are induced by the presence of the interfacial agent.

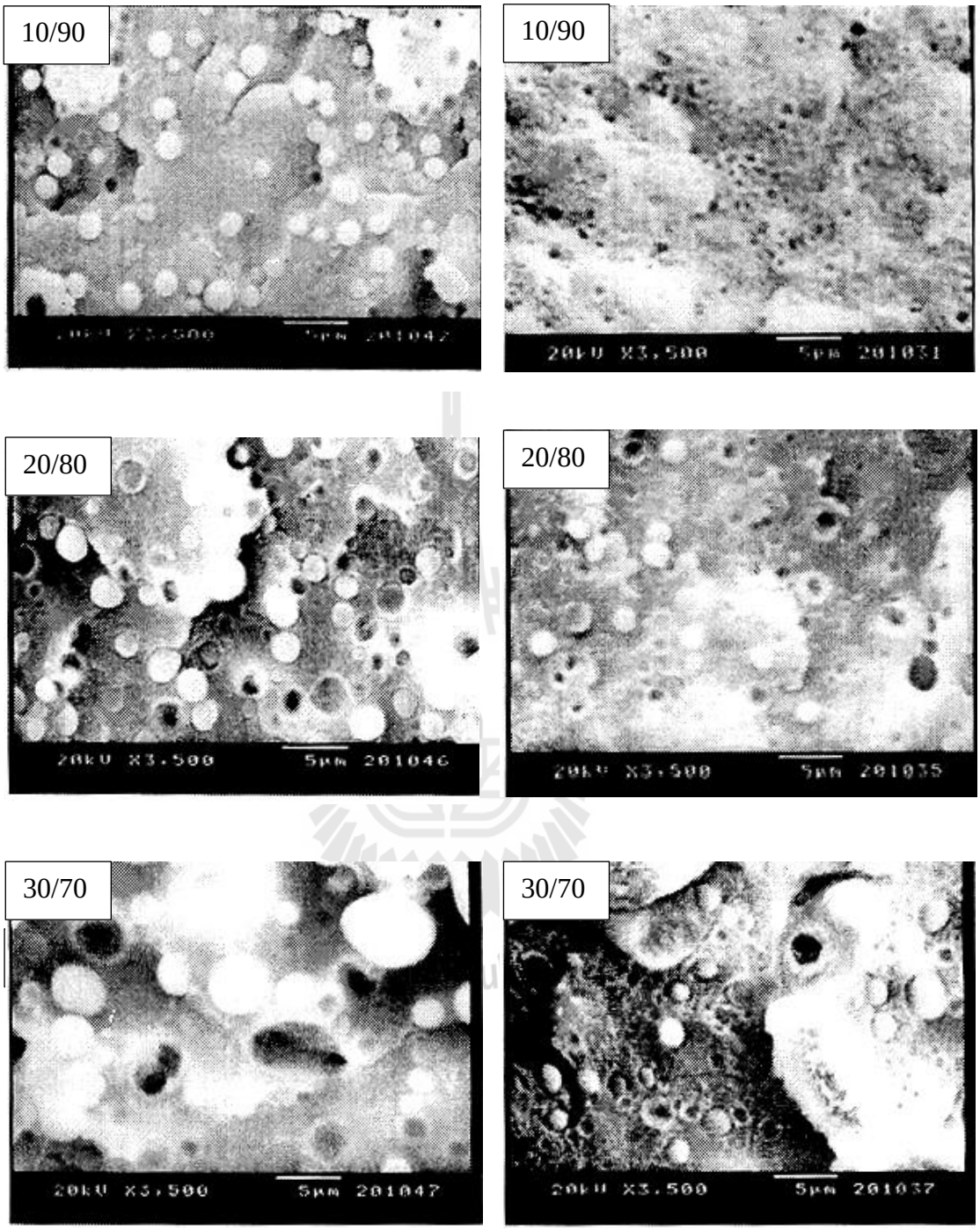

Figure 2.6 SEM micrograph of uncompatibilized and compatibilized PET/HDPE blend with 10 wt.% SEBS triblock copolymer (Iñiguez, Michel, Romero and Nuñez, 2000)

Laurienzo, Immirzi and Malinconico (2001) studied the effect of poly (ethylene terephthalate)-co-(ε-caprolactone) copolymer as a compatibilizer on phase morphology of PET/HDPE blends. PET, HDPE and compatibilizer content in blends was 30 wt%, 70 wt% and 10 wt%, respectively. SEM micrograph of uncompatibilized and compatibilized blend was shown in Figure 2.7. It was observed that the non-compatibilized blend exhibited a clear two-phase morphology with poor adhesion between the phases. The PET phase was dispersed into the HDPE matrix as continuous phase (Figure 2.7 (a1)) and spherical domains (Figure 2.7 (a2)). The suggested that this phase structure was characteristic of immiscible blends in which the content of the dispersed phase was high (typically more than 20 and less than 40%). For compatibilized blend, it was evident that the PET phase was no longer co-continuous but slightly spherical (Figure 2.7 (b1)). Few larger spherical domains (about 2 μm in size) coexisted with domains of sub-micronic dimensions (Figure 2.7 (b2)). It could be concluded that the addition of TCL copolymer both reduced the average size of most PET particles (less than 1 μm) and increased the interfacial area between PET and HDPE phase.

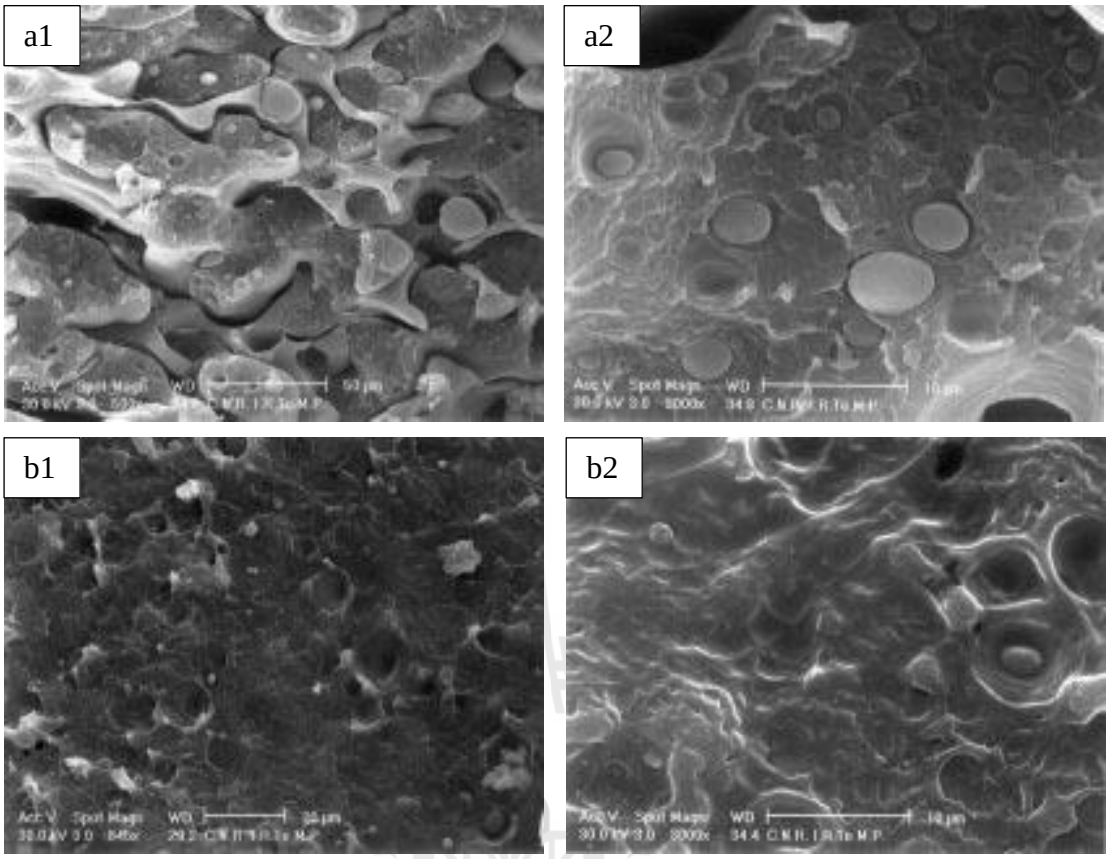

Figure 2.7 SEM micrograph of uncompatibilized and compatibilized PET/HDPE (30/70) blends (Laurienzo, Immirzi and Malinconico, 2001).

Torres, Robin and Boutevin (2001) studied the compatibilization of PET/HDPE (30/70 wt%) blend using grafted copolymers (HDPE-g-GMA). The compatibilizer content in PET/HDPE blend was 5 wt% of the blend. SEM micrograph of uncompatibilized and compatibilized blend was illustrated in Figure 2.8. They found that the PET/HDPE (30/70 wt %) blend without compatibilizer possessed a coarse morphology with larger-size domains, as compared to compatibilized blend. The large particle size, with no evidence of adhesion between matrix and dispersed phase confirmed the incompatibility of the two components. In

comparison, compatibilized blend with only 5 wt % compatibilizer led to a well disperse of PET particles inside the HDPE matrix, smaller size domains, and an improvement of interfacial adhesion.

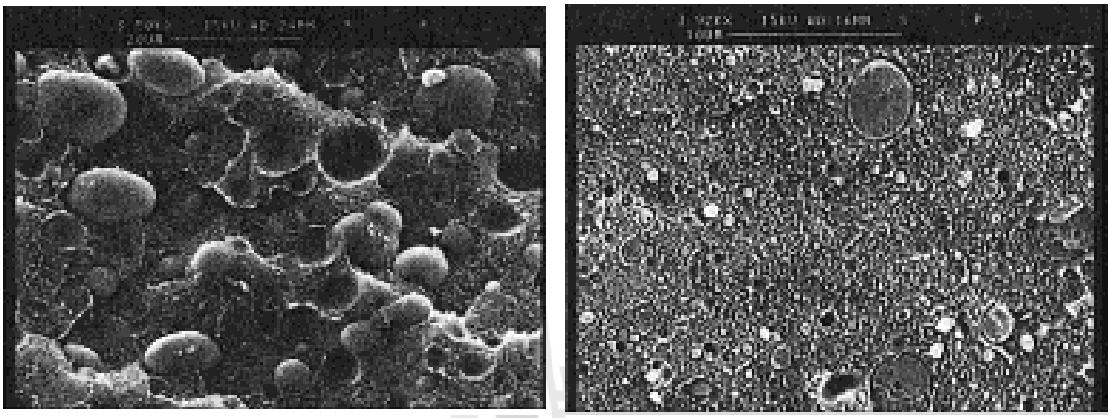

Uncompatibilized blend Compatibilized blend

Figure 2.8 SEM micrograph of uncompatibilized and compatibilized PET/HDPE (30/70) blends (Torres, Robin and Boutevin, 2001).

Fasce, Seltzer and Frontini (2005) observed phase morphology of uncompatibilized and compatiblized HDPE/PET blend. The HDPE/PET blend was prepared at 50 wt% HDPE and 50 wt.% PET. The ethylene/methacrylate acid copolymer (EMA) was used as a compatibilizer at a content of 1 wt.%. SEM micrographs of the blend were displayed in Figure 2.9. It was found that the uncompatibilized blend exhibited a typical of incompatible blend morphology, comprising discrete domains of the discontinuous component, and craters and voids left when particles attached only by weak mechanical adherence were pulled out during fracture. No evidence of interfacial interactions or adhesion between both components exists. The blend compatibilized with 1 wt.% EMA exhibited a finer

dispersion of the PET phase, i.e., more particles of smaller dimensions, though some lack of homogeneity was still observed. Despite of blend composition (50/50) no signs of co-continuous structure were displayed by SEM micrographs.

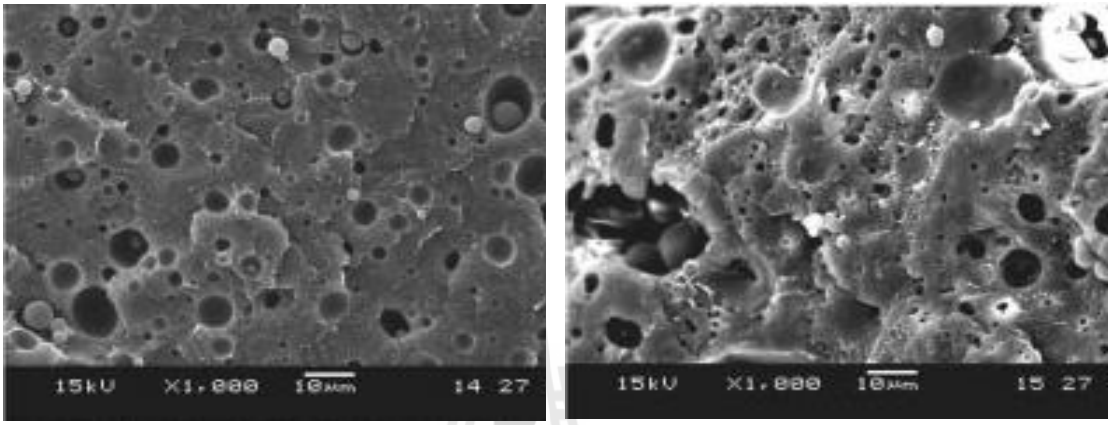

50/50 50/50/1wt.% EMA

Figure 2.9 SEM micrograph of uncompatibilized and compatibilized HDPE/PET blend with 1 wt.% EMA (Fasce, Seltzer and Frontini, 2005).

2.6.2 HDPE/PET blend

2.6.2.1 Effect of blend composition

Mbarek, Jaziri, Chalamet and Carrot (2010) investigated the influence of blend composition on phase morphology of HDPE/PET blends. The HDPE content in their blend system was 5, 10, 15 and 20 wt %. They showed that the morphologies HDPE/PET were typical of immiscible blends. The HDPE dispersed phases were generally coarse and irregular in size because of the immiscibility between PET and HDPE. In addition, the dispersed particle sizes almost linearly with the concentration of HDPE as shown in Figure 2.10. Also, they found some cavities

left on the fracture surface of sample. They suggested that was mainly related to the lack of adhesion between the HDPE droplets and the PET matrix.

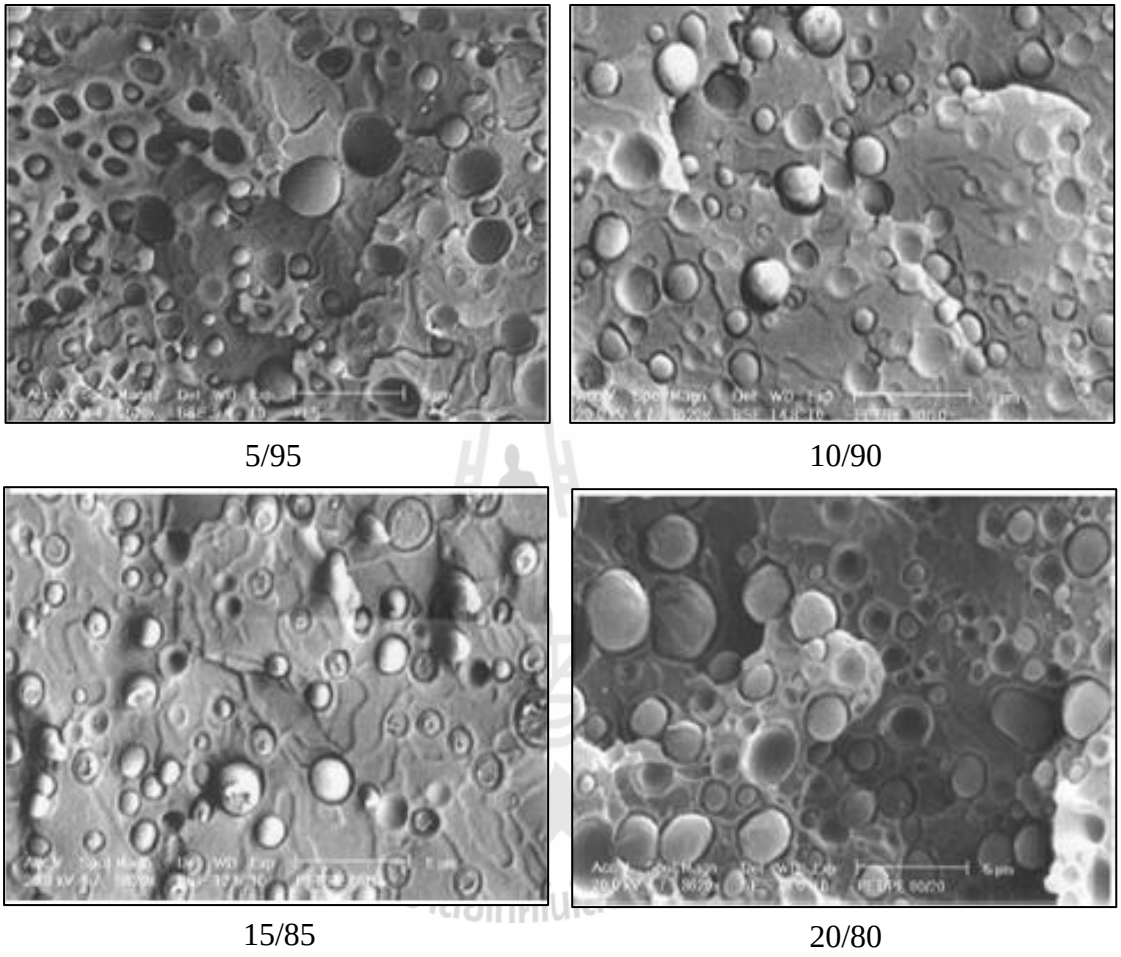

Figure 2.10 SEM micrographs of HDPE/PET blends at various compositions (Mbarek, Jaziri, Chalamet and Carrot, 2010).

2.6.2.2 Effect of compatibilization

Chareunkvun (2007) investigated morphologies of the uncompatibilized and compatibilized HDPE/PET (20/80) blends. The HDPE-g-MAH was used as a compatbilizer at a content of 2, 4, 6 and 8 phr. SEM micrographs of

uncompatibilized and compatibilized blends were illustrated in Figure 2.11. It was observed that the uncompatibilized HDPE/PET blend exhibited a coarse morphology with larger domain size in comparison to the compatibilized blends. Also, the larger particle size did not show an adhesion between the matrix and dispersed phase. This confirmed the incompatibility of the two components. For compatibilized blend, HDPE-g-MAH controlled morphology of uncompatibilized blends by preventing coalescence and reduction of the interfacial tension between HDPE and PET phase. In addition, the dispersed phase sizes depend on the compatibilizer content. The improvement in the interfacial adhesion and reduction in the size of the dispersed phase with increasing the compatibilizer content were also observed.

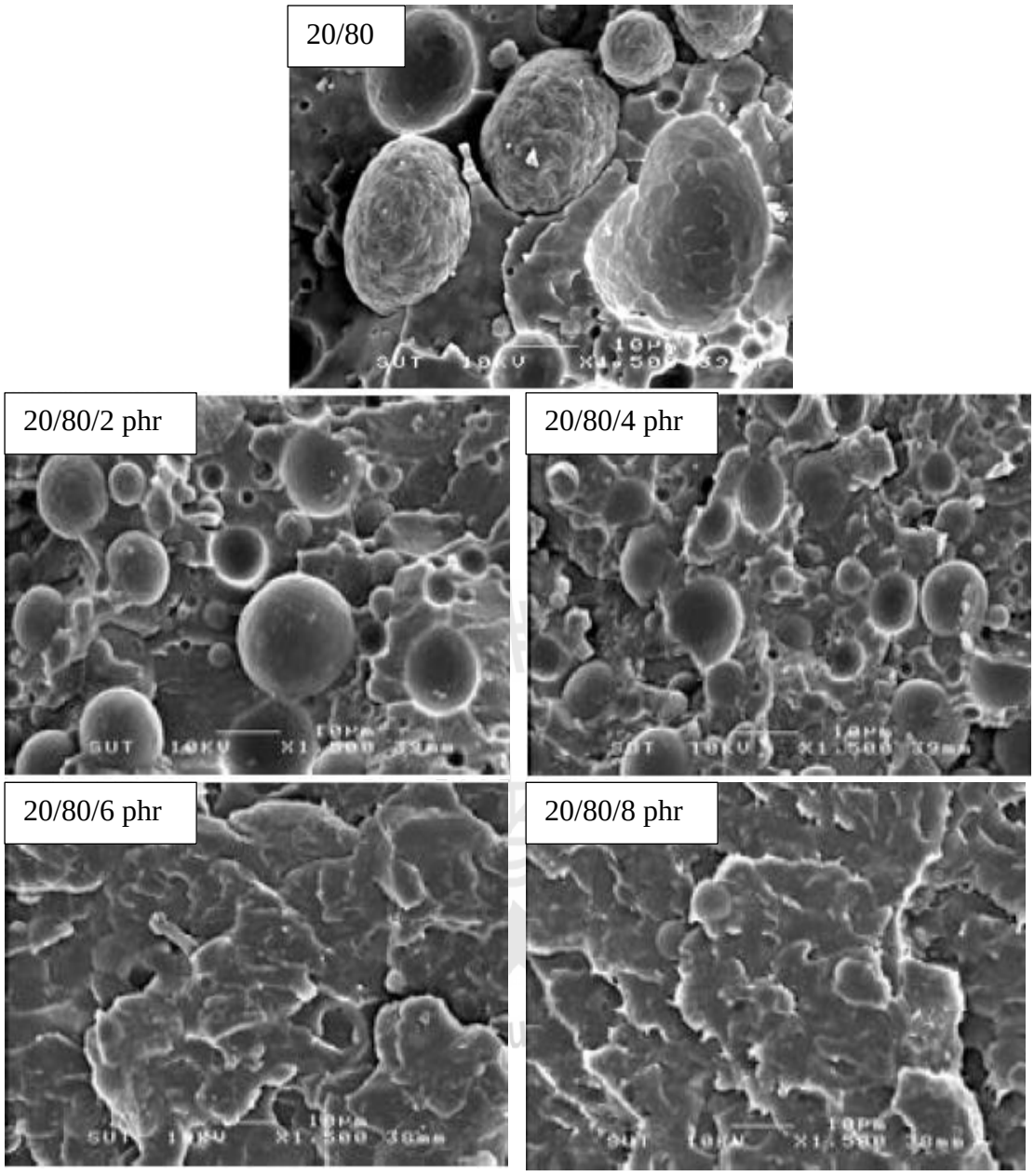

Figure 2.11 SEM micrograph of uncompatibilized and compatibilized HDPE/PET blend with various contents of HDPE-g-MAH (Chareunkvun, 2007).

Kim, Park, Kim, and Suh (2000) studied the influence of blend composition on phase morphology of HDPE/PET blend. They studied at HDPE/PET blend composition of 10/90, 30/70, 50/50 and 90/10 wt.%. It was observed that when

the weight ratios of the HDPE/PET blends were 90/10 and 50/50, the dispersed phase was PET and the matrix was HDPE (Figure 2.12 (a, b)). The reverse was true for the HDPE/PET blends prepared in the weight ratio of 30/70 and 10/90 (Fig. 2.12 (c, d)). It was observed that the particles size of minor phase increased as increasing its content. Also, SEM micrograph exhibited holes on the matrix formed by the pullout of particles indicated that there was little adhesion between the continuous and the dispersed phases.

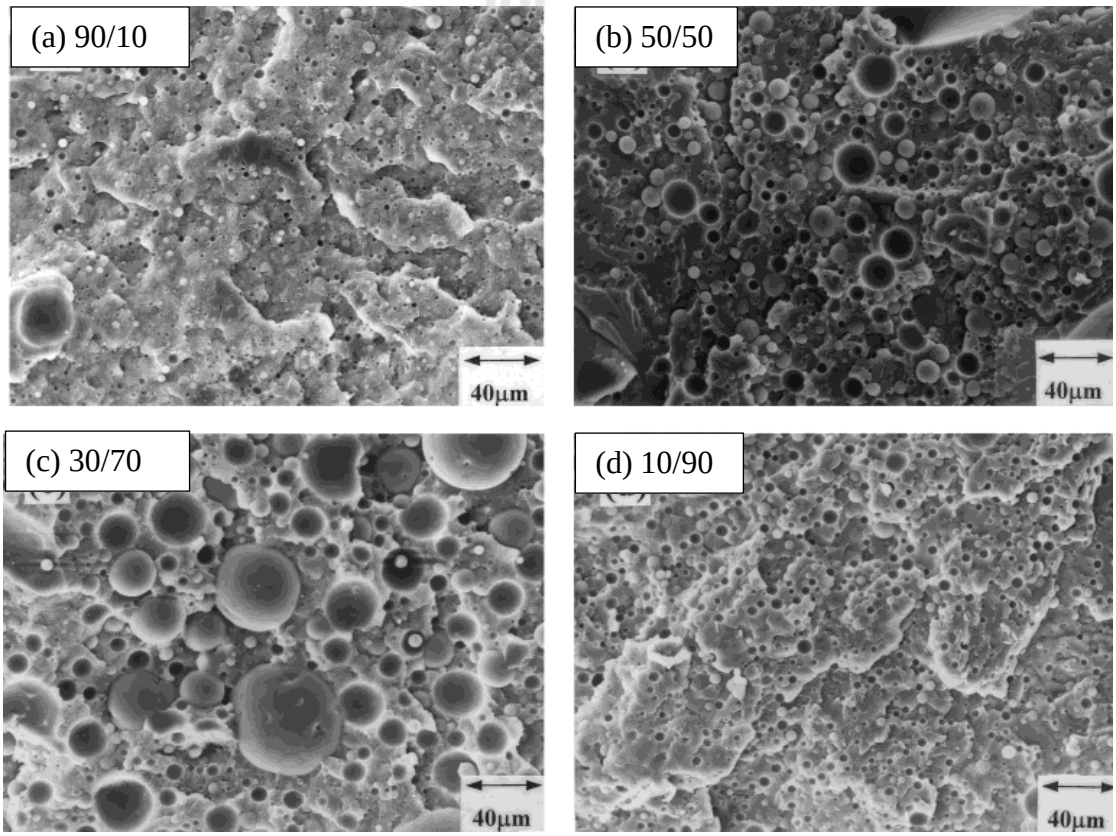

Figure 2.12 SEM micrographs of HDPE/PET blends at various compositions (Kim, Park, Kim, and Suh, 2000).

2.7 Factor affecting phase morphology of PBS blend and PBT blend.

2.7.1 PBS blend

2.7.1.1 Effect of blend composition

Tsi, Tsen, Shu, Chuang and Chen (2009) investigated the effect of blend composition on phase morphology of poly (butylene succinate) (PBS) and propylene-co-ethylene copolymer resin (PER) blends. The composition of PBS/PER blend ranged from 90/10 to 10/90 (wt.%). SEM micrographs of the blend were illustrated in Figure 2.13. They found that most of the PBS/PER blends consisted of two distinct phases (a sea-island morphology) comprising a dispersed phase (island-phase) and a continuous phase (sea-phase). The PER component in the sea island morphology of PBS-rich blends such as PBS/PER (90/10) and PBS/PER (80/20) was dispersed as spherical particles of diameters 3–10 μm. PBS/PER (70/30) displays an apparently singular phase (close to a homogeneous morphology). PBS/PER (60/40) displayed an irregular fiber shape. When the PER content in the blends exceeds 50 wt%, the sea-island morphology of the PBS-rich blends was reversed to form a sea-island morphology of PER-rich blends. Therefore, PBS/PER (50/50) displayed a mixed morphology including both sea-island and fiber-shape regions. When the PBS/PER blends had PER contents between 60 and 90 wt%, the PBS was in the form of a spherical dispersed phase of particle size in the region of 0.8–75 μm and the PER forms a continuous phase. It was also found that the size of spherical particles (island-phase size) in the sea-island morphologies increased as the concentration of the island-phase was increased. Noticeably, it could be seen that the PER island-phase in

the PBS-rich blends consisted of larger spherical particles than the PBS island-phase in the PER-rich blends at the same concentration of the island phase. Thus, the particle sizes in PBS/PER (90/10) and PBS/PER (10/90) were 3–4 μm and 0.8–3 μm, respectively. This might be due to the different diffusion rates of the chains in the process of nucleation and growth. Because PER was a thermoplastic elastomer and has high entropy, the PER macromolecular chains in the PBS-rich blends assemble at a high diffusion rate, resulting in the formation of large spherical particles.

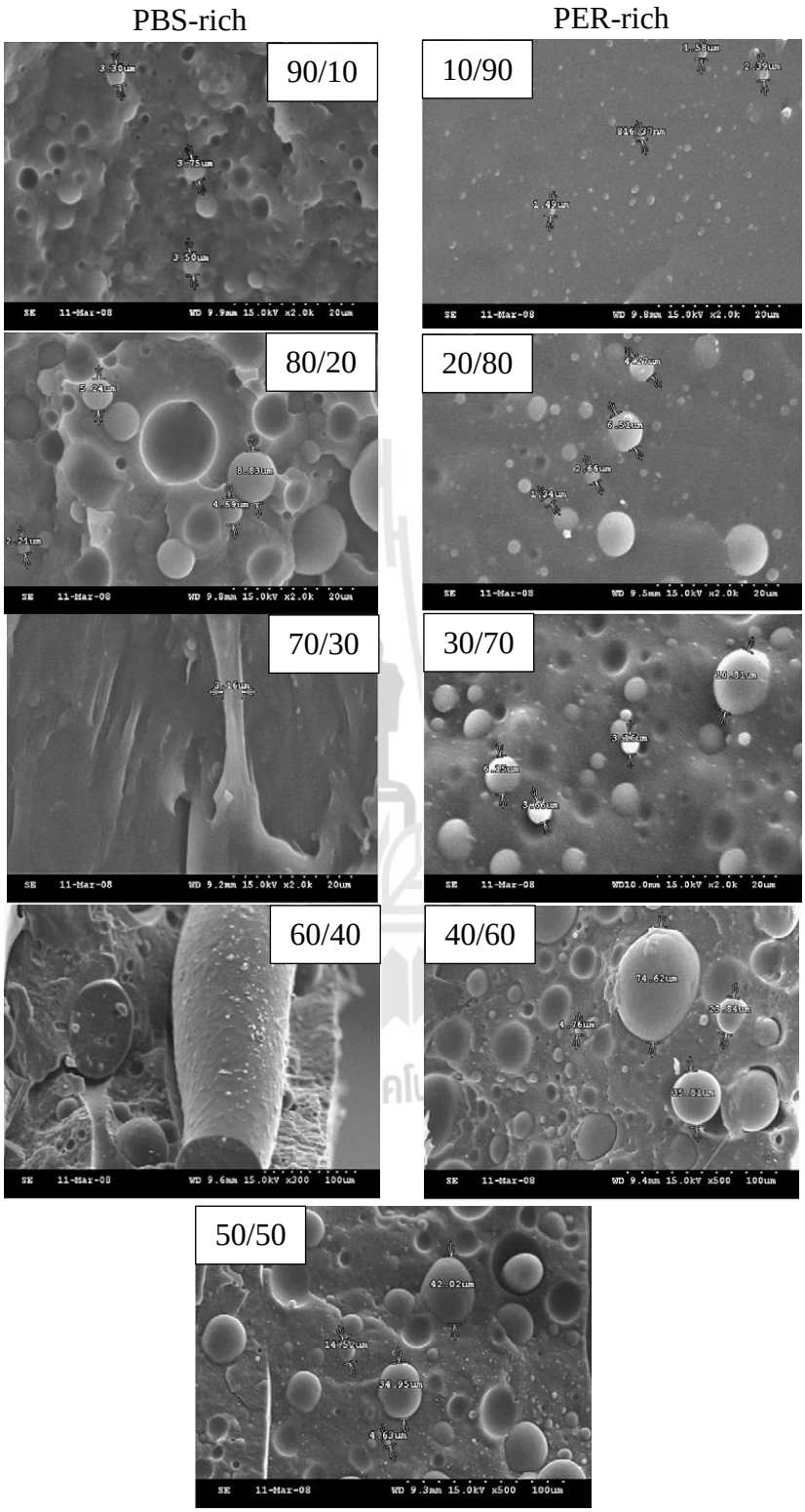

Figure 2.13 SEM micrographs of PBS/PER blend at various blend compositions (Tsi, Tsen, Shu, Chuang and Chen, 2009).

2.7.2 PBT blend

2.7.2.1 Effect of blend composition

Kang *et al*. (1999) studied the effect of blend composition on phase morphology of LLDPE/PBT blend. The composition of LLDPE/PBT was 20/80 40/60, 60/40 and 80/20wt.%. They found that the morphology of the blends, prepared by melt mixing, changed as a function of composition. In Figure 2.14, the LLDPE particles below 40 wt % of LLDPE were dispersed in the PBT matrix. However, at 60 wt % of LLDPE, a co-continuous morphology was obtained. When the concentration of LLDPE was above 50 wt %, phase inversion took place. The blend having 80/20 composition exhibited much finer domain morphology than that of 20/80 composition. They suggested that when the components have different melt viscosity, the morphology of the blends depends on whether the minor component has a lower viscosity or a higher viscosity. If the minor component has a lower viscosity than that of the major one, the minor component will be finely dispersed.

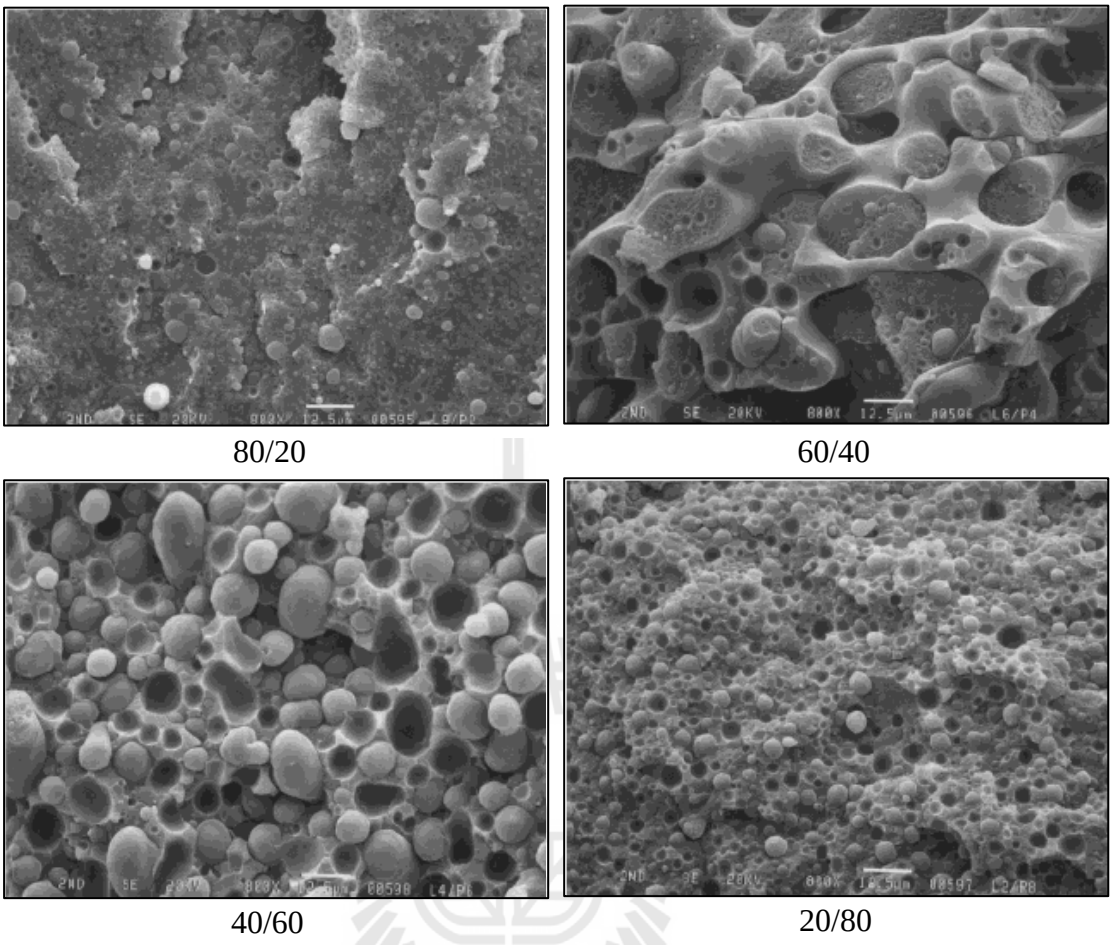

Figure 2.14 SEM micrographs of LLDPE/PBT blends at various compositions (Kang *et al*., 1999).

2.7.2.2 Effect of viscosity ratio

Kang *et al*. (1999) studied the effect of viscosity ratio on phase morphology of the blend between LLDPE and PBT. The PBT/LLDPE and LLDPE/PBT blend was prepared at composition of 20/80 wt.%. It was observed that PBT was a minor phase for the system of PBT/LLDPE blend. In turn, LLDPE was a minor phase in the system of LLDPE/PBT blend. In comparison, the particles size of PBT was finer than that of LLDPE. This was due to the fact that PBT was less viscous

than LLDPE. Therefore, the PBT/LLDPE blend system had a lower viscosity ratio (viscosity ratio = η_d/η_m) comparing to the LLDPE/PBT blend system. The lower viscosity ratio of the blend led to a smaller size of dispersed particles. Figure 2.15 showed SEM micrograph of PBT/LLDPE (20/80 wt.%) and LLDPE/PBT (20/80 wt.%).

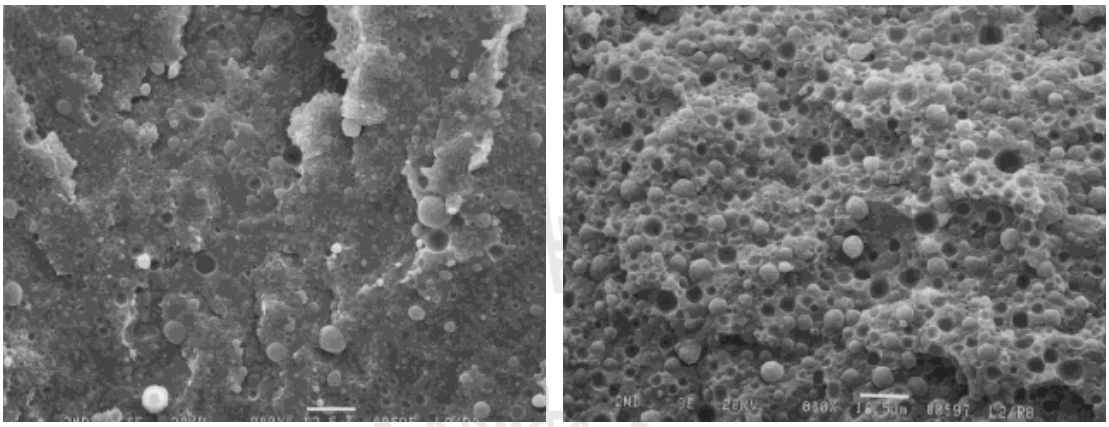

PBT/LLDPE (20/80 wt.%) LLDPE/PBT (20/80 wt.%)

Figure 2.15 SEM micrographs of PBT/LLDPE (20/80 wt.%) and LLDPE/PBT (20/80 wt.%) (Kang *et al*., 1999).

CHAPTER III

EXPERIMENTAL

3.1 Materials

The materials used in this study were high density polyethylene (HDPE) and poly (butylene succinate) (PBS). Beside those, high density polyethylene grafted with 0.9 wt.% maleic anhydride (HDPE-g-MAH) and ethylene-propylene rubber containing 43 wt.% ethylene and 53 wt.% propylene grafted with 1.14 wt.% maleic anhydride (EPR-g-MAH) were used as compatibilizers. The characteristic and some physical properties of those polymers were listed in Table 3.1.

Table 3.1 Characteristics and some physical properties of HDPE, PBS, HDPE-g-MAH and EPR-g-MAH.

Properties	Materials			
	HDPE	PBS	HDPE-g-MAH	EPR-g-MAH
Manufacturer	SCG Chemical	Mitsubishi Chemical	Du Pont™	Exxon Mobil Chemical
Trade name	EL-Lene™	GS Pla	Fusabond® MB100D	Exxelor 1803
Melting temperature (°C)	130	110	136	-
Glass transition temperature (°C)	-	-	-	-57
Density (g/cm^3)	0.96	1.26	0.96	0.86

3.2 Preparation of blend between HDPE and PBS

3.2.1 PBS/HDPE blend

3.2.1.1 Mixing process

The pellets of HDPE and PBS were initially dried in an oven at 60ºC for 12 h to remove moisture before blending preparation. The PBS/HDPE blend was prepared at PBS content of 20 wt.%, 30 wt.%, 40 wt.% and 50 wt.%. Firstly, HDPE and PBS pellets were pre-mixed in a plastic bag. Then, the melt mixing process was operated in an internal mixer at a temperature of 170°C under a rotor speed of 70 rpm and a mixing time of 10 min. The blends of PBS/HDPE were cooled down to room temperature before grounding by a grinding machine. The grinded pellet was stored in a zipper bag and dried at 60°C for 12 h to avoid moisture infiltration, before further molded by an injection machine.

3.2.1.2 Molding process

The tensile (dumbbell-shape), flexural and impact specimens of PBS/HDPE blend were prepared using an injection molding machine (Chuan Lih Fa, CLF 80T). The injection molding process was carried out with a melting temperature of 180°C, a screw speed of 130 rpm, an injection speed of 47 mm/s, a holding pressure of 617 kg/cm^3, a mold temperature of 30°C and a cooling time of 20 s.

3.2.2 HDPE/PBS blend

3.2.2.1 Mixing process

The pellets of PBS and HDPE were initially dried in an oven at 60ºC for 12 h to remove moisture before blending preparation. The HDPE/PBS blend was prepared at HDPE content of 20 wt.%, 30 wt.%, 40 wt.% and 50 wt.%. Firstly, PBS and HDPE pellets were pre-mixed in a plastic bag. Then, the melt mixing

process was operated in an internal mixer at a temperature of 170°C under a rotor speed of 70 rpm and a mixing time of 10 min. The blends of HDPE/PBS were cooled down to room temperature before grounding by a grinding machine. The grinded pellet was stored in a zipper bag and dried at 60°C for 12 h to avoid moisture infiltration, before further molded by an injection machine.

3.2.2.2 Molding process

The tensile (dumbbell-shape), flexural and impact specimens of HDPE/PBS blend were prepared using an injection molding machine (Chuan Lih Fa, CLF 80T). The injection molding process was carried out with a melting temperature of 180°C, a screw speed of 130 rpm, an injection speed of 47 mm/s, a holding pressure of 617 kg/cm^3, a mold temperature of 30°C and a cooling time of 20 s.

3.3 Preparation of compatibilized blend between HDPE and PBS

3.3.1 PBS/HDPE blend

3.3.1.1 Mixing process

The pellets of HDPE, PBS, HDPE-g-MAH and EPR-g-MAH were initially dried in an oven at 60ºC for 12 h to remove moisture before blending preparation. The compatibilized PBS/HDPE blend was prepared at PBS content of 30 wt%. The HDPE-g-MAH or EPR-g-MAH content was 2, 4, 6, and 8 phr. Firstly, HDPE, PBS, and HDPE-g-MAH or EPR-g-MAH pellets were pre-mixed in a plastic bag. Then, the melt mixing process was operated in an internal mixer at a temperature of 170°C under a rotor speed of 70 rpm and a mixing time of 10 min. The blends of PBS/HDPE were cooled down to room temperature before grounding by a grinding

machine. The grinded pellet was stored in a zipper bag and dried at 60°C for 12 h to avoid moisture infiltration, before further molded by an injection machine.

3.3.1.2 Molding process

The tensile (dumbbell-shape), flexural and impact specimens of compatibilized PBS/HDPE blend were prepared using an injection molding machine (Chuan Lih Fa, CLF 80T). The injection molding process was carried out with a melting temperature of 180°C, a screw speed of 130 rpm, an injection speed of 47 mm/s, a holding pressure of 617 kg/cm^3, a mold temperature of 30°C and a cooling time of 20 s.

3.3.2 HDPE/PBS blend

3.3.2.1 Mixing process

The pellets of PBS, HDPE, HDPE-g-MAH and EPR-g-MAH were initially dried in an oven at 60ºC for 12 h to remove moisture before blending preparation. The compatibilized HDPE/PBS blend was prepared at HDPE content of 30 wt%. The HDPE-g-MAH or EPR-g-MAH content was 2, 4, 6, and 8 phr. Firstly, PBS, HDPE and HDPE-g-MAH or EPR-g-MAH pellets were pre-mixed in a plastic bag. Then, the melt mixing process was operated in an internal mixer at a temperature of 170°C under a rotor speed of 70 rpm and a mixing time of 10 min. The blends of PBS/HDPE were cooled down to room temperature before grounding by a grinding machine. The grinded pellet was stored in a zipper bag and dried at 60°C for 12 h to avoid moisture infiltration, before further molded by an injection machine.

3.3.2.2 Molding process

The tensile (dumbbell-shape), flexural and impact specimens of compatibilized HDPE/PBS blend were prepared using an injection molding machine

(Chuan Lih Fa, CLF 80T). The injection molding process was carried out with a melting temperature of 180°C, a screw speed of 130 rpm, an injection speed of 47 mm/s, a holding pressure of 617 kg/cm^3, a mold temperature of 30°C and a cooling time of 20 s.

3.4 Characterization of blend between HDPE and PBS

3.4.1 Flow properties

According to ASTM D1238, a melt flow index (MFI) of neat HDPE, neat PBS and the blends was determined by a melt flow indexer (Kayeness, D4004HV) at 180°C with a standard weight of 2.16 kg.

The apparent shear viscosity of neat HDPE, neat PBS and the blends was measured using a capillary rheometer (Rosand Malvern Instruments, Rh2200) at 180°C and a shear rate range of 10–7,000 s^{-1}. The viscosity ratio of the blend was also calculated at shear rate range between 3,000 and 4,000 s^{-1} using equation (3.1).

$$\text{Viscosity ratio} = \frac{\eta_d}{\eta_m} \tag{3.1}$$

where η_d is viscosity of a dispersed phase and η_m is viscosity of a matrix phase.

3.4.2 Mechanical properties

Tensile properties of neat HDPE, neat PBS and the blends were determined in accordance with ASTM D638 (Type I specimens) using a universal testing machine equipped with a load cell of 5 kN (Instron, 5565). The specimen was tested at a crosshead speed of 10 mm/min and a gauge length of 50 mm. The dimension of test specimens was 12.9 mm in width, 3.3 mm in thickness, and 165 mm

in length. At least five specimens were tested for neat HDPE, neat PBS and the blends.

Flexural properties of neat HDPE, neat PBS and the blends were tested according to ASTM D790 (procedure B) using a universal testing machine equipped with a load cell of 5 kN (Instron, 5565). The testing was performed at a crosshead speed of 14 mm/min under a fixed span length of 53 mm. The dimension of test specimens was 127 mm in length, 13 mm in width, and 3.3 mm in depth.

Unnotched Izod impact strength of neat HDPE, neat PBS and the blends was evaluated on an impact tester (Atlas, BPI), equipped with 5.4 J hammer following ASTM D256. At least five specimens were tested.

3.4.3 Thermal property

Thermal degradation of neat HDPE, neat PBS and the blends was investigated using a thermogravimetric analyzer (TA Instrument, SDT 2960). The sample was heated from 30°C to 800°C under a nitrogen atmosphere, with a heating rate of 20°C/min.

3.4.4 Melting and crystallizing behavior

Melting temperature (T_m), crystallization temperature (T_c) of HDPE and PBS phase were determined using a differential scanning calorimeter (DSC) (Perkin Elmer, UNIX DSC7). Under a nitrogen atmosphere, the sample was first heated to 200°C, held at 200°C for 5 min, cooled down to 30°C, and then re-heated to 200°C. The heating and cooling rate was 5°C/min. The melting temperature and crystallization temperature of HDPE and PBS phase were obtained according to ASTM D3417.

3.4.5 Fracture surface morphology

3.4.5.1 Preparation of SEM sample

The middle part of flexural specimen of neat HDPE, neat PBS and the blends were cut using a cutter. Then, the parts were soaked in liquid nitrogen prior to fracture along the flow direction using a wrench, following diagram in Figure 3.1. After fracture, PBS phase of PBS/HDPE blend was removed by chloroform etching at ambient temperature (Sung, Hyun, Kwon and Choi, 2002), and HDPE phase of HDPE/PBS blend was etched using xylene at 50ºC (Laokijcharoen and Coran, 1998).

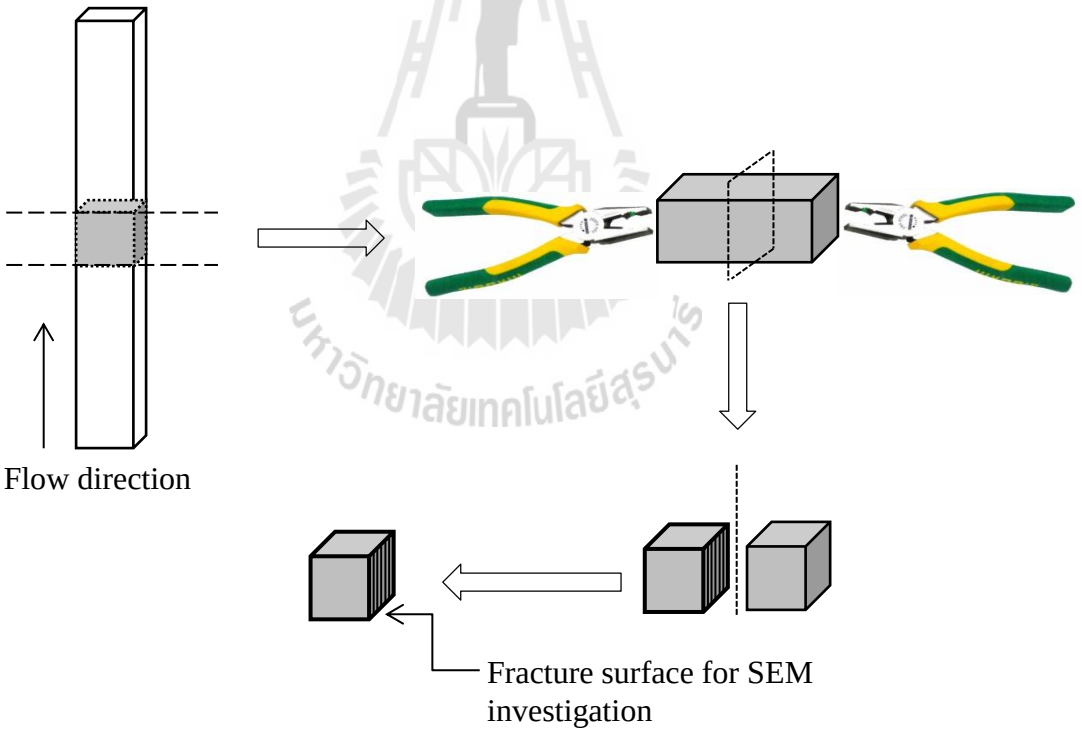

Figure 3.1 A diagram for SEM sample preparation

3.4.5.2 SEM investigation

The SEM samples of neat HDPE, neat PBS and the blends were coated with gold using an ion sputtering device for 9 min at a current of 10 mA to avoid charging under an electron beam and make it electrically conductive. The fracture surface morphology of neat HDPE, neat PBS and the blends was investigated using SEM (JEOL, JSM 6010LV) operated at an accelerating voltage of 15 kV.

3.4.6 Water absorption

The samples were immersed in distilled water at room temperature. The weight gain was monitored until reaching the equilibrium. Five samples were tested in neat HDPE, neat PBS and their blends. The weight gain during immersion test was calculated using an equation (3.2), as shown below :

$$\text{Weight gain, } \% = \frac{(W_i - W_d)}{W_d} \times 100 \qquad (3.2)$$

where W_i is sample weight after immersion and W_d is sample weight after drying in an oven.

3.4.7 Biodegradability by natural soil burial test

The biodegradability of the neat HDPE, neat PBS and their blends was simulated via natural soil burial. The dimensions of test specimens were 63.5 mm in length, 13 mm in width, and 3.3 mm in depth. The specimens were horizontally embedded in natural soil in the depth of 10 cm, as shown in Figure 3.2. Then, the buried area was daily watered in the morning and the evening.

Figure 3.2 The arrangement of samples in soil before burial test

The biodegradability of the samples was measured during natural soil burial for 4 months (Kim, Yang and Kim, 2005). After duration of soil burial test of 30, 45, 60, 75, 100 and 120 days, the buried specimens were dug out, cleaned and dried in an oven. Then, the samples were weight using an electronic precision balance. The percentage of weight loss was calculated using equation (3.3). In addition, the percentage of weight loss was averaged from at least 5 test specimens.

$$\text{Weight loss}, \% = \frac{(W_i - W_b)}{W_i} \times 100 \tag{3.3}$$

where W_i is an initial sample weight and W_b is a sample weight after dried.

CHAPTER IV

RESULTS AND DISCUSSION

This chapter is divided into two main topics. The first topic reveals results from the blends which HDPE is a matrix phase called PBS/HDPE blend. The second topic focuses on the blend that PBS is a matrix phase called HDPE/PBS blend. Additionally, the effect of blend composition and compatibilization on physical properties of those blends were discussed.

4.1 PBS/HDPE blend

4.1.1 Effect of PBS content on physical properties

4.1.1.1 Flow properties

The dependence of apparent shear viscosity on apparent shear rate of neat HDPE, neat PBS and PBS/HDPE blends are presented in Figure 4.1. The apparent shear viscosity of the neat HDPE was higher than that of neat PBS. Neat HDPE and neat PBS both exhibited shear thinning behavior of which shear viscosity decreased as shear rate increased. At high shear rate, more polymer chains aligned in the shear direction resulting in better molecular flow ability of polymer molecules leading to the lower of viscosity (Ahmad, Wahit, Kadir and Dahlan, 2012). This shear thinning behavior was also observed from PBS/HDPE blend, as shown in Figure 4.1. In addition, the apparent shear viscosity of the blend decreased with increasing PBS content. Within the shear rate range of injection molding process at 190ºC, shear viscosities of HDPE and PBS was 46-59 Pa.s and 9-11 Pa.s, respectively. The

viscosity ratio of the blend calculated through equation 3.1 was in a range of 0.19 to 0.20.

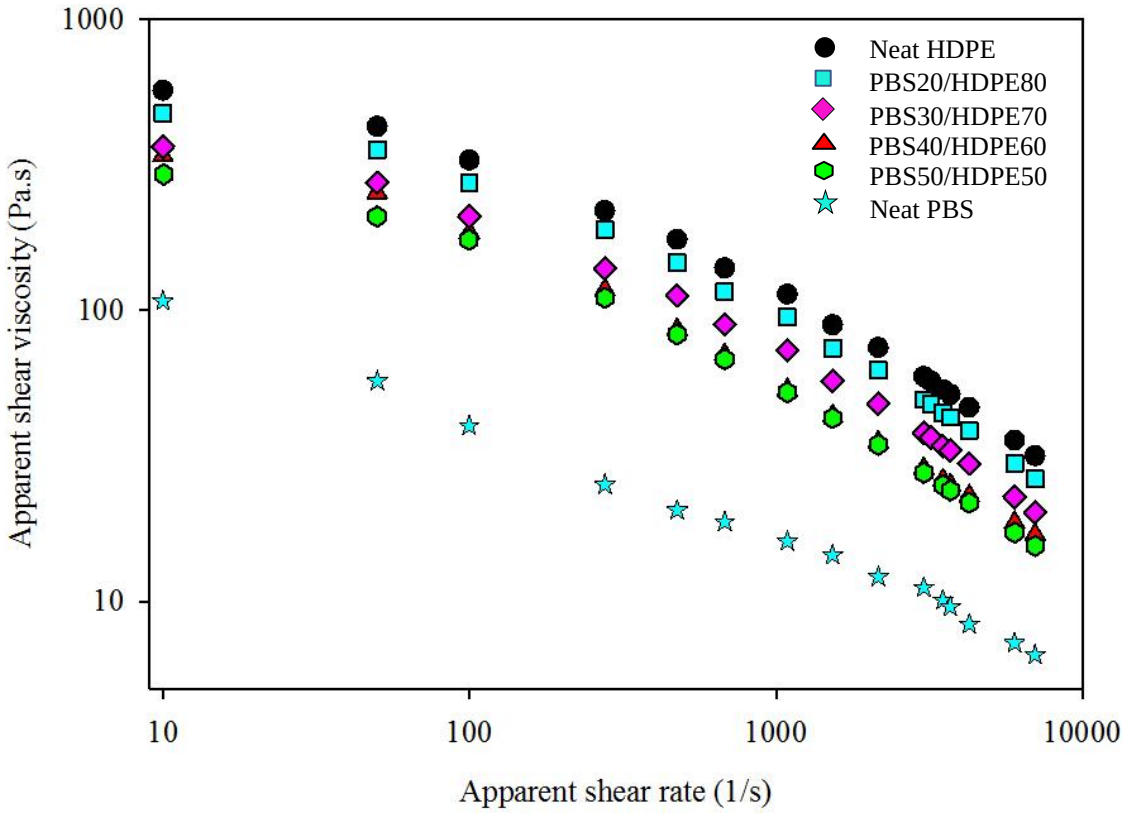

Figure 4.1 Plot of apparent shear viscosity as a function of apparent shear rate of neat HDPE, neat PBS and PBS/HDPE blend at various contents of PBS.

Melt flow index (MFI) of neat HDPE, neat PBS and PBS/HDPE blend at various contents of PBS is shown in Table 4.1. It illustrates that MFI of neat PBS was higher than that of neat HDPE. The MFI of the PBS/HDPE blends increased with increasing PBS content.

Table 4.1 Melt flow index (MFI) at 180°C with a standard weight of 2.16 kg of neat HDPE, neat PBS and PBS/HDPE blend.

Sample	MFI (g/10min)
Neat HDPE	11.6
PBS20/HDPE80	12.0
PBS30/HDPE70	13.8
PBS40/HDPE60	15.3
PBS50/HDPE50	18.5
Neat PBS	26.1

4.1.1.2 Failure behavior and phase morphology

Engineering stress-strain curves and SEM micrographs of neat HDPE and neat PBS are concurrently presented in Figure 4.2. Noticeably, the tensile specimen of neat HDPE did not break under an instrumentation limit of 800% elongation. The tensile curve of neat HDPE exhibited yielding and cold drawing region. Additionally, the SEM micrograph of neat HDPE revealed a rough and blocky structure, as observed from its fractured surface morphology illustrated in Figure 4.2(a), in which it is typical for ductile fracture. The freeze fractured surface of neat HDPE corresponded well with ductile behavior of neat HDPE as shown in the stress-strain curve (Brough, Haward, and Healey, 2004).

Stress-strain curve of neat PBS is illustrated in Figure 4.2. It shows yielding and cold drawing region before it ruptured at elongation of 313%. The SEM micrograph of neat PBS, shown in Figure 4.2(b), contained a rough and blocky structure of fractured surface. This fractured surface morphology confirmed that PBS failed in a ductile manner. However, neat PBS ruptured at a lower strain than neat

HDPE. This might be due to PBS fractured surface contained a larger blocky and the fractured surface of neat PBS was smoother than neat HDPE.

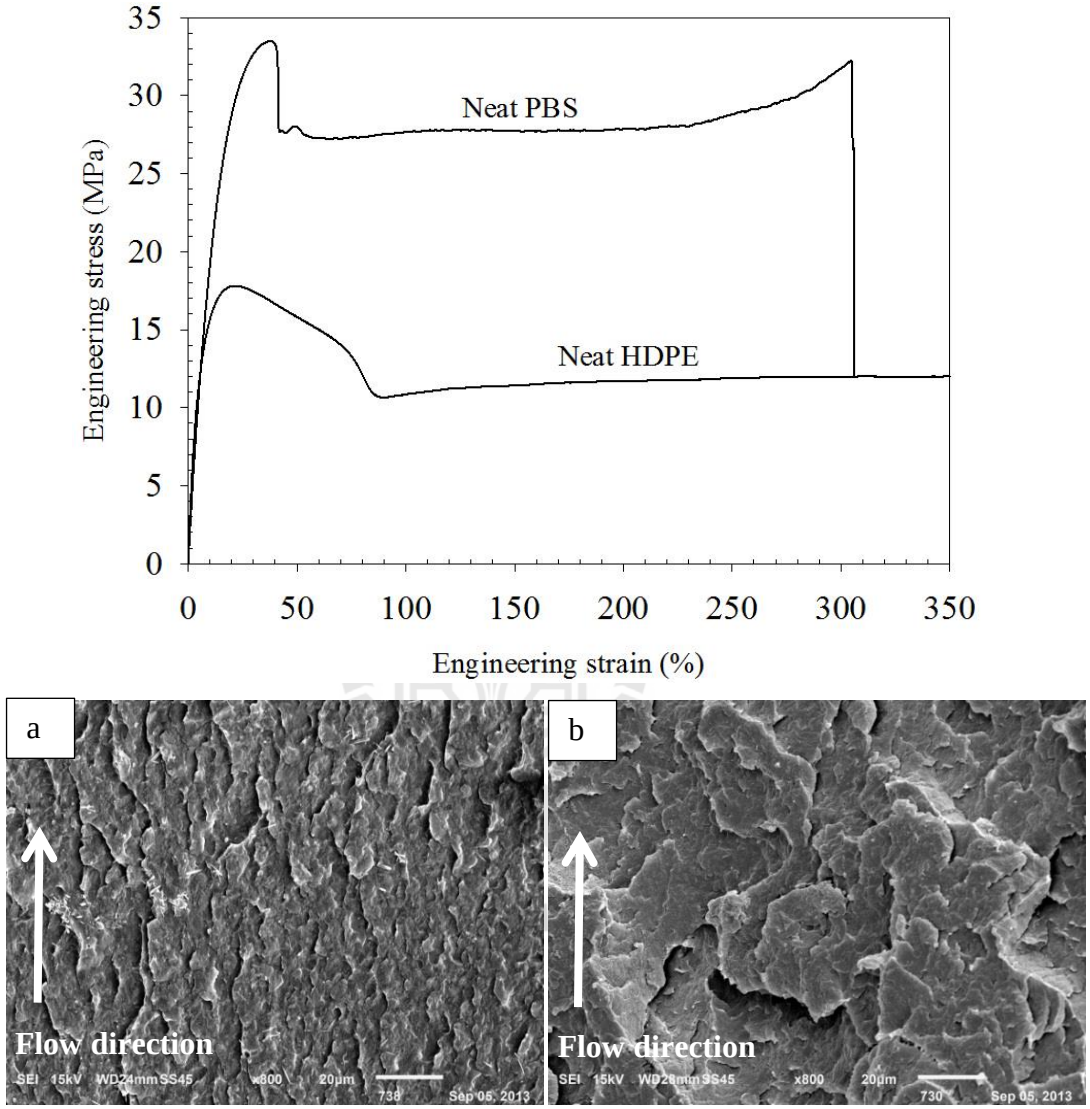

Figure 4.2 Tensile stress-strain curves and SEM micrographs of neat HDPE (a) and neat PBS (b).

PBS/HDPE blend at 20 wt.% PBS still broke in a ductile manner of which tensile curve exhibited yielding and then cold drawing before ruptured at elongation of 200%, as observed in stress-strain curve in Figure 4.3. The ductility of the blend was much lower than that of neat HDPE. The fractured surface morphology of PBS20/HDPE80 blend is illustrated in Figure 4.3(a). It revealed that the addition of 20 wt.% PBS into HDPE matrix gave rise to a heterogeneous phase morphology with spherical PBS dispersed in HDPE matrix. This heterogeneous phase morphology was a consequence of high interfacial tension between PBS and HDPE phases. In addition, smoother surface of HDPE matrix was also observed from the freeze fractured surface. This was an indication of reduction in ductility of HDPE matrix. However, according to the low content of PBS, therefore the size of PBS domain was fine. It was in a range of <1 μm to 4 μm.

With increasing PBS content to 30 wt.%, the stress-strain curve of the blend is shown in Figure 4.3. It reveals that the blend was more brittle than the blend at 20 wt% PBS. The PBS30/HDPE70 blend failed and fractured in a brittle manner at even lower elongation of 24%. The fractured surface morphology of PBS30/HDPE70 blend is demonstrated in Figure 4.3. It revealed a larger size of PBS dispersed phase, including spherical, elongated and worm-like. Approximately, the dispersed PBS size was in a range of <1 μm to 9 μm. The increase in size of dispersed PBS was strongly affected by the content of PBS. In addition, increasing content of PBS resulted in an increase of number of PBS particles, leading to more particle-particle collision. Therefore, increasing content of PBS resulted in an increase in coalescence of particles Furthermore, under injection shear stress, these collided particles underwent deformation in the direction of flow field as a result they were in

worm-like shape (Harrats, Thomas and Groeninckx, 2006; Wallheinke, Pötschke, Macosko and Stutz, 1999). Also, it might be due to a high interfacial tension between PBS and HDPE, this led to the existence of the ellipsoid drop.

PBS/HDPE blend at 40 wt.% PBS failed and subsequently fractured at a strain of 40%, as shown in Figure 4.3. Phase morphology of the blend at 40 wt.% PBS is shown in Figure 4.3(c). It revealed that adding 40 wt.% PBS into HDPE matrix led to a creation of fibrillation of phase domain. The diameter fibril was in a range of 4 μm to 9 μm. It was also observed a partial of co-continuous phase morphology at this blend composition. The fibrillation took place by PBS particles were stretched in the direction of the melt flow and were accompanied by their coalescence, leading to a producing of continuous fibrils (Lafitte, Espuche and Gérard, 2011). In addition, it was previously reported that elongational flow during the filling stage of injection molding process was also effective in transforming droplets into fibrous domains (Li, 2000). Moreover, the fiber formation was favored for the blends containing higher concentrations of the dispersed phase (Harrats, 2009; Chapleau and Favis, 1995.)

With adding 50 wt.% PBS, The blend failed and fractured in a brittle manner at 29% strain, as shown in stress-strain curve in Figure 4.3. Phase morphology of PBS50/HDPE50 blend, as shown in Figure 4.3(d), was in co-continuous type as expected. In conventional terms, co-continuous phase morphology could be generated at the same volume of each component in binary blend (Harrats, Thomas and Groeninckx, 2006). It had been previously found that phase morphology of PBT/PP blend at 50 wt.% PBT was also in a co-continuous type (Tsai and Chang, 1996).

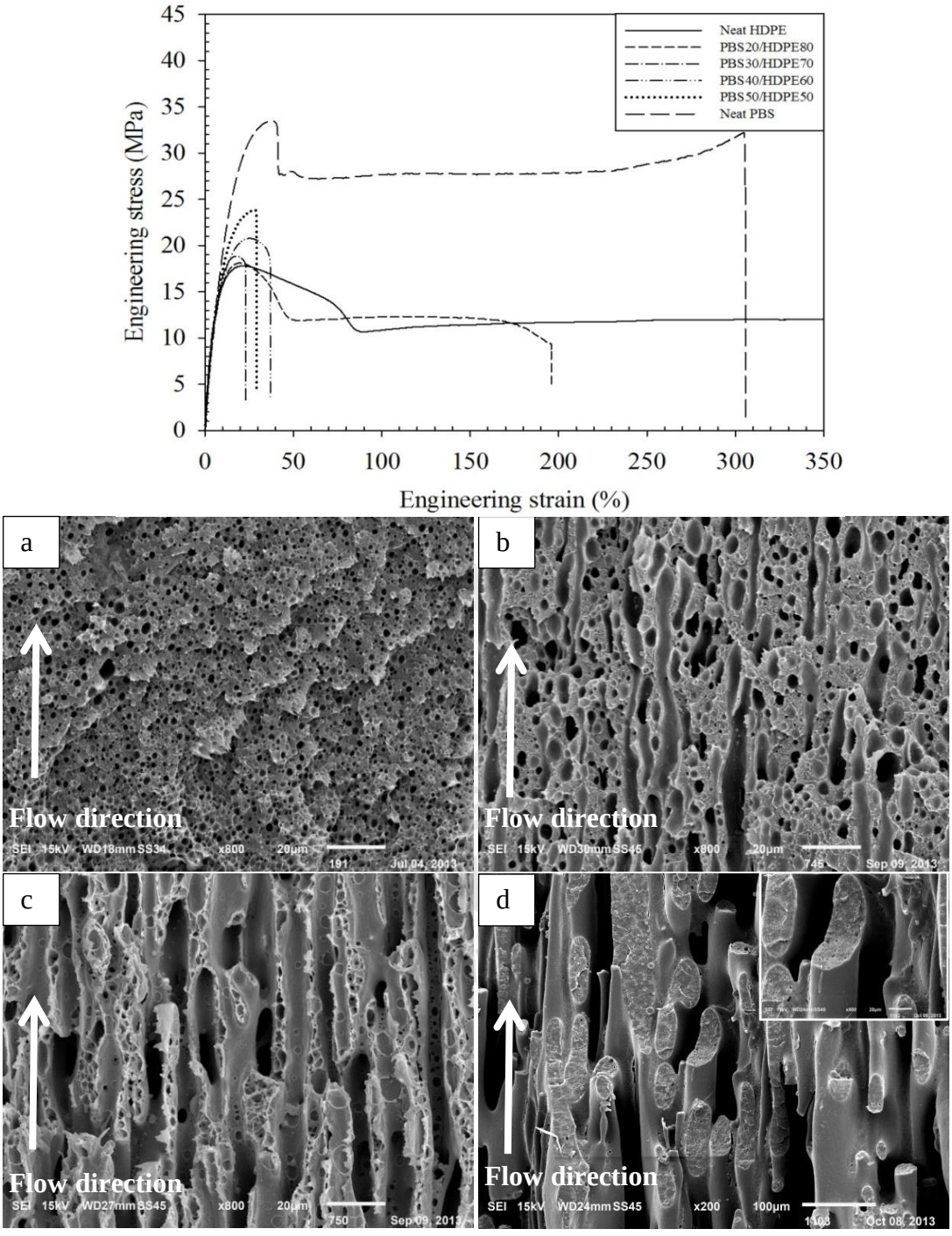

Figure 4.3 Tensile stress-strain curves and SEM micrographs of PBS etching specimens at magnification of x800 of PBS/HDPE blend at 20 wt.% PBS (a), 30 wt.% PBS (b), 40 wt.% PBS (c) and at a magnification of x200 and x800 of 50 wt.% PBS (d).

4.1.1.3 Mechanical properties

Young's modulus of neat HDPE, neat PBS and PBS/HDPE blends is presented in Figure 4.4. Young's modulus of neat HDPE was higher than that of neat PBS. Adding PBS into HDPE matrix resulted in a decrease of Young's modulus of the blend. Furthermore, Young's modulus of PBS/HDPE blend decreased continuously with increasing PBS content.

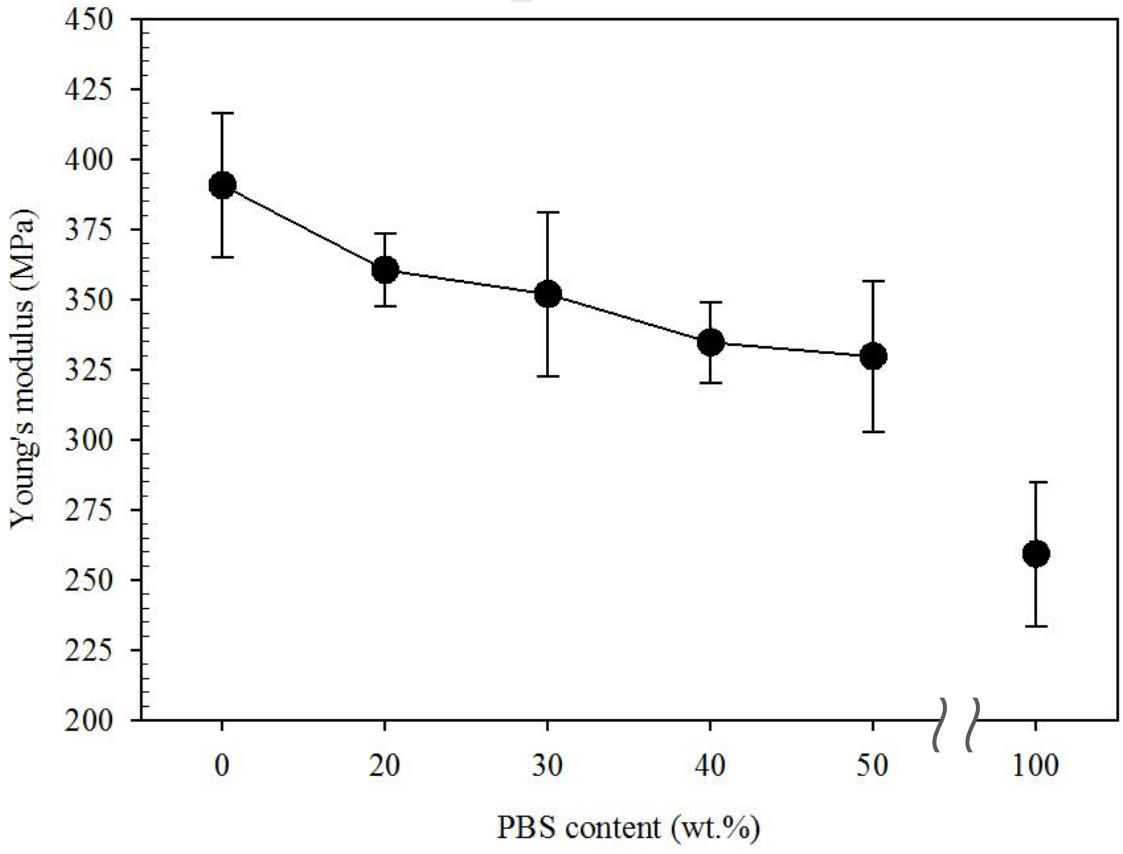

Figure 4.4 Plot of Young's modulus of PBS/HDPE blend vs. PBS content.

The prediction of longitudinal and transverse modulus of the blends is comparatively plotted with Young's modulus obtained from an experimental in Figure 4.5. It illustrates that Young's modulus of PBS/HDPE blends obtained from

the experimental was line in between the longitudinal modulus (E_L) and transverse modulus (E_T) of which calculated using “Rule of mixture” and “Inverse rule of mixtures” as following equations (Maksimov, Meri and Kalnin and Zicans, 2003) :

$$E_L = E_m V_m + E_d V_d \tag{4.1}$$

$$\frac{1}{E_T} = \frac{V_m}{E_m} + \frac{V_d}{E_d} \tag{4.2}$$

where V_m and V_d are volume fraction of matrix and dispersed phase, respectively. E_m and E_d are modulus of matrix and dispersed phase, respectively.

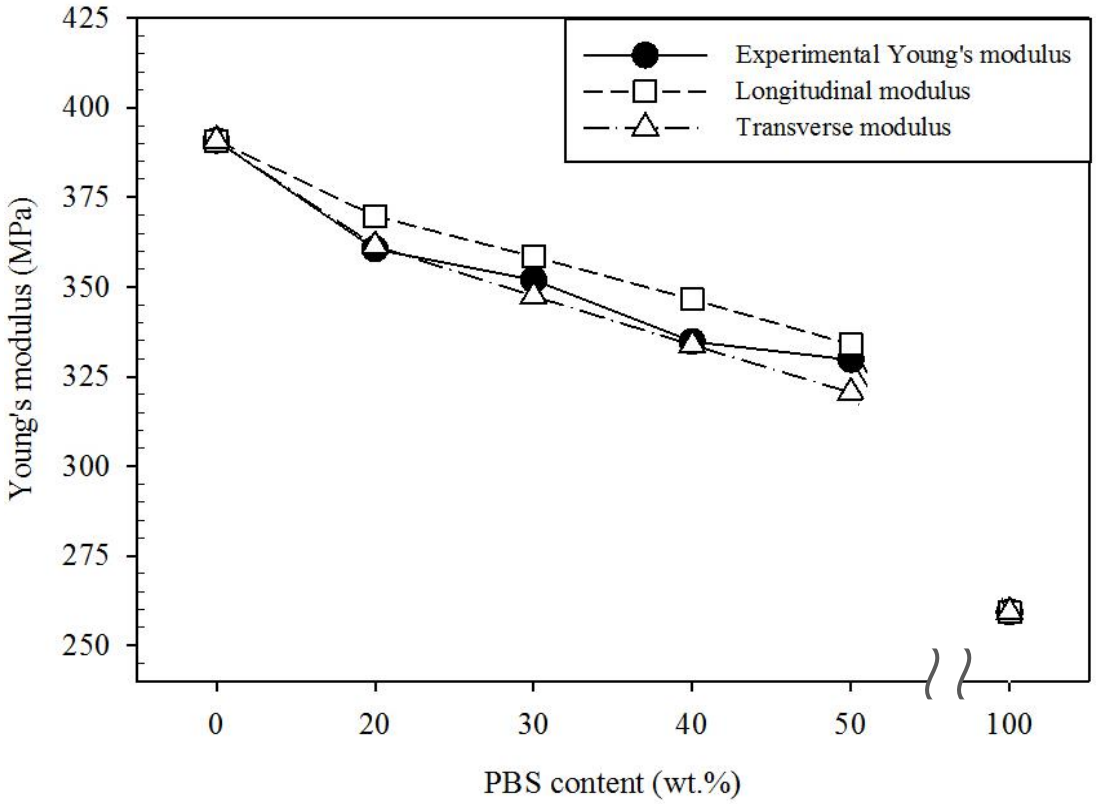

Figure 4.5 Plot of longitudinal and transverse modulus compared with Young's modulus obtained from an experimental of PBS/HDPE blend vs. PBS content.

Elongation at break of neat PBS and PBS/HDPE blends is also shown in Figure 4.6. As mentioned previously, elongation at break of neat HDPE, under tensile test of a crosshead speed of 10 mm/min, was not obtained because it was far beyond an instrumentation limit of 800%. Addition of 20 wt.% PBS into HDPE matrix resulted in a decrease of elongation at break of the blend. This decreasing elongation at break was a result of heterogeneous phase morphology of the PBS/HDPE blend at 20 wt.% PBS. During tensile loading, micro-cracking occurred leading to void creation at HDPE-PBS interface. Then, the voids at interface were

propagated, as a result, the blend sample failed. As increasing PBS content to 30 wt.%, the elongation at break of HDPE/PBS blend still decreased. This result might be correlated with a larger size and a non-uniform in shape of PBS domain as previously shown in SEM micrograph. The larger size of dispersed PBS created more incompatible HDPE-PBS interfacial contact leading to a failure of blend sample at lower strain. However, elongation at break of PBS/HDPE blend did not further decrease with adding 40-50 wt.% PBS. The unchanging elongation at break of the blend with adding PBS 40-50 wt.% PBS related well with its phase morphology. The fibrillation of PBS domain in PBS/HDPE blend at 40 wt.% PBS induced elongation, as observed in Figure 4.3(c). Therefore, elongation at break of PBS/HDPE blend at 40 wt.% PBS did not further decrease. Similarly, co-continuous phase morphology of PBS/HDPE blend at 50 wt.% PBS, as shown in Figure 4.3(d) also maintained the unchanging of elongation at break. This was because both phases in the co-continuous morphology were able to maintain mechanical performance in all direction (Bell, 2007). This might result in a restriction of elongation at break of the blend. The similar result was previously reported in the system of PET/HDPE blend. It was found that blending HDPE with small amount of PET resulted in much decrease of elongation at break while adding more PET to 30-50 wt.% did not make a further decrease of elongation at break of the blend (Kim, Park, Kim, and Suh, 2000). Moreover, these results also corresponded with Pietrasanta, Robin, Torres, and Boutevin's work (1999). They found that blending HDPE with 10-20 wt.% PET resulted in a large decrease of elongation at break while adding more PET to 40-60 wt.% did not promote a decrease of elongation at break of the blend.

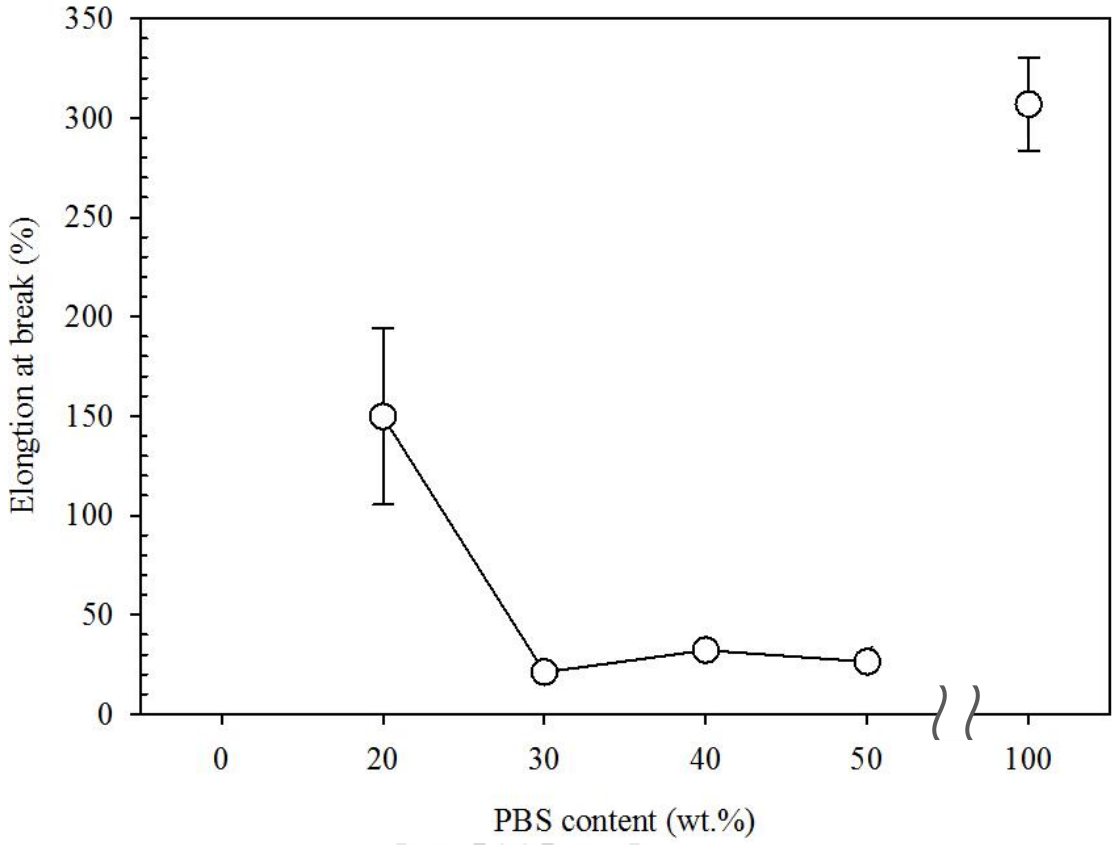

Figure 4.6 Plot of elongation at break of PBS/HDPE blend vs. PBS content.

Yield strength of neat HDPE, neat PBS and PBS/HDPE blends is shown in Figure 4.7. It demonstrates that the yield strength of neat PBS was higher than that of the blend. Adding 20 wt.% PBS into HDPE matrix did not affect yield strength of the blend. However, the blend containing 30 to 50 wt.% PBS fractured in a brittle manner. The ductile to brittle transition was defined from stress-strain curve of the blend occurring within HDPE content range of 20-30 wt.%. The decrease in yield strength of the blend was a consequence of the fact that the yield strength of HDPE was lower than that of PBS and they were not compatible.

Stress at break of neat HDPE, neat PBS and PBS/HDPE blends is also shown in Figure 4.7. As mentioned previously, stress at break of neat HDPE,

under tensile test of a crosshead speed of 10 mm/min, was not able to detect because it was far beyond an instrumentation limit. On the other hand, stress at break of neat PBS was 28 MPa. Stress at break of PBS/HDPE blend of the blend significantly improved as increasing PBS content. It was previously reported that stress at break of the PET was higher than that of HDPE. This led to an increase of stress at break of PET/HDPE blend with increasing PET content (Mbarek, Jaziri, Chalamet and Carrot, 2010). In addition, tensile properties of the blends were listed in Table 4.2.

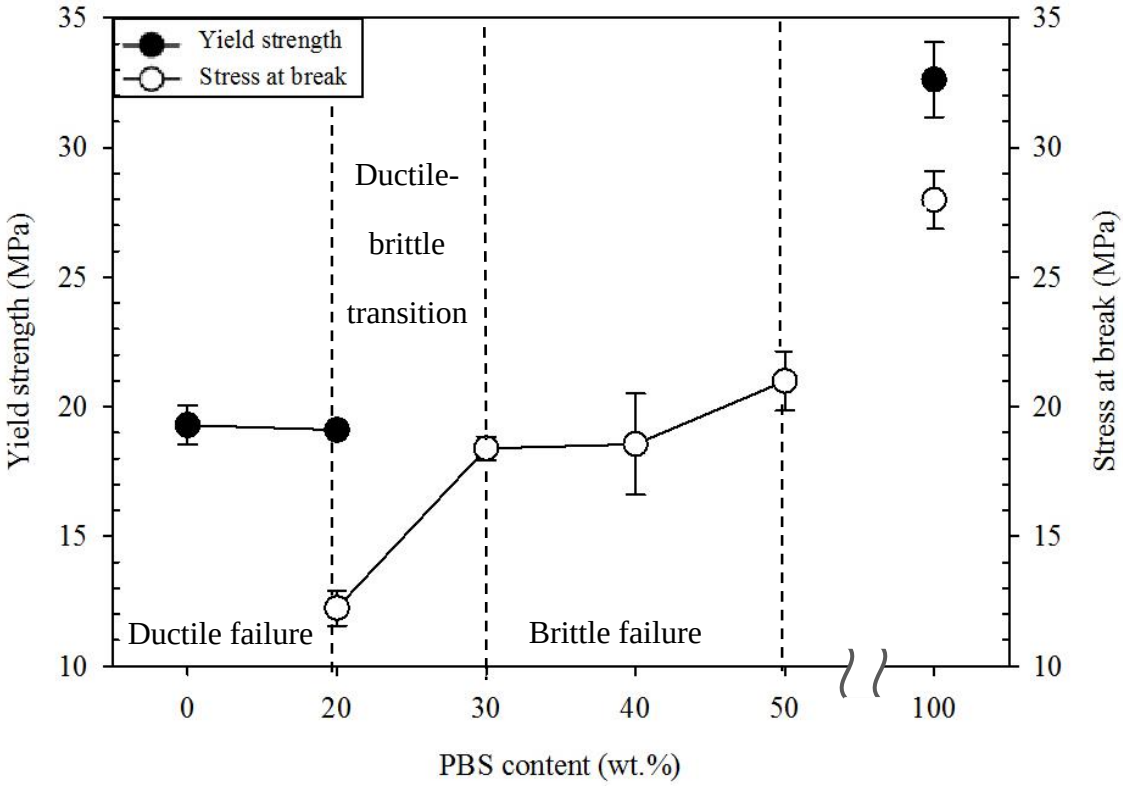

Figure 4.7 Plot of yield strength and stress at break of PBS/HDPE blend vs. PBS content

Table 4.2 Tensile properties of neat HDPE, neat PBS and PBS/HDPE blend

Sample	Young's modulus (MPa)	Elongation at break (%)	Yield strength (MPa)	Stress at break (MPa)
Neat HDPE	390.7±25.7	Not break	19.3±0.8	Not break
PBS20/HDPE80	360.5±12.9	149.7±44.4	19.1±0.1	12.2±0.7
PBS30/HDPE70	359.1±29.1	21.1±1.8	Brittle failure	18.4±0.5
PBS40/HDPE60	334.7±14.5	32.2±2.1	Brittle failure	18.6±1.9
PBS50/HDPE50	329.7±26.9	26.4±2.6	Brittle failure	21.0±1.1
Neat PBS	259.3±25.8	306.6±23.4	32.6±1.4	28.0±1.1

Flexural strength and flexural modulus of neat HDPE, neat HDPE and PBS/HDPE blend at various contents of PBS are presented in Figure 4.8. It illustrates that flexural strength of neat HDPE was lower than that of neat PBS. Adding PBS into HDPE matrix brought about an increase in flexural strength of the blend. As increasing PBS content, the flexural strength of the PBS/HDPE blend slightly increased. Figure 4.8 also shows that flexural modulus of neat HDPE was higher than that of neat PBS. Addition 20 wt% PBS into HDPE matrix gave rise to a decrease of flexural modulus of the blend. However, adding more 20 wt.% PBS did not have any subsequent effect on flexural modulus of the blend. In addition, flexural properties of the blend were summarized in Table 4.3.

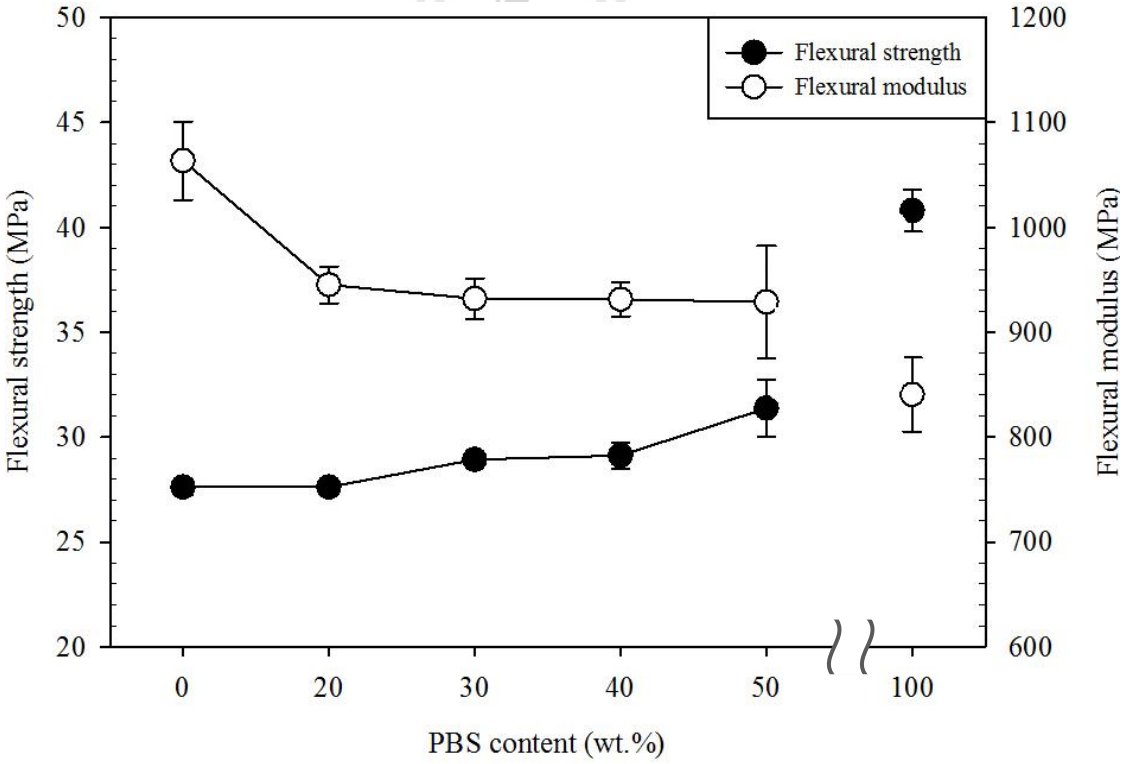

Figure 4.8 Plot of flexural strength and flexural modulus of PBS/HDPE blend vs. PBS content.

Table 4.3 Flexural properties of neat HDPE, neat PBS and PBS/HDPE blend

Sample	Flexural strength (MPa)	Flexural modulus (MPa)
Neat HDPE	27.6±0.4	1,063.5±37.5
PBS20/HDPE80	27.6±0.3	945.1±17.5
PBS30/HDPE70	28.9±0.3	931.9±19.5
PBS40/HDPE60	29.1±0.6	931.3±16.0
PBS50/HDPE50	31.4±1.4	928.8±53.3
Neat PBS	40.8±1.0	840.6±35.2

Unnot ched Izod impact strength of neat HDPE, neat PBS and PBS/HDPE blends is shown in Table 4.4. The impact strength of neat HDPE and neat PBS was not obtained; it was beyond an instrumentation limit of a 135 kJ/m^2. From Table 4.2, it illustrates that the addition 20 to 30 wt.% PBS into HDPE matrix resulted in a significant decrease of the impact strength of the blend. The decreasing impact strength was due to high interfacial tension between PBS and HDPE. A high interfacial tension resulted in an immature stress transfer which could not prevent cracks initiation at the interface from growing until catastrophic failure occurs. However, increasing PBS to 40 and 50 wt.% led to an increase of impact strength of the blend, especially, at 50 wt.% PBS, impact strength of the blend largely increased. The improvement of impact strength of PBS/HDPE blend at 40 wt.% PBS correlated with its fibrillar phase morphology (Bandyopadhyay, Iyer, Majumder, Satapathy, and Ghosh, 2013). Fibrils promoted a crack-tip shielding of which tended to bridge the crack and opposed a crack opening of the blend (Nalla, Kinney and Ritchie, 2003).

The improved impact strength of PBS/HDPE blend at 50 wt.% PBS corresponded well with its co-continuous phase morphology (Harrats, Thomas and Groeninckx, 2006; Utracki and Dumoulin, 2003). This was because both phases in the co-continuous morphology were able to contribute to mechanical performance in all direction, often resulting in synergistic effect (Bell, 2007).

Table 4.4 Unnotched Izod impact strength of neat HDPE, neat PBS and PBS/HDPE blend.

Sample	Unnotched Izod impact strength (kJ/m^2)
Neat HDPE	Not break
PBS20/HDPE80	33.5±1.2
PBS30/HDPE70	26.4±1.1
PBS40/HDPE60	35.5±0.9
PBS50/HDPE50	Not break
Neat PBS	Not break

4.1.1.4 Thermal degradation temperature and weight loss

TGA and DTGA curves of neat HDPE, neat PBS and PBS/HDPE blends are presented in Figure 4.9. As shown in Figure 4.9(a), neat HDPE and neat PBS degraded with single thermal transition at a temperature range of 423-506ºC and 350-433ºC, respectively. Adding 20 wt% PBS into HDPE made the blend thermally degraded in two stages. The first transition occurred at a temperature range of 352-430ºC corresponding to the thermal degradation of PBS phase. The second transition occurred at a temperature range of 423-508°C, due to thermal degradation

of HDPE phase. Adding 30, 40 and 50 wt.% PBS into HDPE matrix resulted in an insignificant change of degradation temperature range of PBS and HDPE phase. The PBS phase degraded at a temperature range of 355-430, 355-433 and 355-433 ºC whereas HDPE matrix degraded at a temperature range of 427-506, 426-506 and 431-504 ºC, respectively. In addition, the TGA curves show the percentage of HDPE and PBS corresponding to the blend ratios.

For degradation temperature, the degradation temperature of HDPE matrix in the PBS/HDPE blends was independent of PBS content, as shown in DTGA curves in Figure 4.9(b). On the other hand, degradation temperature of PBS domain slightly increased from 406°C to 413°C when its content was increased from 20 wt.% to 50 wt.%. The improvement of thermal stability of PBS phase might be related with its crystallinity (Song, Chen, Yu, Linliu and Tseng, 1996; Poletto, Zattera, Forte and Santana, 2012).

In addition, the temperature range for degradation, the degradation temperature and weight loss of PBS domain and HDPE matrix were summarized in Table 4.5.

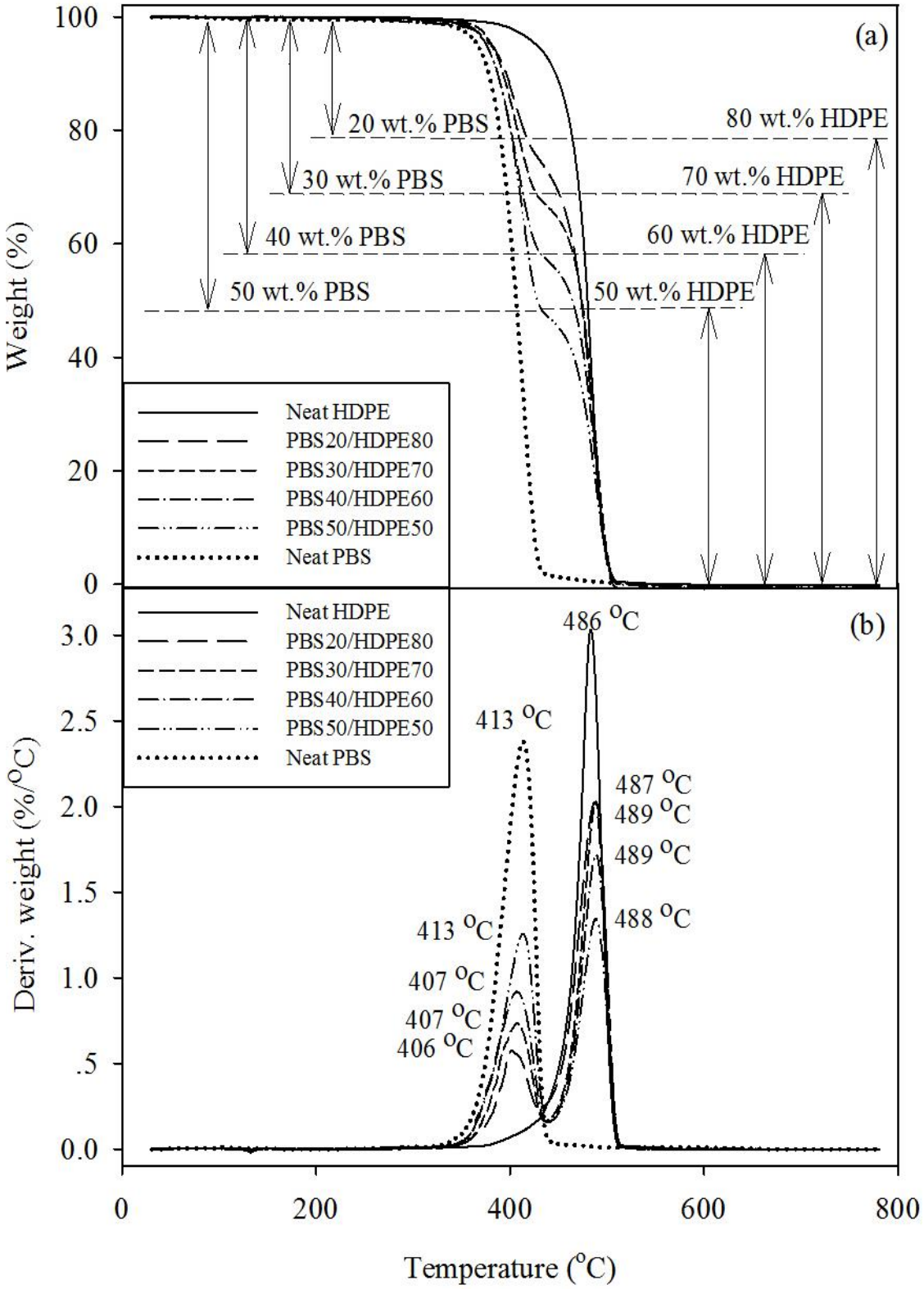

Figure 4.9 TGA (a) and DTGA (b) thermograms of neat HDPE, neat PBS and PBS/HDPE blend at various PBS contents.

Table 4.5 The temperature range for degradation ($T_{d,range}$), Peak temperatures (T_{peak}) and weight loss of neat HDPE, neat PBS, and PBS/HDPE blend at various PBS contents.

Sample	PBS phase			HDPE phase		
	T_{peak} (ºC)	Weight loss (%)	$T_{d,range}$ (ºC)	T_{peak} (ºC)	Weight loss (%)	$T_{d,range}$ (ºC)
Neat HDPE	-	-	-	486	100.0	423-506
PBS20/HDPE80	406	19.9	352-430	487	79.6	423-508
PBS30/HDPE70	407	29.7	355-430	489	69.9	427-506
PBS40/HDPE60	407	39.9	355-433	489	59.6	426-506
PBS50/HDPE50	413	49.9	355-433	488	49.6	431-504
Neat PBS	413	100.0	350-433	-	-	-

4.1.1.5 Melting and crystallizing behavior

DSC curve from the first heating scan of neat HDPE, neat PBS and PBS/HDPE blend at various contents of PBS are shown in Figure 4.10 It illustrates that neat HDPE exhibited an endothermic peak at 128.8°C corresponding to its melting temperature. Neat PBS exhibited an exothermic peak at 90.3°C subsequent with endothermic peak at 109.8°C. The exothermic peak was caused by the recrystallization of PBS called cold-crystallization (Yasuniwa, Tsubakihara, Satou and Iura, 2005). It was previously reported that cold-crystallization occurring during heating scan of PBS at a temperature around 93.0°C, due to the thermal history during cooling and reheating (Yoo and Im, 1999). The endothermic peak at 109.8°C corresponded to a melting temperature of PBS. Addition of PBS into HDPE matrix hardly affected a cold-crystallization temperature of PBS phase, melting temperature of HDPE phase and melting temperature of PBS phase itself, as well.

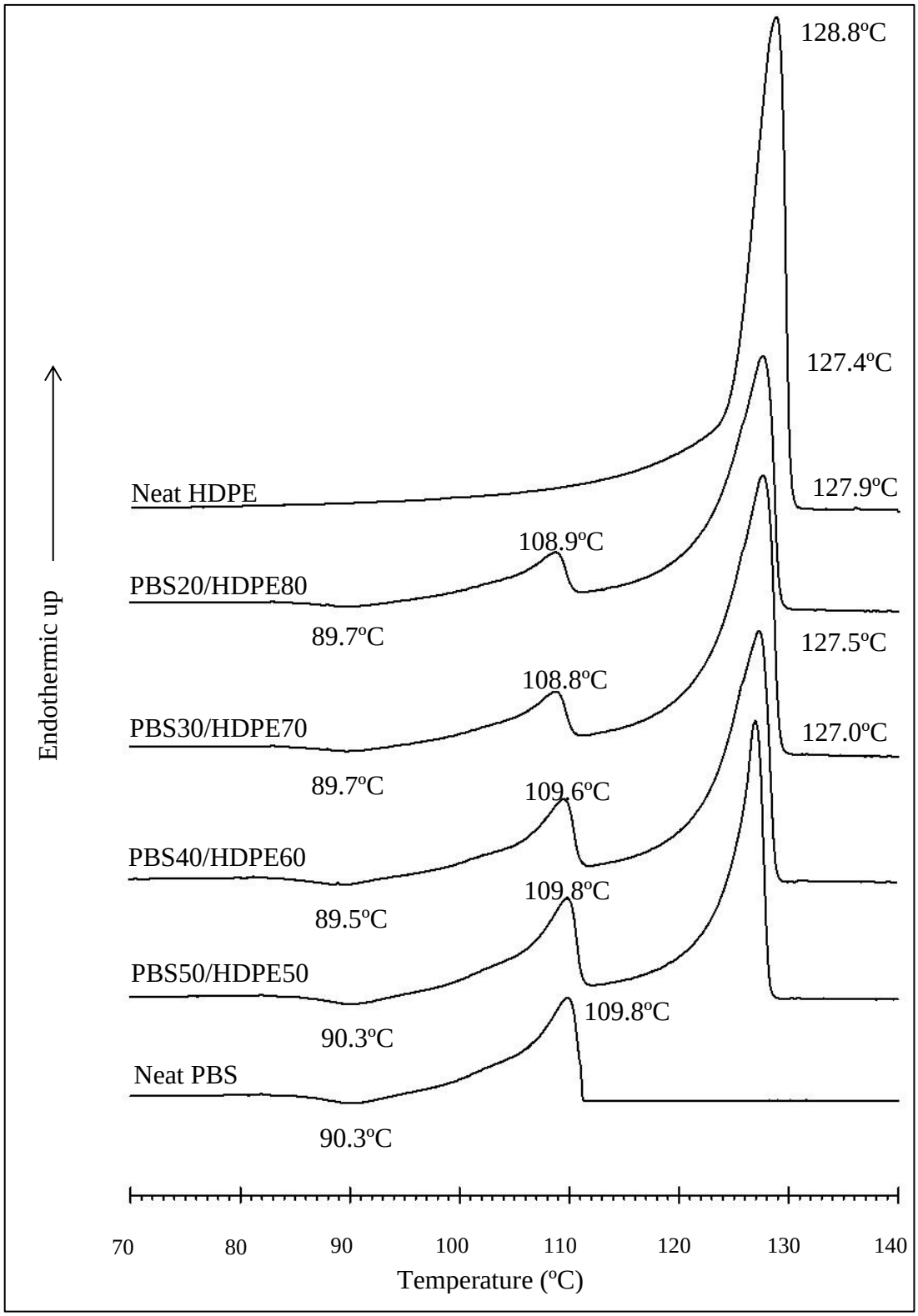

Figure 4.10 DSC curve from the first heating scan of neat HDPE, neat PBS and PBS/HDPE blend at various PBS contents.

The DSC curves from the cooling scan of neat HDPE, neat PBS and PBS/HDPE blend at various contents of PBS are presented in Figure 4.11. The crystallization temperature of neat HDPE and neat PBS was observed at 116.7°C and 85.1°C, respectively. Adding PBS into HDPE matrix made an insignificant change the crystallization temperature of HDPE phase and PBS phase itself. Noticeably, the crystallization temperature of PBS phase in the blend at 20 wt.% PBS was much lower than that of neat PBS. This probably due to, at small amount of PBS, the crystallization of PBS molecular chains was inhibited by HDPE chains leading to a retardation of PBS crystallization process.

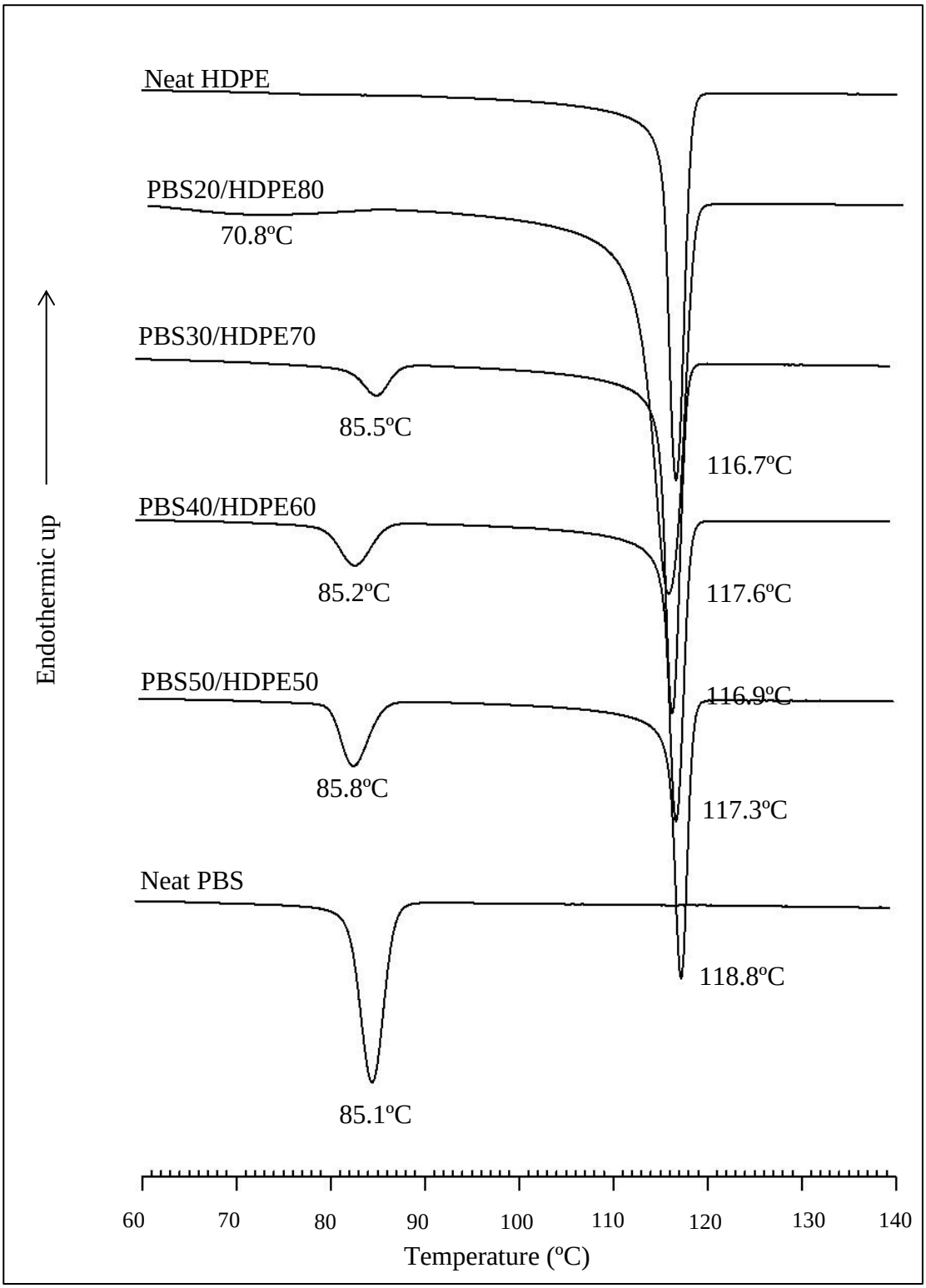

Figure 4.11 DSC curves from cooling scan of neat HDPE, neat PBS and PBS/HDPE blend at various PBS contents.

The DSC curve from the second heating scan of neat HDPE, neat PBS and PBS/HDPE blend at various contents of PBS are shown in Figure 4.12. DSC curve of neat HDPE exhibits an endothermic peak at 129.0°C corresponded to melting temperature of HDPE. The DSC curve neat PBS shows double endothermic peak of PBS at temperature of 100.1°C and 109.0°C. It was report that PBS had two spherulitic forms, α form and β form (Xu and Guo, 2010). The spherulite of α form melted at higher temperature than the spherulite of β form. However, the melting endotherm of β spherulite might or might not be observed from a DSC thermogram depending on heating scan, cooling scan and their thermal history. Therefore, the lower temperature peak might possibly be the endotherm of β form of PBS.

In addition, adding PBS into HDPE matrix did insignificantly influence melting temperature of HDPE phase. Similarly, the adding PBS into HDPE matrix did insignificantly affect the melting temperature of PBS phase at both low and high melting temperature. However, DSC curve of the blend at 20 wt.% PBS exhibited only a small shoulder prior to melting peak at high temperature of PBS phase, 109.1°C. This probably due to adding small amount of PBS gave rise to a perfect form of PBS crystallizes. Therefore, the melting peak of PBS at low temperature of which belonged to metastable spherulite (β form) melting was not clearly observed.

As well, melting temperature and cold crystallization temperature from the first heating scan, crystallization temperature, and melting at low and high temperature from the second heating scan of PBS/HDPE blend at various contents PBS are summarized in Table 4.6.

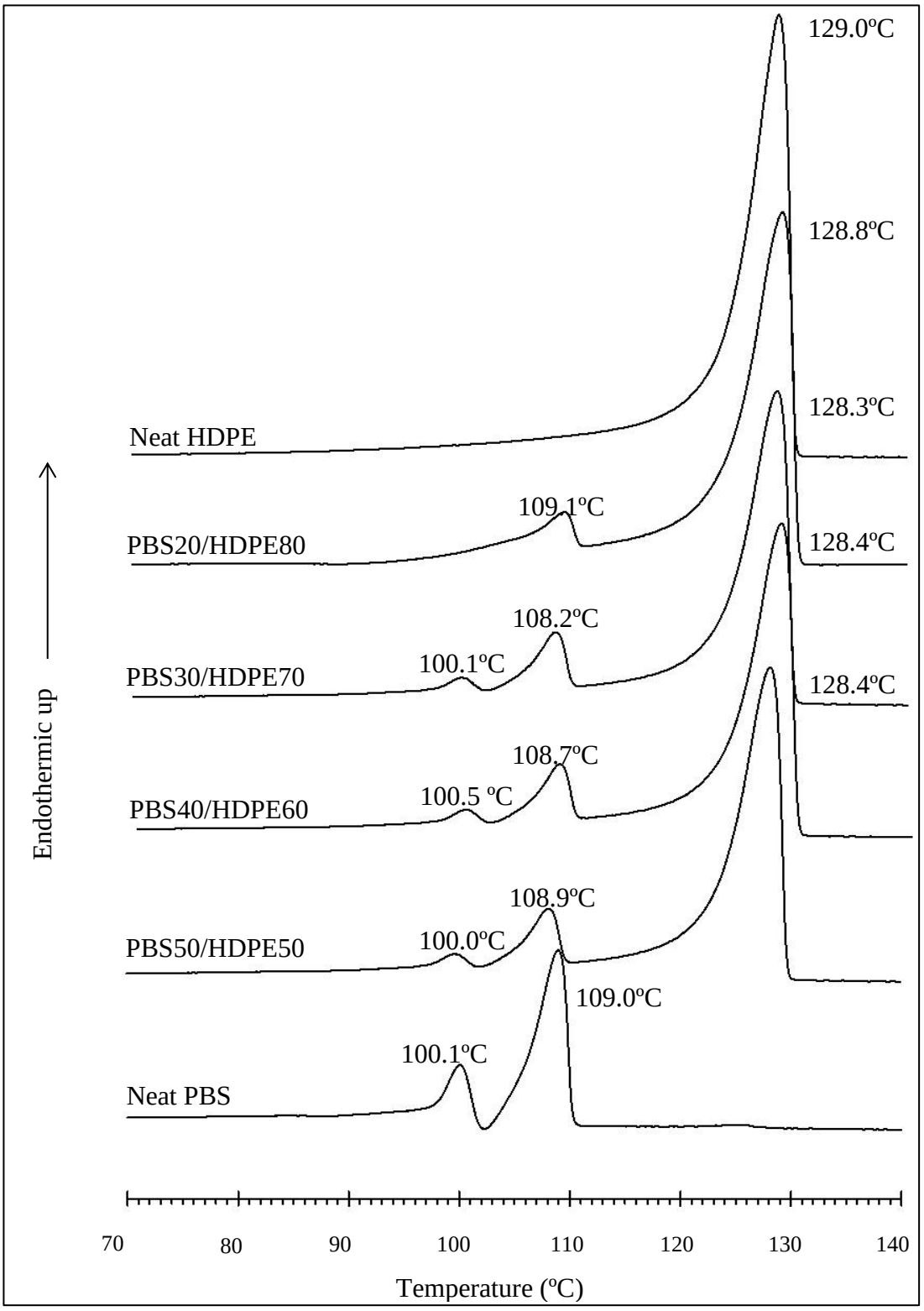

Figure 4.12 DSC curve from the second heating scan of neat HDPE, neat PBS and PBS/HDPE blend at various PBS contents.

Table 4.6 Melting temperature and cold crystallization temperature from the first heating scan, crystallization temperature and melting at low and high temperature of neat HDPE, neat PBS and PBS/HDPE blend.

Sample	First heating scan			Crystallization temperature (^{o}C)		Second heating scan	
	Melting temperature (^{o}C)		Cold crystallization temperature (^{o}C)			Melting temperature (^{o}C)	
	HDPE matrix	PBS domain	PBS domain	HDPE matrix	PBS domain	HDPE matrix	PBS domain
Neat HDPE	128.8	-	-	116.7	-	129.0	-
PBS20/HDPE80	127.4	108.9	89.7	117.6	70.8	128.8	109.1
PBS30/HDPE70	127.9	108.8	89.7	116.9	85.5	128.3	101.1,108.2
PBS40/HDPE60	127.5	109.6	89.5	117.3	85.2	128.4	100.5,108.7
PBS50/HDPE50	127.0	109.8	90.3	118.8	85.8	128.4	100.0,108.9
Neat PBS	-	109.8	90.3	-	85.1	-	100.1,109.0

4.1.1.6 Water absorption

Plot of water absorption (%) and immersion time of neat HDPE, neat PBS and PBS/HDPE blends is shown in Figure 4.13. The water absorption of neat HDPE was much lower than that of neat PBS. This was a consequence of hydrophobicity of HDPE. In contrast, PBS is higher in hydrophilicity facilitated by its ester groups along the PBS main chains. These groups were able to bind with water molecules via hydrogen bond (Merdas, Thominette, Tcharkntchi and Verdu, 2002). It also shows that the water absorption of neat PBS rapidly increased within 6 days of immersion time. After, 42 and 51 days of immersion, the water absorption of neat HDPE and neat PBS reached to equilibrium of water absorption, respectively. Adding PBS into HDPE matrix brought about an increase of water absorption of the blends. The increase in water absorption of the PBS/HDPE blend corresponded with the increase in size of PBS dispersed phase as shown in SEM micrographs. The larger size of PBS dispersed phase resulted in the larger interfacial voids leading to more moisture available for absorbed water molecules. In addition, the PBS/HDPE blend containing 20 wt.%, 30 wt.%, 40 wt.% and 50 wt.% PBS gained an equilibrium at immersion times of 39 days, 42 days, 45 days and 45 days, respectively. In addition, immersion time and water content of neat HDPE, neat PBS and PBS/HDPE blends at equilibrium. is summarized in Table 4.7.

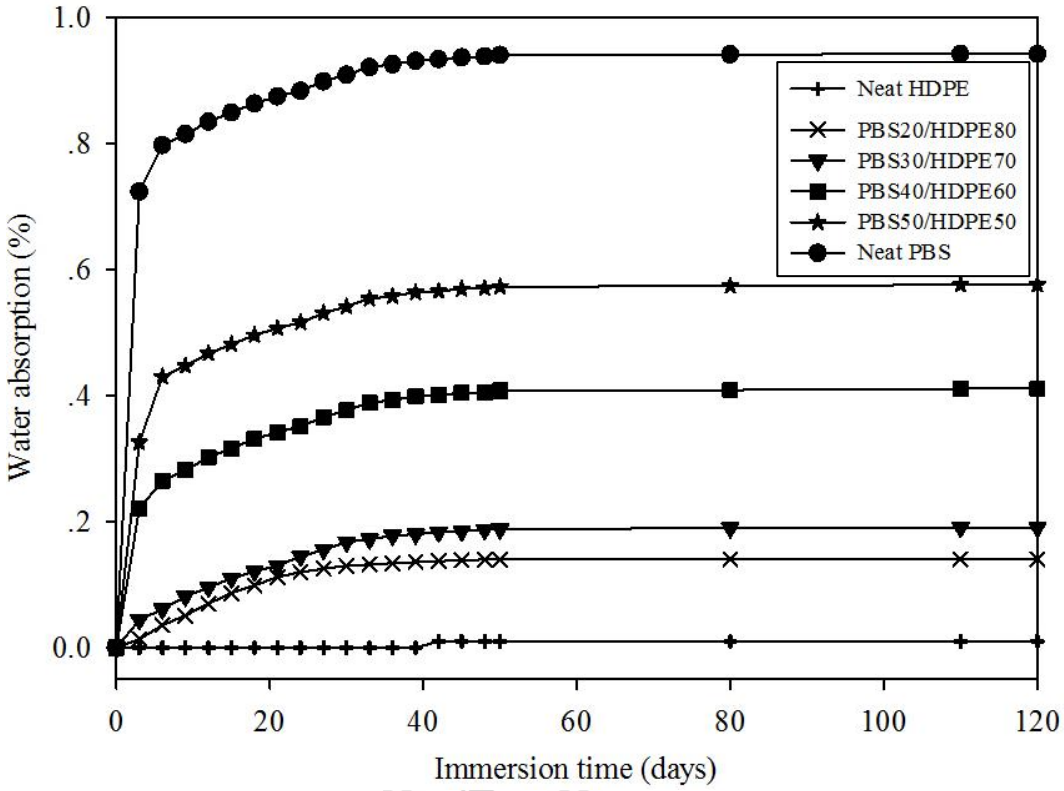

Figure 4.13 Plot of water absorption vs. immersion time of neat HDPE, neat PBS and PBS/HDPE blends.

Table 4.7 Immersion time and water content of neat HDPE, neat PBS and PBS/HDPE blends at equilibrium.

Sample	Immersion time (day)	Water content at equilibrium (%)
Neat HDPE	42	0.01%
PBS20/HDPE80	39	0.14%
PBS30/HDPE70	42	0.18%
PBS40/HDPE60	45	0.40%
PBS50/HDPE50	45	0.58%
Neat PBS	51	0.94%

4.1.1.7 Biodegradability by natural soil burial test

The plot of weight loss (%) and burial time of neat HDPE, neat PBS and PBS/HDPE blends is shown in Figure 4.14. It illustrates that the weight loss increased with burial period for all the specimens. The weight loss of neat HDPE was much lower than that of neat PBS. This was a consequence of hydrophobicity of HDPE. In contrast, PBS is higher in hydrophilicity facilitated by its ester groups along the PBS main chains. These groups were able to bind with moisture (Kim and Park, 1999). In addition, PBS could be degraded by micro-organisms encountering in soil (Liu, Yu, Cheng and Yang, 2009). After using dilution plating method to identify the number of viable micro-organisms in soil, it was confirmed by National Center for Genetic Engineering and Biotechnology (BIOTEC) that the *Aspergillus Niger* was a micro-organism encountering in soil. This predicated that PBS could be biodegraded by the *Aspergillus Niger* micro-organism. This result corresponded well with the previously reported which informed that PBS could be biodegraded by micro-organisms including *Aspergillus Niger, Penicillium, Bacillus, and Thermopolyspora*. Among them, *Aspergillus Niger* was the best PBS-degrading micro-organism (Zhao *et al.*, 2005). For the blend, the weight loss increased as increasing PBS content, due to biodegradable of the blend included PBS.

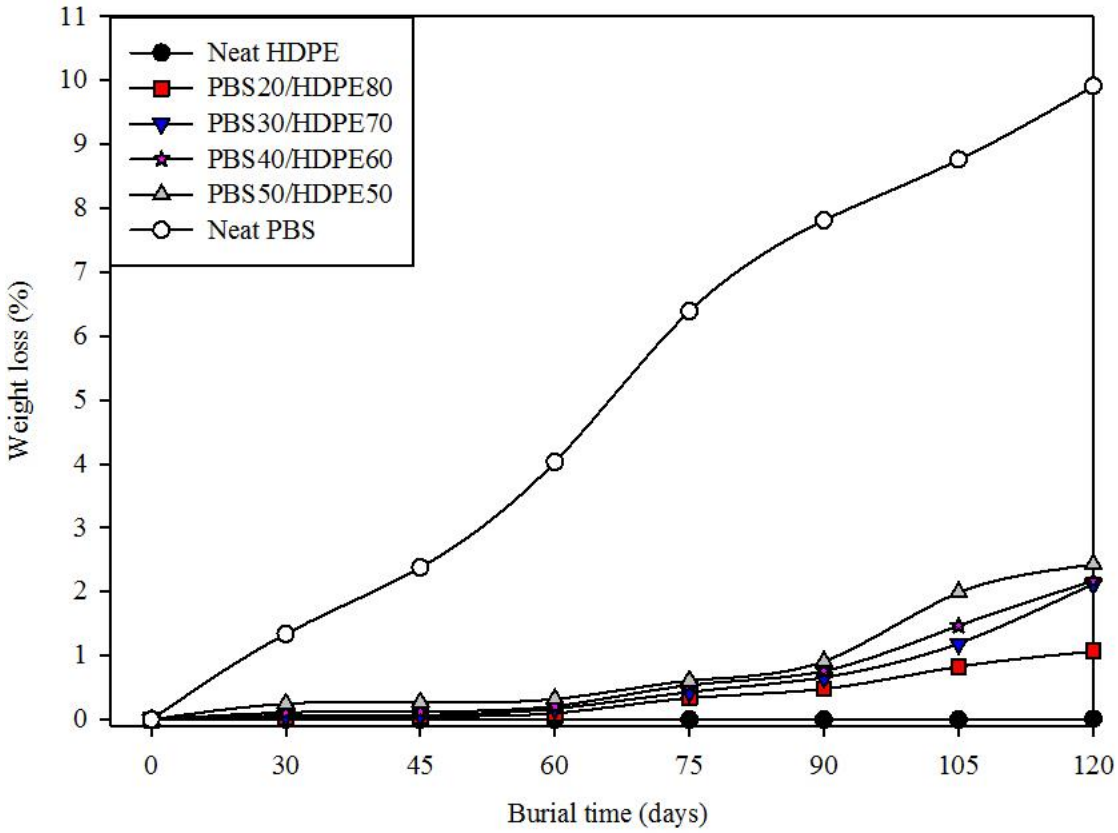

Figure 4.14 Plot of weight loss and burial time of neat HDPE, neat PBS and PBS/HDPE blend.

Figure 4.15 shows optical photographs of the surfaces of the samples buried in the soil for 120 days. It illustrates that the surface and color of neat HDPE sample did not change within 120 days of burial time. The biodegradation of neat PBS occurred at 30 days of burial time, as observed from the occurrence of dark area and rougher surface. In addition the biodegradation of neat PBS was more severe as the burial time increased.

At 20 to 30 wt.% PBS, The surface of the blend still unchanged. Seemingly, the color of the blends sample seemed to be darker after 60 days of burial times.

With adding 40 wt.% PBS, the white spot occurred at the edge of the blend sample after 30 days of burial time. The whitening spot implied that the biodegradation occurred. Furthermore, the biodegradation of the blend was more clearly, as seen in the dark spot after burial time of 90 days.

As increasing PBS to 50 wt.%, the small dark spot occurred at the edge of the blend sample after 30 days of burial time. After the 45 days, the whitening part spreaded to the surface of the blend sample. Furthermore, the surface of the blend was rougher after 45 days of burial time. In addition, the biodegradation was more drastic as seen in the darken part at the blend sample surface after burial time of 75 days.

In addition, the increase in biodegradability of PBS/HDPE blend at various content of PBS is summarized in Table 4.8.

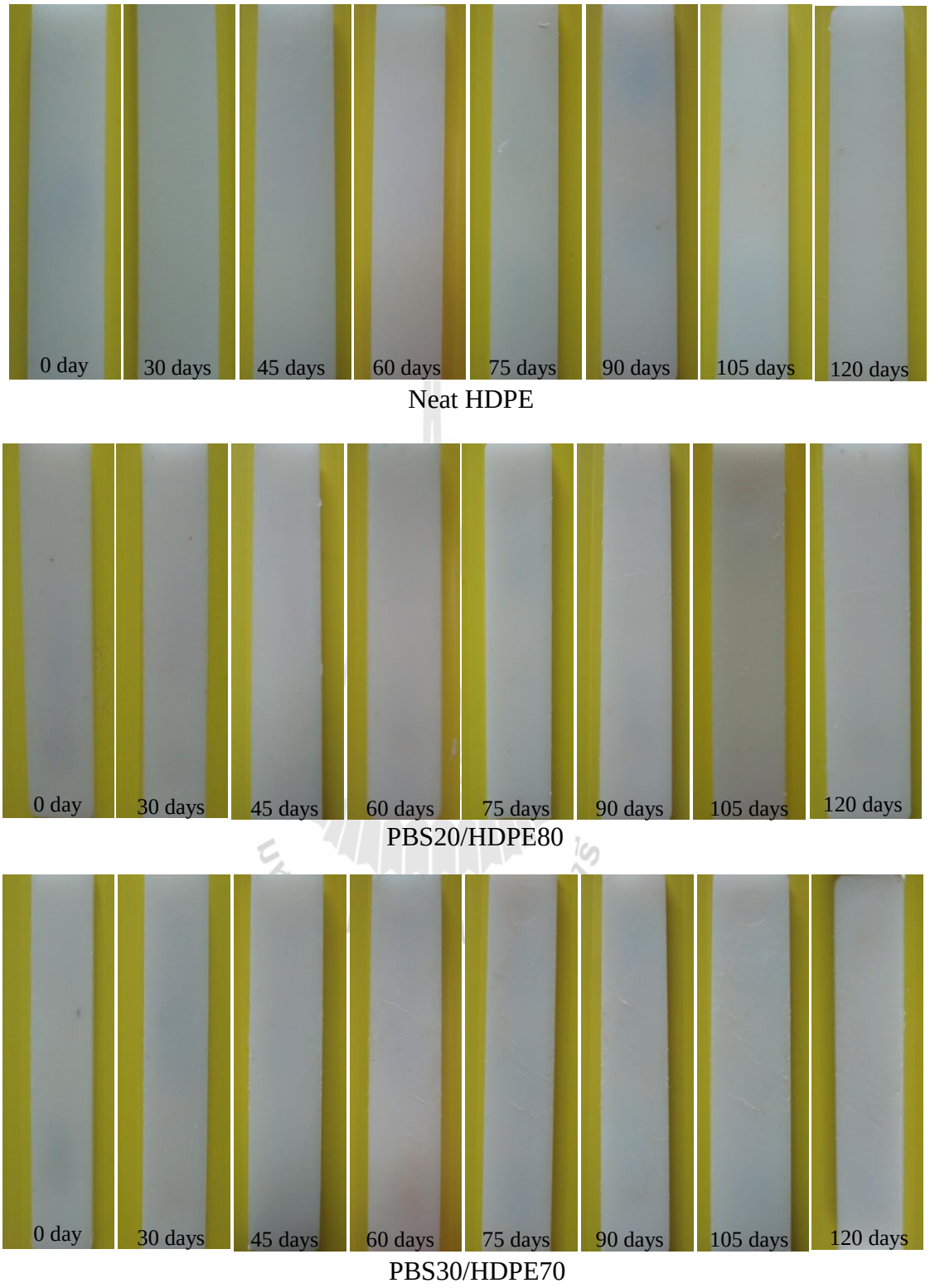

Figure 4.15 Optical micrographs of buried samples of neat PBS, neat HDPE and PBS/HDPE blend at several burial times of 0 to 120 days.

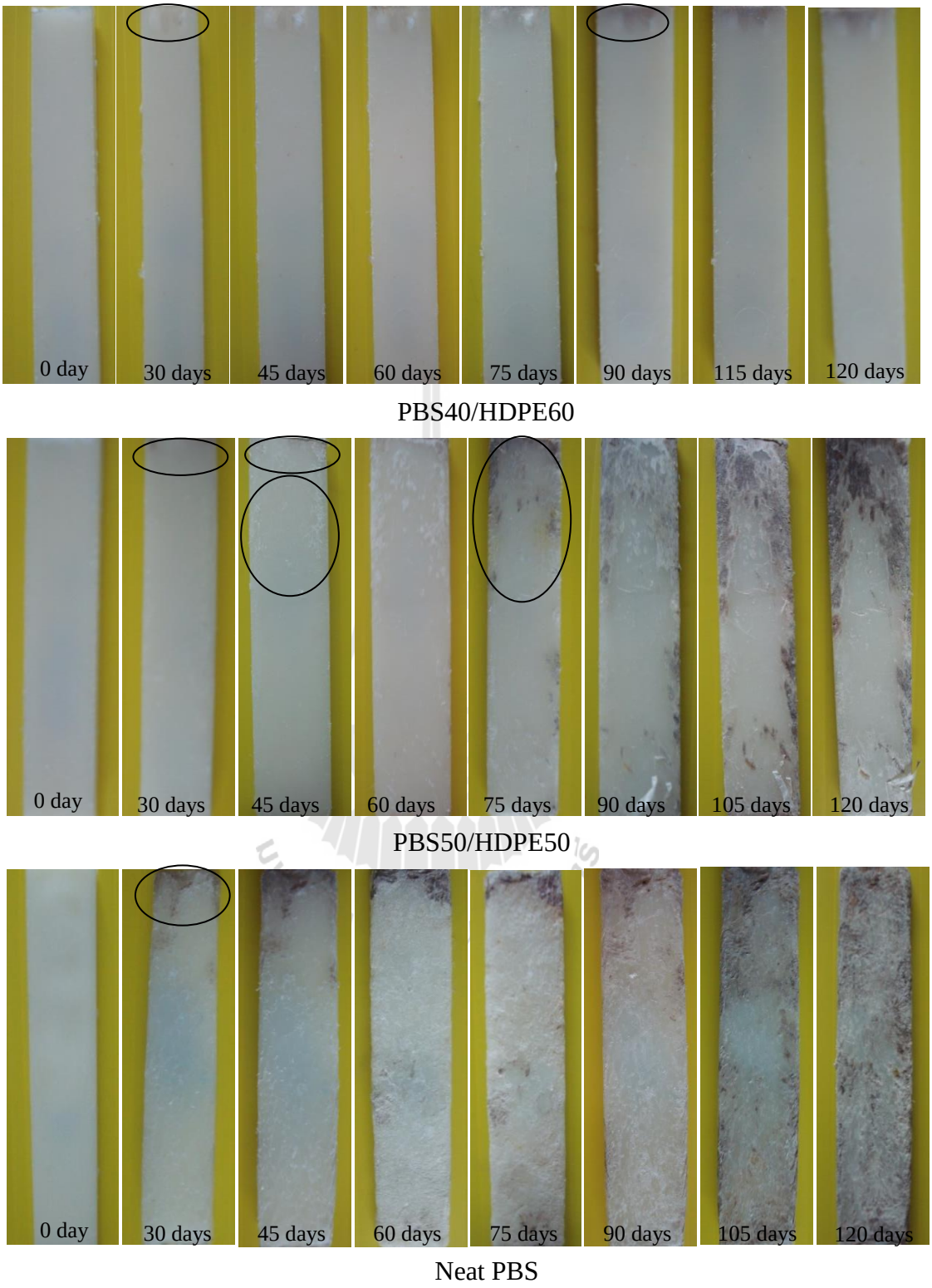

Figure 4.15 Optical micrographs of buried samples of neat PBS, neat HDPE and PBS/HDPE blend at several burial times of 0 to 120 days. (Continued)

Table 4.8 The increase in biodegradability of PBS/HDPE blend at various content of PBS comparing neat HDPE.

Sample	Biodegradability (%)	Increase in biodegradability (%)
Neat HDPE	0.01	-
PBS20/HDPE80	1.07	1.06
PBS30/HDPE70	2.12	2.11
PBS40/HDPE60	2.17	2.16
PBS50/HDPE50	2.44	2.43
Neat PBS	9.90	-

4.1.2 Effect of compatibilization on physical properties

Base on mechanical properties, the PBS/HDPE blend containing 30 wt.% PBS gave an acceptable Young's modulus and tensile strength. Therefore, this blend composition was further study the compatibilization effect. The compatibilizer type and content on physical properties of compatibilized PBS/HDPE blend was revealed. The compatibilizers were HDPE-g-MAH and EPR-g-MAH. The compatibilizer contents were 2, 4, 6, and 8 phr.

4.1.2.1 Flow property

The dependence of apparent shear viscosity on apparent shear rate of uncompatibilized and compatibilized PBS30/HDPE70 blend with HDPE-g-MAH and EPR-g-MAH at various contents is presented in Figure 4.16 (a) and Figure 4.16 (b), respectively. Figure 4.16 (a) illustrates that the shear thinning behavior was observed from both uncompatibilized and compatibilized PBS30/HDPE70 blends. In

comparison, the viscosity of the uncompatibilized blend was lower than that of compatibilized blend. Furthermore, the viscosity of compatibilized blend slightly increased with increasing HDPE-g-MAH content. The slight increase in the viscosity could be related to the occurrence of interfacial interactions, H-bonding and interchain diffusion. The H-bonding was between MAH groups of HDPE-g-MAH and ester groups of PBS. The interchain diffusion was between molecular chains of HDPE and HDPE backbone of HDPE-g-MAH (Qi, Nie, Zhou, Mao and Zhang, 2006; Pracella, Rolla, Chionna and Galeski, 2002; Nashar, Maziad and Sadek, 2008).

Figure 4.16 (b) demonstrates that both uncompatibilized and compatibilized PBS/HDPE blends exhibited shear thinning behavior. Adding EPR-g-MAH into binary blend led to an increase of viscosity of the blend. However, increasing EPR-g-MAH content resulted in a slight increase of viscosity of the compatibilized blend. The slight increase in the viscosity of compatibilized blend might be due to the occurrence of interactions between MAH groups of EPR-g-MAH and ester groups of PBS, together with physical entanglement between HDPE chains and EPR backbone.

In comparison, the shear viscosity of the compatibilized blend using HDPE-g-MAH and EPR-g-MAH at a shear rate range corresponding to that during injection molding process, 3,000-4,000 s^{-1} was insignificantly different, as illustrated in Table 4.9.

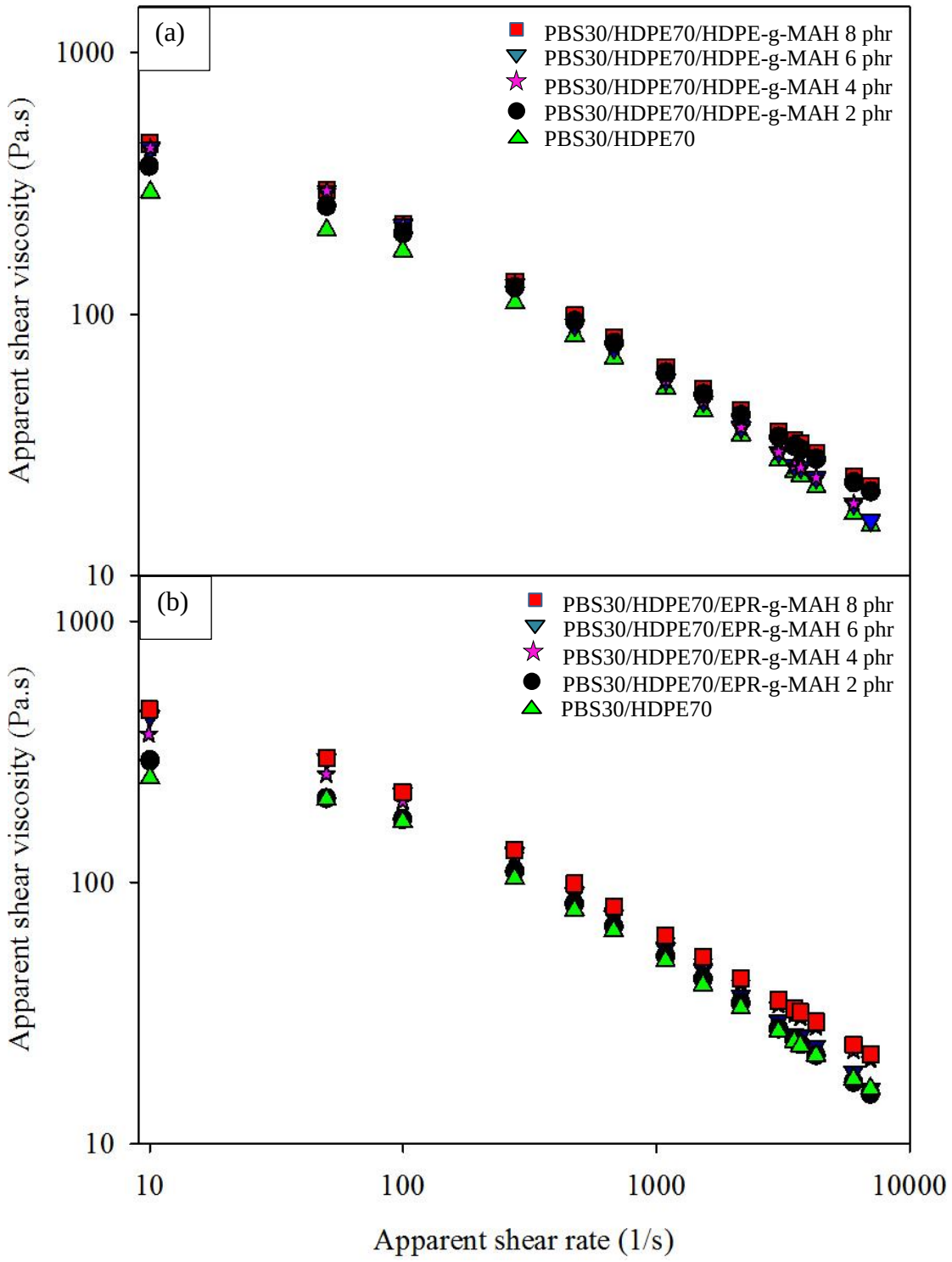

Figure 4.16 Plot of apparent shear viscosity as a function of apparent shear rate of uncompatibilized and compatibilized PBS30/HDPE70 blend with various contents of HDPE-g-MAH (a) and EPR-g-MAH (b).

Table 4.9 Shear viscosity range within the shear rate range of injection molding of uncompatibilized and compatibilized PBS30/HDPE70 blend with HDPE-g-MAH and EPR-g-MAH.

Compatibilizer content	Shear viscosity at a shear rate of 3,000-4,000 s^{-1} (Pa.s)	
	HDPE-g-MAH	EPR-g-MAH
0 phr	27.6-21.8	27.6-21.8
2 phr	33.9-27.9	28.6-22.8
4 phr	29.7-23.7	33.9-27.9
6 phr	29.7-23.7	29.7-24.0
8 phr	35.4-29.3	35.4-29.2

Melt flow index (MFI) at 180°C with a standard weight of 2.16 kg of uncompatibilized and compatibilized PBS30/HDPE70 blends with various contents of HDPE-g-MAH and EPR-g-MAH is presented in Table 4.10. It illustrates that the MFI of PBS30/HDPE70 blend compatibilized with HDPE-g-MAH was slightly lower than that of uncompatibilized blend. As increasing HDPE-g-MAH content, the MFI of the compatibilized PBS30/HDPE70 blend decreased. For the PBS30/HDPE70 blend compatibilized with EPR-g-MAH, the addition of EPR-g-MAH into PBS30/HDPE70 blend led to a decrease of MFI as compared to uncompatibilized blend. Adding more EPR-g-MAH content into the PBS30/HDPE70 blend brought about a slight decrease of MFI. In comparison, the MFI of the compatibilized blends using HDPE-g-MAH and EPR-g-MAH as compatibilizers was not significantly different.

Table 4.10 Melt flow index (MFI) at 180°C with a standard weight of 2.16 kg of uncompatibilized and compatibilized PBS30/HDPE70 blend with various contents of HDPE-g-MAH and EPR-g-MAH.

Compatibilizer content	Melt flow index (g/10min)	
	HDPE-g-MAH	EPR-g-MAH
0 phr	13.8	13.8
2 phr	13.5	13.1
4 phr	13.0	12.9
6 phr	12.8	12.3
8 phr	12.0	11.8

4.1.2.2 Failure behavior and phase morphology

Engineering stress-strain curves of uncompatibilized and compatibilized PBS30/HDPE70 blend at various contents of HDPE-g-MAH are presented concurrently with their SEM image in Figure 4.17. As shown in the stress-strain curve, uncompatibilized PBS30/HDPE70 blend fractured in a brittle manner at 19 MPa stress and 24% strain. As shown in Figure 4.17(a), phase morphology of uncompatibilized PBS30/HDPE70 blend clearly exhibited two-phase morphologies. The PBS domains were non-uniform in size and shape, including spherical, elongated and worm-like dispersed in HDPE matrix. Also, its phase morphology reveals a lack of adhesion between PBS domain and HDPE matrix as observed from a smooth surface of interfacial area between PBS domain and HDPE matrix.

After adding 2phr HDPE-g-MAH into PBS30/HDPE70 blend, the compatibilized blend still fractured in a brittle manner. However, the maximum stress of the blend appeared at higher stress comparing to uncompatibilized blend.

The phase morphology of the blend compatibilized with 2 phr HDPE-g-MAH is shown in Figure 4.17(b). It reveals that PBS dispersed phase was more uniform in size and shape, mostly in spherical shape. Approximately, size of PBS domain was in range of <2μm to 7 μm.

As increasing HDPE-g-MAH content to 4 phr, HDPE-g-MAH did not significant influence the fracture behavior of the blend, as observed from its stress-strain curve shown in Figure 4.17. However, its phase morphology revealed that the PBS dispersed phase became finer within a size range of <1μm to 5 μm and its shape was more homogeneous, as observed in Figure 4.17(c).

With increasing HDPE-g-MAH contents to 6 and 8 phr, the blend still fractured in a brittle manner. However, the blend fractured at higher strain, as observed from their stress-strain curve shown in Figure 4.17. In addition, their maximum stress was comparable to that of the blend compatibilized with 2 and 4 phr HDPE-g-MAH. The blend compatibilized with 6 phr and 8 phr HDPE-g-MAH fractured at 26% and 28 % strain, respectively. This was indication in higher toughness of the blend conpatibilized with 6 and 8 phr HDPE-g-MAH. The phase morphology of the blend compatibilized with 6 and 8 phr HDPE-g-MAH is presented in Figure 4.17(d) and Figure 4.17(e), respectively. Their phase morphologies revealed a good dispersion of the PBS phase. In addition, shape and particle size of the PBS domain was more uniform. Moreover, the particle size of the PBS domains decreased with adding more HDPE-g-MAH contents. The PBS particle size of the blend conpatibilized with 6 and 8 phr HDPE-g-MAH was in range of <1μm to 5 μm. This was due to compatibilizer controlled phase morphology by preventing coalescence (Pang, Jia, Hua, Hourston and Song, 2000). In addition, the blend was possibly lower

in interfacial with adding HDPE-g-MAH. This resulted in a higher capillary number of the blend system; therefore the deformability of the dispersed PBS was governed by the shear stress acting on the domain. As a result, the finer and uniform droplet was obtained.

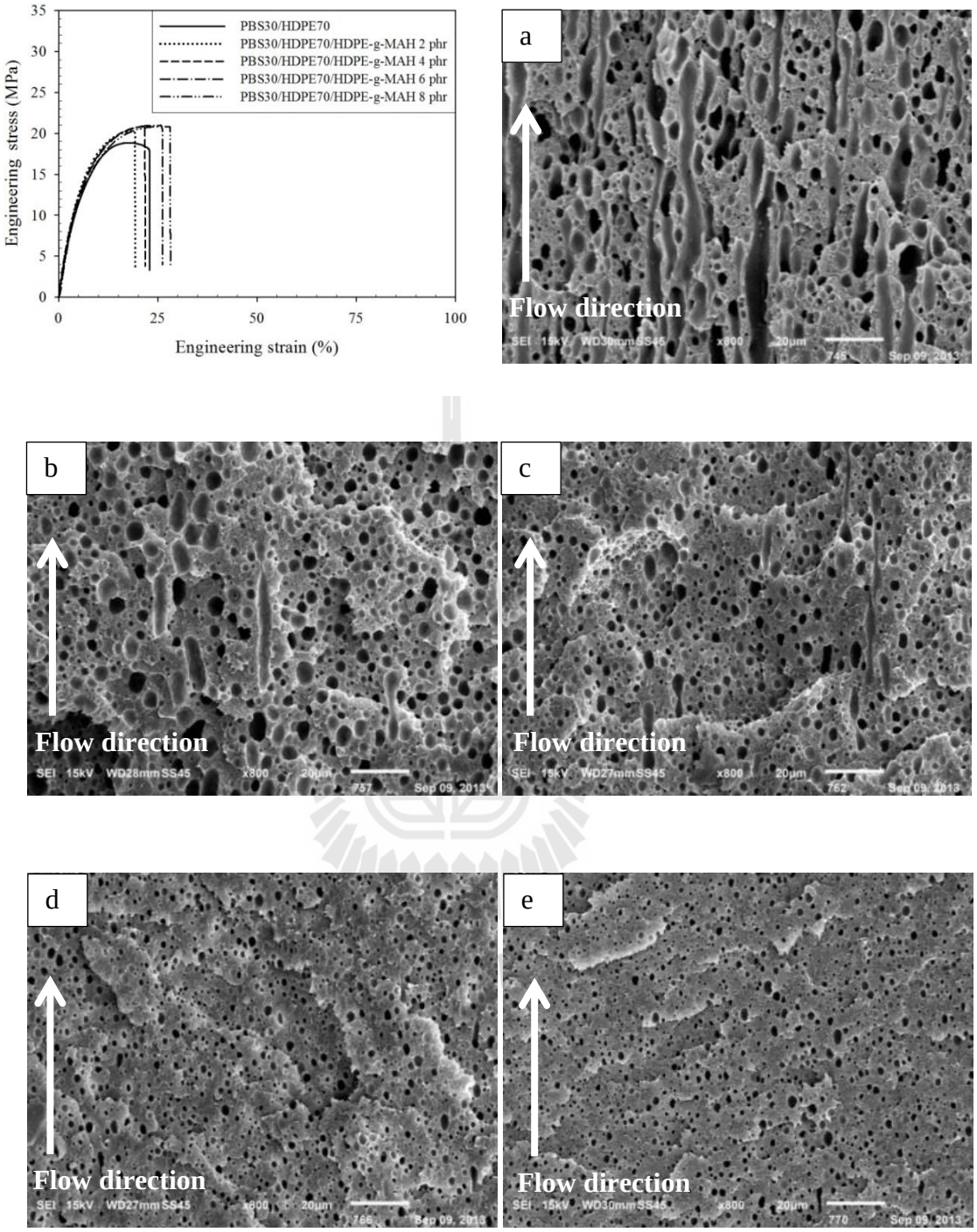

Figure 4.17 Tensile stress-strain curves and SEM micrographs of PBS etching specimens at magnification of x800 of uncompatibilized and compatibilized PBS30/HDPE70 blend with HDPE-g-MAH at 0 phr (a), 2 phr (b), 4 phr (c), 6 phr (d) and 8 phr (e).

As observed from Figure 4.18, stress-strain curve exhibited that the blend compatbilized with 2 phr EPR-g-MAH fractured in a brittle manner at higher strain comparing to uncompatibilized blend. The blend compatbilized with 2 phr EPR-g-MAH ruptured at stress of 19 MPa and 36% strain, as observed from its stress-strain curve in Figure 4.18. Adding 2 phr EPR-g-MAH into PBS/HDPE blend gave rise to more uniform in size and shape of PBS domains, as shown in Figure 4.18(b). Phase morphology of the compatibilized blend included elongated and spherical of PBS domains. In addition, the spherical PBS was finer than that of uncompatibilized blend. In estimation, the PBS particle size was in range of <2μm to 7 μm.

As increasing EPR-g-MAH content to 4 phr, the blend broke at higher stress and strain, as observed from stress-strain curve shown in Figure 4.18. The blend fractured at stress of 18 MPa and strain of 46%. The blend fractured at higher strain indicated that the blend was tougher. Phase morphology of the blend compatibilized with 4 phr EPR-g-MAH is displayed in Figure 4.18(c). It revealed that the size of spherical PBS did not further decrease. The size of PBS domain was in a size range of <2μm to 8 μm. However, it illustrates that the HDPE matrix was more ability to plastically flow.

With adding EPR-g-MAH content to 6 and 8 phr, the compatibilizing effect together with the elastic properties of EPR-g-MAH significantly affected the fracture behavior of the blend, as observed in stress-strain curve shown in Figure 4.18. The blend compatibilized with 6 and 8 phr EPR-g-MAH fractured at 50% and 51% strain, respectively. Their phase morphologies revealed that spherical PBS domain was more uniform in size and shape, as observed in Figure

4.18(d) and Figure 41.8(e), respectively. The approximate domain size was <2μm to 8 μm. Moreover, the ability to plastically flow of HDPE matrix was more pronounced. It confirmed that the toughness of PBS/HDPE blend could be improved using EPR-g-MAH as a compatibilizer.

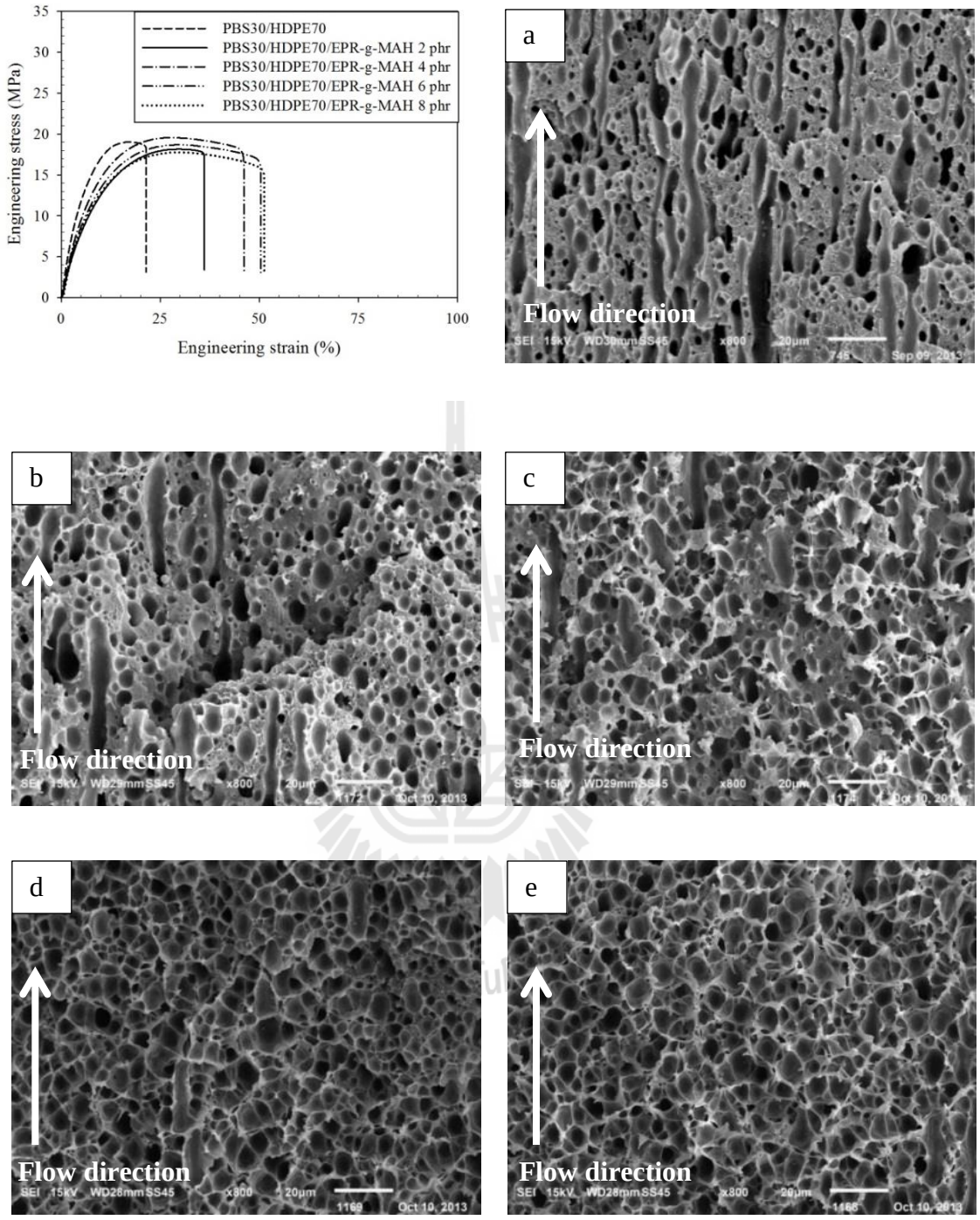

Figure 4.18 Tensile stress-strain curves and SEM micrographs of PBS etching specimens at magnification of x800 of uncompatibilized and compatibilized PBS30/HDPE70 blend with EPR-g-MAH at 0 phr (a), 2 phr (b), 4 phr (c), 6 phr (d) and 8 phr (e).

4.1.2.3 Mechanical properties

Young's modulus of uncompatibilized and compatibilized PBS30/HDPE70 blends at various contents of HDPE-g-MAH and EPR-g-MAH is presented in Figure 4.19. Young's modulus of PBS30/HDPE70 compatibilized with HDPE-g-MAH was higher than that of uncompatibilized blend. The addition of 2 phr HDPE-g-MAH led to a slight increase of Young's modulus of the blend. However, there was almost no change in Young's modulus of the blends when HDPE-g-MAH content was more than 2 phr. It was previously reported that the incorporation of PP-g-MAH compatibilizer more than 2 phr resulted in an insignificant improvement in the Young's modulus of PET/PP blend (Razak, Inuwa, Hassan and Samsudin, 2013). In contrast, Young's modulus of PBS30/HDPE70 blends compatibilized with EPR-g-MAH was lower than that of uncompatibilized blend. Addition of EPR-g-MAH into PBS30/HDPE70 blends resulted in gradual decrease of Young's modulus. This might be due to the elastic characteristic of EPR-g-MAH. Naturally, EPR-g-MAH is rubbery at room temperature which has low Young's modulus with high elasticity. Therefore, adding EPR-g-MAH bring about an inclusion of rubbery amorphous phase. Therefore, the Young's modulus of the PBS30/HDPE70 blends diminished.

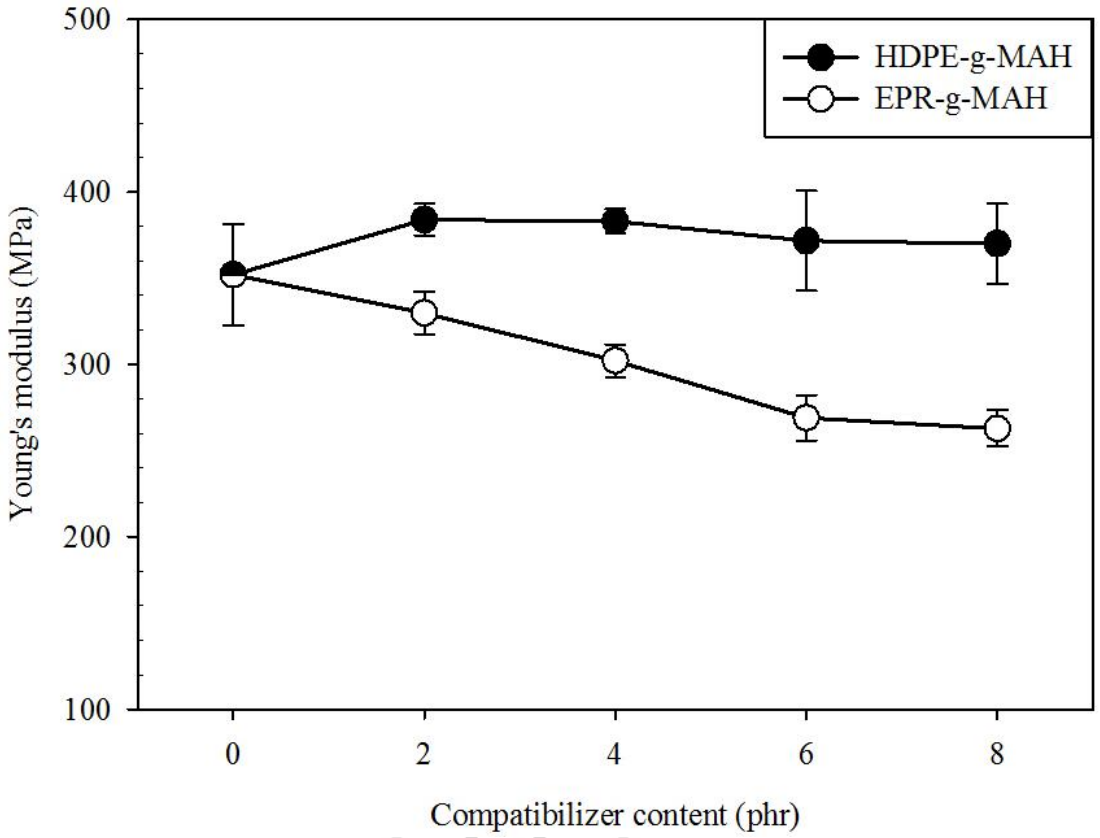

Figure 4.19 Plot of Young's modulus of PBS30/HDPE70 blends at various contents of HDPE-g-MAH and EPR-g-MAH.

Figure 4.20 illustrates that addition 2 phr HDPE-g-MAH led to an insignificant decrease of elongation at break of the blend. However, the elongation at break of the blend tended to increase as adding more HDPE-g-MAH. This had been accounted for by miscibility between HDPE-g-MAH and HDPE phase. Also, it might be due to chemical reactions between reactive functional groups of HDPE-g-MAH with ester groups of PBS, as proposed in Figure 4.22(a) (Pracella, Rolla, Chionna and Galeski, 2002). In addition, these results corresponded well with the results of Young's modulus as previously shown in Figure 4.19. The increase in elongation at break was previously observed in the system of PET/HDPE blend of which PE-g-

MAH was used as a compatibilizer (Boutevin, Lusinchi, Pietrasanta and Robin, 1996). It was found that using PE-g-MAH enhanced the elongation at break of PET/HDPE blend to 150% as compared to PET/HDPE blend without PE-g-MAH.

For the PBS30/HDPE70 compatibilized with EPR-g-MAH, elongation at break of the blend increased continuously with increasing EPR-g-MAH content from 2 phr to 6 phr. As increasing EPR-g-MAH content to 8 phr, the elongation at break of the blend did not give rise to any increment. The enhancement of the elongation at break attributed to the better adhesion of PBS and HDPE phase. Possibly, the improvement of elongation at break of blend was a consequence of a high ability to deform before breaking of EPR-g-MAH elastomer. It was previously reported that the significant improvement of elongation at break of PET/HDPE blend could be achieved using maleic anhydride elastomer compatibilizer (Dimitrova *et al*., 2000).

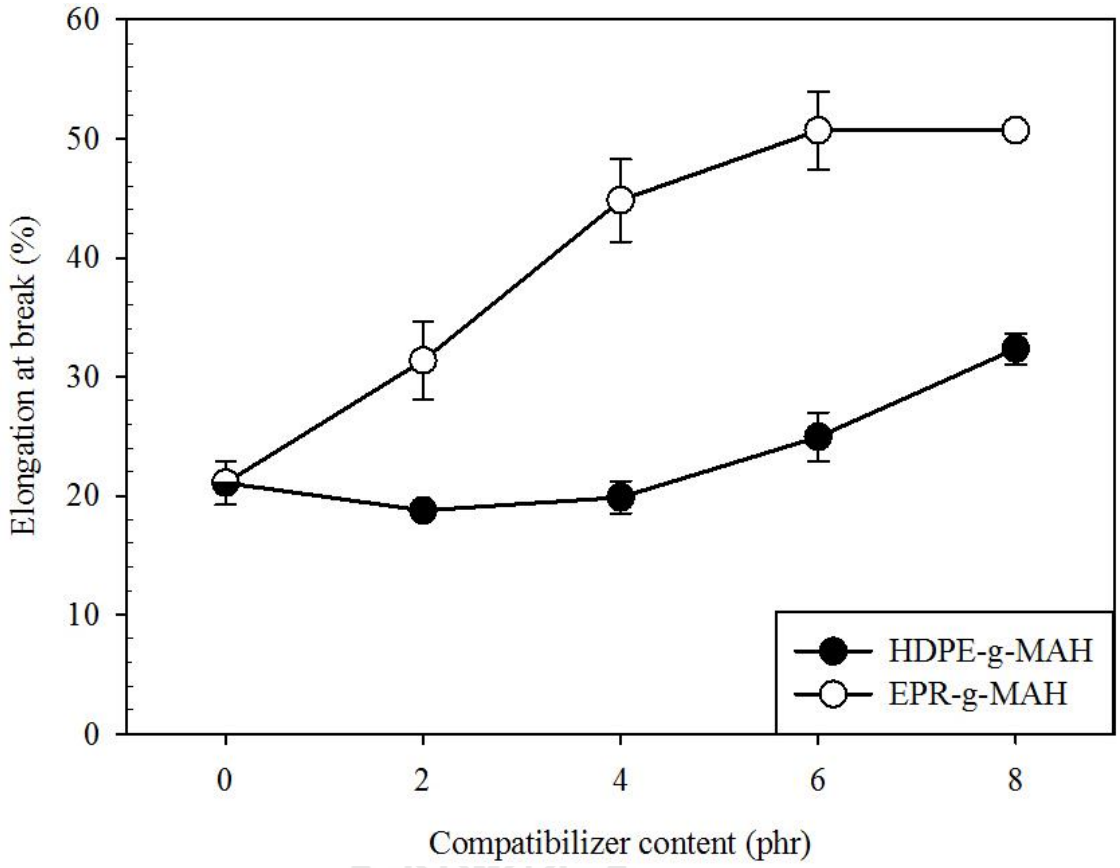

Figure 4.20 Plot of elongation at break of PBS30/HDPE70 blend at various contents of HDPE-g-MAH and EPR-g-MAH.

Figure 4.21 shows the tensile strength of uncompatibilized and compatibilized PBS30/HDPE70 blends at various contents of HDPE-g-MAH. It illustrates that tensile strength of PBS30/HDPE70 compatibilized with HDPE-g-MAH was higher than that of the uncompatibilized blend. Adding 2 phr HDPE-g-MAH into PBS30/HDPE70 blend made the tensile strength of the blend increased. However, the tensile strength of the blend did insignificantly change with adding more HDPE-g-MAH. The slight improvement of tensile strength might be due to a better interfacial adhesion between PBS domain and HDPE matrix. The better adhesion was promoted

by H-bonding between maleic anhydride group of HDPE-g-MAH and ester groups of PBS (Martínez, Benavides and Guerrero, 2007; Lusinchi *et al*., 2001). In addition, the interchain diffusion between HDPE matrix and HDPE backbones of HDPE-g-MA might be occurred due to the solubility parameter of HDPE-g-MAH is approximate the same as that of HDPE (Sewda and Maiti, 2009; Nashar, Maziad and Sadek, 2008; Chiu and Hsiao, 2006). The solubility parameter of HDPE-g-MAH and HDPE is 17.6 $J^{1/2}/cm^{3/2}$ and 17.5 $J^{1/2}/cm^{3/2}$, respectively (Seo, Park, Dao, and Jeong, 2013). The schematic of mechanism for compatibility enhancement between PBS and HDPE using HDPE-g-MAH is presented in Figure 4.22(a).

Tensile strength of the blend compatibilized with EPR-g-MAH is presented in Figure 4.21. It illustrates that the tensile strength of the compatibilized blend was higher than that of uncompatibilized blend. Addition of 2 to 4 phr EPR-g-MAH into PBS30/HDPE70 blend led to an increase of tensile strength of the blend. As increasing EPR-g-MAH content to 6 phr, the tensile strength of the blend insignificantly increased. The improvement of tensile strength could be due to the compatibilizing effect of EPR-g-MAH which provided a better adhesion between PBS and HDPE. The better adhesion between PBS and HDPE was a consequence of interaction between active maleic anhydride functional group of EPR-g-MAH with ester groups of PBS and also physical entanglement between HDPE phase and ethylene-propylene copolymer within amorphous phase of the blend as proposed in Figure 4.22(b). However, the tensile strength of the blend was not significantly improved with adding 8 phr EPR-g-MAH. In addition, tensile properties of PBS30/HDPE70 blends compatibilized with HDPE-g-MAH and EPR-g-MAH were summarized in Table 4.11.

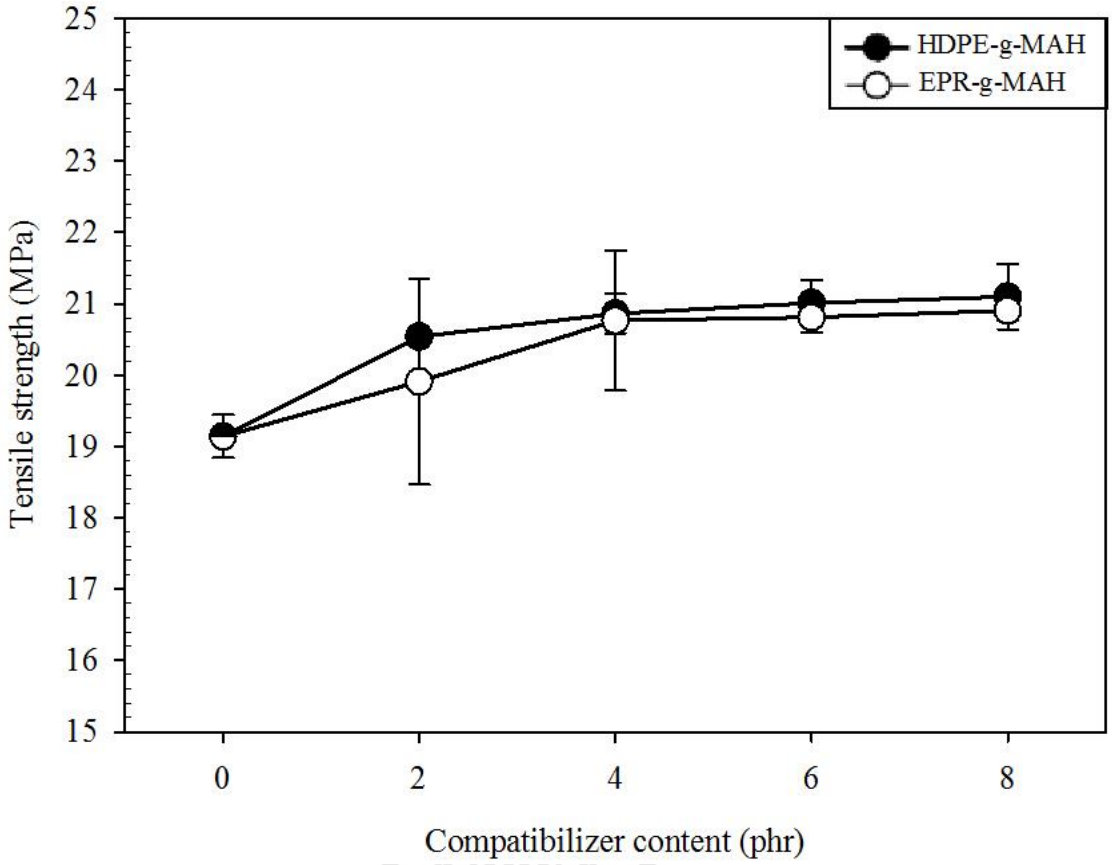

Figure 4.21 Plot of tensile strength of PBS30/HDPE70 blend at various contents of HDPE-g-MAH (a) and EPR-g-MAH (b).

Table 4.11 Tensile properties of PBS30/HDPE70 blend at various contents of HDPE-g-MAH and EPR-g-MAH.

Compatibilizer content (phr)	Young's modulus (MPa)		Elongation at break (%)		Tensile strength (MPa)	
	HDPE-g-MAH	EPR-g-MAH	HDPE-g-MAH	EPR-g-MAH	HDPE-g-MAH	EPR-g-MAH
0 phr	359.1±29.1		21.1±1.8		19.1±0.3	
2 phr	383.9±9.2	329.8±12.3	18.8±0.3	31.4±3.2	20.5±0.1	19.9±1.4
4 phr	383.0±6.9	302.1±9.56	19.9±1.3	44.8±3.4	20.9±0.3	20.8±1.0
6 phr	371.7±28.9	268.8±13.1	24.9±2.0	50.7±3.2	21.0±0.3	20.8±0.2
8 phr	370.0±23.0	262.7±10.6	32.3±1.3	50.70.7	21.1±0.4	20.9±0.1

(a) HDPE-g-MAH

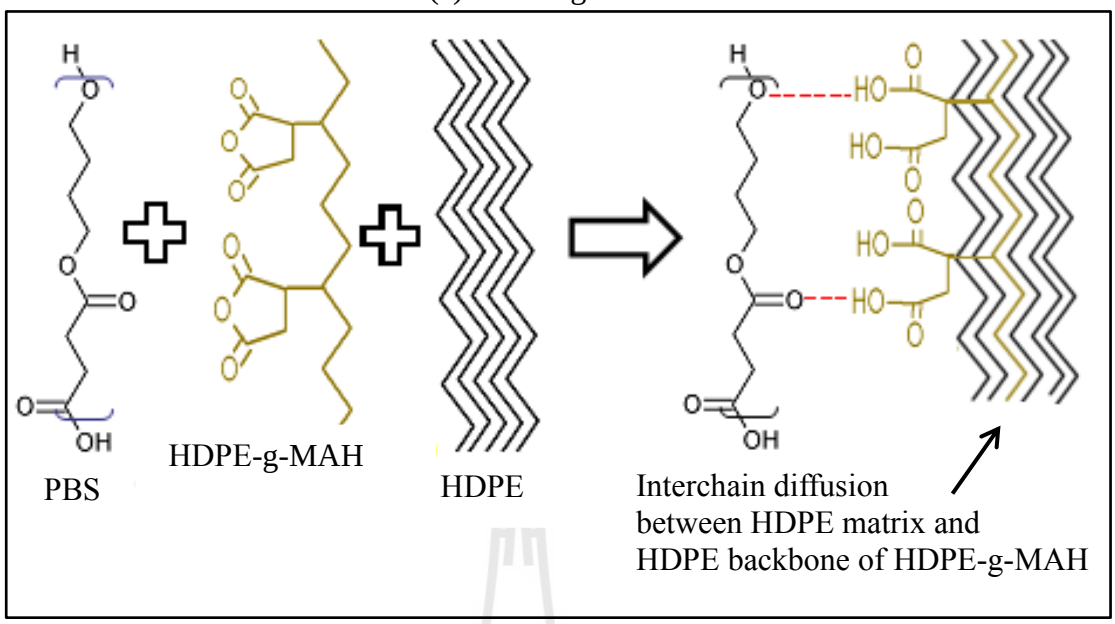

(b) EPR-g-MAH

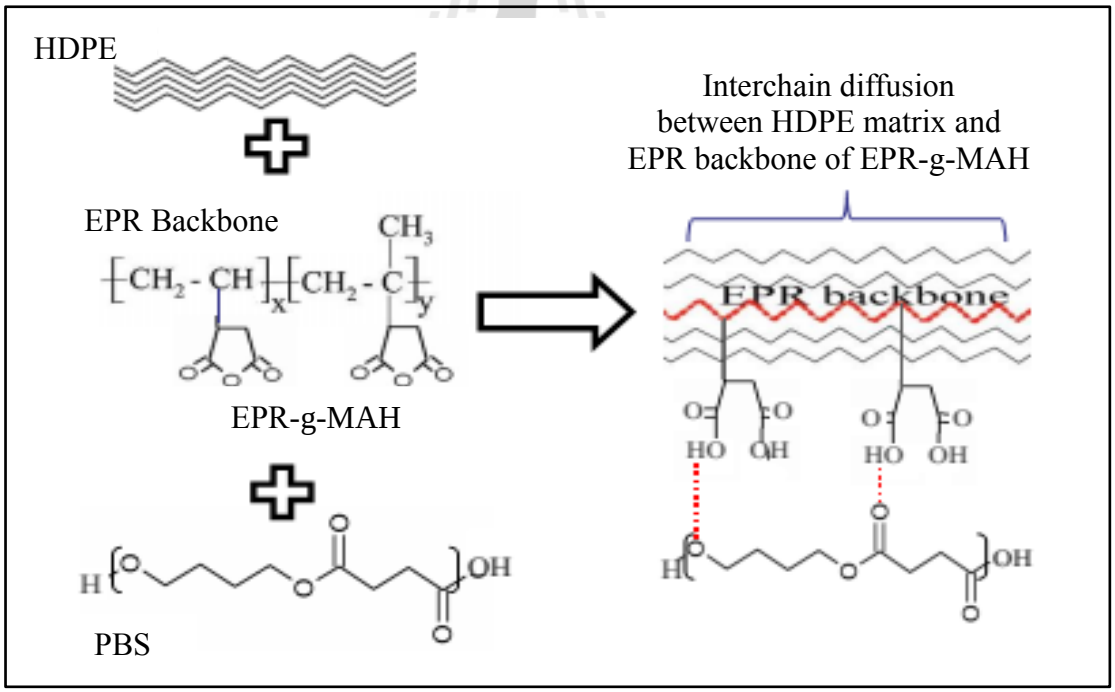

Figure 4.22 Schematic of mechanism for compatibility enhancement between PBS and HDPE using HDPE-g-MAH (a) (Adapted from Pracella, Rolla, Chionna and Galeski, 2002) and EPR-g-MAH (b) (Adapted from Chow, Bakar, Ishak, Kocsis and Ishiaku, 2005) as compatibilizers.

From the tensile results of using HDPE-g-MAH and EPR-g-MAH as compatibilizers, it illustrates that HDPE-g-MAH was more effective for improving Young's modulus of the blend while EPR-g-MAH improved toughness of the blend better than HDPE-g-MAH. The better improvement in toughness of the blend using EPR-g-MAH might be due to a high elasticity of EPR-g-MAH. This similar result was previously reported that elastomeric compatibilizer (SEBS-g-MAH) was more effective for improving elongation at break of PET/PP blend than semi-crystalline compatibilizer (LLDPE-g-MAH) (Papadopoulou, and Kalfoglou, 2000). Comparatively, the efficiency of HDPE-g-MAH and EPR-g-MAH for improving tensile strength and stress at break of the blend was comparable.

For flexural properties, flexural modulus of uncompatibilized and compatibilized PBS30/HDPE70 blends at various contents of HDPE-g-MAH and EPR-g-MAH is presented in Figure 4.23. Flexural modulus of PBS30/HDPE70 blend comaptibilized with HDPE-g-MAH was close to that of uncomaptibilized PBS30/HDPE70 blend. Moreover, the adding more HDPE-g-MAH content did not give rise to further improvement of flexural modulus. On the other hand, flexural modulus of the blend compatibilized with EPR-g-MAH was lower than that of uncompatibilized blend. Furthermore, the more content of EPR-g-MAH, the more decrease in flexural modulus of the blend. The decreasing flexural modulus of the PBS30/HDPE70 blend compatibilized with EPR-g-MAH was a consequence of elastic behavior of EPR-g-MAH.

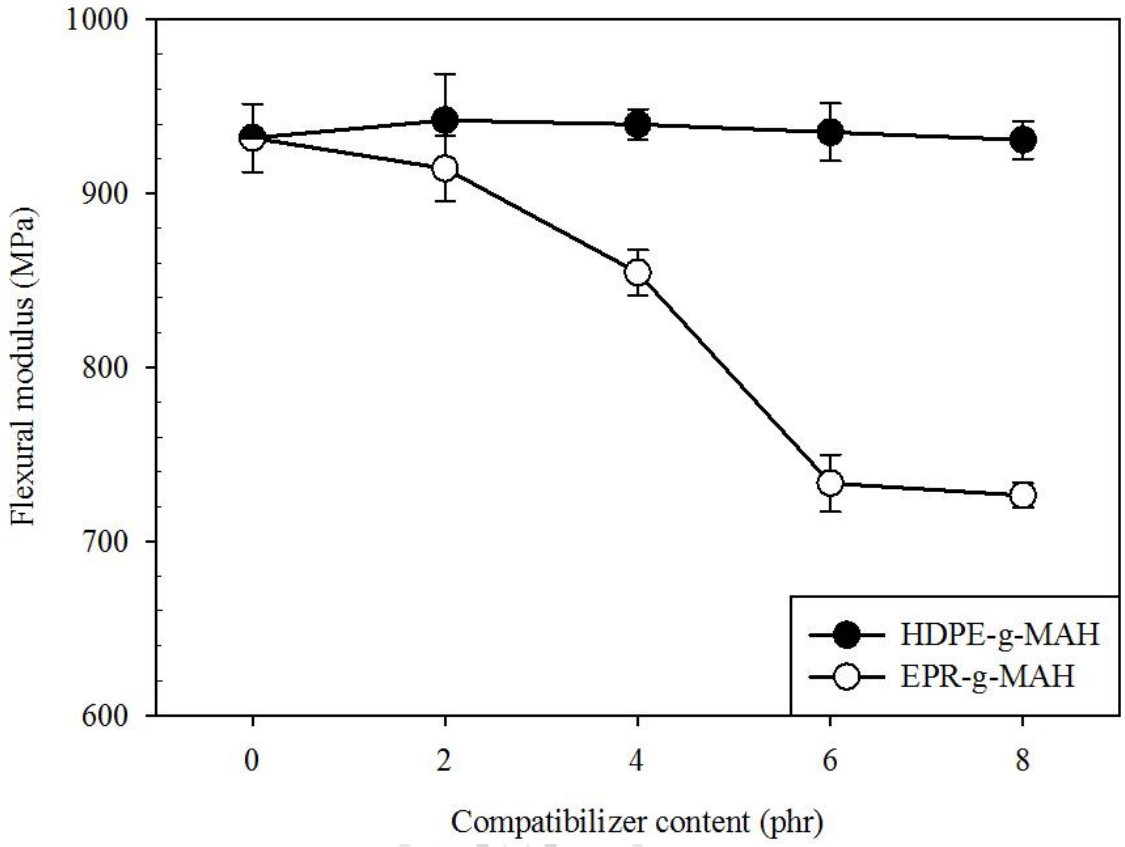

Figure 4.23 Plot of flexural modulus of PBS30/HDPE70 blend at various contents of HDPE-g-MAH and EPR-g-MAH.

Figure 4.24 shows flexural strength of uncompatibilized and compatibilized PBS30/HDPE70 blend at various contents of HDPE-g-MAH and EPR-g-MAH. It reveals that flexural strength of PBS30/HDPE70 compatibilized with HDPE-g-MAH was slightly lower than that of uncompatbilized blend. In addition, addition of HDPE-g-MAH did not much affect flexural strength of the compatibilized blend. The flexural strength of the compatibilized blend decreased insignificantly with increasing HDPE-g-MAH content.

For the blend compatibilized with EPR-g-MAH, flexural strength of compatibilized blend was lower than that of uncompatibilized blend.

Adding EPR-g-MAH into PBS30/HDPE70 blend led to a decrease of flexural strength of the blend and flexural strength of the blend decreased with adding more EPR-g-MAH content. In addition, flexural properties of the blend were listed in Table 4.12.

In comparison, HDPE-g-MAH seems to be more effective for maintaining both the flexural modulus and flexural strength of PBS30/HDPE70 blend than EPR-g-MAH.

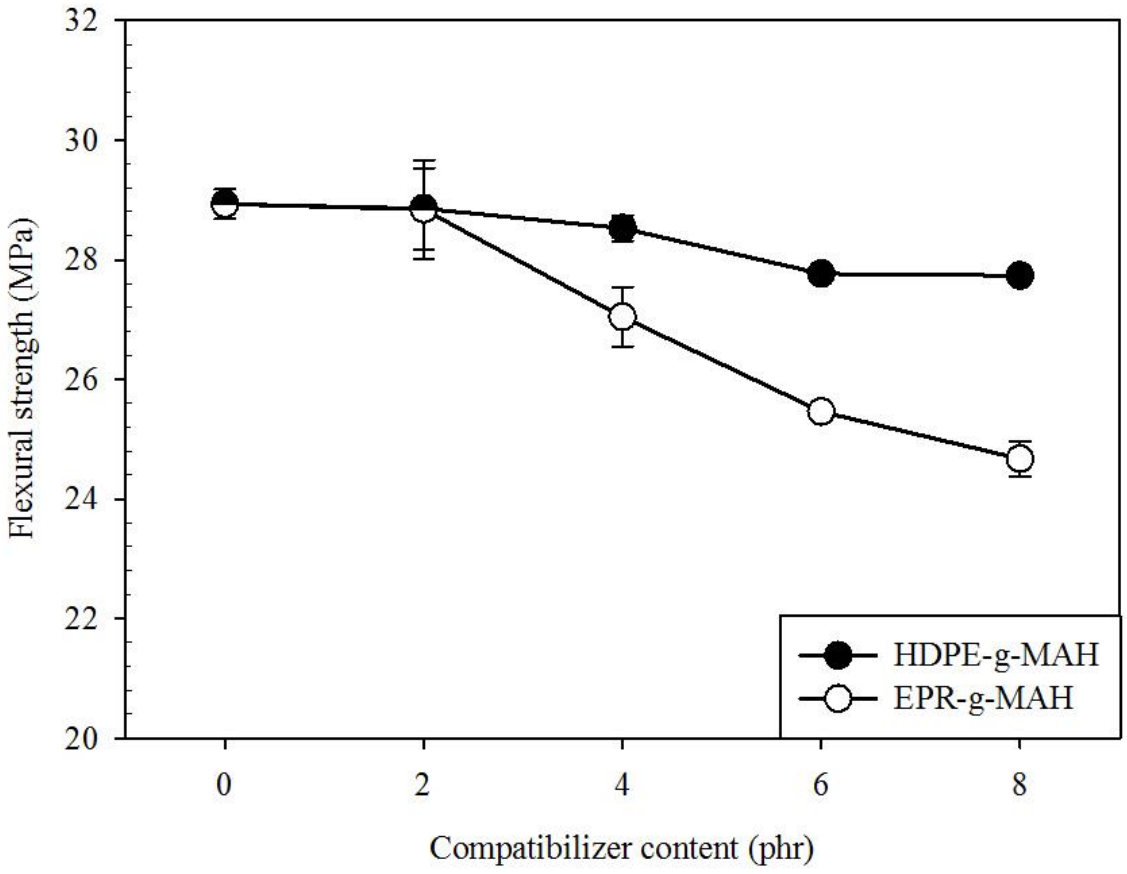

Figure 4.24 Plot of flexural strength of PBS30/HDPE70 blend at various contents of HDPE-g-MAH and EPR-g-MAH.

Table 4.12 Flexural properties of PBS30/HDPE70 blend at various contents of HDPE-g-MAH and EPR-g-MAH.

Compatibilizer content (phr)	Flexural strength (MPa)		Flexural modulus (MPa)	
	HDPE-g-MAH	EPR-g-MAH	HDPE-g-MAH	EPR-g-MAH
0 phr	28.9±0.3		931.9±19.5	
2 phr	28.8±0.7	28.8±0.8	942.1±26.7	914.3±18.8
4 phr	28.5±0.2	27.0±0.5	939.8±8.9	854.5±12.9
6 phr	27.8±0.1	25.4±0.1	935.3±16.6	733.4±16.4
8 phr	27.7±0.1	24.7±0.3	930.9±10.8	726.4±7.1

Unnotched Izod impact strength of PBS30/HDPE70 blend at various contents of HDPE-g-MAH and EPR-g-MAH is presented in Table 4.13. It shows that impact strength of PBS30/HDPE70 blend compatibilized with HDPE-g-MAH was higher than that of uncompatibilized blend. In addition, the impact strength of the blend tended to further increase with increasing HDPE-g-MAH content. Particularly, at 8 phr HDPE-g-MAH, the impact strength of compatibilized blend was beyond the instrumentation limit of 135 kJ/m^2. The increase in impact strength corresponded well with the finer and more uniform in size and shape of PBS dispersed in the blend compatibilized with HDPE-g-MAH as shown previously in Figure 4.17.

Similarly, the impact strength of PBS30/HDPE70 compatibilized with EPR-g-MAH was also improved after the adding of EPR-g-MAH and the unnotched impact strength increased with increasing EPR-g-MAH content. Particularly at 6 phr and 8 phr EPR-g-MAH, the impact strength was greatly improved. The blend sample did not break within an instrumentation limit. The greatly improved in impact strength of PBS30/HDPE70 blend compatibilized with EPR-g-MAH strongly correlated with the finer and more uniform of PBS dispersed phase in the blend compatibilized with EPR-g-MAH as shown in Figure 4.18. Especially, the fibrillation of HDPE matrix was observed in the blend contained 4 phr, 6 phr and 8 phr of EPR-g-MAH. This fibrillation indicated significant improvement in the toughness of the blend. Therefore, it implied that EPR-g-MAH act as a compatibilizer and also a toughener for PBS30/HDPE70 blend.

In summary, both HDPE-g-MAH and EPR-g-MAH were an effective compatibilizer to enhance the impact strength of PBS30/HDPE70 blend.

Comparatively, at the same content of compatibilizer, the compatibilization efficiency of EPR-g-MAH was more effective for developing the impact strength of the PBS30/HDPE7 blend than HDPE-g-MAH.

Table 4.13 Unnotched Izod impact strength of PBS30/HDPE70 blend at various contents of HDPE-g-MAH and EPR-g-MAH.

Compatbilizer content (phr)	Unnotched Izod impact strength (kJ/m2)	
	HDPE-g-MAH	EPR-g-MAH
0	26.4±1.1	26.4±1.1
2	34.2±0.5	38.3±0.8
4	39.7±0.7	45.6±1.2
6	45.7±1.3	Not break
8	Not break	Not break

4.1.2.4 Thermal degradation temperature and weight loss

Figure 4.25 (a) shows TGA thermogram of uncompatibilized and compatibilized PBS30/HDPE70 blend with HDPE-g-MAH. From the curve, it illustrates that uncompatibilized PBS30/HDPE70 blend exhibited two thermal transitions. The first transitions occurred at the temperature range of 355-430°C corresponding to the degradation of PBS. The second transitions occurred within a temperature range of 427-516°C, due to HDPE degradation. Addition of 2 phr HDPE-g-MAH into PBS30/HDPE70 blends made the PBS phase degraded at temperature range of 356-432°C and HDPE phase degrade at temperature range of 427-516°C. As increase HDPE-g-MAH content to 4, 6 and 8 phr, PBS phase degraded at slightly higher temperature range at 357-432°C, 358-434°C and 358-436°C, respectively. On

the other hand, at 4, 6, and 8 phr HDPE-MAH, HDPE phase degrade at temperature range of 430-516°C, 430-517°C and 430-518°C, respectively. The TGA curves illustrate that the adding HDPE-g-MAH into PBS30/HDPE70 did not much affect the degradation temperature range of both PBS and HDPE phase.

Figure 4.25 (b) shows DTGA thermogram of uncompatibilized and compatibilized PBS30/HDPE70 blend with various contents of HDPE-g-MAH and EPR-g-MAH. It illustrates that uncompatibilized PBS30/HDPE70 blend exhibited two thermal degradation peaks. The first degradation peak occurred at a temperature of 407°C corresponding to the degradation of PBS. The second degradation peak occurred at a temperature of 489°C, due to HDPE degradation. Adding 2 phr HDPE-g-MAH into PBS30/HDPE70 blends did not affect degradation temperature of PBS phase while degradation temperature of HDPE phase insignificantly increased. As increasing HDPE-g-MAH content to 4 and 6 phr, the degradation temperature of PBS domain slightly increased whereas the degradation temperature of HDPE matrix remained constant. However, adding 8 phr HDPE-g-MAH made the degradation temperature of PBS domain increased 3ºC whereas the degradation temperature of HDPE matrix insignificantly decreased.

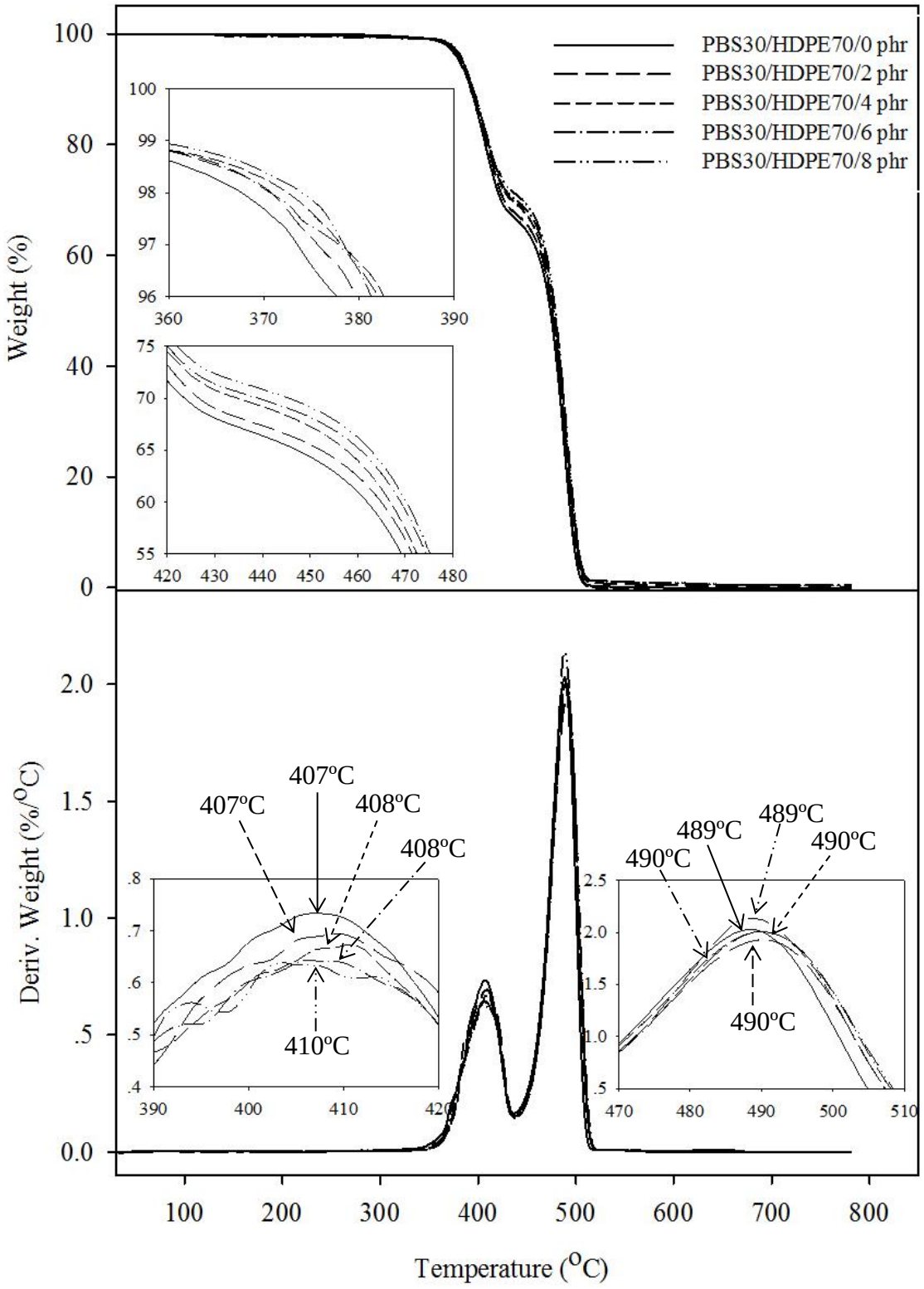

Figure 4.25 TGA and DTGA thermograms of PBS30/HDPE70 blend at various contents of HDPE-g-MAH.

Figure 4.26 (a) shows TGA curve of PBS30/HDPE70 compatibilzed with EPR-g-MAH. From the curve, it illustrates that the compatibilized PBS30/HDPE70 blend with 2 phr of EPR-g-MAH exhibited two thermally degradation. The first transitions occurred at the temperature range of 358-433°C corresponding to the degradation of PBS. The second transitions occurred within a temperature range of 430-516°C, due to HDPE degradation. Addition of 4 phr EPR-g-MAH into PBS30/HDPE70 blends made the PBS phase degraded at temperature range of 358-433°C and HDPE phase degrade at temperature range of 431-518°C. As increasing EPR-g-MAH content to 6 and 8 phr, PBS phase degraded at slightly higher temperature range of 359-433°C and 359-434°C respectively. On the other hand, at 6, and 8 phr EPR-MAH, HDPE phase degraded at temperature range of 431-518°C and 432-518°C, respectively. The TGA curves illustrate that the adding EPR-g-MAH into PBS30/HDPE70 did not much affect the degradation temperature range of both PBS and HDPE phase.

Figure 4.26 (b) shows DTGA curve of PBS30/HDPE70 compatibilzed with EPR-g-MAH. From the curve, it illustrates that adding 2 phr EPR-g-MAH into PBS30/HDPE70 blends greatly affect degradation temperature of both PBS and HDPE phase. The degradation temperature of PBS phase was improved to 8°C. The improvement of thermal stability of PBS domain could be attributed to a finer size and better dispersion of PBS domain as observed from SEM images in Figure 4.19 (Khalf, Nashar and. Maziad, 2010). Also, degradation temperature of HDPE phase was improved to 6°C after adding 2 phr HDPE-g-MAH. However, increasing EPR-g-MAH content insignificantly influenced degradation temperature of both PBS domain and HDPE matrix.

In summarization, EPR-g-MAH was more effective compatibilizer than HDPE-g-MAH for improving thermal stability of PBS30/HDPE70 blend than HDPE-g-MAH. In addition, the temperature range for degradation ($T_{d,range}$), peak temperatures (T_{peak}) and weight loss of PBS30/HDPE70 blends at various contents of HDPE-g-MAH and EPR-g-MAH are summarized in Table 4.14.

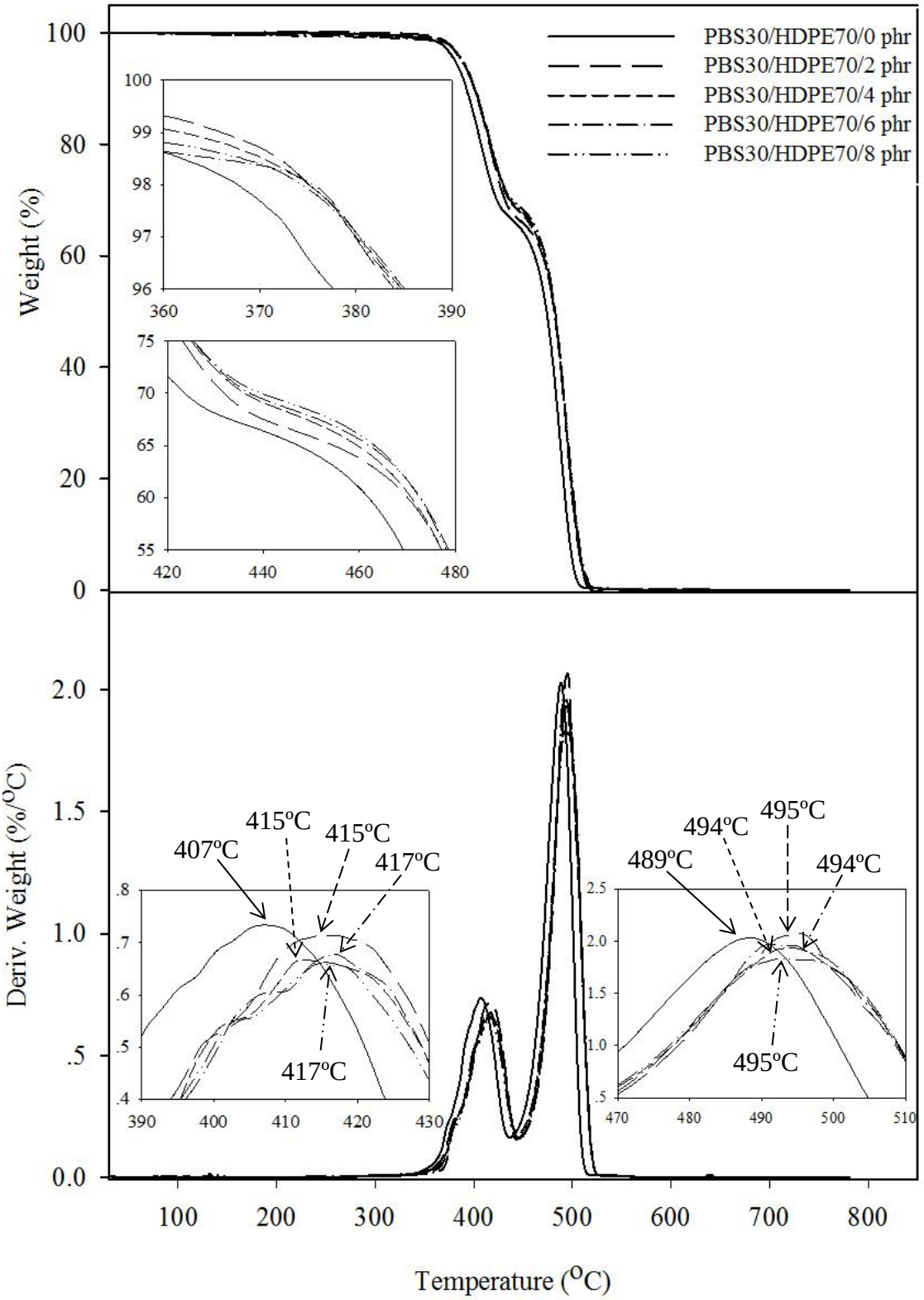

Figure 4.26 TGA and DTGA thermograms of PBS30/HDPE70 blend at various contents of EPR-g-MAH.

Table 4.14 The temperature range for degradation ($T_{d,range)}$, peak temperatures (T_{peak}) and weight loss of PBS30/HDPE70 blend at various contents of HDPE-g-MAH and EPR-g-MAH.

Compatibilizer content	PBS domain						HDPE matrix					
	HDPE-g-MAH			EPR-g-MAH			HDPE-g-MAH			EPR-g-MAH		
	T_{peak} (ºC)	Weight loss (%)	$T_{d,range}$ (ºC)	T_{peak} (ºC)	Weight loss (%)	$T_{d,range}$ (ºC)	T_{peak} (ºC)	Weight loss (%)	$T_{d,range}$ (ºC)	T_{peak} (ºC)	Weight loss (%)	$T_{d,range}$ (ºC)
0 phr	407	29.7	355-430	407	29.7	355-430	489	69.9	427-516	489	69.9	427-516
2 phr	407	28.6	356-432	415	29.1	358-433	490	69.5	427-516	495	68.5	430-516
4 phr	408	28.4	358-434	415	29.2	358-433	490	69.6	430-516	494	68.7	431-518
6 phr	408	28.9	357-432	417	29.7	359-433	490	69.1	430-517	494	68.6	431-518
8 phr	410	28.6	358-436	417	28.5	359-434	489	69.4	430-518	495	69.7	432-518

4.1.2.5 Melting and crystallizing behavior

DSC curves from the first heating scan of PBS30/HDPE70 blends at various contents of HDPE-g-MAH and EPR-g-MAH are shown in Figure 4.27 (a) and Figure 4.27 (b), respectively. As shown in Figure 4.27 (a), the DSC curve of uncompatibilized PBS30/HDPE70 blend exhibited a broad exothermic peak at 89.9°C and two endothermic peaks at 108.8°C and at 127.7°C, respectively. The broad exothermic peak was caused by the cold-crystallization of PBS (Yasuniwa, Tsubakihara, Satou and Iura, 2005). Yoo and Im (1999) also found a broad exothermic peak during heating scan of PBS at around 93.0°C, due to the thermal history during cooling and reheating. The first endothermic peak was due to melting of PBS phase and the second endothermic peak corresponded to the melting of HDPE phase. Adding 2 phr HDPE-g-MAH into PBS30/HDPE70 blend made the broad exothermic peak of PBS shift to a slightly higher temperature while the melting peak of PBS and HDPE phase insignificantly changed. As increasing HDPE-g-MAH content to 4, 6 and 8 phr, the broad exothermic peak of PBS, the melting peak of PBS and HDPE phase almost unchanged.

Figure 4.27 (b) shows DSC curves from the first heating scan of PBS30/HDPE70 blends at various contents of EPR-g-MAH. It illustrates that adding 2 phr EPR-g-MAH made the exothermic peak of PBS, the melting peak of PBS and HDPE phase shift to slightly higher temperature. Noticeably, a small shoulder was observed at around 103°C in the blend compatibilized with EPR-g-MAH. This shoulder corresponded to the difference in size of PBS after adding EPR-g-MAH. As increasing EPR-g-MAH to 4, 6 and 8 phr, the melting behavior of PBS and HDPE phase during the first heating scan was unalterable. These results indicated

that using HDPE-g-MAH and EPR-g-MAH as a compatibilizer for PBS30/HDPE70 blend slightly affected the melting temperature of PBS and HDPE.

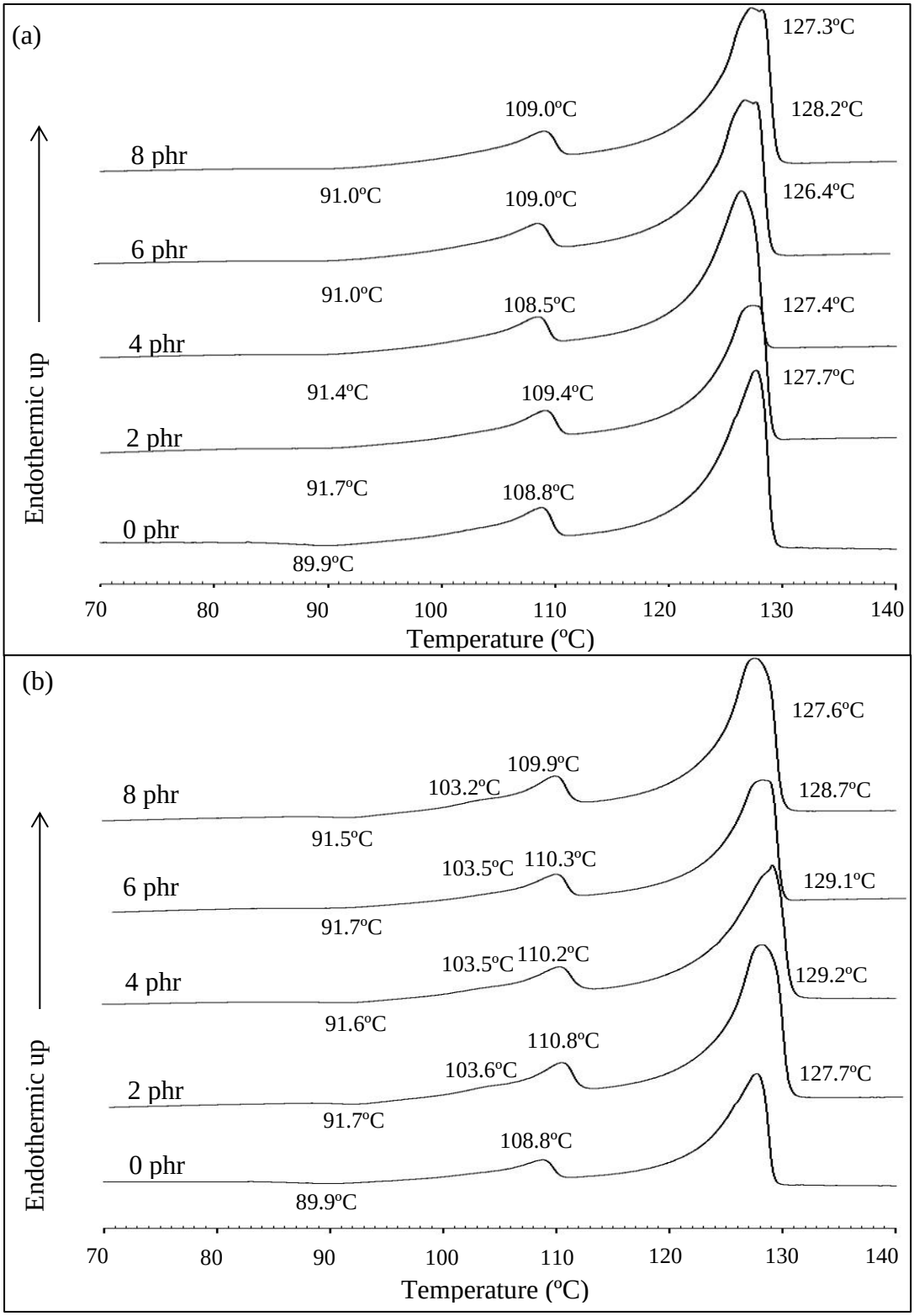

Figure 4.27 DSC curves from the first heating scan of PBS30/HDPE70 blends at various contents of HDPE-g-MAH (a) and EPR-g-MAH (b).

Figure 4.28 (a) shows the DSC curves from the cooling scan of PBS30/HDPE70 blends at various contents of HDPE-g-MAH. The DSC curve of uncompatibilized PBS30/HDPE70 blend shows a crystallization temperature of HDPE and PBS at 116.9 °C and 85.5°C, respectively. With adding 2 phr of HDPE-g-MAH, the crystallization temperature of HDPE increased slightly whereas the crystallization temperature of PBS decreased slightly. As increasing HDPE-g-MAH content to 4, 6 and 8 phr, the crystallization temperature of HDPE and PBS insignificantly changed.

Figure 4.28 (b) shows the DSC curves from the cooling scan of PBS30/HDPE70 blends at various contents of EPR-g-MAH. It illustrates that adding 2 phr of EPR-g-MAH did not much affect the crystallization temperature of HDPE. On the other hand, adding 2 phr of EPR-g-MAH into PBS30/HDPE70 blend gave rise to a retardation of crystallization process of PBS resulting in the lower crystallization temperature of PBS. However, increasing EPR-g-MAH content did insignificant affect the crystallization temperature of HDPE and PBS phase.

These results indicated that the using HDPE-g-MAH as a compatibilizer in PBS30/HDPE70 blend hardly affected the crystallization behavior of PBS and HDPE phase while EPR-g-MAH affected the crystallization behavior of PBS phase by which the crystallization temperature of PBS was lower with adding more EPR-g-MAH content. However, HDPE-g-MAH and EPR-g-MAH content did not much influence the crystallization temperature of PBS and HDPE phase.

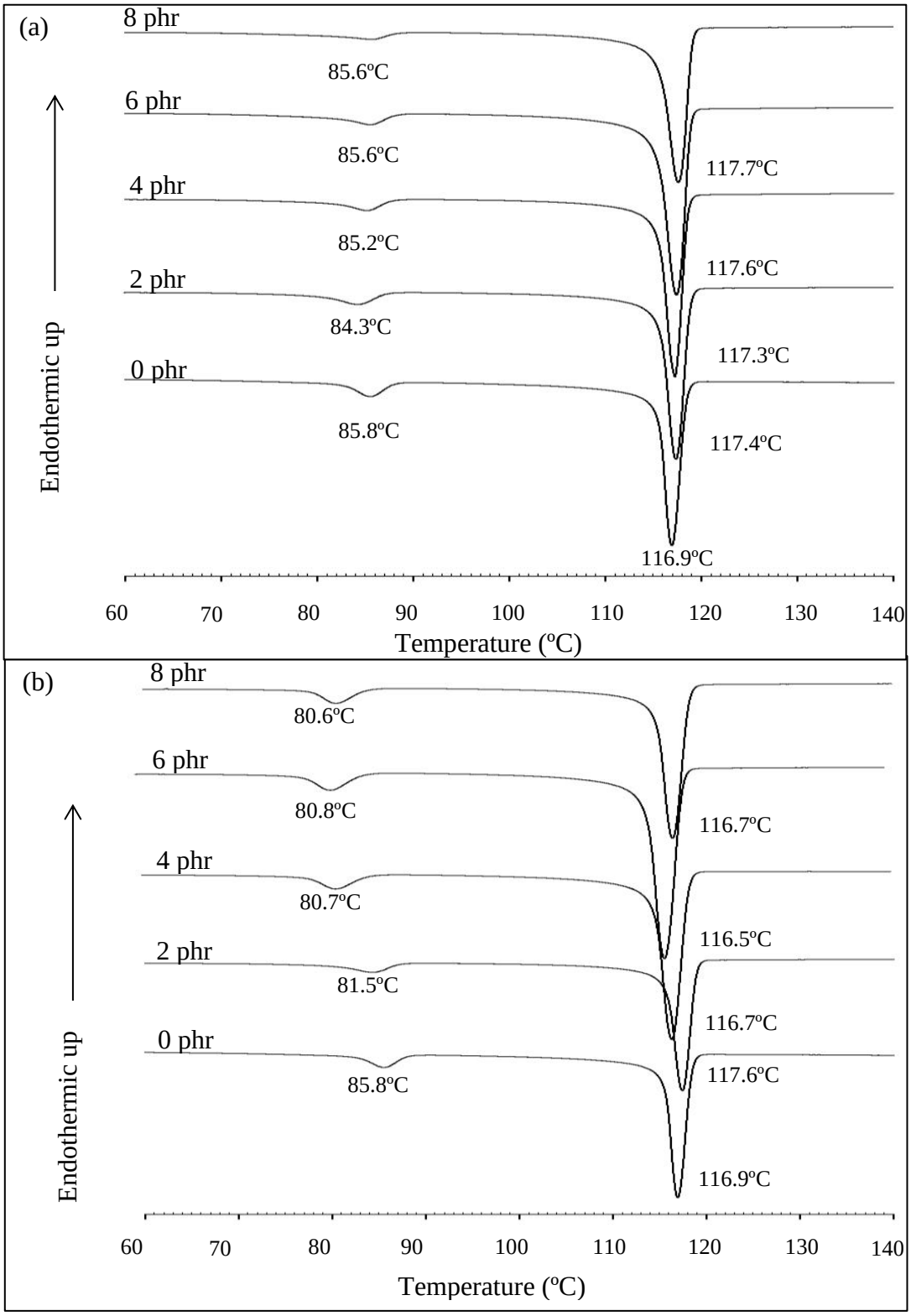

Figure 4.28 DSC curves from cooling scan of PBS30/HDPE70 blend at various contents of HDPE-g-MAH (a) and EPR-g-MAH (b).

Figure 4.29 (a) shows the DSC curves from the second heating scan of PBS30/HDPE70 blends at various contents of HDPE-g-MAH. The DSC curve of uncompatibilized PBS30/HDPE70 blend shows double endothermic peak of PBS at low temperature of 99.6°C and at high temperature of 108.2°C. Also, it shows melting peak of HDPE at 128.3°C. The melting behavior of PBS during the second heating scan could be explained by the co-existence of two crystal forms, β and α form. Metastable β crystal form melted first at low temperature following by α crystal form melted at higher temperature. The compatibilized PBS30/HDPE70 blend with 2, 4, 6 and 8 phr HDPE-g-MAH did insignificantly influence the melting temperature of PBS at both low and high temperature. Also, adding HDPE-g-MAH 2, 4, 6 and 8 phr did insignificantly affect the melting temperature of HDPE phase.

Figure 4.29 (b) shows DSC curves from the second heating scan of PBS30/HDPE70 blends at various contents of EPR-g-MAH. It demonstrates that adding 2 phr EPR-g-MAH resulted in a slight decrease of melting temperature of lower melting peak of PBS whereas a melting temperature at high temperature of PBS phase insignificantly changed. Similar with the first heating scan, the curve of the blend compatibilized with 2 phr EPR-g-MAH still exhibited a small shoulder occurred at 106.7°C prior to a higher melting peak of PBS. This might be a consequence of the difference in size of PBS crystallites. Also, adding 2 phr EPR-g-MAH did not influence the melting temperature of HDPE phase. With adding more EPR-g-MAH, EPR-g-MAH did insignificantly affect the melting behavior including melting at low and high temperature of PBS phase and also melting temperature of HDPE phase.

These results indicated that using HDPE-g-MAH as a compatibilizer for PBS30/HDPE70 blend hardly affected the melting temperature at the low and high temperature of PBS and also the melting temperature of HDPE phase. On the other hand, EPR-g-MAH insignificantly influenced the melting temperature at high temperature of PBS, and the melting temperature of HDPE. However, EPR-g-MAH made the melting temperature at low temperature of PBS slightly decreased. Moreover, the DSC curves of the blend compatibilized with EPR-g-MAH exhibited a shoulder occurring prior to a melting peak at high temperature of PBS phase.

Additionally, melting temperature, cold crystallization temperature from the first heating scan and crystallization temperature of PBS30/HDPE70 blend at various contents of HDPE-g-MAH and EPR-g-MAH are summarized in Table 4.15.

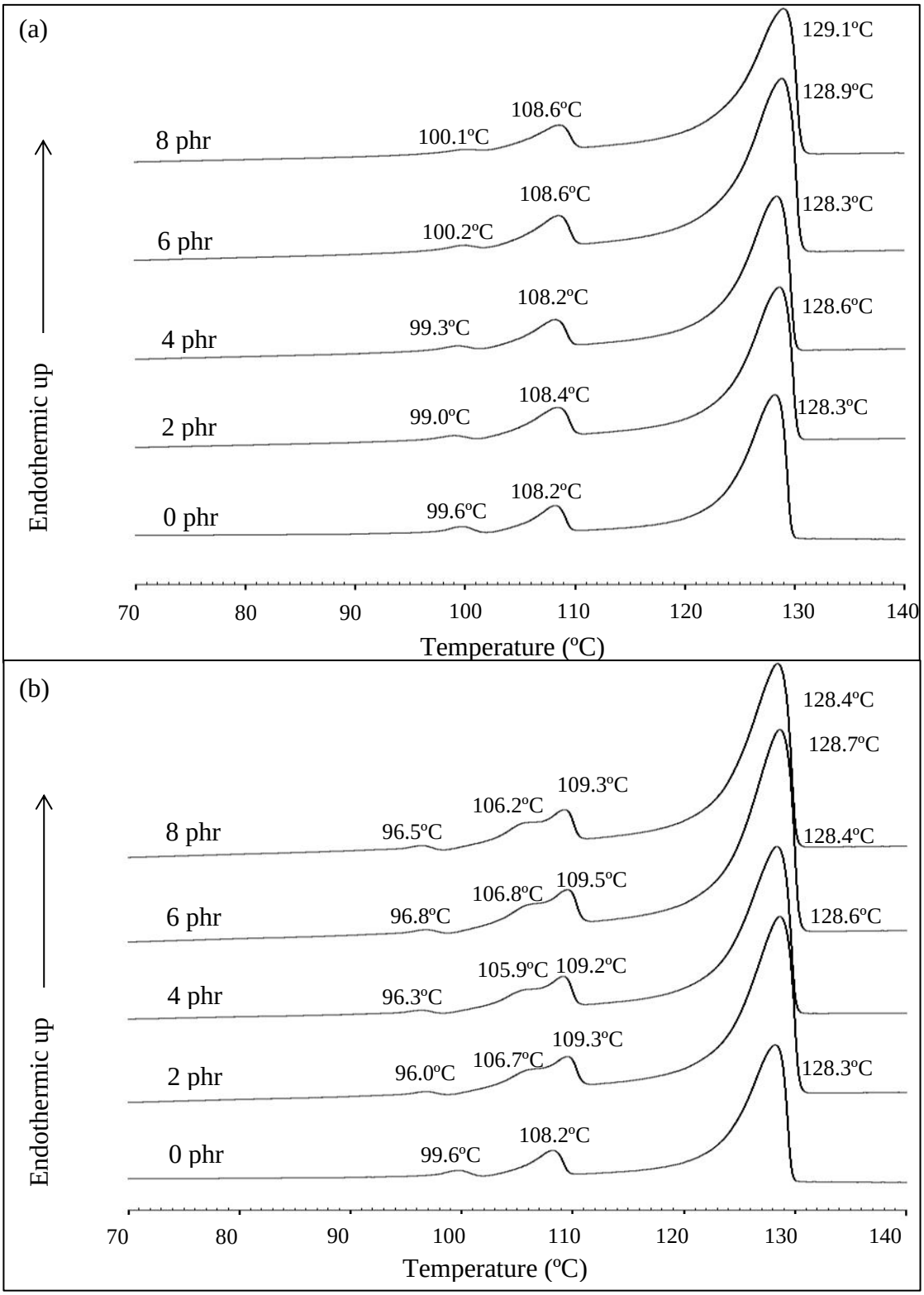

Figure 4.29 DSC curves from the second heating scan of PBS30/HDPE70 blends at various contents of HDPE-g-MAH (a) and EPR-g-MAH (b).

Table 4.15 Melting temperature and cold crystallization temperature from the first heating scan, crystallization temperature and melting at low and high temperature of PBS30/HDPE70 blend at various contents of HDPE-g-MAH and EPR-g-MAH.

Compatibilizer content	First heating scan						Crystallization temperature (^oC)				Second heating scan			
	Melting temperature (^oC)				Cold crystallization temperature (^oC)						Melting temperature (^oC)			
	PBS domain		HDPE matrix		PBS domain		HDPE matrix		PBS domain		HDPE matrix		PBS domain	
	H	E	H	E	H	E	H	E	H	E	H	E	H	E
0 phr	108.8		127.7		89.9		116.9		85.5		128.3		99.6,108.2	
2 phr	109.4	110.8	127.4	129.2	91.7	91.7	117.4	117.6	84.3	81.5	128.6	128.6	99.0, 108.4	96.0, 109.3
4 phr	108.5	110.2	126.4	129.1	91.4	91.6	117.3	116.7	85.2	80.7	128.3	128.4	99.3, 108.2	96.3, 109.2
6 phr	109.2	110.3	128.2	128.7	91.0	91.7	117.6	116.5	85.6	80.8	128.9	128.7	100.2, 108.6	96.8, 109.5
8 phr	109.0	109.9	127.3	127.6	91.0	91.5	117.7	116.7	85.6	80.6	129.1	128.4	100.1, 108.6	96.5, 109.3

Remark : H = HDPE-g-MAH, E= EPR-g-MAH

4.1.2.6 Water absorption

Relationship between water absorption and immersion time of uncompatibilized and compatibilized PBS30/HDPE70 blends with HDPE-g-MAH and EPR-g-MAH is shown in Figure 4.30. As shown in Figure 4.30 (a), the water absorption of the PBS30/HDPE70 blends compatibilized with HDPE-g-MAH was slightly lower than that of the uncompatibilized blend. Furthermore, the adding more HDPE-g-MAH content led to a slight decrease in water absorption. The decrease in water absorption of the compatibilized PBS30/HDPE70 blends as increasing HDPE-g-MAH content corresponded well with improved interfacial adhesion resulted in decreasing interfacial voids between PBS and HDPE phase. The water absorption of PBS30/HDPE70 blend compatibilized with 2, 4, 6and 4 phr of HDPE-g-MAH reached equilibrium water absorption after immersion time of 42, 42, 45 and 45 days, respectively.

Figure 4.30 (b) shows the relationship between water absorption and immersion time of uncompatibilized and compatibilized PBS30/HDPE70 blends with EPR-g-MAH. It illustrates that the water absorption of PBS30/HDPE70 blends compatibilized with EPR-g-MAH was slightly lower than that of the uncompatibilized blend. Moreover, water absorption of the compatibilized PBS30/HDPE70 blends decreased with increasing EPR-g-MAH content. The water absorption of PBS30/HDPE70 blend compatibilized with 2, 4, 6 and 8 phr of EPR-g-MAH reached equilibrium after immersion time of 42, 42, 45 and 45 days, respectively. The reduction of water absorption also correlated with the improved interfacial adhesion as increasing EPR-g-MAH content. It was previously reported that the reduction of water absorption of compatibilized blend was attributed to an

improvement in an interfacial adhesion resulting in avoidance an easy penetration of water molecules into the compatibilized blends and a decrease water accumulation at the interfacial voids (Arbelaiz *et al*., 2005).

In summary, the water absorption of the PBS30/HDPE70 blends compatibilized with EPR-g-MAH and HDPE-g-MAH was insignificant difference. In addition, immersion time and water content of immersion time and water content at equilibrium of PBS30/HDPE70 blends at various contents of HDPE-g-MAH and EPR-g-MAH is summarized in Table 4.16.

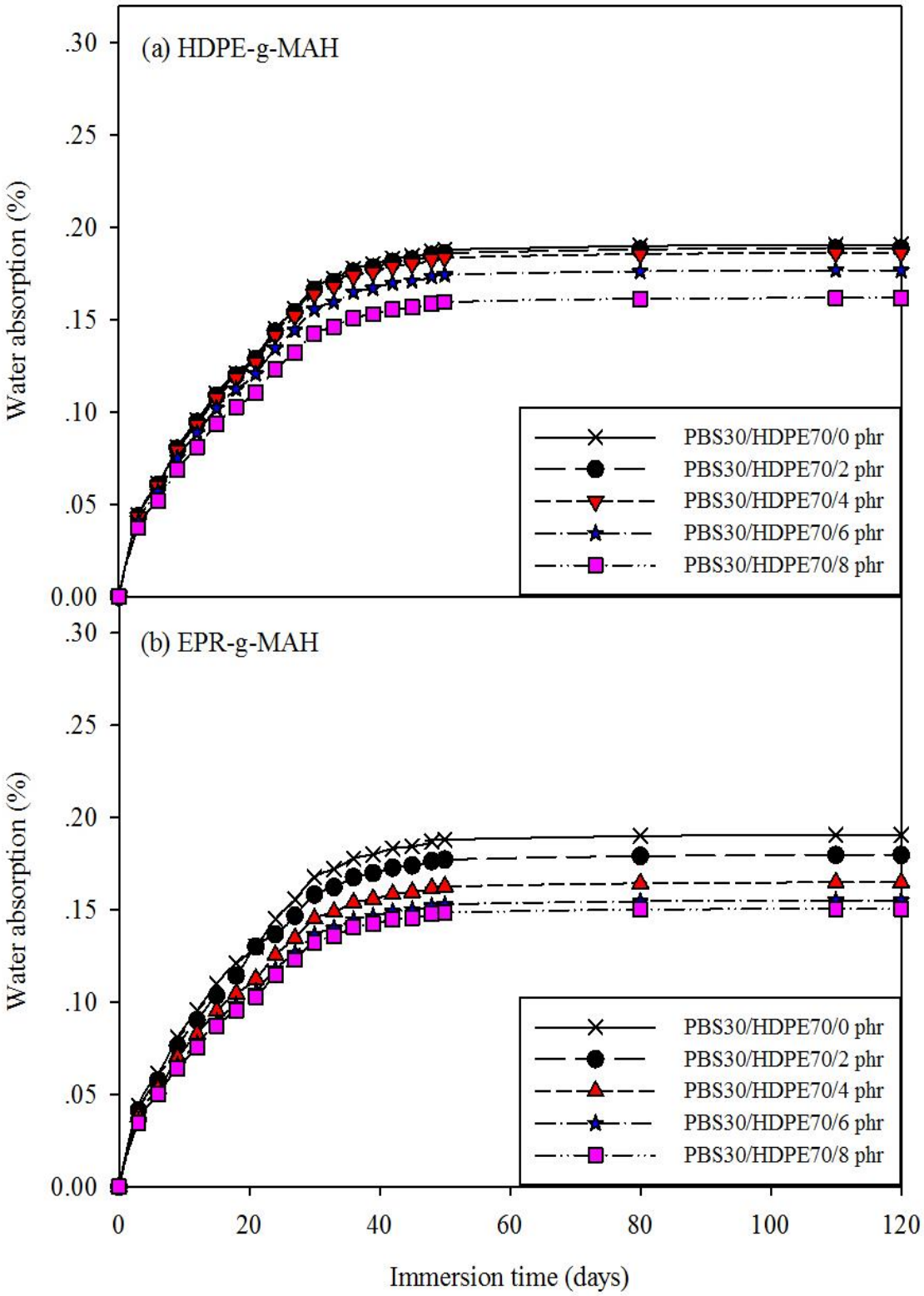

Figure 4.30 Plot of water absorption vs. immersion time of PBS30/HDPE70 blends at various contents of (a) HDPE-g-MAH and (b) EPR-g-MAH.

Table 4.16 Immersion time and water content at equilibrium of PBS30/HDPE70 blends at various contents of HDPE-g-MAH and EPR-g-MAH.

Compatibilizer content	Blend with HDPE-g-MAH		Blend with EPR-g-MAH	
	Immersion time (day)	Water content at equilibrium (%)	Immersion time (day)	Water content at equilibrium (%)
0 phr	42	0.18%	42	0.18%
2 phr	42	0.18%	42	0.17%
4 phr	42	0.18%	42	0.16%
6 phr	45	0.17%	45	0.15%
8 phr	45	0.16%	45	0.14%

4.1.2.7 Biodegradability by natural soil burial test

Plot of weight loss and burial time of uncompatibilized and compatibilized PBS30/HDPE70 blends with HDPE-g-MAH is shown in Figure 4.31 (a). It illustrates that weight loss of compatibilized blend was slightly lower than that of uncompatibilized blend. Adding more HDPE-g-MAH content led to a slight decrease in weight loss of the blends. The decrease in weight loss of compatibilized blend as increasing HDPE-g-MAH content might be due to the compatibilization effect of HDPE-g-MAH. HDPE-g-MAH improved interfacial adhesion between HDPE and PBS. Upon improved interfacial adhesion between HDPE and PBS, the moisture hardly diffused into the compatibilized blend sample.

Plot of weight loss and burial time of uncompatibilized and compatibilized PBS30/HDPE70 blends with EPR-g-MAH is displayed in Figure 4.31 (b). The weight loss of compatibilized blend was higher than that of uncompatibilized blend. In addition, increasing EPR-g-MAH content facilitated more weight loss of the compatibilized blend. This occurrence might because by an amorphous EPR-g-MAH elastomer. It was previously reported that biodegradation preferentially took place in the amorphous regions rather than in the crystalline region (Kim and Park, 1999).

In comparison, the blend compatibilized with EPR-g-MAH could be degraded in natural soil easier than the blend compatibilized with HDPE-g-MAH.

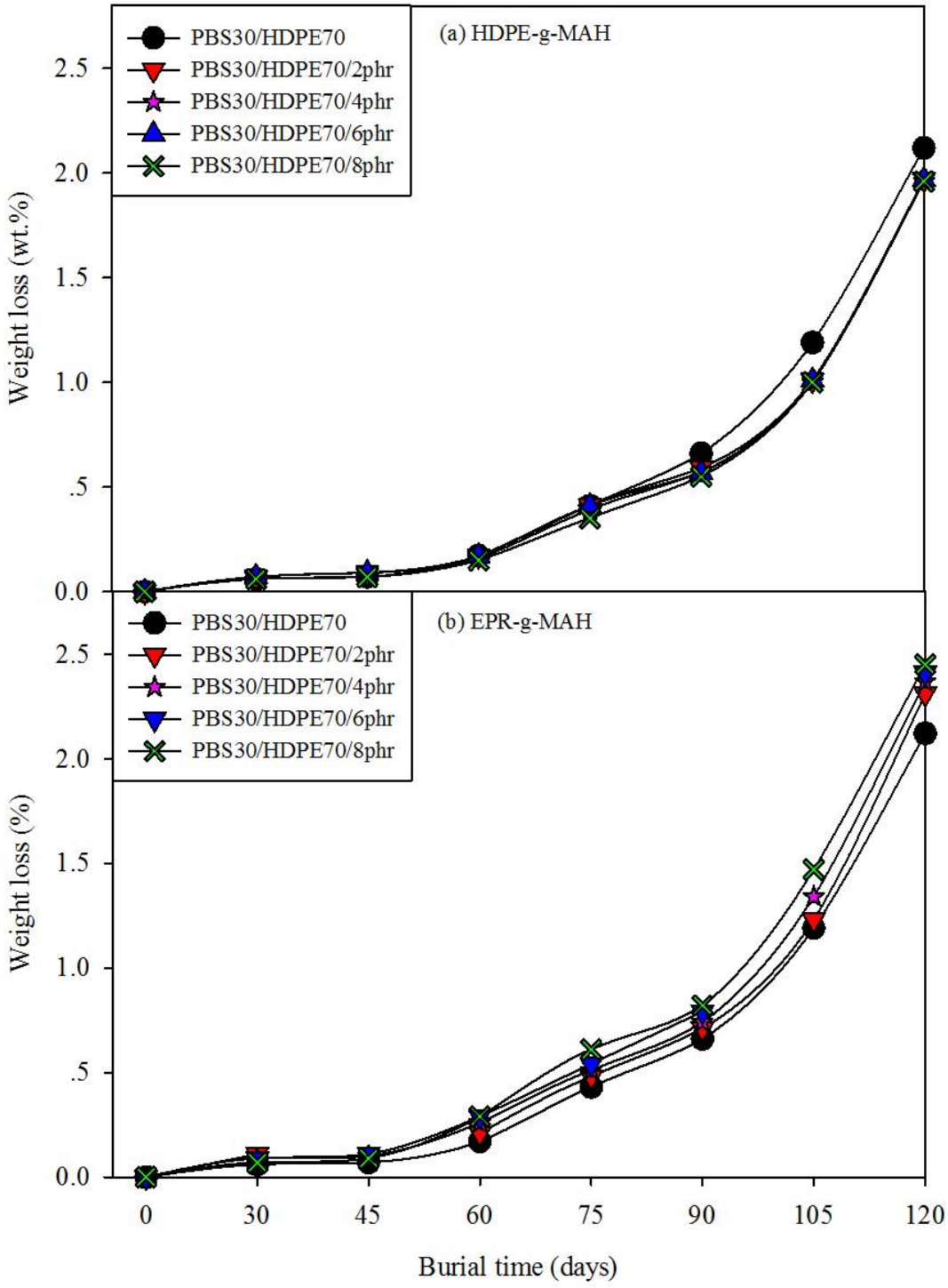

Figure 4.31 Plot of weight loss (%) and burial specimens of PBS30/HDPE70 blends at various contents of HDPE-g-MAH (a) and EPR-g-MAH (b).

Figure 4.32 shows optical photographs of the surfaces of the samples buried in the soil for 120 days. It illustrates that the surface of the uncompatibilized blend unchanged. Seemingly, the color of the blends sample seemed to be darker after 60 days of burial times. However, adding 2 to 8 phr HDPE-g-MAH did not affect the appearance of the blend sample.

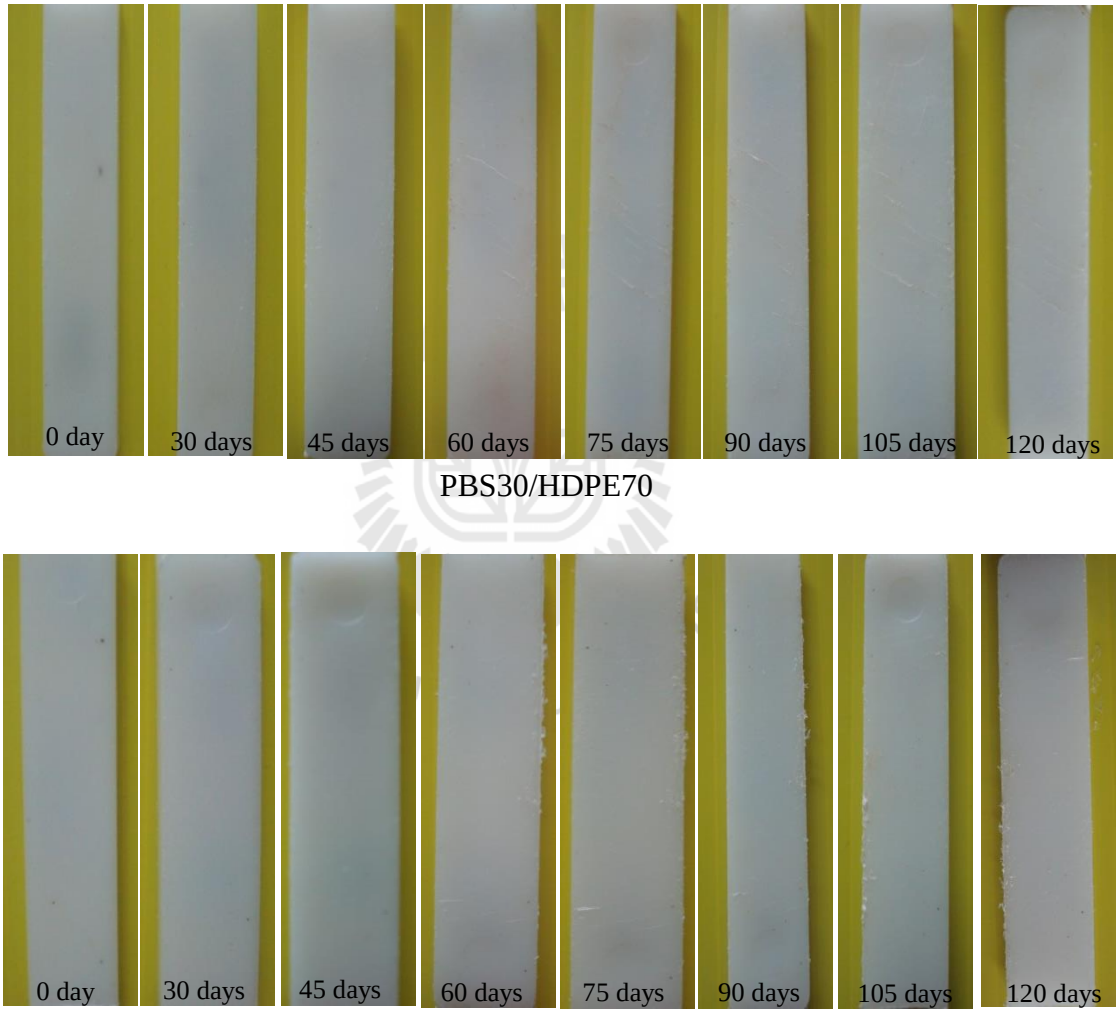

Figure 4.32 Optical micrographs of buried specimens of PBS30/HDPE70 blends at various contents of DHPE-g-MAH at several burial times of 0 to 120 days.

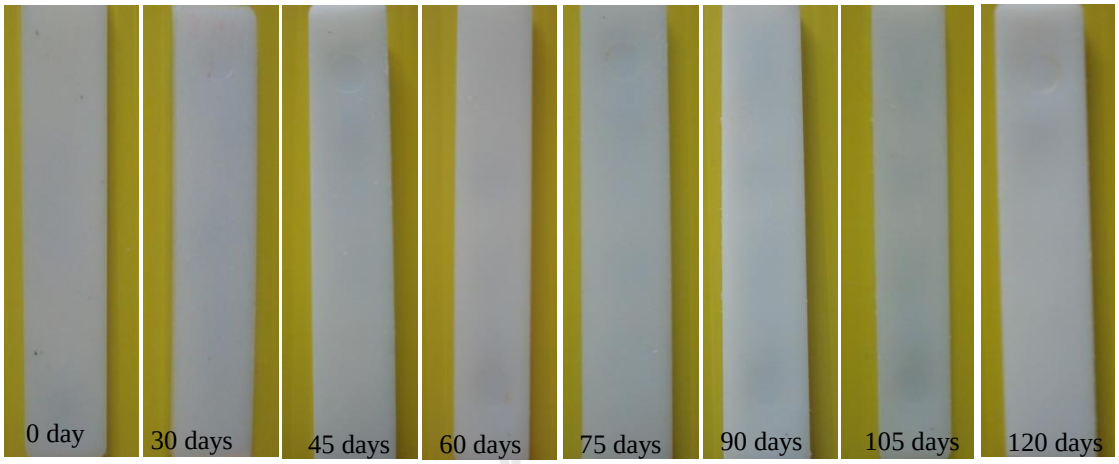

PBS30/HDPE70/HDPE-g-MAH 4 phr

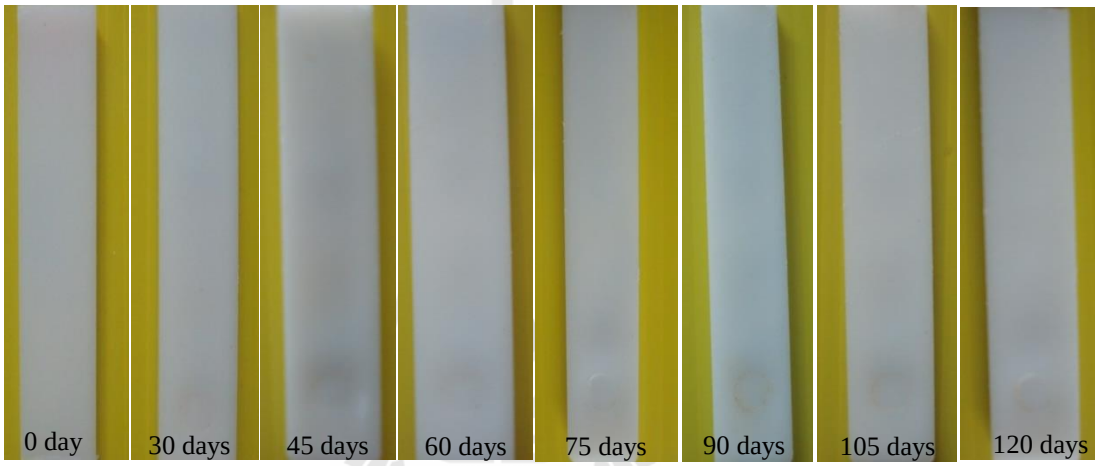

PBS30/HDPE70/HDPE-g-MAH 6 phr

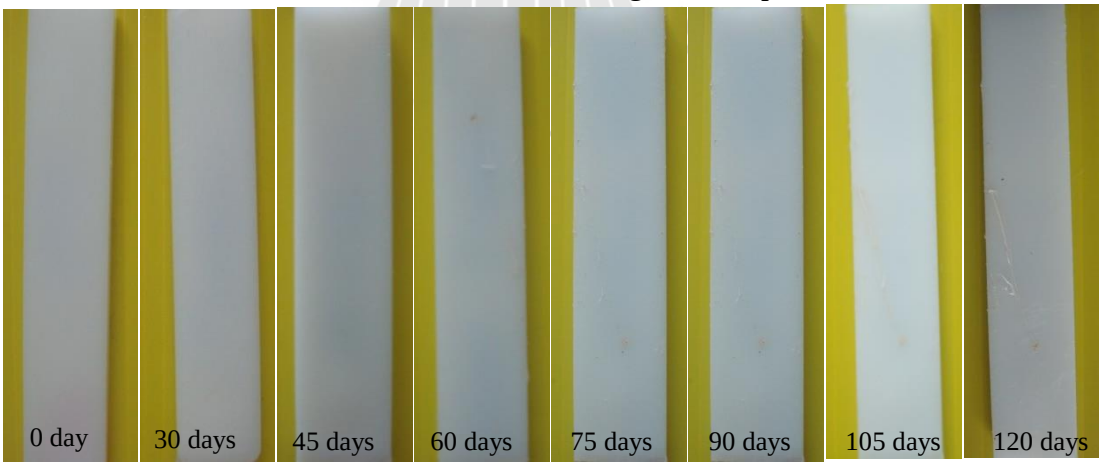

PBS30/HDPE70/HDPE-g-MAH 8 phr

Figure 4.32 Optical micrographs of buried specimens of PBS30/HDPE70 blends at various contents of DHPE-g-MAH at several burial times of 0 to 120 days. (Continued)

Figure 4.33 shows optical photographs of the surfaces of the blend compatibilized with EPR-g-MAH. With adding 2 to 4 phr EPR-g-MAH into the blend, the dark spot occurred at the edge of the blend sample after burial time of 60 days. In addition, the dark spot spreaded as the burial time increased.

As increasing EPR-g-MAH to 6 and 8 phr, the dark streak was observed after burial time of 75 days. Furthermore, the area of a dark streak was more clearly seen as increasing burial time. This implied that the biodegradability of the blend compatibilized with EPR-g-MAH increased with increasing burial time.

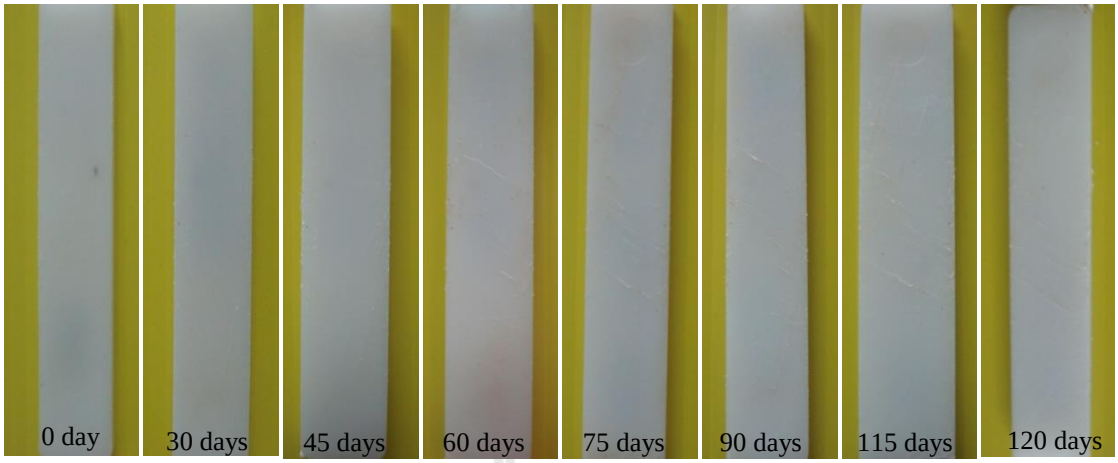

PBS30/HDPE70

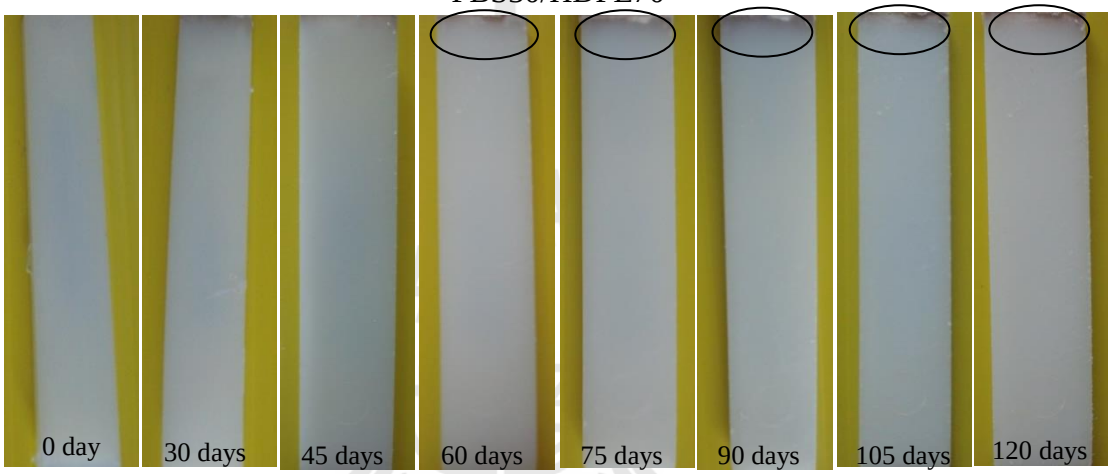

PBS30/HDPE70/EPR-g-MAH 2 phr

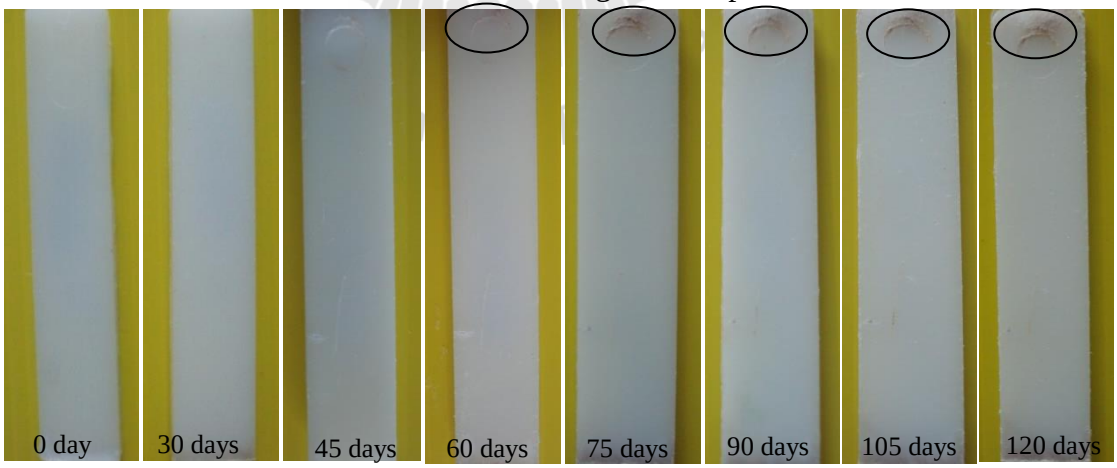

PBS30/HDPE70/EPR-g-MAH 4 phr

Figure 4.33 Optical micrographs of buried specimens of PBS30/HDPE70 blends at various contents of EPR-g-MAH at several burial times of 0 to 120 days.

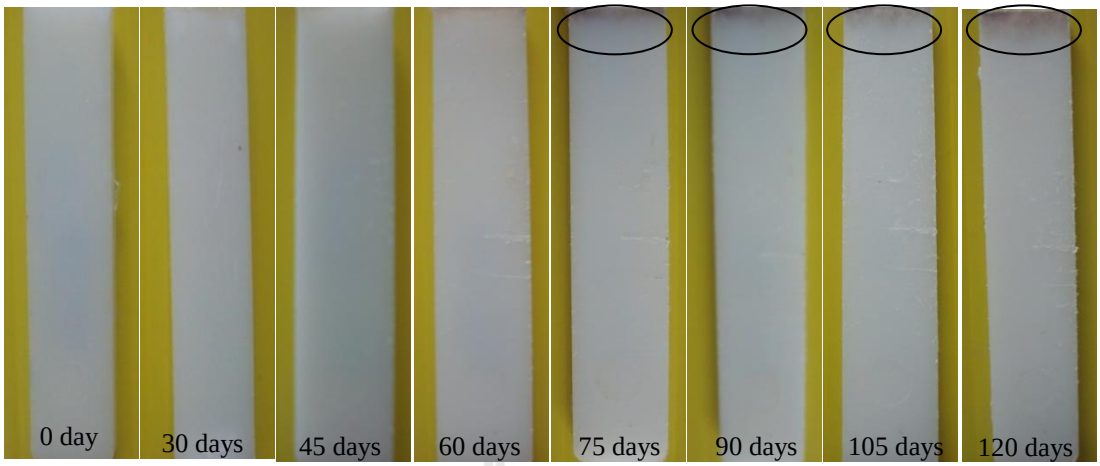

PBS30/HDPE70/EPR-g-MAH 6 phr

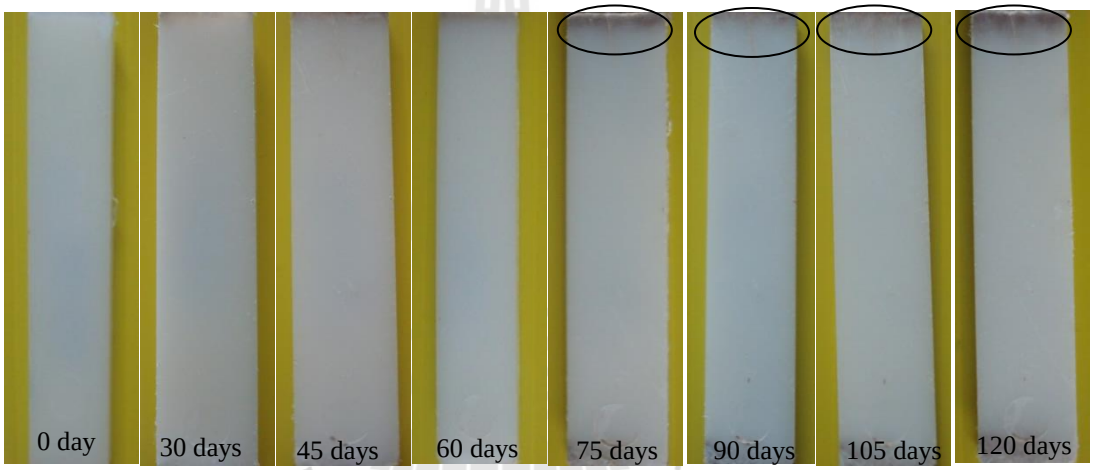

PBS30/HDPE70/EPR-g-MAH 8 phr

Figure 4.33 Optical micrographs of buried specimens of PBS30/HDPE70 blends at various contents of EPR-g-MAH at several burial times of 0 to 120 days. (Continued)

4.2 HDPE/PBS blend

4.2.1 Effect of HDPE content on physical properties

4.2.1.1 Flow properties

The dependence of apparent shear viscosity on apparent shear rate of neat PBS, neat HDPE and HDPE/PBS blends are presented in Figure 4.34. The apparent shear viscosity of neat PBS was lower than that of neat HDPE. Neat PBS and neat HDPE both exhibited shear thinning behavior of which shear viscosity decreased as shear rate increased. At high shear rate, polymer chains more aligned in the shear direction resulting in better molecular flow ability of polymer molecules leading to lower viscosity (Ahmad, Wahit, Kadir and Dahlan, 2012). This shear thinning behavior was also observed from HDPE/PBS blend. In addition, the apparent shear viscosity of the blend increased with increasing HDPE content.

Within the shear rate range of injection molding process (3,000-4,000 s^{-1}) at 190ºC, shear viscosity of PBS and HDPE was 9-11 Pa.s and 46-59 Pa.s, respectively. The viscosity ratio of the blend calculated at the shear rate a range of injection process was in a range of 5.11 to 5.36 depending on HDPE composition.

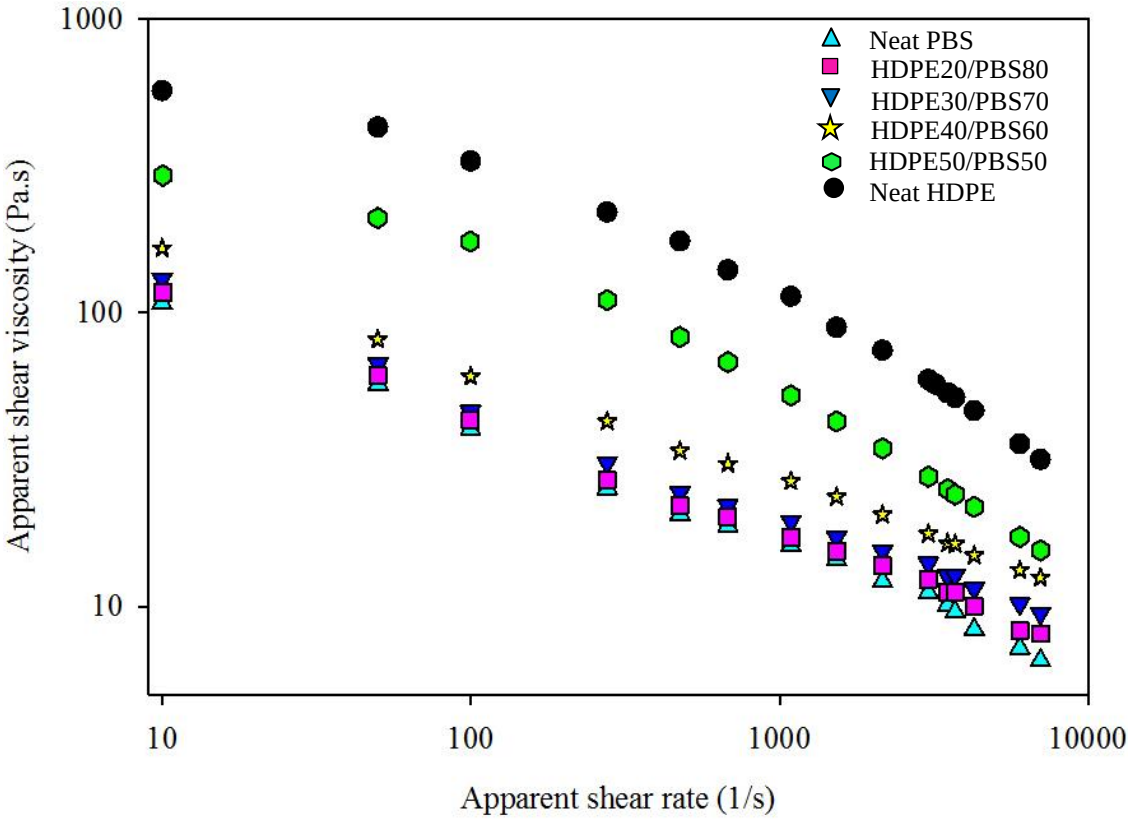

Figure 4.34 Plot of apparent shear viscosity as a function of apparent shear rate of neat PBS, neat HDPE and HDPE/PBS blend at various contents of HDPE.

Melt flow index (MFI) of neat PBS, neat HDPE and HDPE/PBS blend at various contents of HDPE is shown in Table 4.17. It illustrates that MFI of neat PBS was higher than that of neat HDPE. The MFI of HDPE/PBS blends decreased with increasing HDPE content.

Table 4.17 Melt flow index (MFI) at 190°C with a standard weight of 2.16 kg of neat PBS, neat HDPE and HDPE/PBS blends.

Sample	MFI (g/10min)
Neat PBS	26.1
HDPE20/PBS80	24.7
HDPE30/PBS70	22.7
HDPE40/PBS60	21.4
HDPE50/PBS50	18.5
Neat HDPE	11.6

4.2.1.2 Failure behavior and phase morphology

The stress-strain curve of HDPE/PBS blend at 20 wt.% HDPE is displayed in Figure 4.35. It illustrates that failure behavior of HDPE/PBS blend at 20 wt.% HDPE was still in a ductile manner as necking and then large strain deformation took place before fracture at a strain of 218%. The freeze fractured surface morphology of HDPE20/PBS80 blend is illustrated in Figure 4.35 (a). It revealed that the addition of 20 wt.% HDPE into PBS matrix gave rise to a heterogeneous phase morphology with spherical and oval shape of HDPE dispersed in PBS matrix. In approximation, the dispersed HDPE size was in range of 1 μm to 7 μm. This heterogeneous phase morphology was a consequence of immiscibility and high interfacial tension between HDPE and PBS phases. Also, shear viscosity of PBS was much lower than that of HDPE. Accordingly, the viscosity ratio (η_d/η_m) of this blend system was much higher than 1. Therefore, the blend system with high interfacial tension, and high viscosity ratio would obtain. In comparison, the size of HDPE domain was much larger than that of PBS domain of PBS/HDPE blend system.

Even though the interfacial tension of these two blend systems was approximate in the same degree but their viscosity ratios were much different. It turned out that the dispersed phase size of those blend systems was not in the same range due to the difference in viscosity ratio.

As increasing HDPE content to 30 wt.%, stress-strain curve illustrated in Figure 4.35 shows that the blend fractured prior to yielding at 28 % strain. This implied that the blend failed in a brittle manner. The freeze fractured surface morphology of HDPE30/PBS70 blend is illustrated in Figure 4.35 (b), was in non-uniform size and shape with an estimation in size range of 2 μm to 9 μm., including spheres, ovals and large size of elongated HDPE dispersed in PBS matrix. This was due to the high interfacial tension and having viscosity ratio higher than 1 of this blend system, therefore the droplet was hardly broken up. It just deformed and oriented to shear flow direction. In addition, the high interfacial tension between HDPE and PBS gave rise to low capillary number of the blend. This was responsible for the existence of ellipsoid drop shape, as observed from its phase morphology. Also, the interfacial adhesion between PBS matrix and HDPE was not good indicated by the smooth surface of dispersed HDPE. This was responsible for a brittle failure of the blend.

The stress-strain curve of HDPE/PBS blend at 40 wt.% HDPE, in Figure 4.35, exhibits that the blend failed and subsequently fractured without a yielding point at 24% strain. Its stress-strain curve indicated that the blend at 40 wt.% HDPE failed and broke in a brittle manner. The freeze fractured surface morphology of HDPE40/PBS60 blend is displayed in Figure 4.35 (c). It was in non-uniform size and shape of HDPE dispersed phase, including spheres, ovals and large elongated of

dispersed HDPE with an approximate size of 3 μm to 14 μm. The dispersed HDPE size was strongly affected by its composition. With increasing content of HDPE, the number of HDPE particles increased, leading to more particle-particle collision, and then coalescence of HDPE particles occurred.

With adding HDPE content to 50 wt.%, HDPE50/PBS50 blend specimens ruptured prior to yielding at a strain of 29%. The phase morphology of HDPE50/PBS50 blend, as shown in Figure 4.35 (d), was in co-continuous type as expected. Presumably, co-continuous phase morphology could be generated at the same volume fraction of each component in the binary blend (Harrats, Thomas and Groeninckx, 2006). Additionally, it had been previously found that phase morphology of PBT/PP blend at 50 wt.% PBT was also in a co-continuous type (Tsai and Chang, 1996).

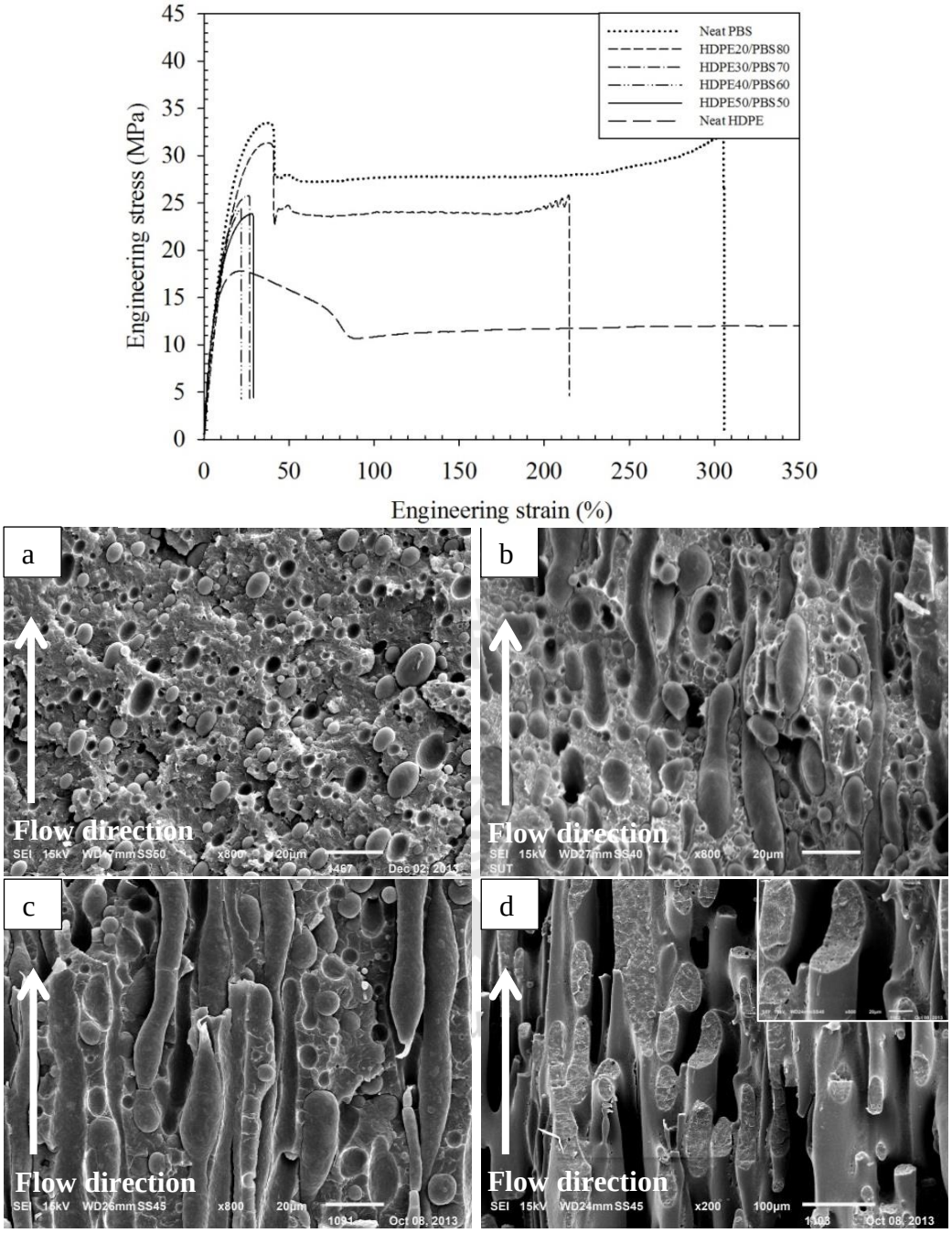

Figure 4.35 Tensile stress-strain curves and SEM micrographs of HDPE etching specimens at magnification of x800 of HDPE/PBS blend at 20 wt.% HDPE (a), 30 wt.% HDPE (b), 40 wt.% HDPE (c) and at a magnification of x200 and x800 of 50 wt.% HDPE (PBS etched) (d).

4.2.1.3 Mechanical properties

Young's modulus of neat PBS, neat HDPE and HDPE/PBS blends is presented in Figure 4.36. Young's modulus of neat PBS was lower than that of neat HDPE. Adding HDPE into PBS matrix resulted in an increase of Young's modulus of the blend. Furthermore, Young's modulus of HDPE/PBS blend increased continuously with increasing HDPE content.

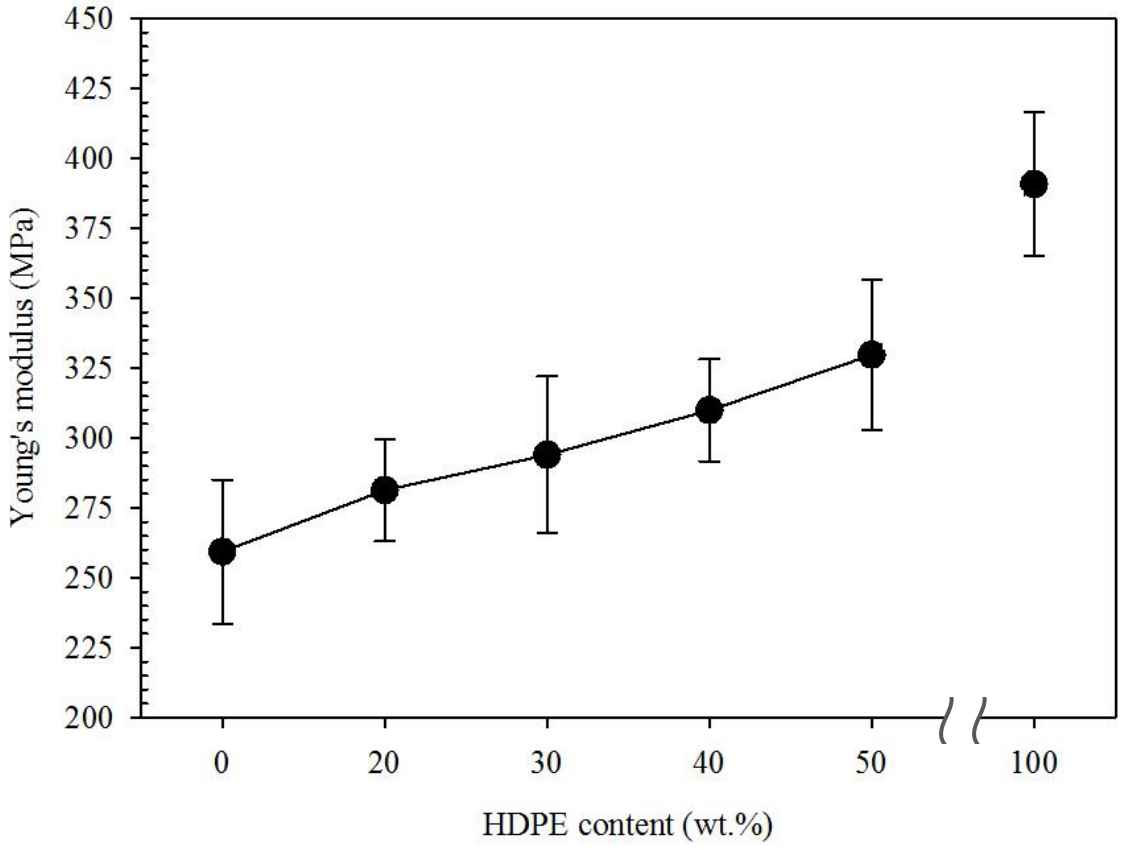

Figure 4.36 Plot of Young's modulus of HDPE/PBS blend vs. HDPE content.

The prediction of longitudinal and transverse modulus as a function of the blend composition is comparatively plotted with Young's modulus obtained from an experimental data in Figure 4.37. It illustrates that Young's modulus

of HDPE/PBS blends obtained from the experimental was line in between the longitudinal modulus (E_L) and transverse modulus (E_T) of which calculated using "Rule of mixture" and "Inverse rule of mixtures" as mention previously in equation 4.1 and 4.2, respectively. However, the Young's modulus of the HDPE/PBS blend at 50 wt.% HDPE was slightly above calculated longitudinal and transverse modulus. This might be due to co-continuous phase morphology.

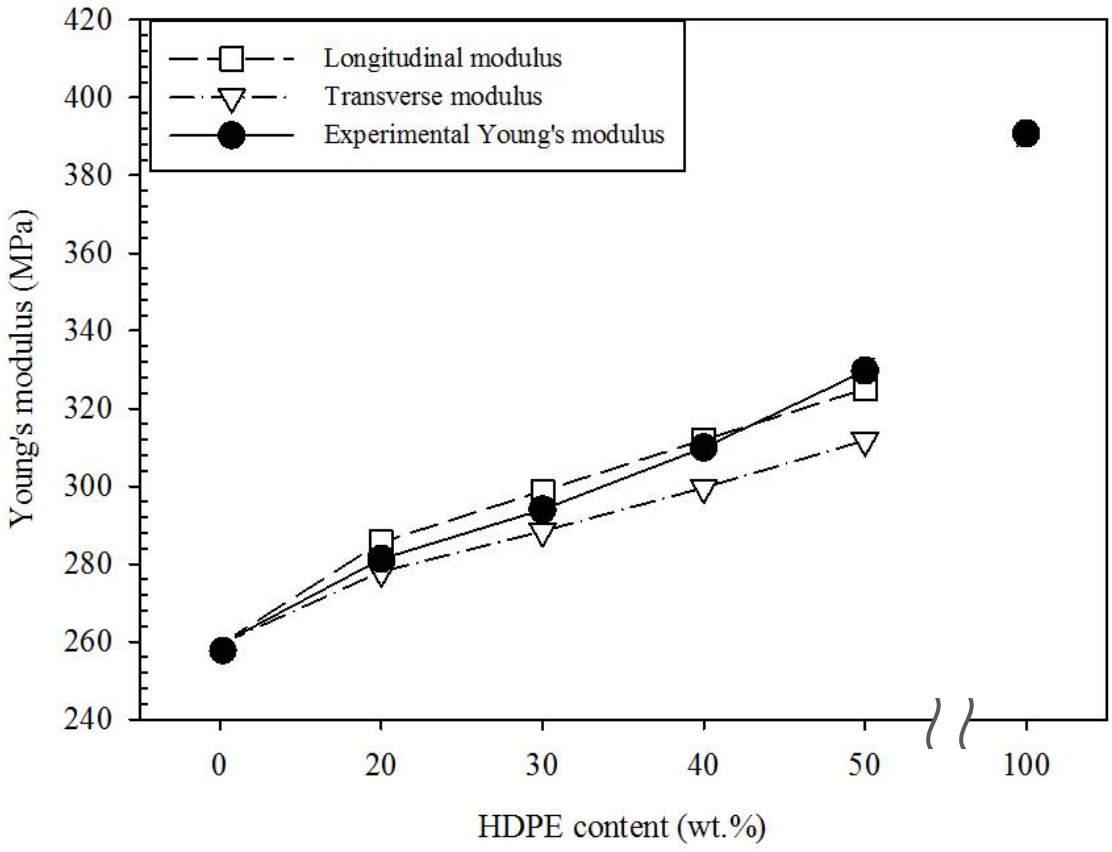

Figure 4.37 Plot of calculated longitudinal and transverse modulus, and Young's modulus obtained from an experimental data of HDPE/PBS blend vs. HDPE content.

The elongation at break of neat PBS and HDPE/PBS blends was also shown in Figure 4.38. As mentioned previously, elongation at break of neat HDPE, under tensile test of a crosshead speed of 10 mm/min, was not obtained because it was far beyond an instrumentation limit of 800%. Addition of 20 wt.% HDPE into PBS matrix resulted in much decrease of elongation at break of the blends. This decreasing elongation at break was a consequence of poor adhesion between HDPE and PBS. During tensile loading, voids at the interface propagated, as a result, the blend broke at lower ultimate strain. As increasing HDPE content to 30 wt.%, the elongation at break of HDPE/PBS blend still decreased gradually. This result might be correlated with a larger size of HDPE domain as previously shown in SEM micrograph, Figure 4.35 (b). The larger size of dispersed HDPE created large particle-particle distance leading to a failure of blend sample at even lower strain. With increasing HDPE content to 40 wt.%, the elongation at break of HDPE/PBS blend almost unchanged as compared to the blend at 30 wt% HDPE. This corresponded with no significant difference in phase morphology between the blend at 30 wt.% and 40 wt.% HDPE. Noticeably, at 50 wt.% HDPE, the elongation at break the blend slightly improved. This correlated with its co-continuous phase morphology maintaining the elongation at break of the blend (Bell, 2007).

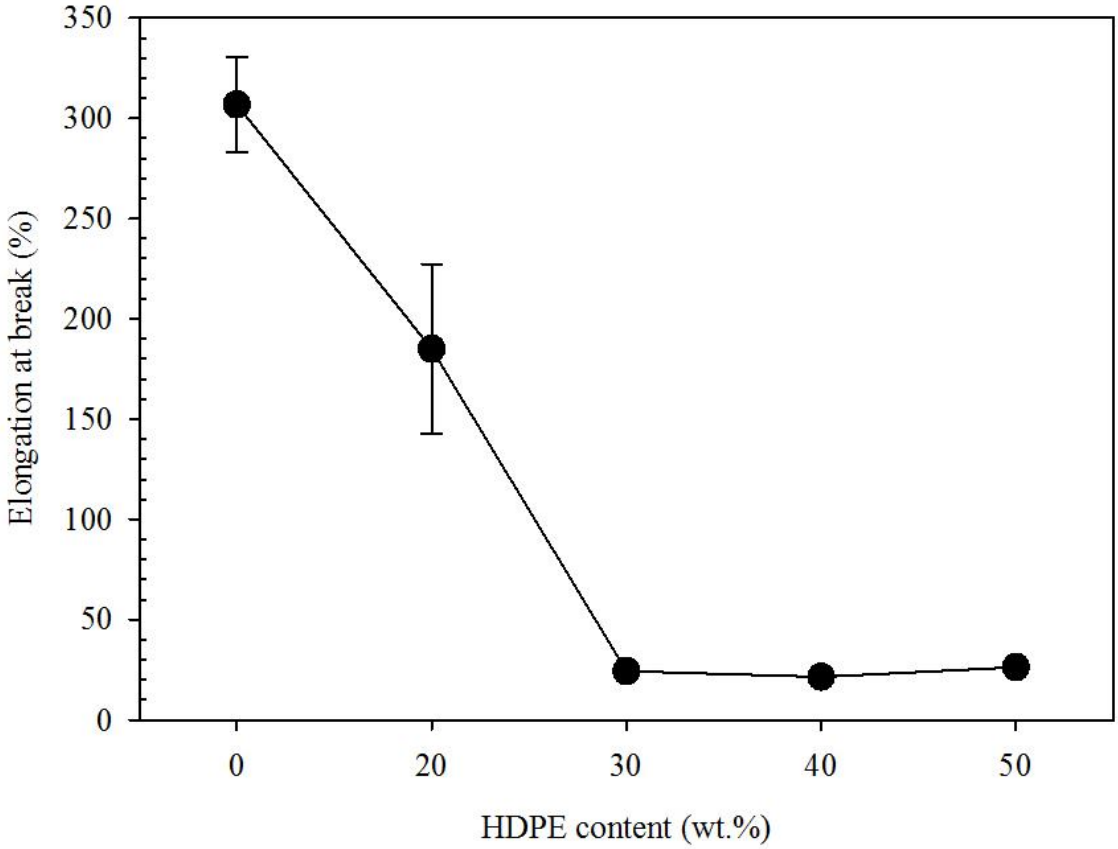

Figure 4.38 Plot of elongation at break of HDPE/PBS blend vs. HDPE content.

Yield strength of neat PBS, neat HDPE and HDPE/PBS blends is shown in Figure 4.39. It demonstrates that the yield strength of neat PBS was higher than that of neat HDPE. Yield strength of HDPE/PBS blend decreased as increasing HDPE content. However, the blend containing 30 to 50 wt.% HDPE fractured in a brittle manner. The ductile to brittle transition of the blend was defined from fracture behavior of the blend from stress-strain curve occurring within HDPE content range of 20-30 wt.%. The decrease in yield strength of the blend was a consequence of the fact that the yield strength of HDPE was lower than that of PBS and they were not compatible. Therefore, adding more HDPE into the blend led to a decrease of yield strength of the blend. Also, the decrease in yield strength of

HDPE/PBS blend might be due to the weak or no adhesion between HDPE and PBS phase. This similar result was previously observed in others polyethylene/polyester blend, including LLDPE/PBT (Kang *et al*., 1999), HDPE/PET (Kim, Park, Kim, and Suh, 2000) and LLDPE/BDP blend (Kim, Kim, Shin, Choi and Jhon, 2001). Stress at break of neat PBS, neat HDPE and HDPE/PBS blends is also shown in Figure 4.39. It illustrates that stress at break of neat PBS was 28 MPa. As mentioned previously, stress at break of neat HDPE, under tensile test of a crosshead speed of 10 mm/min, was not able to detect because it was far beyond a universal testing machine limit. The addition of HDPE into PBS matrix resulted in a significant decrease of stress at break of the blend. In addition, tensile properties of the blend were listed in Table 4.18.

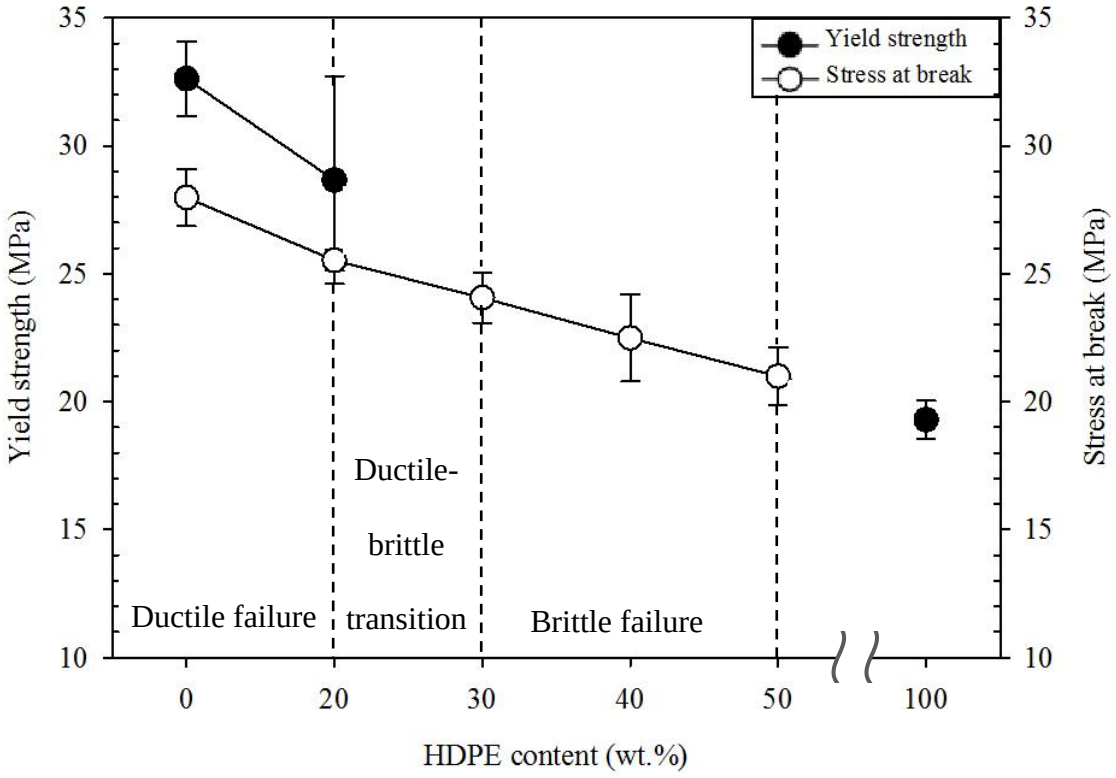

Figure 4.39 Plot of yield strength and stress at break of HDPE/PBS blend vs. HDPE content.

Table 4.18 Tensile properties of neat PBS, neat HDPE and HDPE/PBS blends

Sample	Young's modulus (MPa)	Elongation at break (%)	Yield strength (MPa)	Stress at break (MPa)
Neat PBS	259.3±25.8	306.6±23.4	32.6±1.4	28.0±1.1
HDPE20/PBS80	281.3±18.2	185.0±42.2	28.7±4.1	25.5±0.4
HDPE30/PBS70	294.0±27.9	24.3±1.9	Brittle failure	24.0±0.9
HDPE40/PBS60	309.9±18.3	21.5±1.0	Brittle failure	22.5±1.7
HDPE50/PBS50	329.7±26.9	26.4±2.6	Brittle failure	21.0±1.1
Neat HDPE	390.7±25.7	Not break	19.3±0.8	Not break

Flexural strength and flexural modulus of neat PBS, neat HDPE and HDPE/PBS blend at various contents of HDPE are presented in Figure 4.40. It illustrates that flexural strength of neat PBS was higher than that of neat HDPE. The addition of HDPE into PBS matrix brought about a decrease in flexural strength of the blend. In addition, flexural strength of the HDPE/PBS blend decreased with increasing HDPE content. Flexural modulus of neat PBS was lower than that of neat HDPE. Flexural modulus of HDPE/PBS blends gradually increased as increasing HDPE content. In addition, flexural properties of the blend were summarized in Table 4.19.

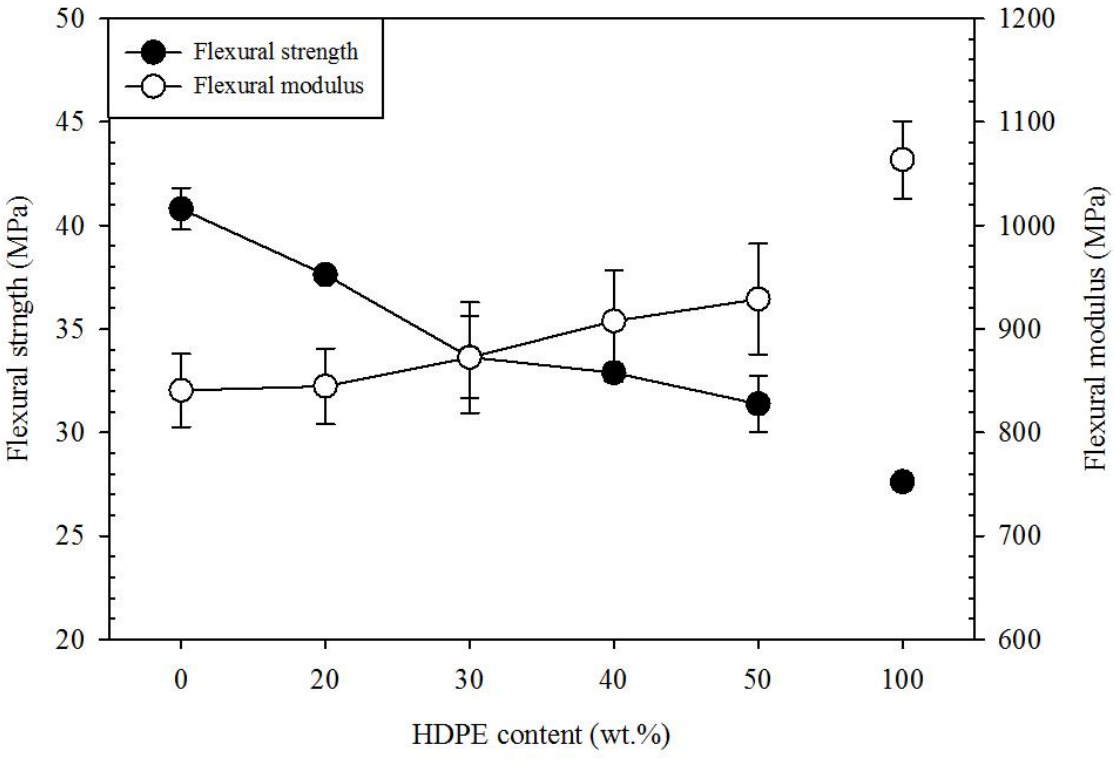

Figure 4.40 Plot of flexural strength and flexural modulus of HDPE/PBS blend vs. HDPE content.

Table 4.19 Flexural properties of neat PBS, neat HDPE and HDPE/PBS blends

Sample	Flexural strength (MPa)	Flexural modulus (MPa)
Neat PBS	40.8±1.0	840.6±35.2
HDPE20/PBS80	37.6±0.3	844.5±36.5
HDPE30/PBS70	33.6±1.9	872.4±53.4
HDPE40/PBS60	32.9±0.4	907.5±49.3
HDPE50/PBS50	31.4±1.4	928.8±53.3
Neat HDPE	27.6±0.4	1,063.5±37.5

Unnotched Izod impact strength of neat PBS, neat HDPE and HDPE/PBS blends is shown in Table 4.20. The impact strength of neat PBS and neat HDPE was not obtained; it was beyond an instrumentation limit of 135 kJ/m^2. From Table 4.16, it illustrates that addition 20 wt.% HDPE into PBS matrix resulted in a significant decrease of the impact strength. The decrease in impact strength was indicated by voids at the blend interface. The interfacial void due to incompatibility of HDPE/PBS blend was revealed by SEM micrograph illustrated in Figure 4.35 (a). With adding 30-40 wt.% HDPE, the impact strength of HDPE/PBS blend slightly increased. The slight increase might be related to the elongated shape and fibrillar structure of dispersed HDPE. These dispersed HDPE acted as a crack-tip shielding, by which these dispersed HDPE resisted the cracking of blend, as proposed in Figure 4.41. However, the impact strength of HDPE/PBS blend was greatly improved by the addition of 50 wt.% HDPE. The great improvement of impact strength correlated well with co-continuous phase morphology of HDPE/PBS blends at 50 wt.% PBS (Harrats,

Thomas and Groeninckx, 2006). This was because both phases in the co-continuous morphology were able to contribute to mechanical performance in all direction (Bell, 2007). The similar result was also observed in LLDPE/BDP blend at 50 wt.% LLDPE (Kim, Kim, Shin, Choi and Jhon, 2001).

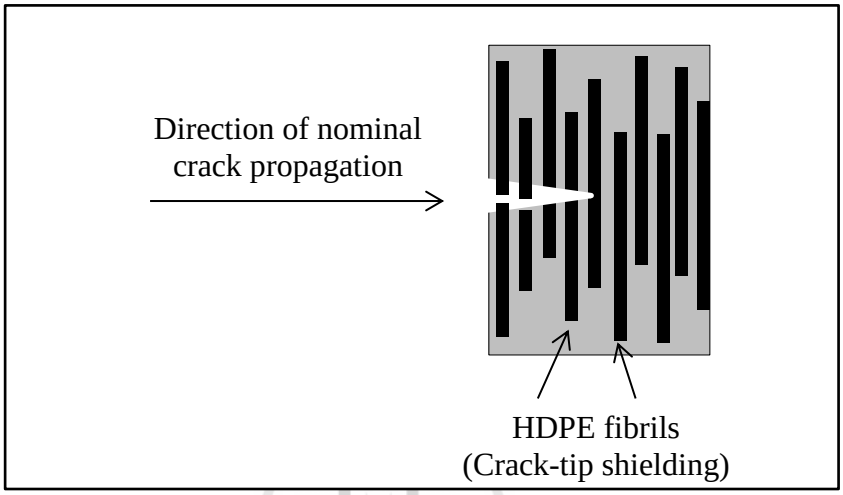

Figure 4.41 Schematic illustration of the possible toughening mechanism in HDPE/PBS blends at 30 wt.% and 40 wt.% HDPE (Adapted from Nalla, Kinney and Ritchie, 2003).

Table 4.20 Unnotched Izod impact strength of neat PBS, neat HDPE and HDPE/PBS blends.

Sample	Unnotched Izod impact strength (kJ/m^2)
Neat PBS	Not break
HDPE20/PBS80	37.0±3.8
HDPE30/PBS 70	39.4±3.0
HDPE40/PBS 60	40.0±3.4
HDPE50/PBS 50	Not break
Neat HDPE	Not break

4.2.1.4 Thermal degradation temperature and weight loss

TGA and DTGA curves of neat PBS, neat HDPE and HDPE/PBS blends are presented in Figure 4.42. Neat PBS and neat HDPE degraded with single thermal transition at temperature range of 350-433ºC and 423-526ºC, respectively. Adding 20 wt% HDPE into PBS matrix made the blend thermally degraded into two stages. The first transition occurred at a temperature range of 353-430ºC corresponding to the thermal degradation of PBS phase. The second transition occurred at a temperature range of 433-509°C, due to thermal degradation of HDPE phase. Adding 30, 40 and 50 wt.% HDPE into PBS made the PBS phase degraded at a temperature range of 355-435ºC, 354-433ºC and 355-433ºC. On the other hand, HDPE phased degraded at a temperature range of 436-504 ºC, 433-509 ºC and 431-504ºC, respectively. In addition, the TGA curves show the percentage of HDPE and PBS corresponding to the blend composition.

As shown in Figure 4.47 (b), adding 20 wt.% HDPE made the degradation temperature of PBS matrix improved insignificantly. In addition, the degradation temperature of HDPE itself remained unchanged. As increasing HDPE content to 30 wt.%, the degradation temperature of PBS and HDPE phase slightly improved. However, with adding more HDPE, the degradation temperature of PBS decreased slightly whereas the degradation temperature of HDPE remained constant. Additionally, the temperature range for degradation, the degradation temperature and weight loss of HDPE domain and PBS matrix were summarized in Table 4.21.

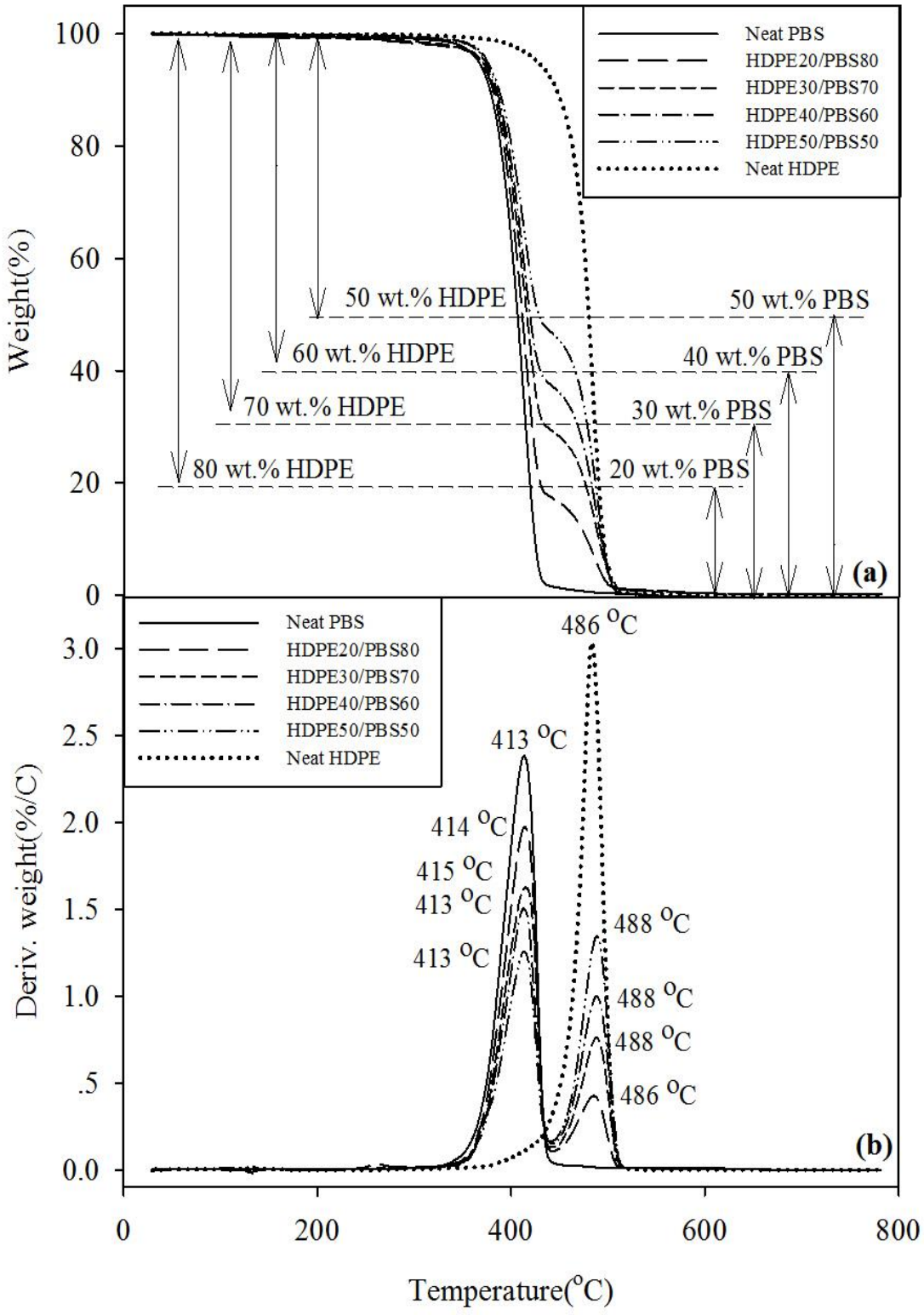

Figure 4.42 TGA (a) and DTGA (b) thermograms of neat PBS, neat HDPE and HDPE/PBS blend at various HDPE contents.

Table 4.21 The temperature range for degradation ($T_{d,range}$), peak temperatures (T_{peak}) and weight loss of neat PBS, neat HDPE, and HDPE/PBS blend at various HDPE contents.

Sample	PBS matrix			HDPE domain		
	T_{peak} (ºC)	Weight loss (%)	$T_{d,range}$ (ºC)	T_{peak} (ºC)	Weight loss (%)	$T_{d,range}$ (ºC)
Neat PBS	413	100.0	350-433	-	-	-
HDPE20/PBS80	414	79.5	353-430	486	19.8	433-509
HDPE30/PBS70	415	70.0	355-435	488	29.9	436-504
HDPE40/PBS60	413	59.6	354-433	488	39.9	433-509
HDPE50/PBS50	413	49.9	355-433	488	49.6	431-504
Neat HDPE	-	-	-	486	100.0	423-506

4.2.1.5 Melting and crystallizing behavior

DSC curve from the first heating scan of neat PBS, neat HDPE and HDPE/PBS blend at various contents of HDPE are shown in Figure 4.43. The DSC curve of neat HDPE reveals an endothermic peak at 128.8°C corresponding to a melting of HDPE. Neat PBS exhibited an exothermic peak at around 90.3°C following with endothermic peak at 109.8°C. The exothermic peak was caused by the recrystallization of PBS, called cold-crystallization (Yasuniwa, Tsubakihara, Satou and Iura, 2005). It was previously reported that the exothermic peak occurred during a heating scan of PBS, at around 93.0°C, due to the thermal history during cooling and reheating (Yoo and Im, 1999). The endothermic peak at 109.8°C corresponded to a melting of PBS. Addition of HDPE into PBS matrix did insignificant affect cold-crystallization and melting temperature of PBS phase, and melting temperature of HDPE phase itself, as well.

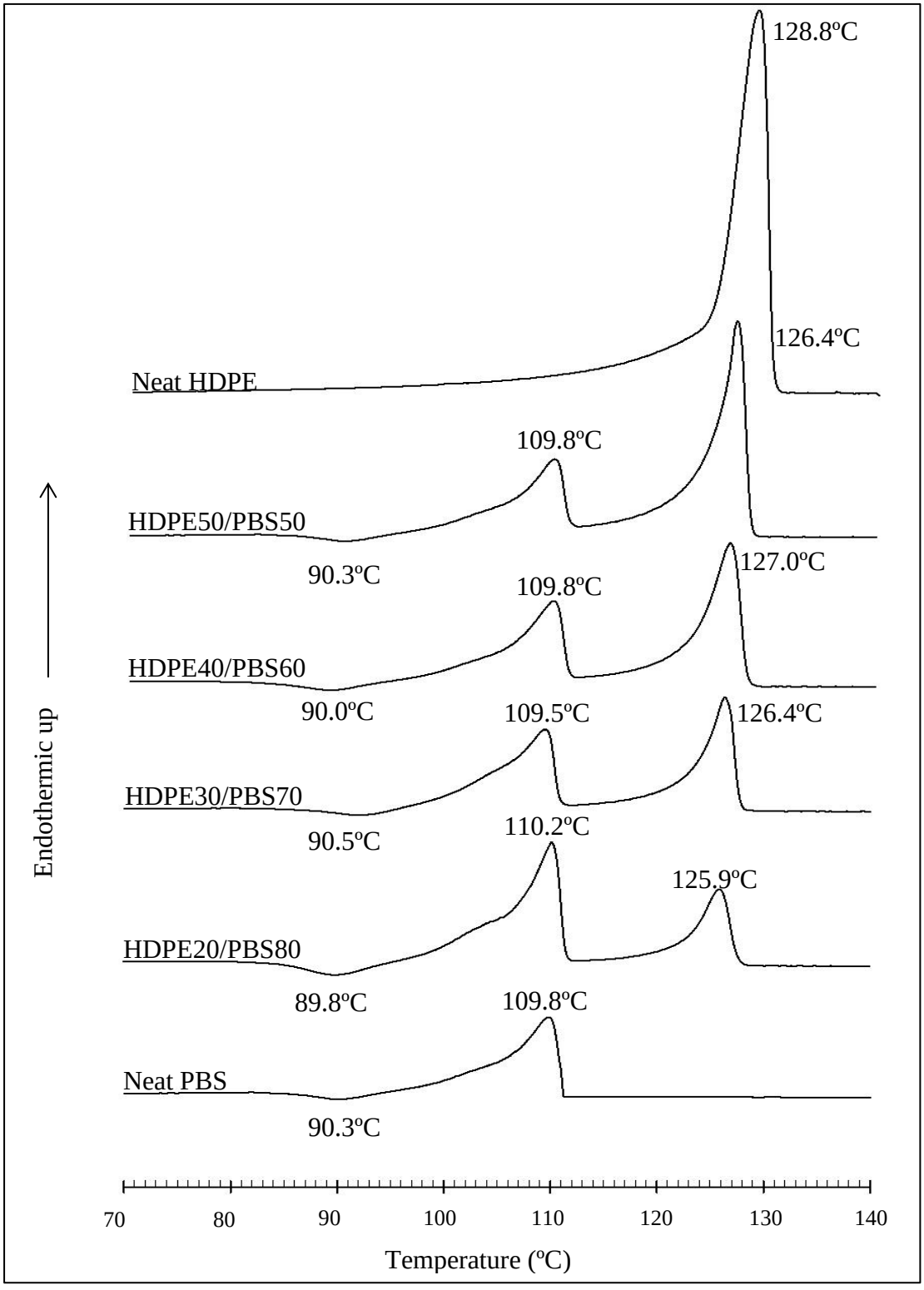

Figure 4.43 DSC curves from the first heating scan of neat PBS, neat HDPE and HDPE/PBS blend at various HDPE contents.

The DSC curves from the cooling scan of neat PBS, neat HDPE and HDPE/PBS blend at various contents of HDPE are presented in Figure 4.44. The crystallization temperature of neat PBS and neat HDPE was observed at 85.1°C and 116.7°C, respectively. The adding HDPE into PBS matrix made an insignificant change the crystallization temperature of PBS phase whereas HDPE itself crystallized at a slight higher temperature.

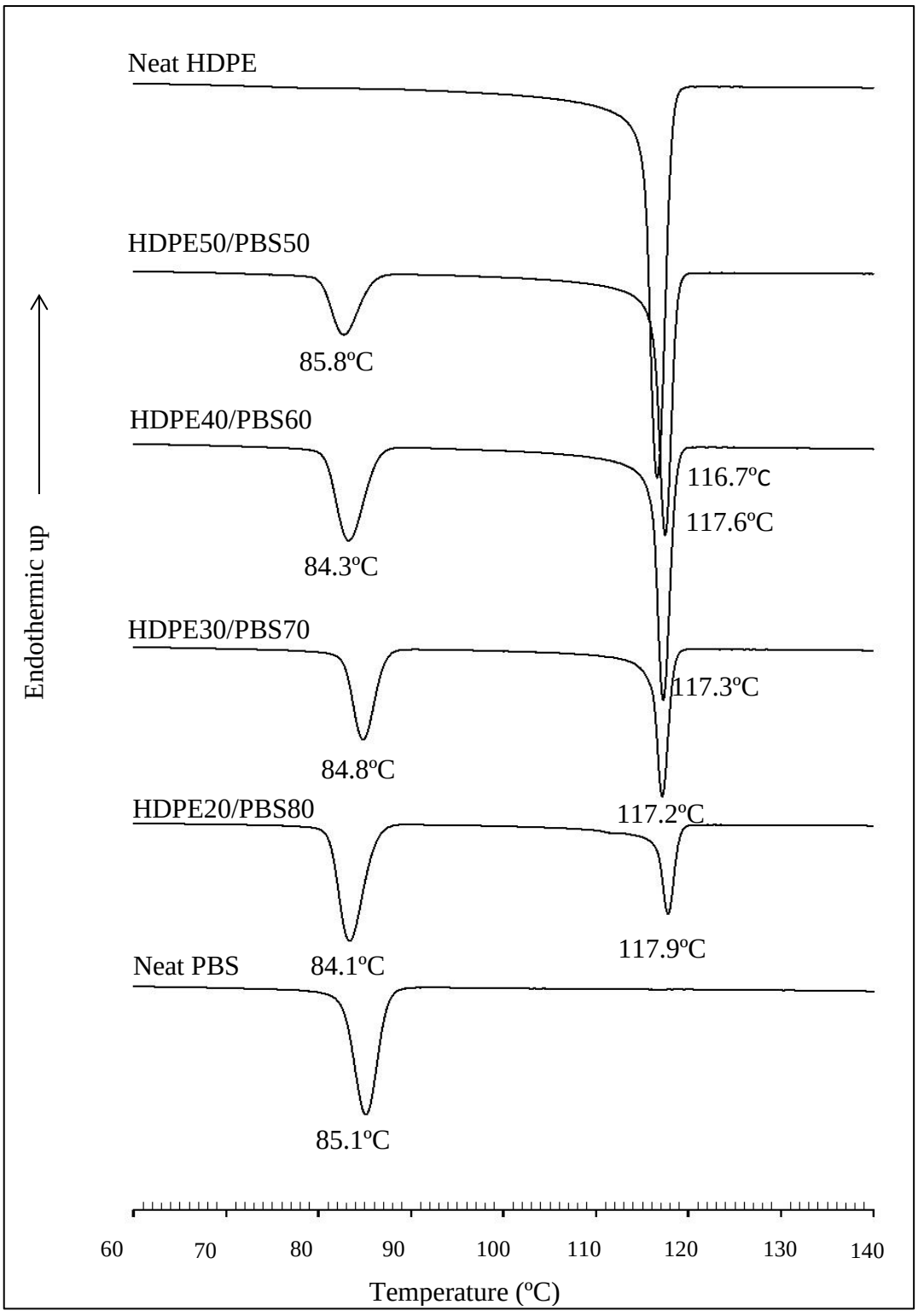

Figure 4.44 DSC curves from cooling scan of neat PBS, neat HDPE and HDPE/PBS blend at various HDPE contents.

The DSC curve from the second heating scan of neat PBS, neat HDPE and HDPE/PBS blend at various contents of HDPE are shown in Figure 4.45. The DSC curve neat PBS shows double endothermic peak of PBS at temperature of 100.1°C and 109.0°C. The double melting peak of PBS could be explained by the present of 2 forms of PBS spherulites. It was the fact that polymers might crystallize into a metastable crystal form (β form), and more stable crystal form (α form). Partly of metastable β crystal melted at low temperature, then the more stable crystallites melted at higher temperature (Yoo and Im, 1999; Qiu, Komura, Ikehara and Nishi, 2003; Lee and Lee, 2005). The DSC curve of neat HDPE exhibits an endothermic melting peak at 129.0°C. Adding HDPE into PBS matrix did insignificantly influence melting behavior of PBS phase at both lower and higher temperature peaks. Also, the melting temperature of HDPE domain was not influence by HDPE content itself.

In addition, the melting temperature and cold crystallization temperature from the first heating scan and crystallization temperature of HDPE/PBS blend at various contents HDPE are summarized in Table 4.22.

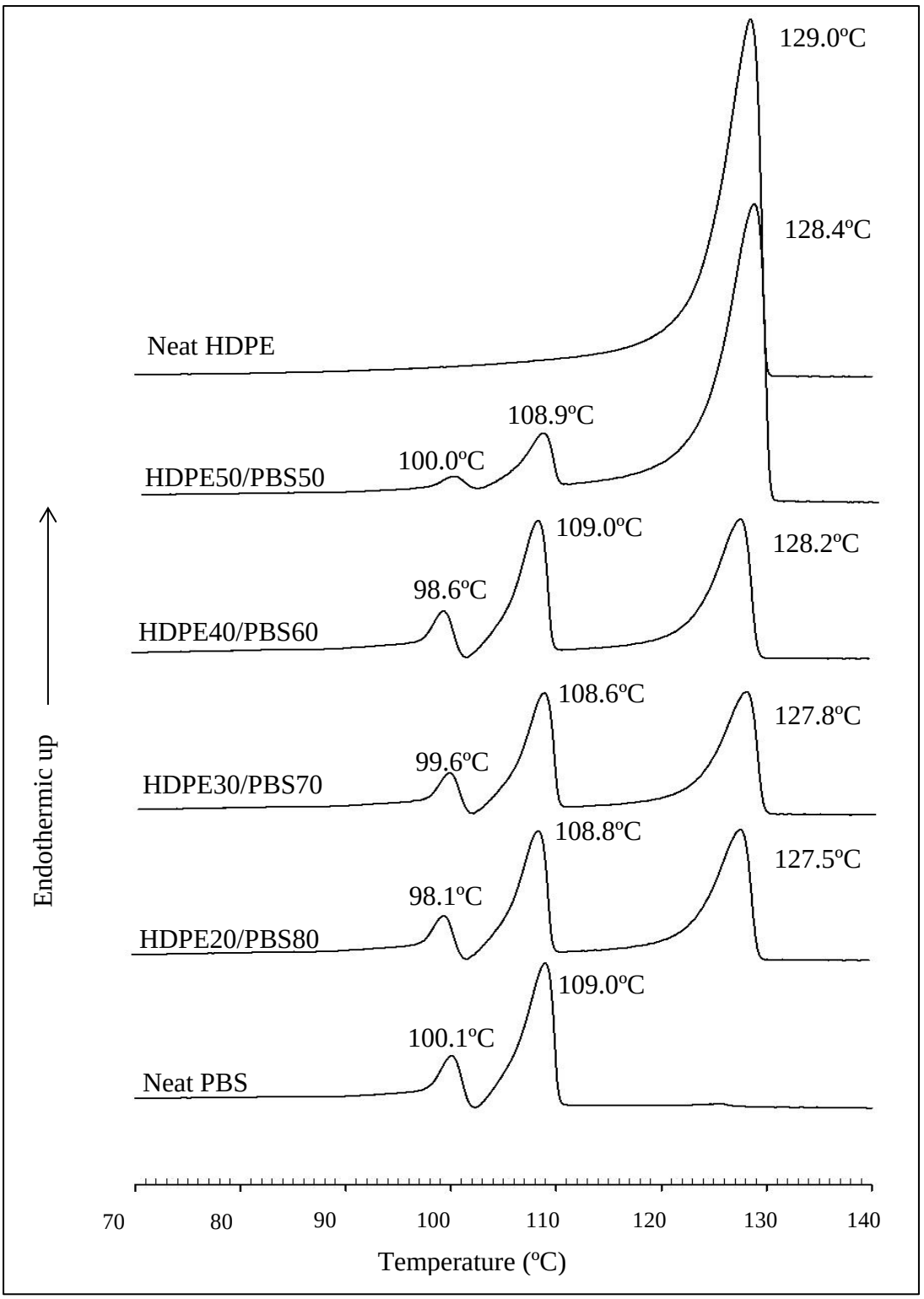

Figure 4.45 DSC curve from the second heating scan of neat PBS, neat HDPE and HDPE/PBS blend at various HDPE contents.

Table 4.22 Melting temperature and cold crystallization temperature from the first heating scan, crystallization temperature and melting at low and high temperature of neat HDPE, neat PBS and HDPE/PBS blend.

Sample	First heating scan			Crystallization temperature (^{o}C)		Second heating scan	
	Melting temperature (^{o}C)		Cold crystallization temperature (^{o}C)			Melting temperature (^{o}C)	
	PBS matrix	HDPE domain	PBS matrix	PBS matrix	HDPE domain	PBS matrix	HDPE domain
Neat PBS	109.8	-	90.3	85.1	-	100.1,109.0	-
HDPE20/PBS80	110.2	125.9	89.8	84.1	117.9	98.1,108.8	127.5
HDPE30/PBS70	109.5	126.4	90.5	84.8	117.2	99.6,108.6	127.8
HDPE40/PBS60	109.8	127.0	90.0	84.3	117.3	98.6,109.0	128.2
HDPE50/PBS50	109.8	127.0	90.3	85.8	118.8	100.0,108.9	128.4
Neat HDPE	-	128.8	-	-	116.7	-	129.0

4.2.1.6 Water absorption

Plot of water absorption (%) and immersion time of neat PBS, neat HDPE and HDPE/PBS blends is shown in Figure 4.46. The water absorption of neat PBS was much higher than that of neat HDPE. This was a consequence of high hydrophilicity of PBS facilitated by its ester groups along the PBS main chains. These groups were able to well interact with water molecules via hydrogen bond (Merdas, Thominette, Tcharkntchi and Verdu, 2002). Also, HDPE hardly absorbed water molecules due to its hydrophobic nature (Puukilainen, Koponen, Xiao, Suvanto, and Pakkanen, 2006). Figure 4.46 also shows that the water absorption of neat PBS rapidly increased within 6 days of immersion time. After, 51 and 42 days of immersion, the water absorption of neat PBS and neat HDPE reached to equilibrium of water absorption, respectively. Adding HDPE into PBS matrix brought about a decrease of water absorption of the blends. The decrease in water absorption of the HDPE/PBS was due to the composition of hydrophobic materials increased, leading to lesser absorbed water molecules of HDPE/PBS blend sample. In addition, the HDPE/PBS blend containing 20 wt.%, 30 wt.%, 40 wt.% and 50 wt.% HDPE gained an equilibrium at immersion times of 51 days, 48 days, 48 days, and 45 days, respectively.

In addition, immersion time and water content of neat PBS, neat HDPE and HDPE/PBS blends at equilibrium is summarized in Table 4.23.

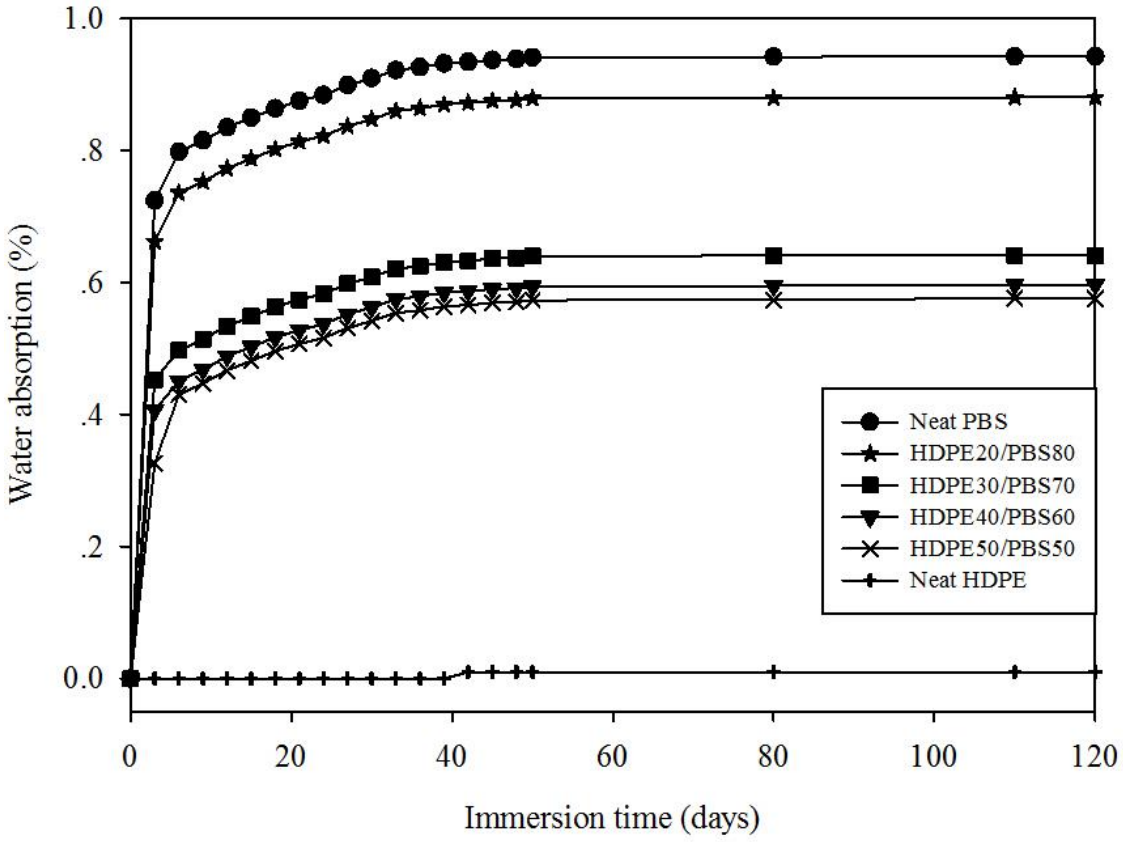

Figure 4.46 Plot of water absorption vs. immersion time of neat PBS, neat HDPE and HDPE/PBS blends.

Table 4.23 Immersion time and water content of neat PBS, neat HDPE and HDPE/PBS blends at equilibrium.

Sample	Immersion time (day)	Water content at equilibrium (%)
Neat PBS	51	0.94%
HDPE20/PBS80	51	0.88%
HDPE30/PBS70	48	0.64%
HDPE40/PBS60	48	0.59%
HDPE50/PBS50	45	0.58%
Neat HDPE	42	0.01%

4.2.1.7 Biodegradation by soil burial test

Plot of weight loss (%) and buried time of neat PBS, neat HDPE and PBS/HDPE blends is shown in Figure 4.47. The weight loss of neat PBS was much higher than that of neat HDPE according to a high hydrophilicity of PBS that were prone to hydrolytic cleavage by micro-organisms, especially, *Aspergillus Niger* micro-organism of which encountered in soil during burial test (Shah, Hasan, Hameed, and Ahmed, 2008). The main problem of lower weight loss of HDPE was degree of hydrophobicity of the polyethylene chains, which impact directly on the rates of depolymerization caused by micro-organism (Łabużek, Nowak and Pająk, 2003; Nowak, Pająk, Bratkowicz and Rymarz, 2011). Adding HDPE into PBS matrix led to a decrease of weight loss of the blend. This was due to HDPE in the blend resisted the microbial attack.

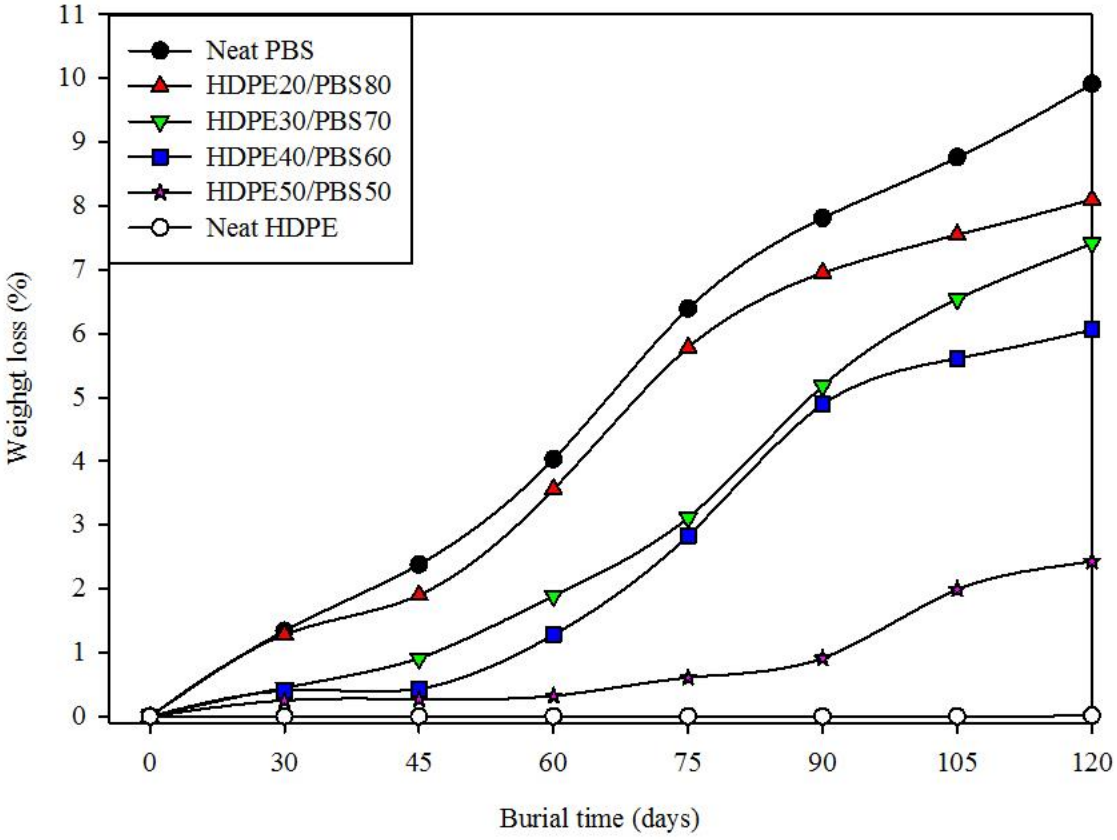

Figure 4.47 Plot of weight loss (%) and burial specimens of neat PBS, neat HDPE and HDPE/PBS blends.

Figure 4.48 shows optical photographs of the surfaces of the samples buried in the soil for 120 days. It illustrates that the biodegradation of neat PBS occurred at 30 days of burial time, as observed from the occurrence of dark area and rougher surface. In addition the biodegradation of neat PBS was more severe as the burial time increased. For neat HDPE, there was no change in the appearance of neat HDPE sample within 120 days of burial time as compared with the sample before burial in soil.

At 20 wt.% HDPE, It was observed that the dark streak occurred after burial time of 30 days. The surface of blend sample was eroded as

observed from the rough surface after burial time of 45 days. In addition, the blend sample was more eroded as the burial time increased.

With adding 30 wt.% HDPE, the roughness of the blend sample less occurred comparing the blend at 30 wt.% HDPE. However, a small dark spot was still observed at the edge of the blend sample after 30 days of burial time. In addition, the dark spot area further increased with increasing burial time.

As increasing HDPE content to 40 wt.%, the dark spot occurred at 45 days of burial time. However, the biodegradability of the blend was more severe when the burial time increased, as observed from the expansion of the darken area.

With increasing HDPE to 50 wt.%, the small dark spot occurred at the edge of the blend sample after 30 days of burial time. After the 45 days, the whitening part occurred and spreaded to the surface of the blend sample. Furthermore, the surface of the blend was rougher after 45 days of burial time. In addition, the biodegradation was more drastic as seen in the darken part at the blend sample surface after burial time of 75 days.

In addition, the decrease in biodegradability of HDPE/PBS blend at various content of HDPE is summarized in Table 4.24.

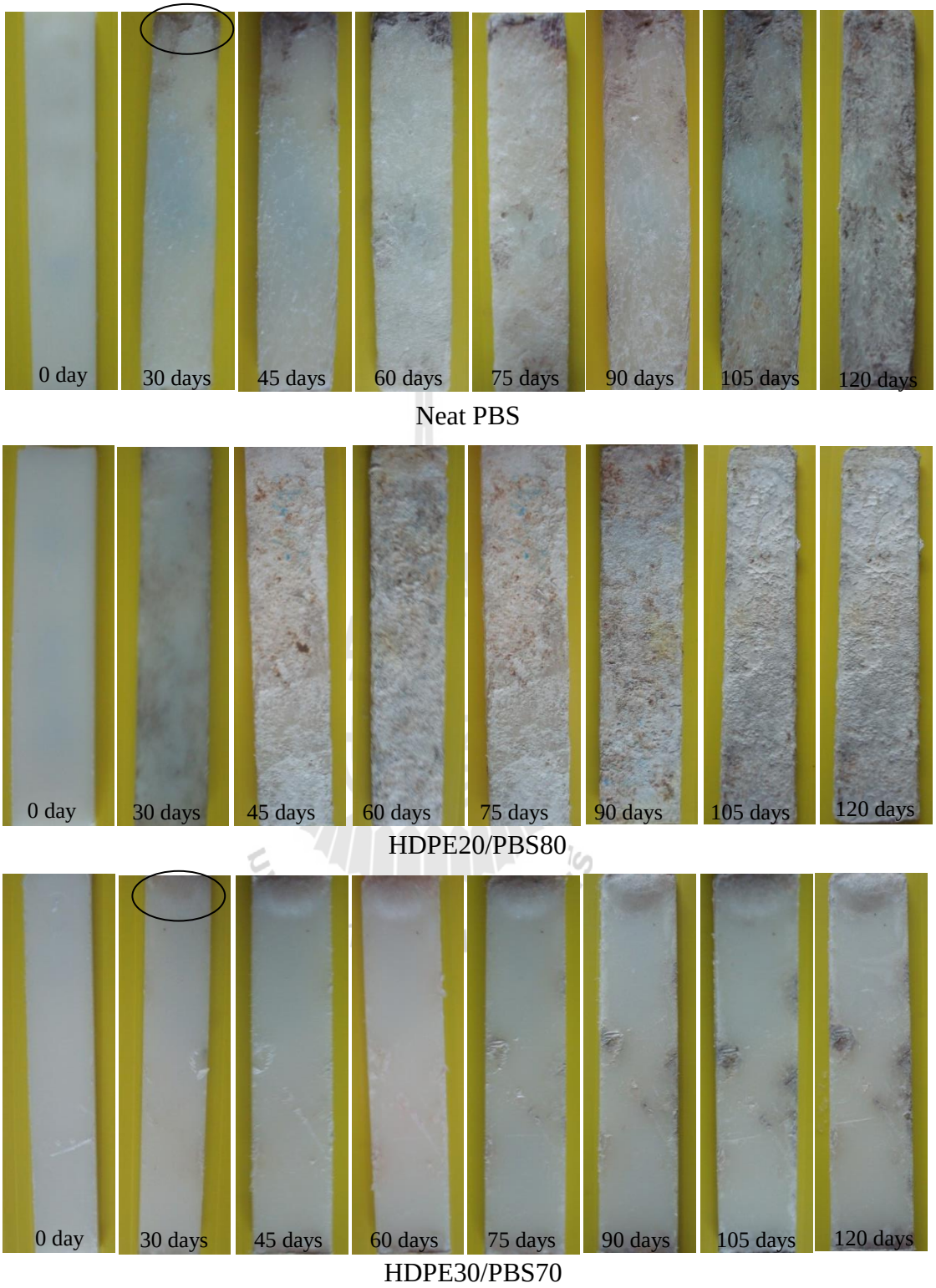

Figure 4.48 Optical micrographs of buried specimens of neat PBS, neat HDPE and HDPE/PBS blends at several burial times of 0 to 120 days.

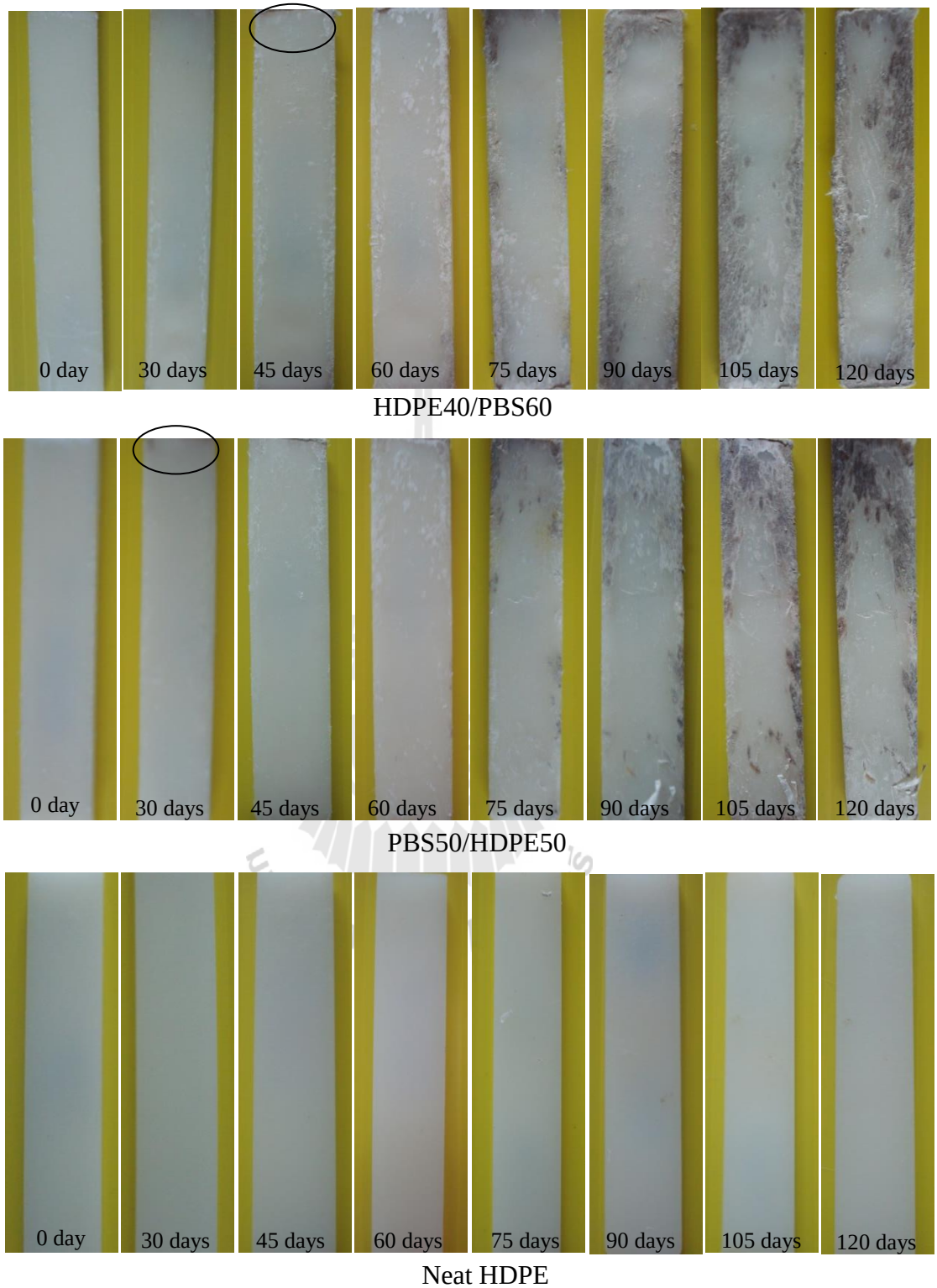

Figure 4.48 Optical micrographs of buried specimens of neat PBS, neat HDPE and HDPE/PBS blends at several burial times of 0 to 120 days. (Continued)

Table 4.24 The decrease in biodegradability of HDPE/PBS blend at various content of HDPE comparing neat PBS.

Sample	Biodegradability (%)	Decrease in Biodegradability (%)
Neat PBS	9.91	-
HDPE20/PBS80	8.10	1.80
HDPE30/PBS70	7.41	2.49
HDPE40/PBS60	6.06	3.85
HDPE50/PBS50	2.43	7.47
Neat HDPE	0.01	-

4.2.2 Effect of compatibilization on physical properties

Base on mechanical properties, the HDPE/PBS blend containing 30 wt.% PBS gave an acceptable Young's modulus and tensile strength. Therefore, this blend composition was further study the compatibilization effect. The effect of compatibilizer type and content on physical properties of compatibilizied HDPE30/PBS70 blend was revealed. The compatibilizers were HDPE-g-MAH and EPR-g-MAH. The compatibilizer contents were 2, 4, 6, and 8 phr.

4.2.2.1 Flow property

The dependence of apparent shear viscosity on apparent shear rate of uncompatibilized and compatibilized HDPE/PBS blend with HDPE-g-MAH and EPR-g-MAH at various contents is presented in Figure 4.49(a) and Figure 4.49(b), respectively. Figure 4.49(a) illustrates that the shear thinning behavior was observed from both uncompatibilized and compatibilized HDPE/PBS blends. In comparison, the viscosity of the uncompatibilized blend was lower than that of

compatibilized blend. Furthermore, the viscosity of compatibilized blend slightly increased with increasing HDPE-g-MAH content. This slight increase in the viscosity implied the occurrence of interfacial interactions, H-bonding and interchain diffusion (Qi, Nie, Zhou, Mao and Zhang, 2006). The H-bonding occurred between maleicanhydride groups of HDPE-g-MAH and ester groups of PBS. The interchain diffusion was between molecular chains of HDPE and HDPE backbone of HDPE-g-MAH.

Figure 4.49(b) demonstrates that both uncompatibilized and compatibilized HDPE/PBS blend exhibited shear thinning behavior. Adding EPR-g-MAH into the binary blend led to an increase of viscosity of the blend. However, increasing EPR-g-MAH content resulted in a slight increase of viscosity of the compatibilized blend. The similar result had been reported in HDPE/PET blend using elastomeric compatibilizer such as SEBS-g-MA (Pracella, Pazzagli and Galeski, 2002).The slight increase in the viscosity of compatibilized blend implied to the occurrence of interactions between MAH groups of EPR-g-MAH and ester groups of PBS, together with physical entanglement between HDPE chains and EPR backbone.

In comparison, the shear viscosity of the compatibilized blend using HDPE-g-MAH and EPR-g-MAH at a shear rate range corresponding to that during injection molding process, 3,000-4,000 s^{-1} was insignificantly different, as illustrated in Table 4.25.

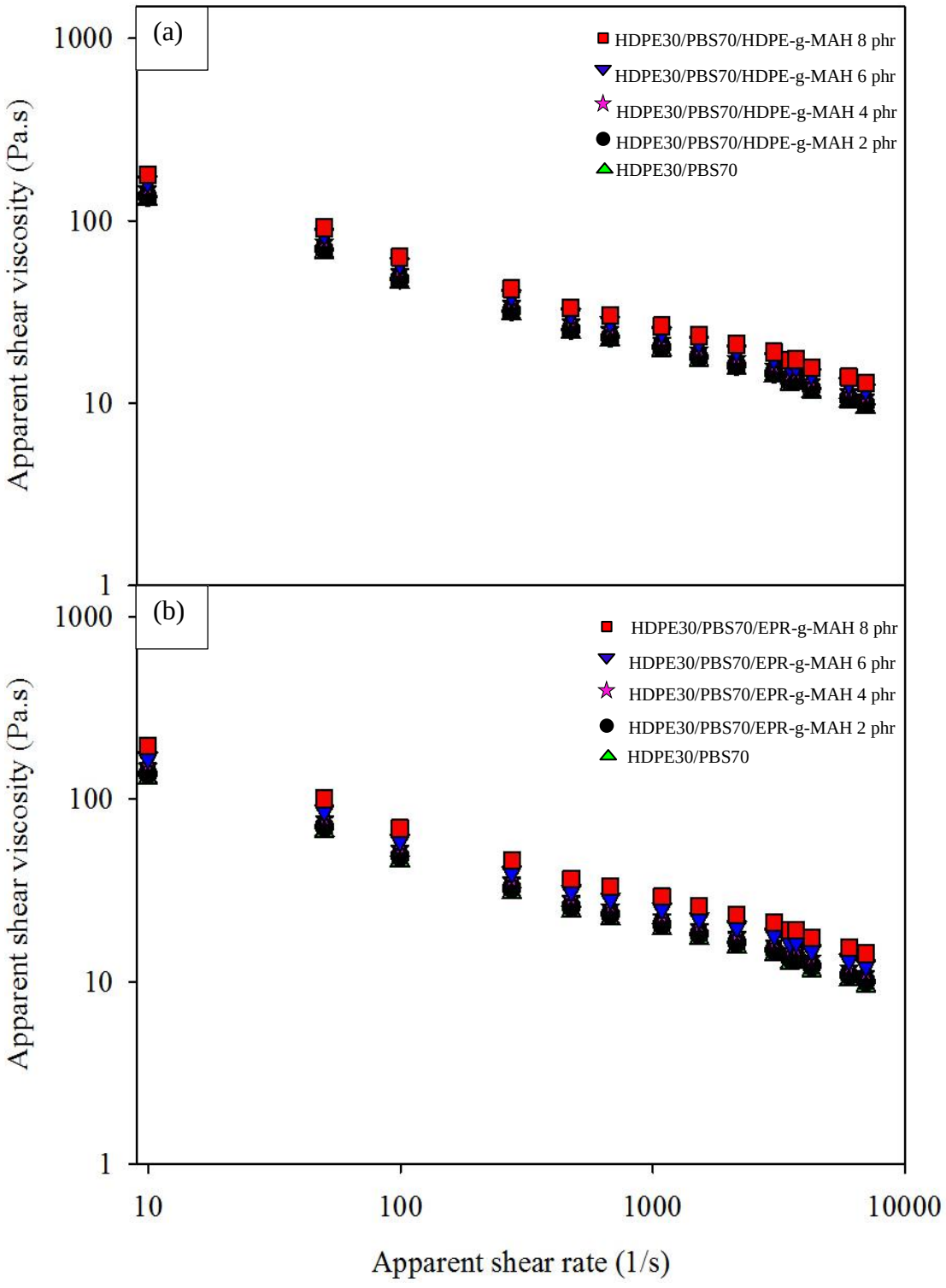

Figure 4.49 Plot of apparent shear viscosity as a function of apparent shear rate of uncompatibilized and compatibilized HDPE30/PBS70 blend at various contents of HDPE-g-MAH (a) and EPR-g-MAH (b).

Table 4.25 Shear viscosity range within the shear rate range of injection molding of uncompatibilized and compatibilized HDPE30/PBS70 blend with HDPE-g-MAH and EPR-g-MAH.

Compatibilizer content	Shear viscosity range (Pa.s)	
	Blend with HDPE-g-MAH	Blend with EPR-g-MAH
0 phr	14.02-11.51	14.02-11.51
2 phr	14.58-11.98	14.87-12.21
4 phr	15.89-13.05	16.36-13.44
6 phr	17.48-14.36	18.14-14.90
8 phr	19.05-15.65	21.12-17.35

Melt flow index (MFI) at 180°C with a standard weight of 2.16 kg of uncompatibilized and compatibilized HDPE30/PBS70 blend with various contents of HDPE-g-MAH and EPR-g-MAH is presented in Table 4.26. It illustrates that the MFI of HDPE30/PBS70 blend compatibilized with HDPE-g-MAH was slightly lower than that of uncompatibilized blend. This result corresponded well with the result of HDPE/PET blend using HDPE-g-MAH (Pawlak, Morawiec, Pazzagl and Pracella, Galeski, 2002). As increasing HDPE-g-MAH content, the MFI of the compatibilized HDPE30/PBS70 blend decreased. For the HDPE30/PBS70 blend compatibilized with EPR-g-MAH, the addition of EPR-g-MAH into PBS30/HDPE70 blend led to a decrease of MFI. Adding more EPR-g-MAH content into the HDPE30/PBS70 blend brought about a gradual decrease of MFI. In comparison, the MFI of the compatibilized blends using HDPE-g-MAH and EPR-g-MAH as compatibilizers was insignificantly different.

Table 4.26 Melt flow index (MFI) at 180°C with a standard weight of 2.16 kg of uncompatibilized and compatibilized HDPE30/PBS70 blend with various contents of HDPE-g-MAH and EPR-g-MAH.

Compatibilizer content	MFI (g/10min)	
	HDPE-g-MAH	EPR-g-MAH
0 phr	22.7	22.7
2 phr	22.0	21.6
4 phr	20.7	20.4
6 phr	19.5	18.9
8 phr	19.0	18.7

4.2.2.2 Failure behavior and phase morphology

Engineering stress-strain of uncompatibilized and compatibilized HDPE30/PBS70 blend at various contents of HDPE-g-MAH is presented concurrently with their SEM images in Figure 4.50. As shown in the stress-strain curve, the uncompatibilized HDPE30/PBS70 blend failed and fractured in a brittle manner at 24 MPa stress and 28% strain. As shown in Figure 4.50(a), phase morphology of uncompatibilized HDPE30/PBS70 blend clearly exhibited two separate phases morphology. The HDPE domains were non-uniform in size and shape, including spherical, elongated and worm-like dispersed in PBS matrix. The approximate domain size was in a range of 4 μm to 11 μm.

After adding 2 and 4 phr HDPE-g-MAH into HDPE30/PBS70 blend, the failure behavior of the compatibilized blend were still in a brittle manner similar to those of uncompatibilized blend, as observed from its stress-strain curve

illustrated in Figure 4.50. The blend compatibilized with 2 phr HDPE-g-MAH fracture at stress and strain of 26 MPa and 36%, respectively whereas the blend compatibilized with 4 phr fracture at stress and strain of 27 MPa and 41%, respectively. Phase morphologies of the HDPE/PBS compatibilized with 2 and 4 phr HDPE-g-MAH are shown in Figure 4.50(b) and (c), respectively. With adding 2 and 4 phr HDPE-g-MAH, HDPE domain was still non-uniform in size, and shape. It was sphere, elongated, and worm-like shape. However, size of HDPE domain of the compatibilized blend was smaller than that of uncompatibilized HDPE/PBS blend. The approximate domain size of compatibilized blend was 3-8 μm. The decrease in size of HDPE domain was a consequence of the decreased interfacial tension between HDPE domain and PBS matrix by added HDPE-g-MAH. The decrease in interfacial tension gave rise to an increase of capillary number contributing the smaller size of domain phase (Harrats, Thomas and Groeninckx, 2006).

With increasing HDPE-g-MAH content to 6 and 8 phr, the toughness of the blend improved, as observed from their stress strain curves. They illustrate that failure behavior of the blends was in a ductile manner with clear defined yielding point. However, they still ruptured at ultimate strain less than 100%; 72% and 79% for the blend compatibilized with 6 and 8 phr HDPE-g-MAH, respectively. Phase morphology of the blends compatibilized with HDPE-g-MAH of 6 and 8 phr are presented in Figure 4.50(d) and (e), respectively. These reveal that adding 6 and 8 phr HDPE-g-MAH led to a creation of fibrillation of HDPE domain. Diameter of the fibrillar domain was small, approximate 2-5 μm. The much lower in interfacial tension due to added more HDPE-g-MAH was responsible for decreased domain diameter. It also made HDPE domain capable to large deformation, under shear force,

in flow direction without occurrence of breaking up. As a matter of fact melting sequence of matrix and dispersed phase was also a key factor determining phase morphology of the blend. For the PBS blend, PBS matrix melted first following by the melting of HDPE domain; this melting sequence also accompanied with other two key factors, high interfacial tension and high viscosity ratio, in a creation of fibrillar structure. In addition, it was previously reported that the presence of compatibilizer could lead to the formation of elongated droplets (Levitt and Macosco, 1999).

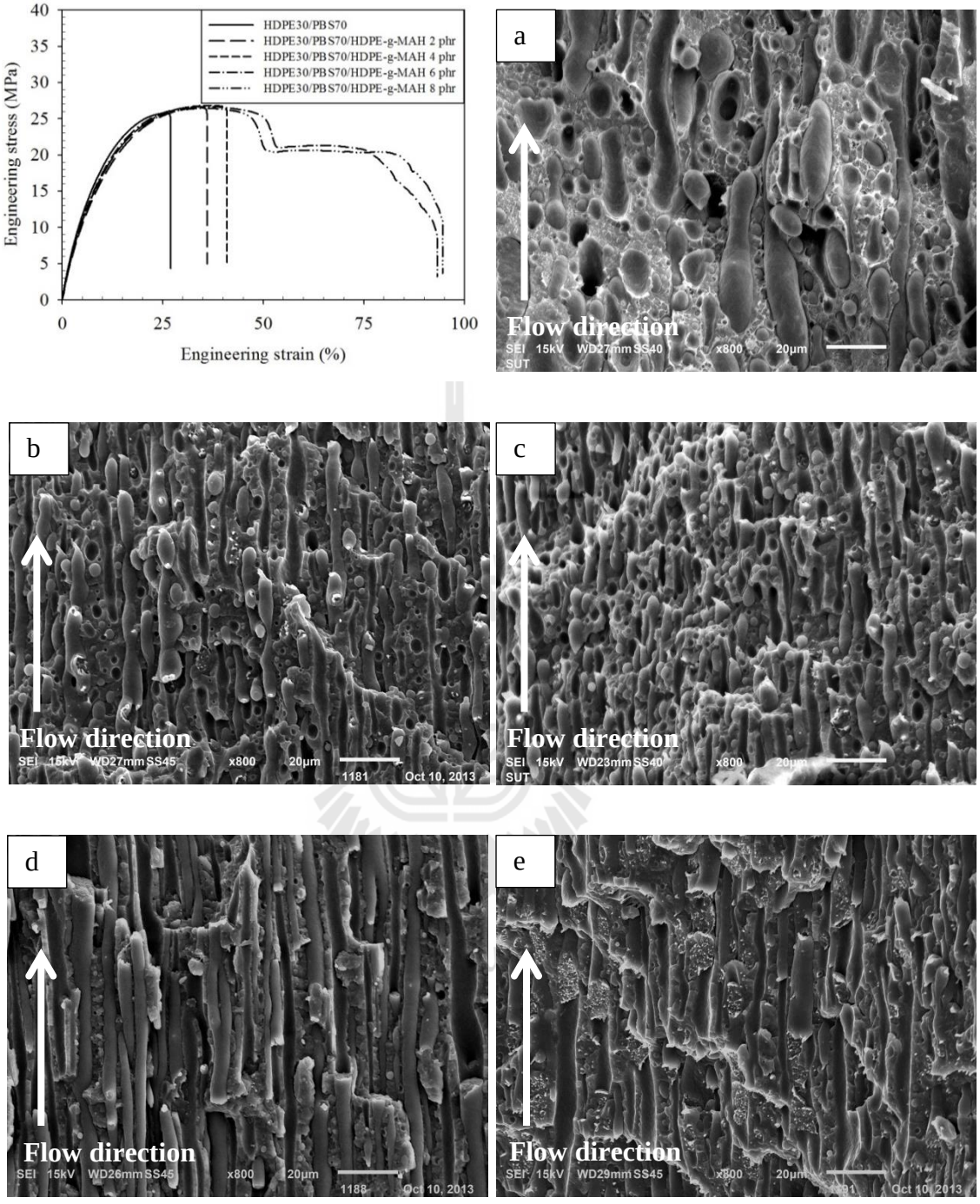

Figure 4.50 Tensile stress-strain curves and SEM micrographs of HDPE etching specimens at magnification of x800 of uncompatibilized and compatibilized HDPE30/PBS70 blend with HDPE-g-MAH at 0 phr (a), 2 phr (b), 4 phr (c), 6 phr (d) and 8 phr (e).

Engineering stress-strain curves of the blend compatibilized with 2 phr EPR-g-MAH fractured at a lower strain comparing to uncompatibilized blend. Its stress-strain curve exhibited that the blend failed and fractured in a brittle manner at 13 MPa stress and 18% strain, as observed from Figure 4.51. From its phase morphology in Figure 4.51(b), it revealed that HDPE domain was in spherical shape incorporated with some elongated particles. In approximation, diameter of the spherical domain was in a range of 2 μm to 15 μm.

As increasing EPR-g-MAH to 4 phr, EPR-g-MAH rarely affected the fracture behavior of the compatibilized blend, as observed from their stress-strain curve. The blend failed and fractured at 14 MPa stress and 18% strain. However, adding adding 4 phr EPR-g-MAH did insignificant affect phase morphology of the compatibilized blend. Its phase morphology was still in a spherical shape with approximate size of 2 μm to 20 μm with incorporation of some elongated particles, as shown in Figure 4.51(c).

With adding 6 and 8 phr EPR-g-MAH into HDPE/PBS blend, stress-strain curve exhibited that the blend still failed and fractured in a brittle manner. The blend compatibilized with 6 phr of EPR-g-MAH failed and fractured at 15 MPa stress and 18% strain whereas the blend at 8 phr EPR-g-MAH failed and fractured at 15 MPa stress and at slightly higher strain, 23%. Adding 6 and 8 phr EPR-g-MAH into HDPE/PBS blend gave rise to more uniform in shape of HDPE domain, as shown in Figure 4.51(e) and Figure 4.51(e), respectively. HDPE domains were mostly in spherical shape. Diameter of the HDPE domain was approximate 2-25 μm. It was previously reported in the similar system, PP/PBT blend using EPDM-g-GMA elastomeric as a compatibilizer, that EPDM-g-GMA controlled morphology as

generated by an elastic repulsion of EPDM-g-GMA. When two droplets approached, they were not able to coalescence due to repulsion of EPDM-g-GMA. (Ao et al., 2007). The similar result was also observed in HDPE/PET blend using elastomeric compatibilizer such as SEBS-g-MAH. (Pawlak, Morawiec, Pazzagl and Pracella, Galeski, 2002).

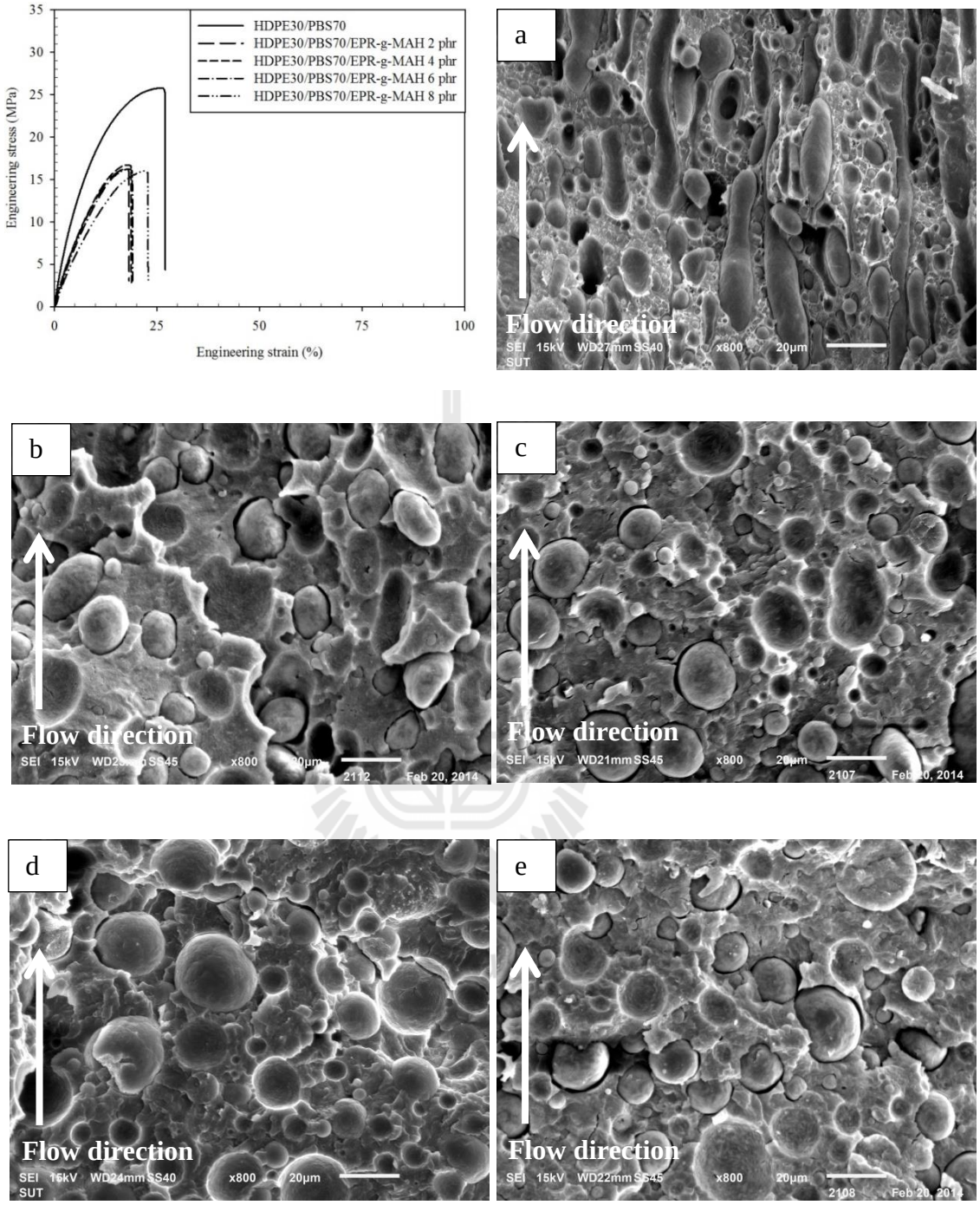

Figure 4.51 Tensile stress-strain curves and SEM micrographs of HDPE etching specimens at magnification of x800 of uncompatibilized and compatibilized HDPE30/PBS70 blend with EPR-g-MAH at 0 phr (a), 2 phr (b), 4 phr (c), 6 phr (d) and 8 phr (e).

4.2.2.3 Mechanical properties

Young's modulus of uncompatibilized and compatibilized HDPE30/PBS70 blends at various contents of HDPE-g-MAH and EPR-g-MAH is presented in Figure 4.52. Young's modulus of HDPE30/PBS70 blend compatibilized with HDPE-g-MAH was slight lower than that of uncompatibilized blend. Adding 2 to 8 phr HDPE-g-MAH into HDPE/PBS blend led to an insignificant decrease in Young's modulus of the blend. The similar result was previously found in the system of HDPE/PET blend using ethylene/glycidyl methacrylate copolymers (E/GMA) and ethylene/ethyl acrylate/glycidyl methacrylate terpolymers (E/EA/GMA) as compatibilizers. It had been reported that the Young's modulus of compatibilized was lower than that of uncompatibilized blend (Pietrasanta, Robin, Torres and Boutevin, 1999; Mbarek, Jaziri, Chalamet and Carrot, 2010). Similarly, Young's modulus of HDPE30/PBS70 blend compatibilized with EPR-g-MAH was lower than that of uncompatibilized blend. Addition of EPR-g-MAH into HDPE30/PBS70 blends resulted in a gradually decrease of Young's modulus. This might be due to the elastic characteristic of EPR-g-MAH. Naturally, EPR-g-MAH is rubbery at room temperature which has low Young's modulus with high elasticity. Adding EPR-g-MAH bring about an inclusion of rubbery amorphous phase. Therefore, the Young's modulus of the PBS30/HDPE70 blends diminished. It was previously reported that Young's modulus of nylon 6 blended with EPR-g-MAH decreased as increasing EPR-g-MAH content (Okada, Keskkula, Paul, 2001).

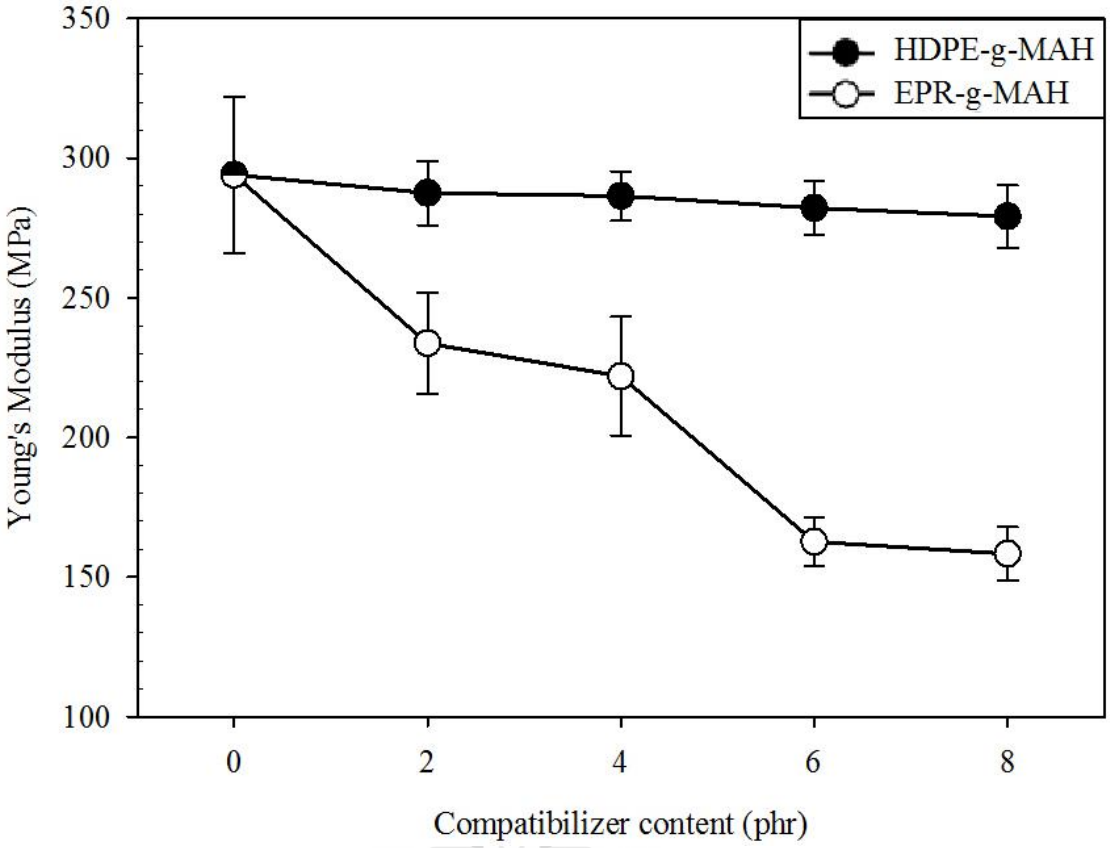

Figure 4.52 Plot of Young's modulus of HDPE30/PBS70 blends at various contents of HDPE-g-MAH and EPR-g-MAH.

From Figure 4.53, it illustrates that the elongation at break of compatibilized blend was higher than that of uncompatibilized blend. The addition of 2 to 4 phr HDPE-g-MAH led to a significant increase of elongation at break of the blend. As increasing HDPE-g-MAH to 6 and 8 phr, the elongation at break of the blend improved greatly. The improvement of elongation at break attributed to the better adhesion between HDPE and PBS phase. The better adhesion occurred due to chemical reactions between MAH of HDPE-g-MAH with ester groups of PBS concurrently with the interchain diffusion of HDPE backbone of HDPE-g-MAH and HDPE phase. In addition, this result corresponded well with their fibrillar phase

morphology as shown in Figure 4.50(d) and Figure 4.50(d), respectively. Figure 4.53 also shows elongation at break of the blend compatibilized with EPR-g-MAH. It illustrates that adding 2 phr EPR-g-MAH brought about a slight decrease of elongation at break of the blend. As increasing EPR-g-MAH to 4 and 6 phr, elongation at break of the blend insignificantly changed. The insignificantly change of elongation at break correlated well with their unchanged in phase morphology, as previously shown in Figure 4.51. However, adding EPR-g-MAH more than 6 phr resulted in a slight improved of elongation at break of the blend.

In comparison, HDPE-g-MAH was more effective for improving elongation at break of the blend than EPR-g-MAH. This might be a consequence of a large difference of solubility parameter between HDPE and EPR-g-MAH of which resulted in a poor diffusion between HDPE and EPR backbone of EPR-g-MAH. The solubility parameter of HDPE, HDPE-g-MAH and EPR-g-AMH is 17.5 $J^{1/2}/cm^{3/2}$, 17.6 $J^{1/2}/cm^{3/2}$ and 7.9 $J^{1/2}/cm^{3/2}$, respectively (Seo, Park, Dao, and Jeong, 2013; Ito and Guillet, 1979).

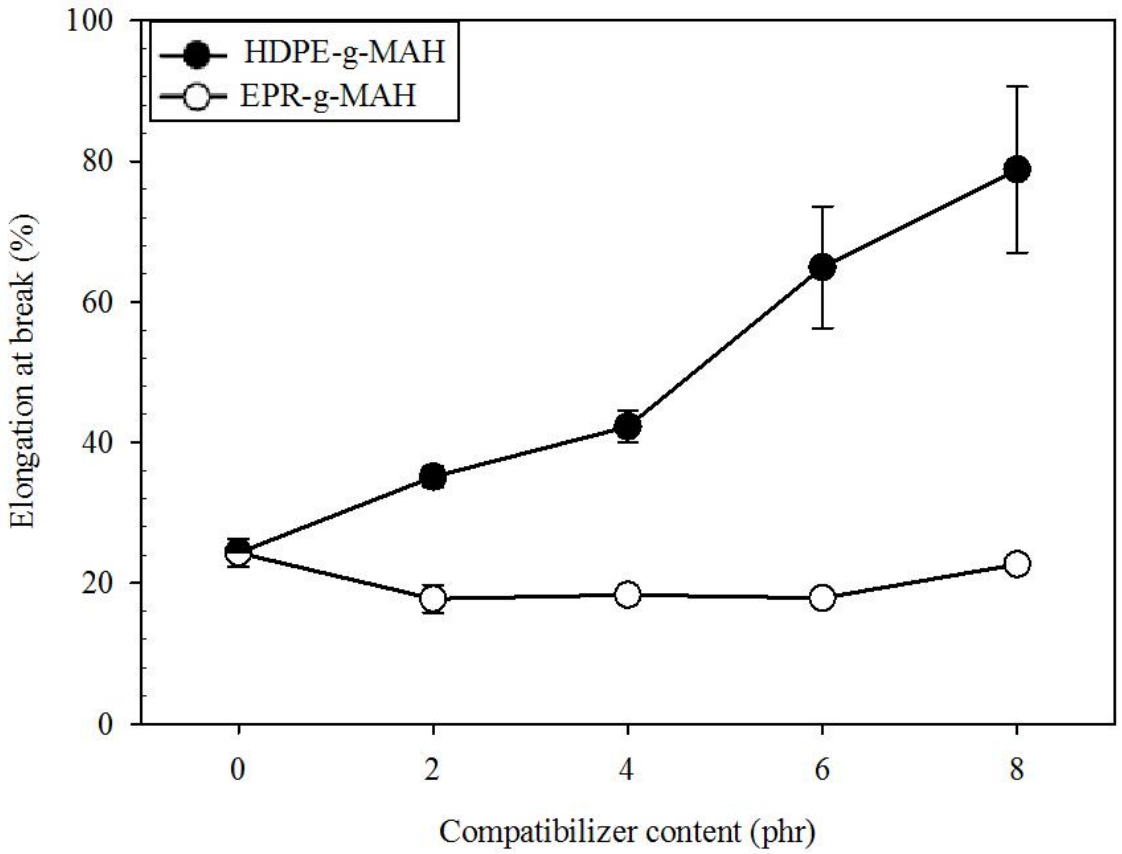

Figure 4.53 Plot of elongation at break of HDPE30/PBS70 blends at various contents of HDPE-g-MAH and EPR-g-MAH.

Figure 4.54 shows the tensile strength of uncompatibilized and compatibilized HDPE30/HDPE70 blend at various contents of HDPE-g-MAH. It illustrates that tensile strength of PBS30/HDPE70 compatibilized with HDPE-g-MAH was higher than that of the uncompatibilized blend. Adding 2 phr HDPE-g-MAH into HDPE30/HDPE70 blend made the tensile strength of the blend increased slightly. However, the tensile strength of the blend did insignificantly change with adding more HDPE-g-MAH. The slight improvement of tensile strength might be due to a better interfacial adhesion between HDPE domain and PBS matrix. The better adhesion was promoted by H-bonding between maleic anhydride group of HDPE-g-

MAH and ester groups of PBS (Martínez, Benavides and Guerrero, 2007; Lusinchi, Boutevin, Torres and Robin, 2001). In addition, because of solubility parameter of HDPE and HDPE-g-MAH is the same as HDPE-g-MAH, therefore the interchain diffusion between HDPE matrix and HDPE backbones of HDPE-g-MAH might be occurred.

For the HDPE30/HDPE70 compatibilized with EPR-g-MAH, as displayed in Figure 4.54. Adding 2 phr EPR-g-MAH into HDPE30/HDPE70 blend led to a decrease of tensile strength of the blend. However, adding more EPR-g-MAH did not make any significant change in tensile strength of the blend. In addition, tensile properties of HDPE30/PBS70 blends compatibilized with HDPE-g-MAH and EPR-g-MAH were summarized in Table 4.27.

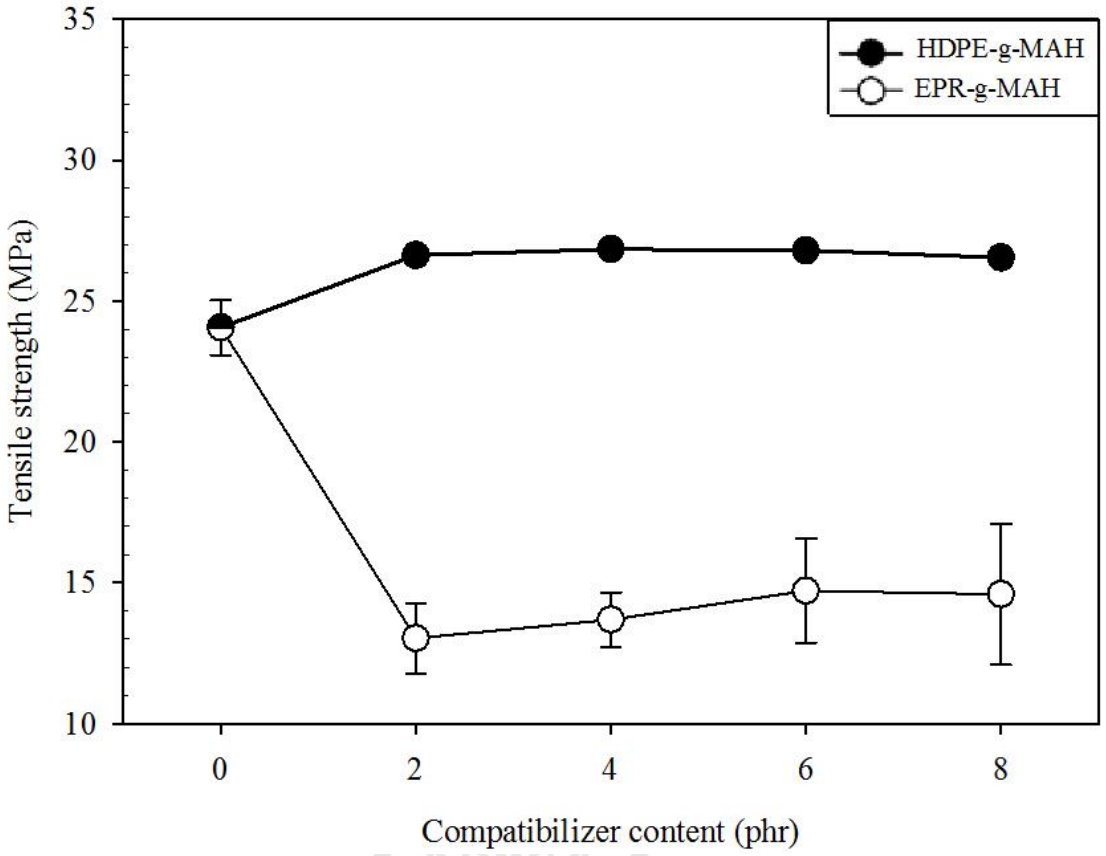

Figure 4.54 Plot of tensile strength of HDPE30/PBS70 blends at various contents of HDPE-g-MAH (a) and EPR-g-MAH (b).

From the tensile results using HDPE-g-MAH and EPR-g-MAH as compatibilizers, Seemingly, HDPE-g-MAH was more effective for maintaining tensile properties including Young's modulus, elongation at break, tensile strength of the blend.

Table 4.27 Tensile properties of HDPE30/PBS70 blends at various contents of HDPE-g-MAH and EPR-g-MAH.

Compatibilizer content (phr)	Young's modulus (MPa)		Elongation at break (%)		Tensile strength (MPa)	
	HDPE-g-MAH	EPR-g-MAH	HDPE-g-MAH	EPR-g-MAH	HDPE-g-MAH	EPR-g-MAH
0 phr	294.0±27.9		24.3±1.9		24.0±0.9	
2 phr	287.5±11.5	233.7±18.1	35.1±1.4	17.8±1.9	26.6±0.1	13.0±1.2
4 phr	286.4±8.8	221.9±21.2	43.2±2.2	18.3±0.8	26.8±0.3	13.7±0.9
6 phr	282.2±9.7	162.7±8.8	64.9±8.6	17.9±0.9	26.8±0.1	14.7±1.8
8 phr	271.9±11.3	158.3±9.5	78.8±11.8	22.7±0.3	26.5±0.1	14.6±2.5

For flexural properties, flexural modulus of uncompatibilized and compatibilized HDPE30/PBS70 blends at various contents of HDPE-g-MAH and EPR-g-MAH is presented in Figure 4.55. Flexural modulus of HDPE30/PBS70 blend comaptibilized with HDPE-g-MAH was lower than that of uncomaptibilized blend. Adding 2 phr HDPE-g-MAH resulted in a decrease of flexural modulus of the blend. However, adding more HDPE-g-MAH did not much affect flexural modulus of the blend. On the other hand, adding EPR-g-MAH into HDPE/PBS blend made the flexural modulus of the blend decreased. Moreover, adding more EPR-g-MAH resulted in a gradually decrease of flexural modulus of the blend. The gradually decrease of flexural modulus of the blend as increasing EPR-g-MAH content was a result of a high elasticity of EPR-g-MAH.

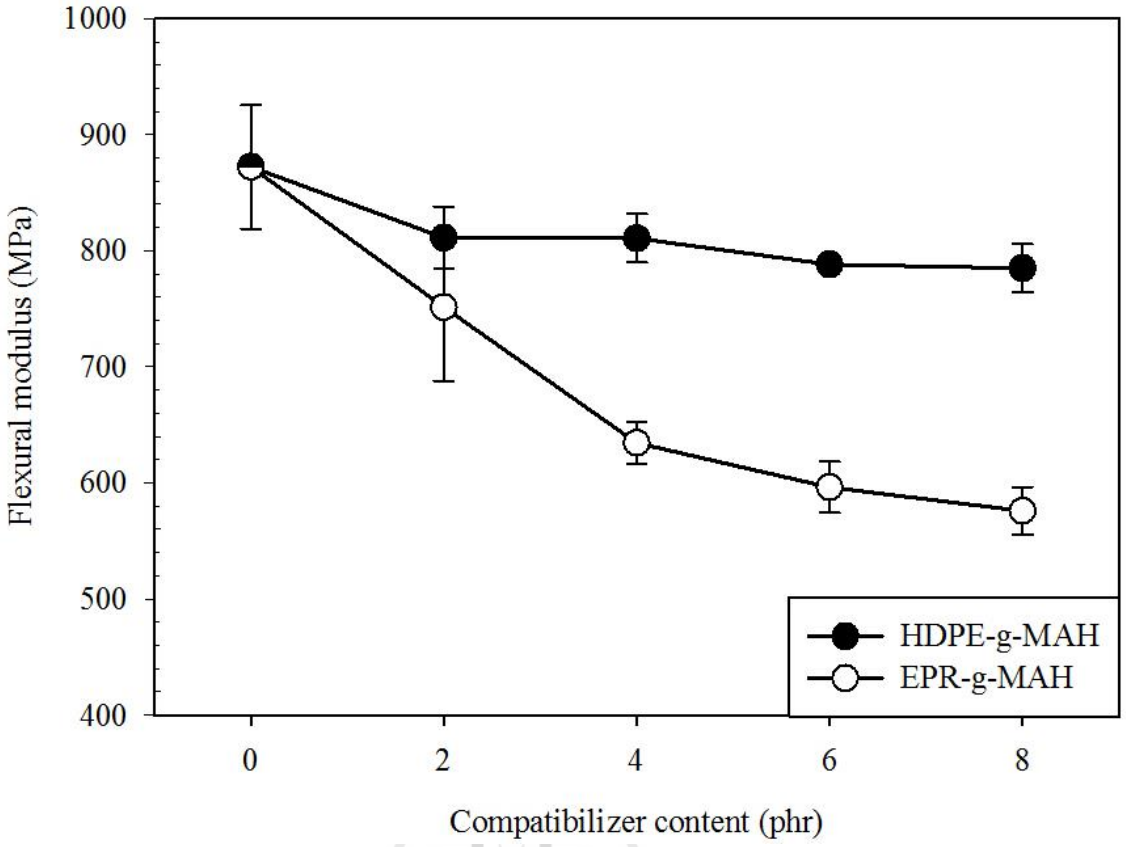

Figure 4.55 Plot of flexural modulus of HDPE30/PBS70 blends at various contents of HDPE-g-MAH and EPR-g-MAH.

Figure 4.56 shows flexural strength of uncompatibilized and compatibilized HDPE30/PBS70 blend at various contents of HDPE-g-MAH and EPR-g-MAH. It reveals that flexural strength of HDPE30/PBS70 compatibilized with HDPE-g-MAH was slightly lower than that of uncompatbilized blend. The addition of 2 phr HDPE-g-MAH brought about a slight decrease of flexural strength of the compatibilized blend. However, the flexural strength of the compatibilized blend did not further decrease as increasing HDPE-g-MAH content. Similarly, the flexural strength of the blend compatibilized with EPR-g-MAH was slightly lower than that of uncompatibilized blend. Adding 2 phr EPR-g-MAH into HDPE30/PBS70 blend led to

a decrease of flexural strength of the blend. However, adding more EPR-g-MAH content did not create a further decrease of flexural strength of the blend. In addition, flexural properties of HDPE30/PBS70 blends compatibilized with HDPE-g-MAH and EPR-g-MAH were summarized in Table 4.28.

In comparison, HDPE-g-MAH seems to be more effective for maintaining both the flexural modulus and flexural strength of HDPE30/PBS70 blend than EPR-g-MAH.

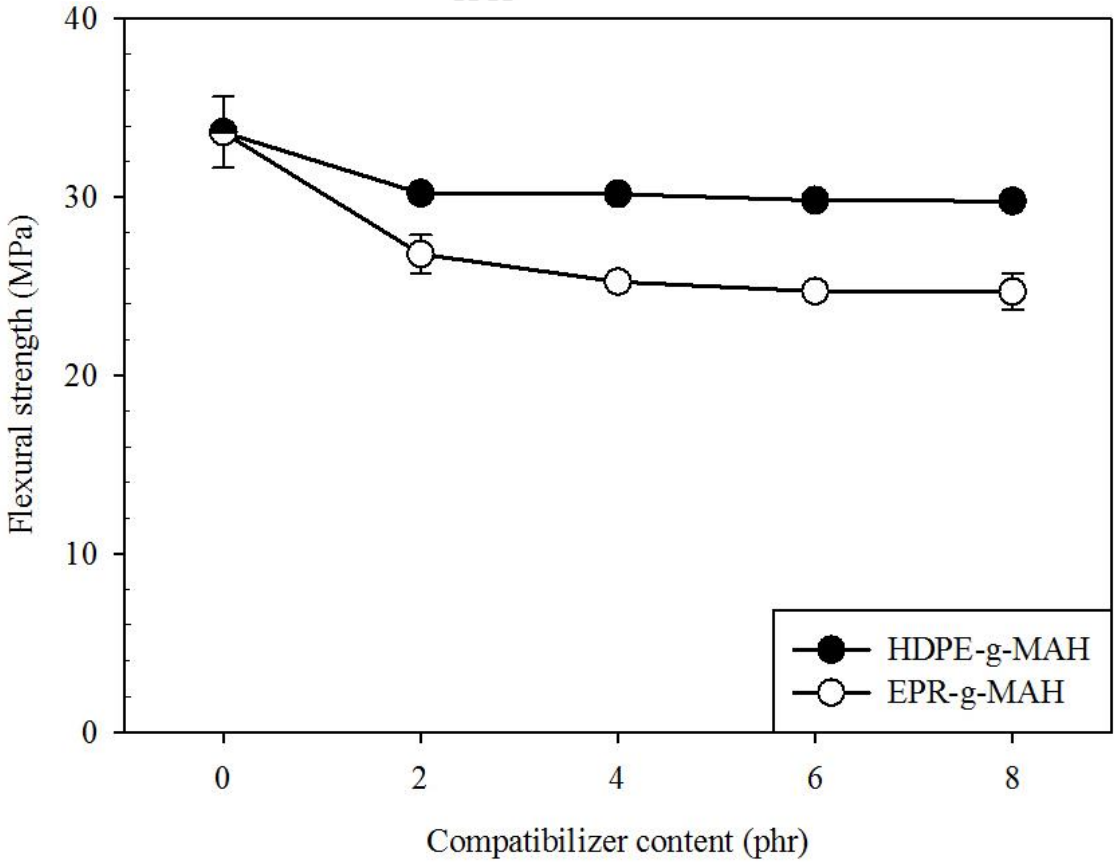

Figure 4.56 Plot of flexural strength of HDPE30/PBS70 blends at various contents of HDPE-g-MAH and EPR-g-MAH.

Table 4.28 Flexural properties of HDPE30/PBS70 blends at various contents of HDPE-g-MAH and EPR-g-MAH.

Compatibilizer content (phr)	Flexural strength (MPa)		Flexural modulus (MPa)	
	HDPE-g-MAH	EPR-g-MAH	HDPE-g-MAH	EPR-g-MAH
0 phr	33.6±1.9		872.4±53.4	
2 phr	30.2±0.1	26.8±1.0	811.3±26.8	751.5±63.6
4 phr	30.1±0.1	25.3±0.4	810.8±20.8	634.5±17.9
6 phr	29.8±0.4	24.7±0.4	788.2±6.2	596.2±21.9
8 phr	29.7±0.2	24.7±1.0	785.0±20.6	575.9±20.6

Unnotched Izod impact strength of HDPE30/PBS70 blend at various contents of HDPE-g-MAH and EPR-g-MAH is presented in Table 4.29. It shows that impact strength of HDPE30/PBS70 blend compatibilized with HDPE-g-MAH was higher than that of uncompatibilized blend. Adding 2 and 4 phr HDPE-g-MAH resulted in an increase of impact strength of the blend. This improvement strongly correlated with their finer size of HDPE domains, as displayed in Figure 4.55(b) and Figure 4.55(c), respectively. In addition, the impact strength of the blend tended to further increase with increasing HDPE-g-MAH content. Particularly, at 6 and 8 phr HDPE-g-MAH, the impact strength of compatibilized blend was beyond the instrumentation limit of 135 kJ/m^2. The large improvement of impact strength of the blend at 6 and 8 phr HDPE-g-MAH corresponded well with their fibrillar phase morphology, as shown in Figure 4.55(d) and Figure 4.55(e), respectively. Fibrils promoted a crack-tip shielding of which tended to bridge the crack and opposed a crack opening of the blend (Nallaa, Kinney and Ritchie, 2003). Also, the much increase in the impact strength could be related to the occurrence of interfacial interactions, H-bonding and interchain diffusion. The H-bonding was between MAH groups of HDPE-g-MAH and ester groups of PBS. The interchain diffusion was between molecular chains of HDPE and HDPE backbone of HDPE-g-MAH, as proposed in Figure 4.22(a) (Qi, Nie, Zhou, Mao and Zhang, 2006; Pracella, Rolla, Chionna and Galeski, 2002; Nashar, Maziad and Sadek, 2008).

Similarly, the impact strength of HDPE30/PBS70 compatibilized with EPR-g-MAH was also improved after the adding 2 phr EPR-g-MAH. Furthermore, the impact strength of the blend greatly improved with increasing EPR-g-MAH to 4, 6 and 8 phr EPR-g-MAH. The blend sample did not break within

an instrumentation limit. The greatly improved in impact strength of HDPE30/PBS70 blend compatibilized with EPR-g-MAH correlated with the more uniform in shape of HDPE domains in the blend compatibilized with EPR-g-MAH as shown in Figure 4.56. Possibly, the great improvement of impact strength of the blend might correlate with a rubbery characteristic of EPR-g-MAH.

In summary, HDPE-g-MAH and EPR-g-MAH were an effective compatibilizer to enhance the impact strength of HDPE30/PBS70 blend. In comparison, at the same content of compatibilizer, EPR-g-MAH seems to be an effective compatibilizer for developing the impact strength of the HDPE30/PBS70 blend as compare to HDPE-g-MAH.

Table 4.29 Unnotched Izod impact strength of HDPE30/PBS70 blends at various contents of HDPE-g-MAH and EPR-g-MAH.

Compatbilizer content (phr)	**Unnotched Izod impact strength (kJ/m^2)**	
	HDPE-g-MAH	**EPR-g-MAH**
0	39.4±3.0	39.4±3.0
2	45.1±1.0	50.1±1.2
4	52.1±0.9	Not break
6	Not break	Not break
8	Not break	Not break

4.2.2.4 Thermal degradation temperature and weight loss

TGA and DTGA thermogram of uncompatibilized and compatibilized HDPE30/PBS70 blend with HDPE-g-MAH is shown in Figure 4.57. Figure 4.57(a) shows TGA curve of HDPE30/PBS70 compatibilzed with HDPE-g-MAH. From the curve, it illustrates that uncompatibilized HDPE30/PBS70 blend exhibited two thermal transitions. The first transition occurred at a temperature range of 355-435°C corresponding to the degradation of PBS. The second transition occurred within a temperature range of 436-504°C due to HDPE degradation. Addition of 2 phr HDPE-g-MAH into HDPE30/PBS70 blend made the PBS phase degraded at temperature range of 357-438°C and HDPE phase degrade at temperature range of 439-504°C. As increasing HDPE-g-MAH content to 4, 6 and 8 phr, PBS phase degraded at slightly higher temperature range at 357-443°C, 358-454°C and 358-460°C, respectively. On the other hand, at 4, 6, and 8 phr HDPE-MAH, HDPE phase degraded at temperature range of 444-508°C, 456-517°C and 461-518°C, respectively. The results implied that adding HDPE-g-MAH into HDPE30/PBS70 made an initial degradation temperature of PBS phase slightly increased whereas initial degradation temperature of HDPE phase markedly improved.

Figure 4.57(b) shows DTGA curve of HDPE30/PBS70 compatibilzed with HDPE-g-MAH. It illustrates that uncompatibilized HDPE30/PBS70 blend exhibited two thermal degradation. The first degradation peak occurred at the temperature of 416 °C corresponding to the degradation of PBS. The second degradation peak occurred within a temperature of 488°C, due to HDPE degradation. Adding 2 to 8 phr HDPE-g-MAH into HDPE30/PBS70 blend did insignificant affect the degradation temperature of both PBS and HDPE phase.

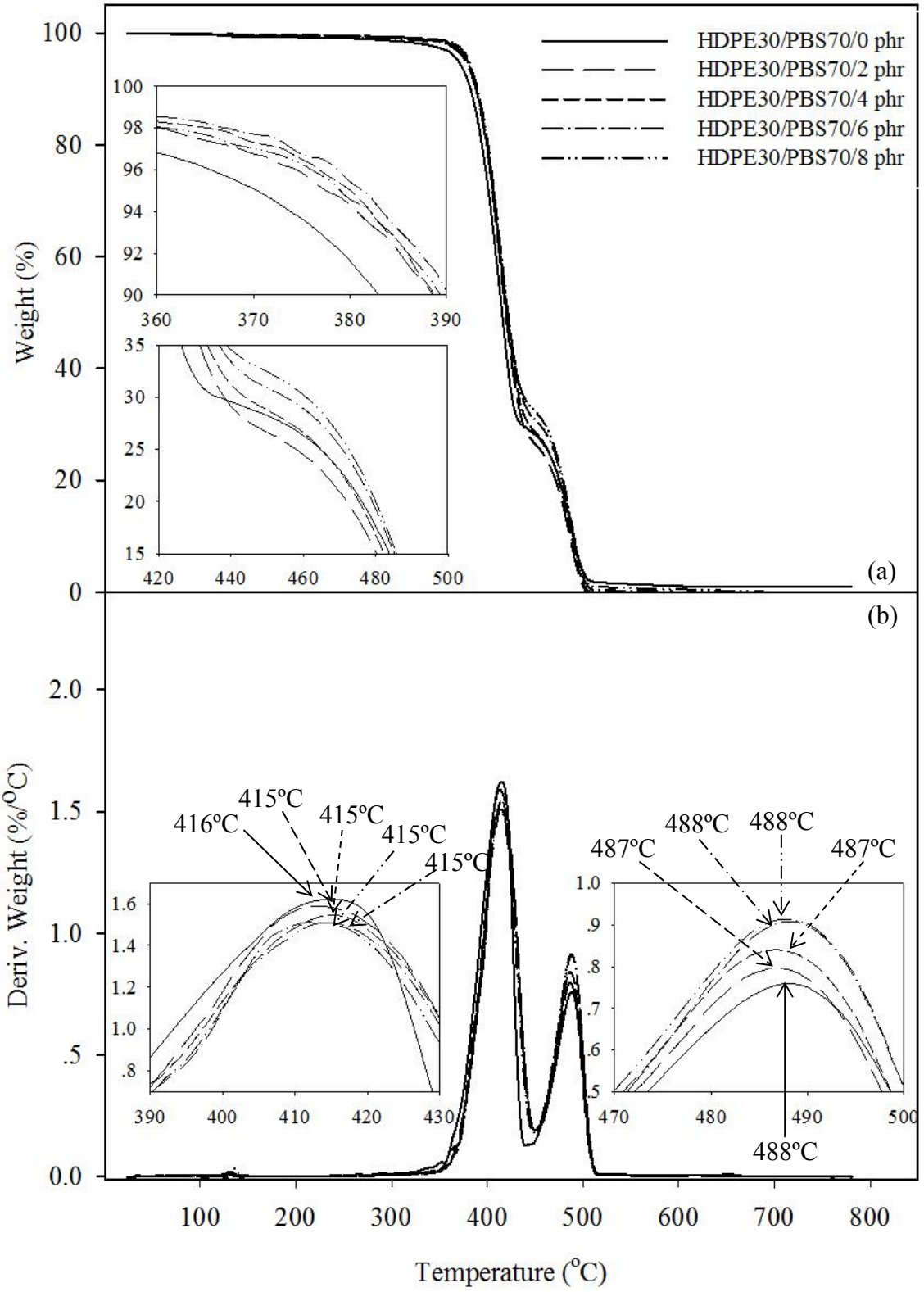

Figure 4.57 TGA (a) and DTGA (b) thermograms of HDPE30/PBS70 blends at various contents of HDPE-g-MAH.

Figure 4.58(a) shows TGA curves of HDPE30/PBS70 compatibilzed with EPR-g-MAH. From the curve, it illustrates that the blend compatibilized with 2 phr of EPR-g-MAH thermally degraded into two stages. The first transition occurred at a temperature range of 371-462°C corresponding to the degradation of PBS. The second transition occurred within a temperature range of 463-516°C due to degradation of HDPE phase. Addition of 4 phr EPR-g-MAH into HDPE30/PBS70 blend made the PBS phase degraded at a temperature range of 371-458°C and HDPE phase degraded at a temperature range of 459-518°C. As increasing EPR-g-MAH to 6 and 8 phr, PBS phase degraded at a slight higher temperature range at 371-452°C and 371-461°C respectively. On the other hand, at 6, and 8 phr EPR-MAH, HDPE phase degraded at temperature range of 453-514°C and 462-518°C, respectively. From TGA curves, it also implied that adding EPR-g-MAH into HDPE30/PBS70 improved the initial degradation temperature of both PBS and HDPE phase. However, this improving was independent of EPR-g-MAH content.

Figure 4.58(b) shows DTGA curve of HDPE30/PBS70 compatibilzed with EPR-g-MAH. It illustrates the adding 2 phr of EPR-g-MAH into HDPE30/PBS70 blends greatly affect degradation temperature of both PBS and HDPE phase. The degradation temperature of PBS phase was improved to 5°C and degradation temperature of HDPE phase was improved to 7°C. The degradation temperature of PBS and HDPE phase was 421°C and 495°C, respectively. However, as increasing EPR-g-MAH, the degradation temperature of PBS and HDPE phase was independent of EPR-g-MAH content.

In summary, adding HDPE-g-MAH into the blend slightly improved initial degradation temperature of PBS phase whereas initial degradation

temperature of HDPE phase markedly improved. However, adding HDPE-g-MAH into the blend did insignificant affect the degradation temperature of both PBS and HDPE phase. Adding EPR-g-MAH also improved the initial degradation temperature of both PBS and HDPE phase. However, the initial degradation temperature of PBS and HDPE was independent of EPR-g-MAH content. Comparatively, at the same content of compatibilizer, EPR-g-MAH was more effective for improving both initial degradation temperature and degradation temperature of PBS and HDPE phase than HDPE-g-MAH.

In addition, the temperature range for degradation ($T_{d,range}$), the peak temperature (T_{peak}) and weight loss of HDPE30/PBS70 blends at various contents of HDPE-g-MAH and EPR-g-MAH are summarized in Table 4.30.

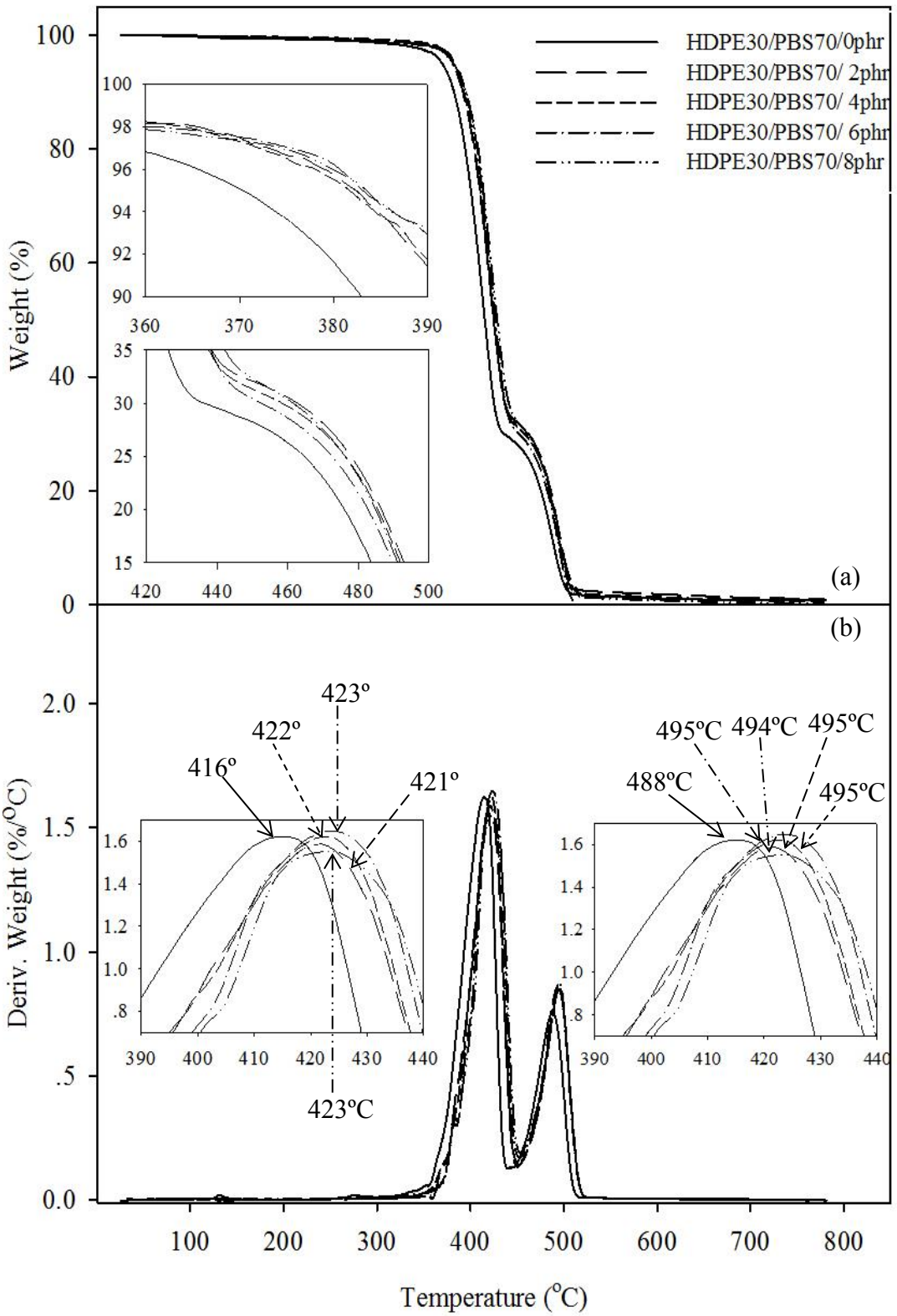

Figure 4.58 TGA and DTGA thermograms of HDPE30/PBS70 blends at various contents of EPR-g-MAH.

Table 4.30 The temperature range for degradation ($T_{d,range}$), peak temperatures (T_{peak}) and weight loss of HDPE30/PBS70 blends at various contents of HDPE-g-MAH and EPR-g-MAH.

Compatibilizer content	HDPE domain						PBS matrix					
	HDPE-g-MAH			EPR-g-MAH			HDPE-g-MAH			EPR-g-MAH		
	T_{peak} (ºC)	Weight loss (%)	$T_{d,range}$ (ºC)	T_{peak} (ºC)	Weight loss (%)	$T_{d,range}$ (ºC)	T_{peak} (ºC)	Weight loss (%)	$T_{d,range}$ (ºC)	T_{peak} (ºC)	Weight loss (%)	$T_{d,range}$ (ºC)
0 phr	488	29.9	436-504	488	29.9	436-504	415	70.0	355-435	416	70.0	355-435
2 phr	487	28.6	439-504	495	30.0	463-516	415	69.5	357-438	421	69.8	371-462
4 phr	487	28.4	444-508	495	29.9	459-518	415	69.6	357-443	422	69.9	371-462
6 phr	488	30.0	456-517	495	29.9	453-514	415	69.8	358-454	423	69.9	371-462
8 phr	488	29.9	461-518	494	29.9	462-518	414	69.8	358-460	423	69.9	371-461

4.2.2.5 Melting and crystallizing behavior

DSC curves from the first heating scan of HDPE30/PBS70 blends at various contents of HDPE-g-MAH are shown in Figure 4.59 (a). The uncompatibilized HDPE30/PBS70 blend exhibited an exothermic peak at 91.7°C and two endothermic peaks at 109.5°C and at 126.4°C, respectively. The exothermic peak was caused by the recrystallization of PBS upon heating (Yoo and Im, 1999). It was previously reported that the exothermic peak of PBS occurred at around 95°C during heating scan, due to the thermal history of cooling and reheating (Yasuniwa, Tsubakihara, Satou and Iura, 2006; Wang, Zhou, Li, 2007). The first endothermic peak was due to melting of PBS phase and the second endothermic peak corresponded to the melting of HDPE phase. Adding 2, 4, 6 and 8 phr HDPE-g-MAH into HDPE30/PBS70 blend did insignificantly affect the exothermic peak and melting temperature of PBS phase. In addition, the melting peak of HDPE phase insignificantly increased after adding HDPE-g-MAH at 2, 4, 6 and 8 phr.

Figure 4.59 (b) shows DSC curves from the first heating scan of HDPE30/PBS70 blends at various contents of EPR-g-MAH. It illustrates that adding EPR-g-MAH made the recrystallization of PBS phase slightly decreased. However, adding 2 phr EPR-g-MAH did insignificantly influence the melting peak of PBS and HDPE phase. Noticeably, a small shoulder was observed at around 102°C in the blend compatibilized with EPR-g-MAH. The occurrence of a shoulder might indicate that EPR-g-MAH making PBS crystallized into different size. As increasing EPR-g-MAH to 4, 6 and 8 phr, the melting behavior of the blend during the first heating scan was unvarying.

In summary, adding HDPE-g-MAH did insignificantly affect the cold-crystallization temperature of PBS whereas EPR-g-MAH affected the slight decrease of cold-crystallization temperature of PBS. For the melting of PBS, adding HDPE-g-MAH into the blend did insignificantly affect the melting temperature of PBS phase. In turn, adding EPR-g-MAH did insignificantly influence the melting peak of PBS. A small shoulder of melting peak of PBS was observed at around 102°C. It implied that PBS had two forms of crystal. For the melting of HDPE, HDPE-g-MAH and EPR-g-MAH did not insignificant affect the melting of HDPE.

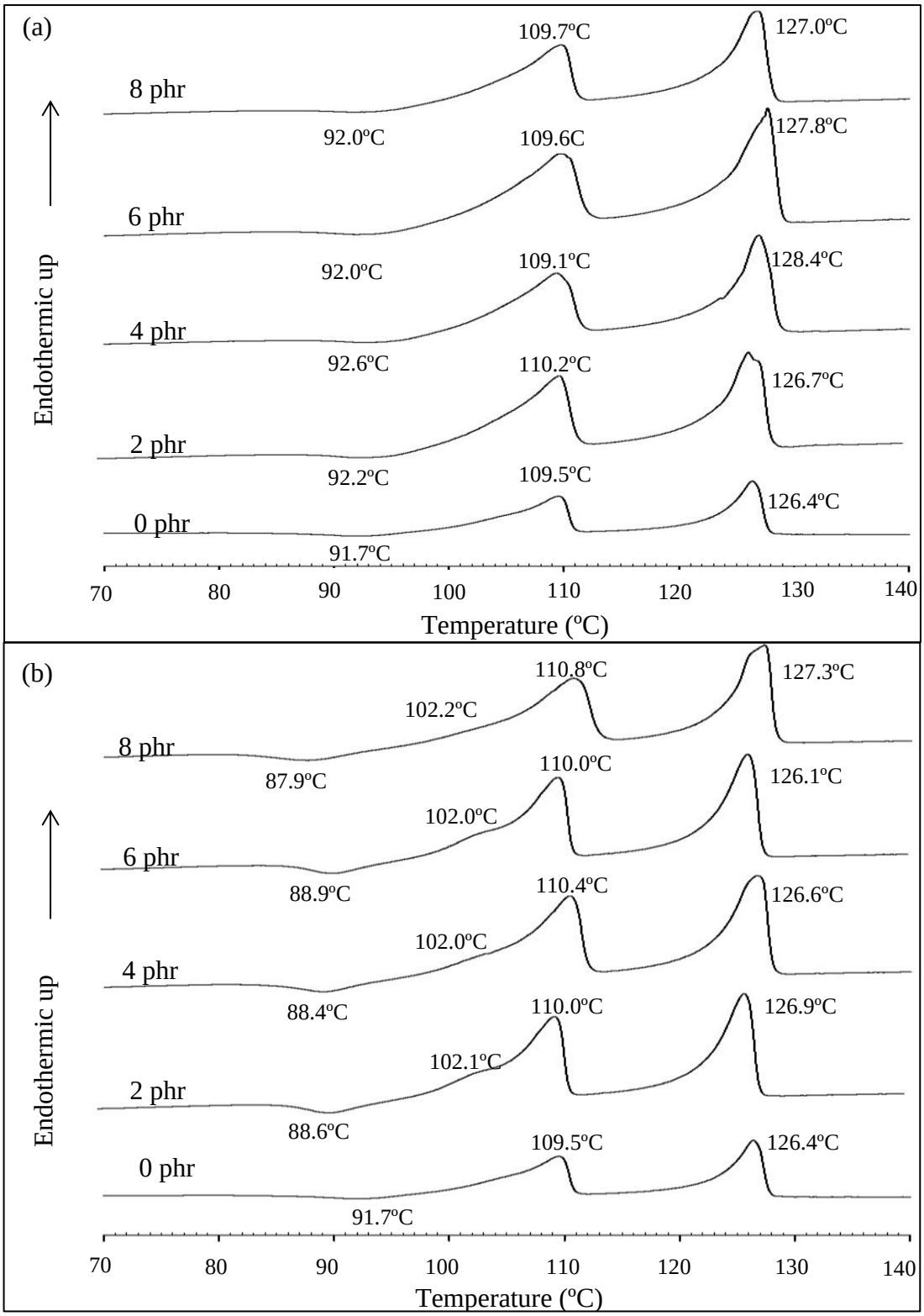

Figure 4.59 DSC curves from the first heating scan of HDPE30/PBS70 blends at various contents of HDPE-g-MAH (a) and EPR-g-MAH (b).

Figure 4.60 (a) shows the DSC curves from the cooling scan of HDPE30/PBS70 blends at various contents of HDPE-g-MAH. The DSC curve of uncompatibilized HDPE30/PBS70 blend exhibited a crystallization temperature of HDPE and PBS at 117.2 and 84.5°C, respectively. With adding 2 phr of HDPE-g-MAH, the crystallization temperature of both HDPE and PBS phase increased slightly. As increasing HDPE-g-MAH content to 4, 6 and 8 phr, the crystallization temperature of HDPE and PBS phase changed insignificantly.

The DSC curves from the cooling scan of HDPE30/PBS70 blend compatibilized with EPR-g-MAH are shown in Figure 4.60 (b). It demonstrates that adding 2 phr of EPR-g-MAH did insignificantly affect the crystallization temperature of HDPE phase. On the other hand, the adding 2 phr EPR-g-MAH into HDPE30/PBS70 blend gave rise to a retardation of crystallization process of PBS which resulted in lower crystallization temperature of PBS phase. However, adding more EPR-g-MAH did insignificant affect the crystallization temperature of both HDPE and PBS phase. It was formerly reported that adding EPR-g-MAH into HDPE/PET blend resulted in 14.3°C decreasing of crystallization temperature of PET phase whereas the crystallization temperature of HDPE phase remained unchanged (Pracella, Rolla, Chionna and Galeski, 2002).

These results indicated that using HDPE-g-MAH as a compatibilizer in HDPE30/PBS70 blend hardly affected the crystallization behavior of HDPE and PBS phase while EPR-g-MAH affected the crystallization behavior of PBS phase by which the crystallization temperature of PBS was lower with adding more EPR-g-MAH. However, the content of HDPE-g-MAH and EPR-g-MAH scarcely influenced the crystallization temperature of HDPE and PBS phase.

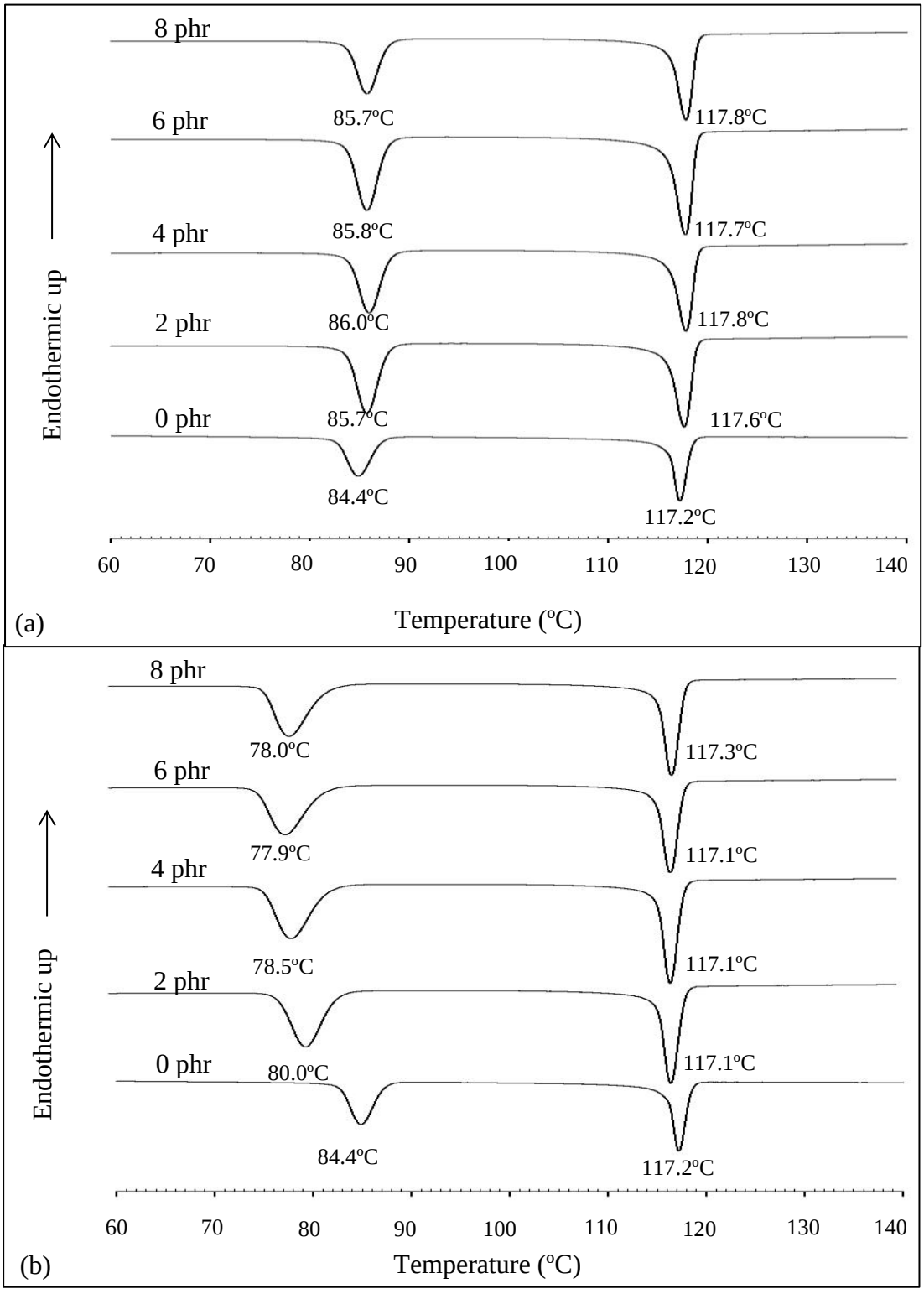

Figure 4.60 DSC curves from the cooling scan of HDPE30/PBS70 blends at various contents of HDPE-g-MAH (a) and EPR-g-MAH (b).

Figure 4.61 (a) shows the DSC curves from the second heating scan of HDPE30/PBS70 blends at various contents of HDPE-g-MAH. The DSC curve of uncompatibilized HDPE30/PBS70 blend shows double endothermic peak of PBS at 99.6°C and 108.6°C. This double melting behavior of PBS could be explained by the existence of 2 forms of spherulites. Also, it shows one endothermic peak of HDPE at 127.8°C corresponded to the melting of HDPE. The compatibilizing HDPE30/PBS70 blend with 2, 4, 6 and 8 phr HDPE-g-MAH made an insignificant change in the melting peak of PBS phase at low and high temperature. Also, HDPE-g-MAH did insignificantly influence the melting temperature of HDPE phase, as well.

Figure 4.61 (b) shows DSC curves from the second heating scan of HDPE30/PBS70 blends at various contents of EPR-g-MAH. It demonstrates that adding 2 phr EPR-g-MAH resulted in a slight decrease of melting peak at low temperature of PBS phase, whereas the melting peak at high temperature of PBS phase insignificantly changed. Similar with the first heating scan, the curve of the blend compatibilized with 2 phr EPR-g-MAH still exhibited a small shoulder occurred at 105.7°C prior to a melting peak of PBS at high temperature. Also, adding 2 phr EPR-g-MAH did not influence the melting temperature of HDPE phase. Adding more EPR-g-MAH did insignificantly affect the melting behavior of both HDPE and PBS phase.

These results indicated that using HDPE-g-MAH as a compatibilizer for HDPE30/PBS70 blend hardly affected the melting temperature at the low and high temperature of PBS, and also the melting temperature of HDPE phase. In addition, EPR-g-MAH scarcely influenced melting temperature at the high temperature of PBS, and the melting temperature of HDPE while it made the melting

at low temperature of PBS decreased. Moreover, the DSC curves of the blend compatibilized with EPR-g-MAH exhibited a shoulder occurring prior to the melting at high temperature of PBS phase.

Additionally, melting temperature and cold crystallization temperature from the first heating scan and crystallization temperature of HDPE30/PBS70 blend at various contents of HDPE-g-MAH and EPR-g-MAH are summarized in Table 4.31.

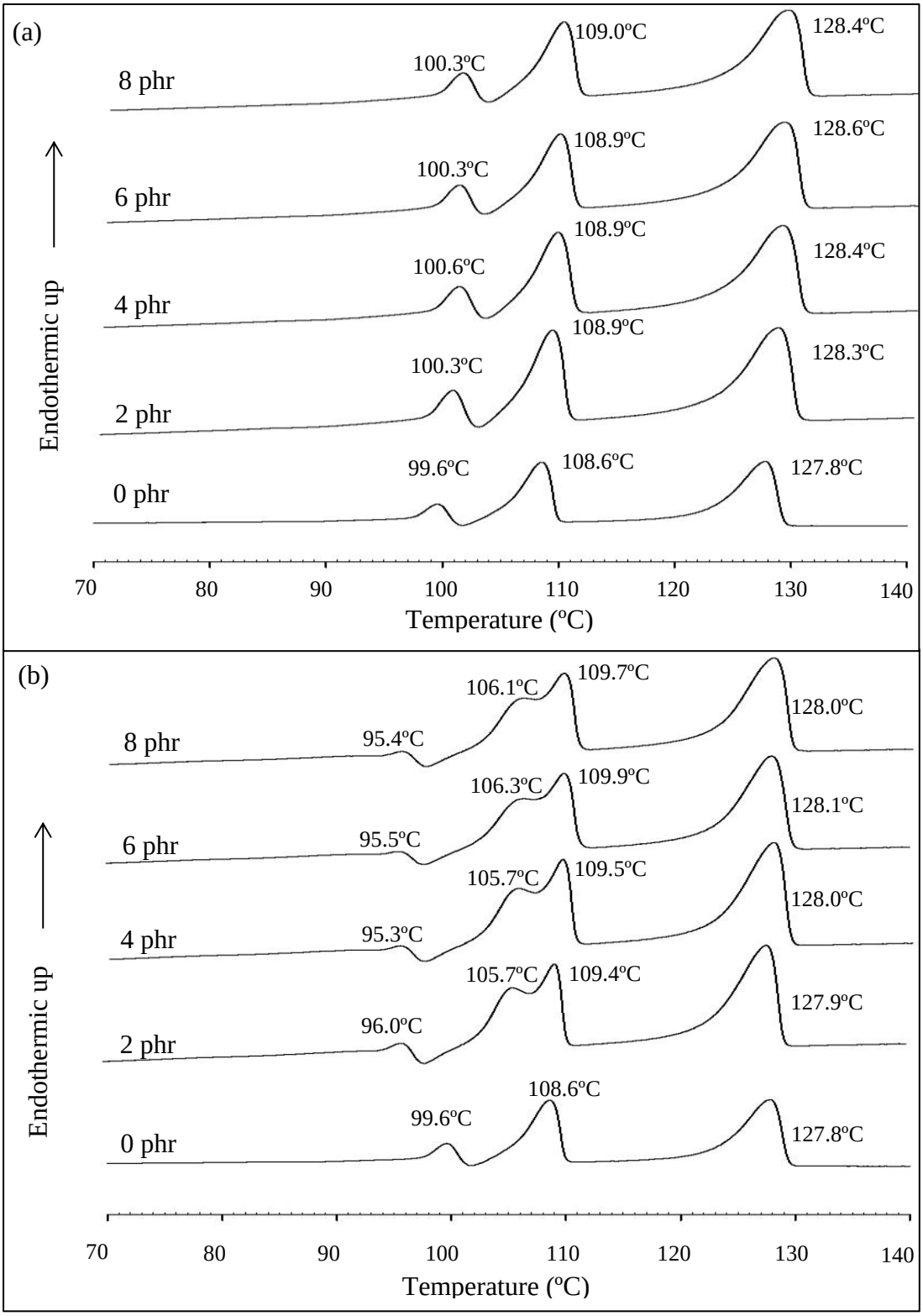

Figure 4.61 DSC curves from the second heating scan of HDPE30/PBS70 blends at various contents of HDPE-g-MAH (a) and EPR-g-MAH (b).

Table 4.31 Melting temperature and cold crystallization temperature from the first heating scan, crystallization temperature and melting at low and high temperature of HDPE30/PBS70 blend at various contents of HDPE-g-MAH and EPR-g-MAH.

Compatibilizer content	First heating scan						Crystallization temperature (^{o}C)				Second heating scan			
	Melting temperature (^{o}C)				Cold crystallization temperature (^{o}C)						Melting temperature (^{o}C)			
	HDPE domain		PBS matrix		PBS matrix		HDPE domain		PBS matrix		HDPE domain		PBS matrix	
	H	E	H	E	H	E	H	E	H	E	H	E	H	E
0 phr	126.4		109.5		91.7		117.2		84.4		127.8		99.6,108.6	
2 phr	126.7	126.9	110.2	110.0	92.2	88.6	117.6	117.1	85.7	80.0	128.3	127.9	100.3, 108.9	96.0, 109.4
4 phr	128.4	126.6	109.1	110.4	92.6	88.4	117.8	117.1	86.0	78.5	128.4	128.0	100.6, 108.9	95.3, 109.5
6 phr	127.8	126.1	109.6	110.0	92.0	88.9	117.7	117.3	85.8	77.9	128.6	128.1	100.3, 108.9	95.5, 109.9
8 phr	127.0	127.3	109.7	110.8	92.0	87.9	117.8	117.6	85.7	78.0	128.4	128.0	100.3, 109.0	95.4, 109.7

Remark : H = HDPE-g-MAH, E= EPR-g-MAH

4.2.2.6 Water absorption

Relationship between water absorption and immersion time of uncompatibilized and compatibilized HDPE30/PBS70 blends with HDPE-g-MAH and EPR-g-MAH is shown in Figure 4.62. As shown in Figure 4.62 (a), the water absorption of the HDPE30/PBS70 blends compatibilized with HDPE-g-MAH was slightly lower than that of the uncompatibilized blend. Adding more HDPE-g-MAH content led to a slight decrease in water absorption. The reduction of water absorption of compatibilized blend was attributed to an improvement in an interfacial adhesion resulting in avoidance an easy penetration of water molecules into the compatibilized blends and a decrease water accumulation at the interfacial voids. The water absorption of HDPE30/PBS70 blend compatibilized with 2, 4, 6 and 8 phr HDPE-g-MAH reached equilibrium after immersion time of 48, 48, 51 and 51 days, respectively.

Similarly, the water absorption of HDPE30/PBS70 blends compatibilized with EPR-g-MAH was slightly lower than that of the uncompatibilized blend, as illustrated in Figure 4.62 (b). As increasing EPR-g-MAH content, the water absorption of the compatibilized HDPE30/PBS70 blends slightly decreased. In addition, the water absorption of HDPE30/PBS70 blend compatibilized with 2, 4, 6 and 8 phr EPR-g-MAH reached equilibrium after immersion time of 48, 48, 48 and 51 days, respectively.

In summary, the water absorption of the HDPE30/PBS70 blends compatibilized with EPR-g-MAH and HDPE-g-MAH was insignificant difference. In addition, immersion time and water content at equilibrium of

HDPE30/PBS70 blends at various contents of HDPE-g-MAH and EPR-g-MAH is summarized in Table 4.32.

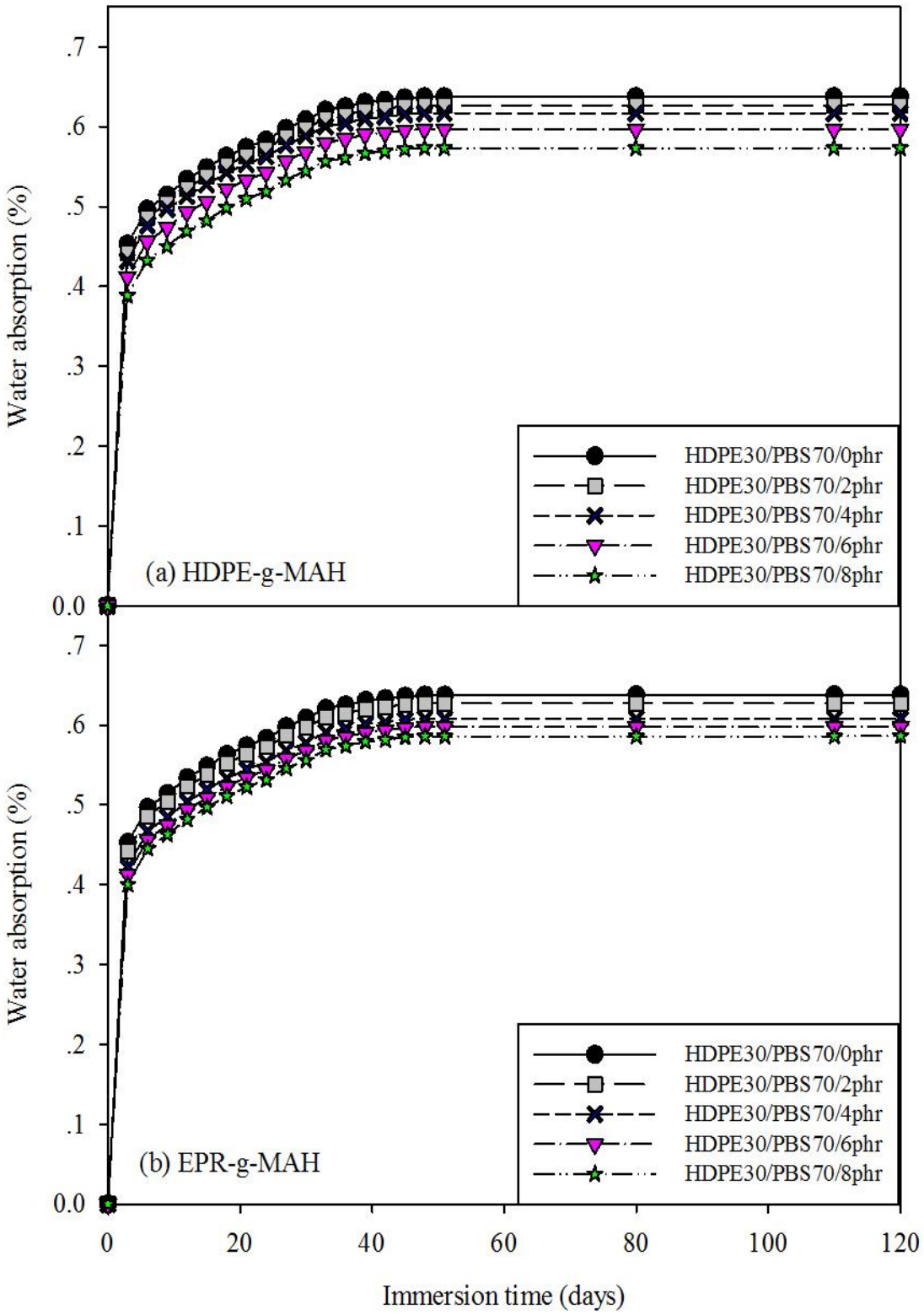

Figure 4.62 Plot of water absorption vs. immersion time of HDPE30/PBS70 blends at various contents of HDPE-g-MAH (a) and EPR-g-MAH (b).

Table 4.32 Immersion time and water content at equilibrium of HDPE30/PBS70 blends at various contents of HDPE-g-MAH and EPR-g-MAH.

Compatibilizer content	Blend with HDPE-g-MAH		Blend with EPR-g-MAH	
	Immersion time (day)	Water content at equilibrium (%)	Immersion time (day)	Water content at equilibrium (%)
0 phr	48	0.64%	48	0.64%
2 phr	48	0.63%	48	0.63%
4 phr	48	0.62%	48	0.61%
6 phr	51	0.60%	48	0.60%
8 phr	51	0.57%	51	0.59%

4.2.2.7 Biodegradability by soil burial test

Plot of weight loss (%) and burial time of uncompatibilized and compatibilized HDPE30/PBS70 blends with HDPE-g-MAH is shown in Figure 4.63 (a). It illustrates that weight loss of compatibilized blend was slightly lower than that of uncompatibilized blend. However, adding more HDPE-g-MAH did insignificant affect the weight loss of the blend. The decrease in weight loss of compatibilized blend might be due to the compatibilization effect of HDPE-g-MAH. The interfacial adhesion between HDPE and PBS improved after adding HDPE-g-MAH leading to a decrease of interfacial void.

Plot of weight loss and burial time of uncompatibilized and compatibilized HDPE30/PBS70 blends with EPR-g-MAH is displayed in Figure 4.63 (b). The result implied that weight loss of compatibilized blend was higher than that of uncompatibilized blend. In addition, increasing EPR-g-MAH content led to a slight increase in weight loss of the compatibilized blend. This occurrence might relate with an amorphous EPR-g-MAH elastomer. The biodegradation process preferentially occurred in the amorphous regions rather than crystalline region.

In comparison, the blend compatibilized with EPR-g-MAH could be degraded in natural soil easier than the blend compatibilized with HDPE-g-MAH.

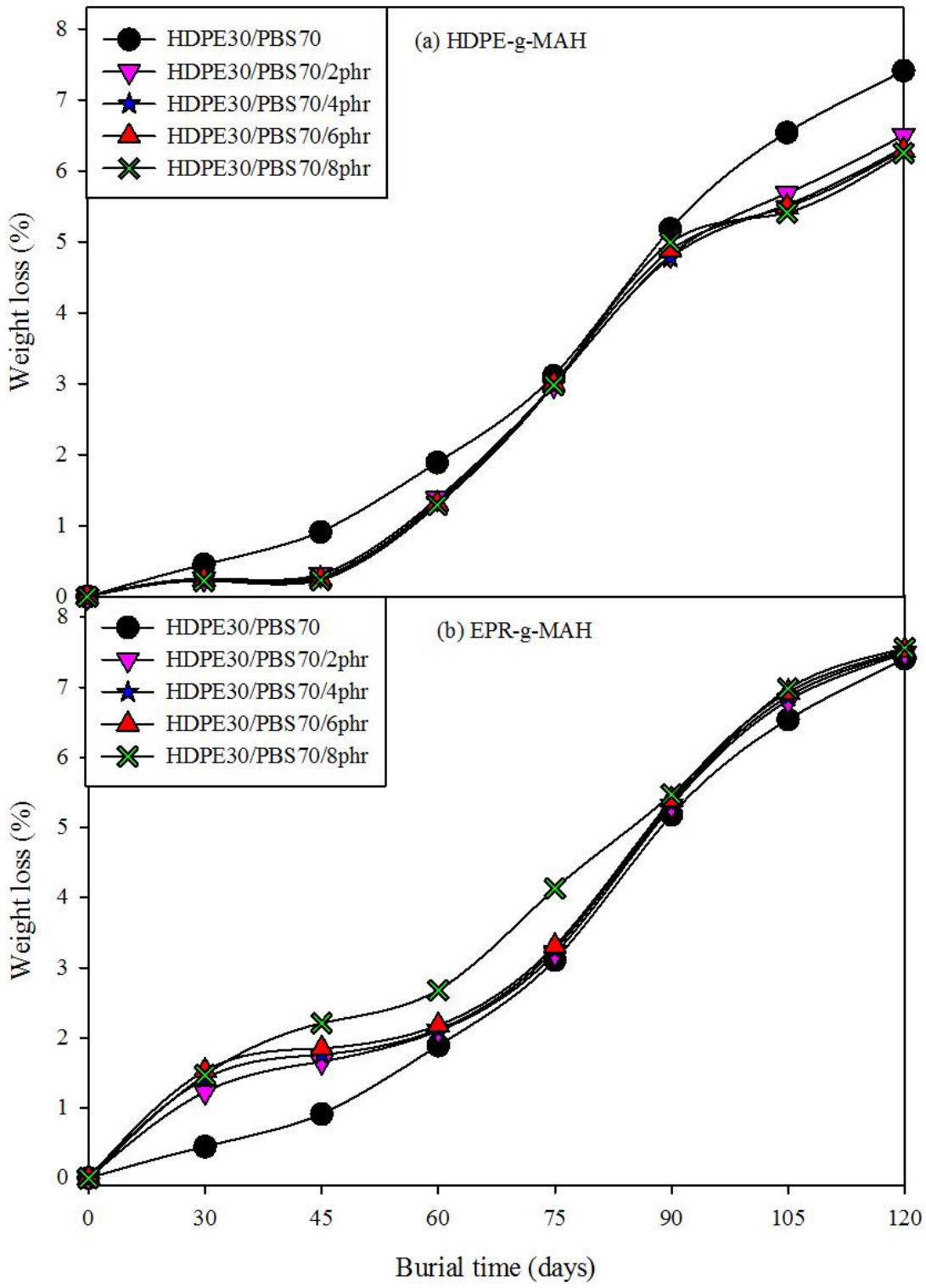

Figure 4.63 Plot of weight loss (%) and burial specimens of HDPE30/PBS70 blends at various contents of HDPE-g-MAH (a) and EPR-g-MAH (b).

The optical micrograph of buried specimens of uncompatibilized and compatibilized HDPE30/HDPE70 blends with various contents of HDPE-g-MAH is displayed in Figure 4.64. With adding 2 to 4 phr HDPE-g-MAH into the blend, the small dark spot occurred after burial time of 45 days. As increasing the burial time, the dark spot was more clearly seen.

As increasing HDPE-g-MAH to 6 and 8 phr, it was observed that the dark spot still occurred after burial time of 45 and 60 days, respectively. However, the area of dark spot decreased. This implied that the biodegradability of the comaptibilized blend decreased.

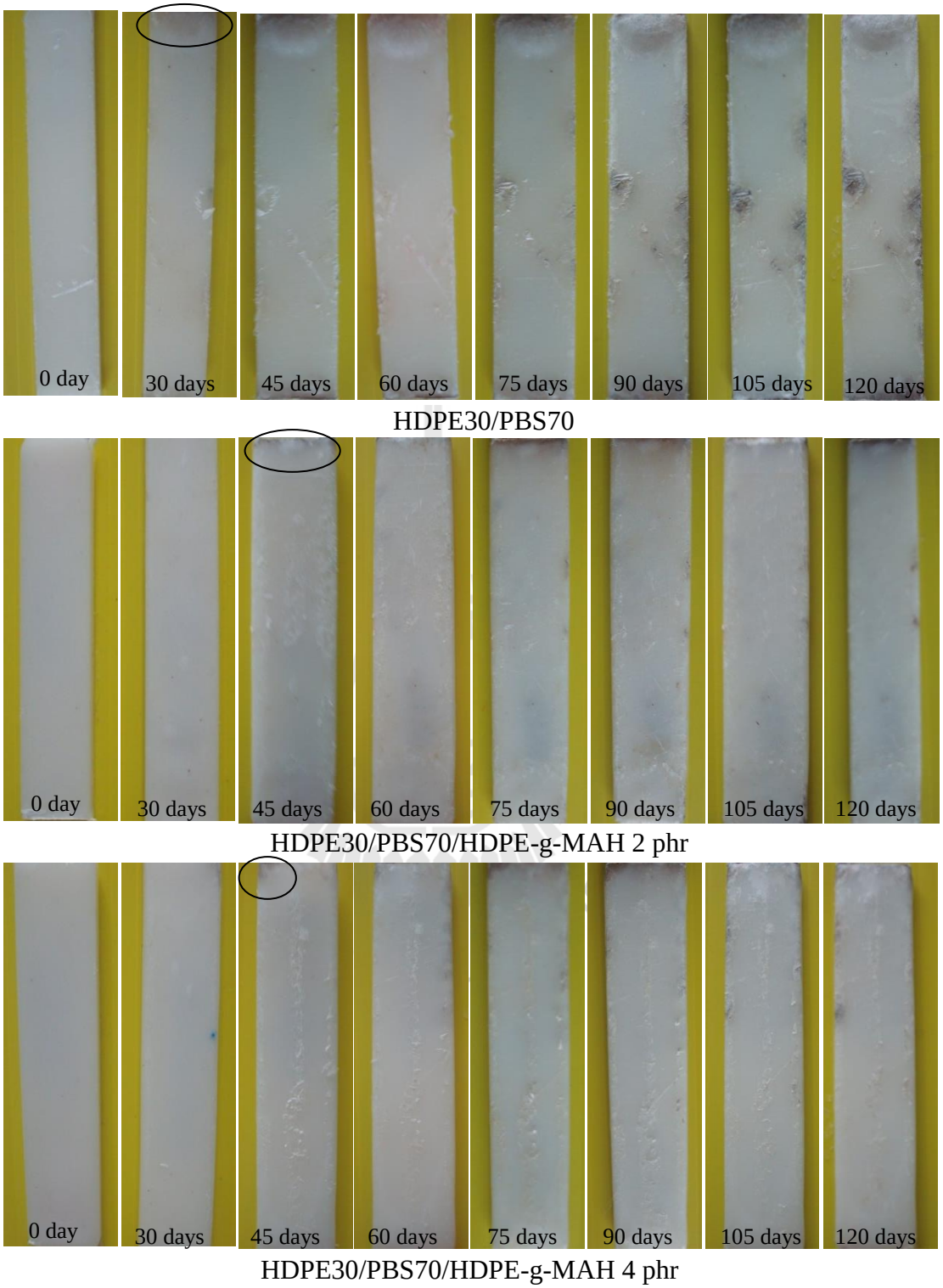

Figure 4.64 Optical micrographs of buried specimens of HDPE30/PBS70 blends at various contents of DHPE-g-MAH at several burial times of 0 to 120 days.

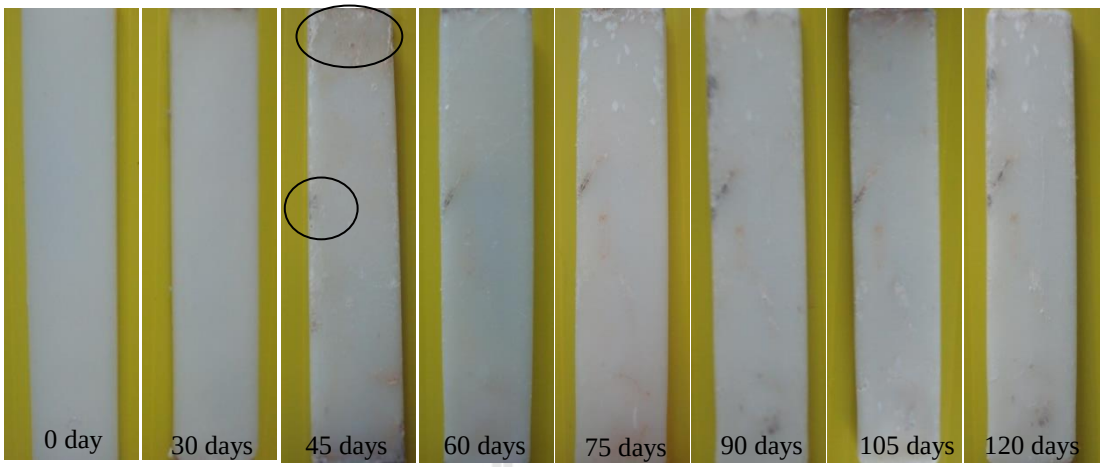

HDPE30/PBS70/HDPE-g-MAH 6 phr

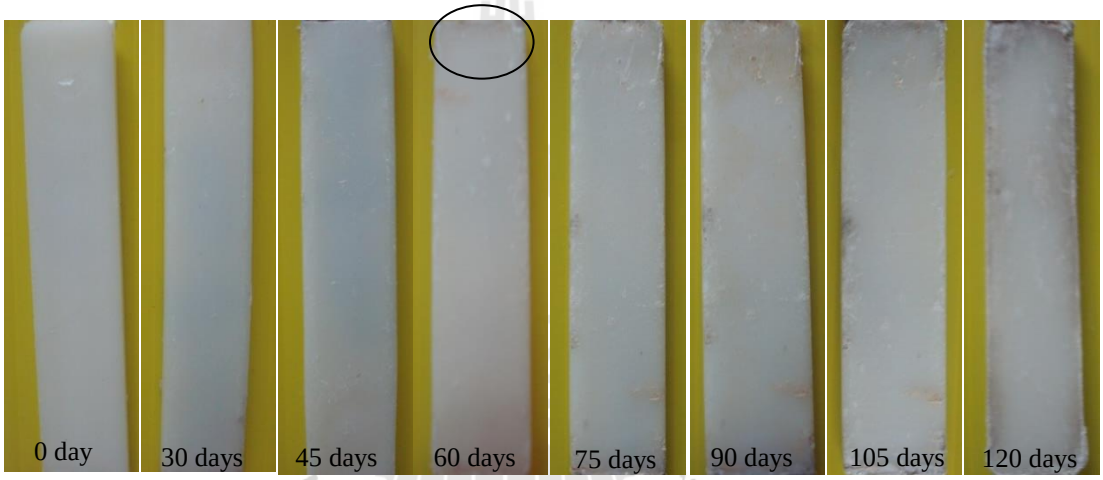

HDPE30/PBS70/HDPE-g-MAH 8 phr

Figure 4.64 Optical micrographs of buried specimens of HDPE30/PBS70 blends at various contents of HDPE-g-MAH at several burial times of 0 to 120 days. (Continued)

The optical micrograph of buried specimens of uncompatibilized and compatibilized HDPE30/HDPE70 blends with various contents of EPR-g-MAH is displayed in Figure 4.65. With adding 2 phr EPR-g-MAH into the blend, the dark streak occurred at the blend sample surface after burial time of 30 days. In addition, the dark streak area was more obviously seen as increasing the

burial time. Similarly, as increasing EPR-g-MAH to 4 phr, the dark streak occurred after burial time of 30 days, by which it was more noticeable than the blend compatibilized with 2 phr EPR-g-MAH. In addition, it illustrated that after 45 days of burial time, the blend sample surface was eroded.

With adding 6 and 8 phr EPR-g-MAH, the dark streak occurred over the blend sample surface after burial time of 30 days. The dark streak was more explicit incorporating with the eroded surface of the blend sample.

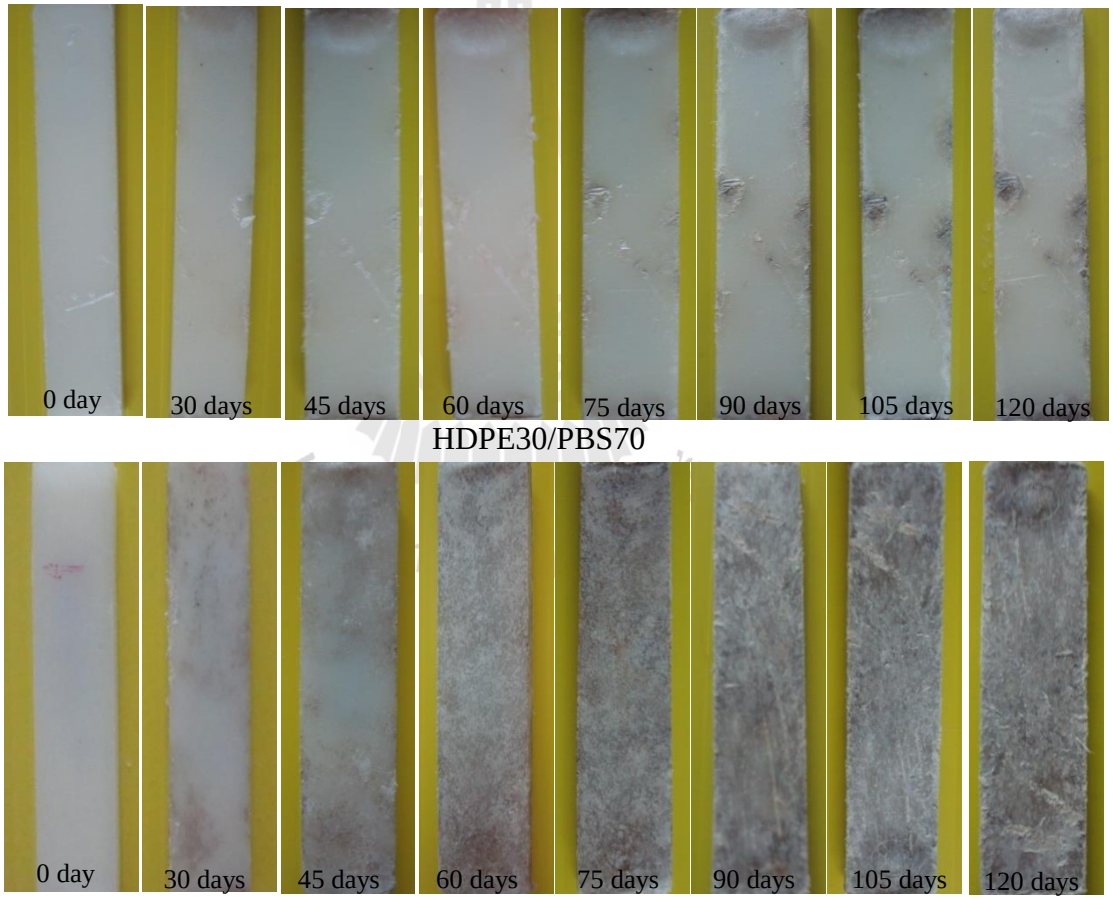

Figure 4.65 Optical micrographs of buried specimens of HDPE30/PBS70 blends at various contents of EPR-g-MAH at several burial times of 0 to 120 days.

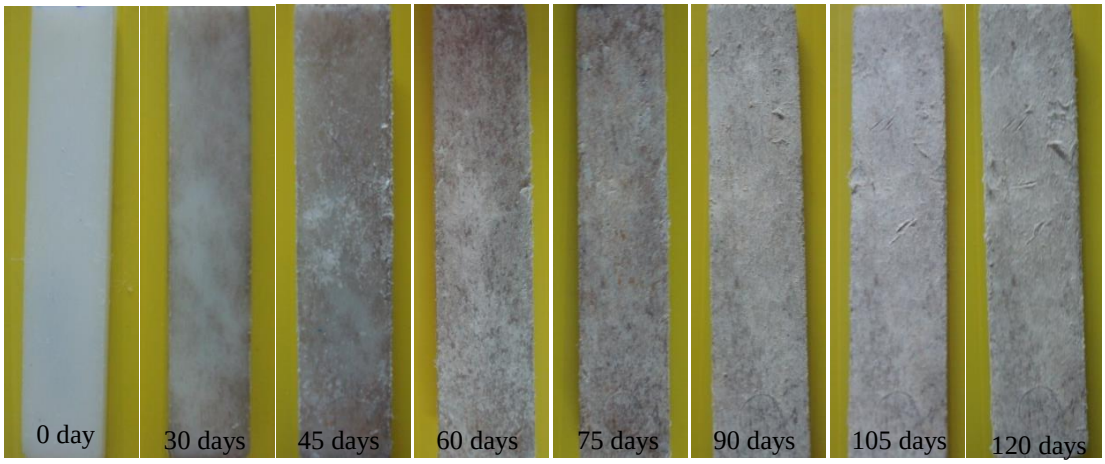

HDPE30/PBS70/EPR-g-MAH 4 phr

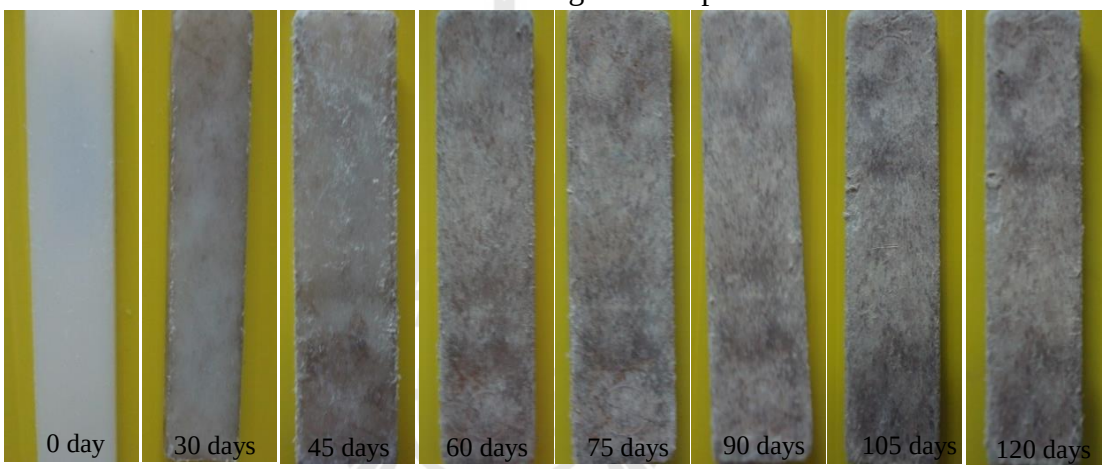

HDPE30/PBS70/EPR-g-MAH 6 phr

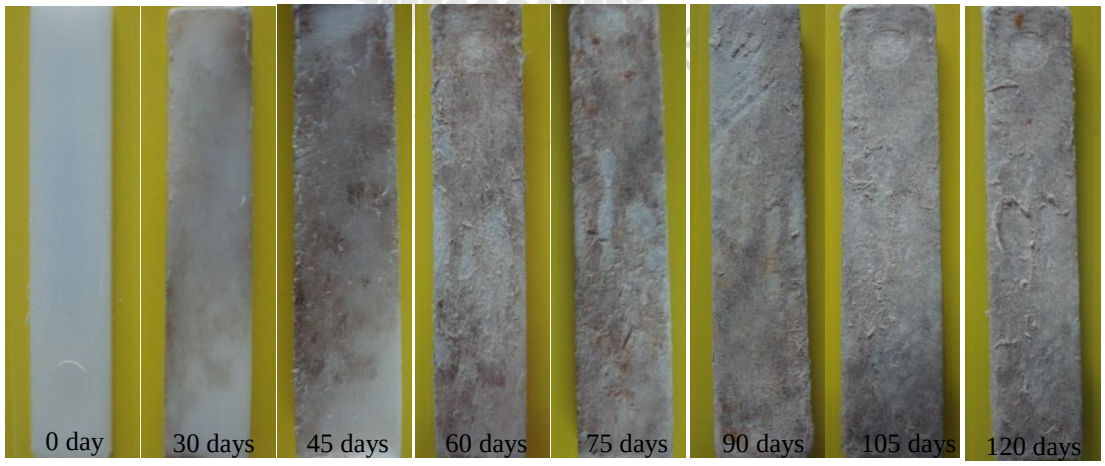

HDPE30/PBS70/EPR-g-MAH 8 phr

Figure 4.65 Optical micrographs of buried specimens of HDPE30/PBS70 blends at various contents of EPR-g-MAH at several burial times of 0 to 120 days. (Continued)

CHAPTER V

CONCLUSIONS

PBS/HDPE blend at 20, 30, 40 and 50 wt.% PBS showed a decreased apparent shear viscosity as increasing PBS content. Failure behavior of the blend containing 20 wt.% was a ductile failure. However, increasing PBS content led to a brittleness of the HDPE bend. The blend morphologies were a spherical domain in a matrix at 20 wt.% PBS, a non-uniform shape of dispersed domain including spherical, elongated and worm-like at 30 wt.% PBS, and fibrillar incorporated with partial co-continuous phase morphology at 40 wt.% PBS. Phase morphology of the blend containing 50 wt.% was the type of co-continuity. Young's modulus, elongation at break and flexural modulus of the blends decreased whereas stress at break and flexural strength of the blend increased with increasing PBS content. Yield strength insignificantly changed with increasing PBS content. Thermal stability of the blend was not much influenced by increasing PBS content. PBS hardly affected melting and crystallization behavior of the blend. In addition, water absorption and biodegradability of the blend increased with increasing PBS content.

Compatibilized PBS/HDPE blend containing 30 wt.% PBS with HDPE-g-MAH resulted in a slight increase in shear viscosity as increasing HDPE-g-MAH content. The compatibilized blend still fractured in a brittle manner. Compatibilized blend with HDPE-g-MAH gave rise to more uniform in size and shape of PBS dispersed phase. The more content of HDPE-g-MAH resulted in the finer of PBS dispersed. Particularly, at HDPE-g-MAH content of 6 and 8 phr, dispersed PBS was

mostly in a spherical shape. Adding HDPE-g-MAH slightly influenced Young's modulus, tensile strength, flexural modulus and flexural strength of the blend whereas it significantly improved elongation at break and impact strength of the blend at HDPE-g-MAH content of 6 to 8 phr. Thermal stability of the blend slightly improved with adding HDPE-g-MAH. However, HDPE-g-MAH insignificantly affected melting and crystallization behavior of the blend. Also, water absorption and biodegradability of the blend slightly decreased with increasing HDPE-g-MAH content. HDPE-g-MAH content of 2 phr was optimum for effectively improving tensile strength and impact strength of the blend without creating any significant change in Young's modulus.

Compatibilized PBS/HDPE blend prepared at 30 wt.% PBS with EPR-g-MAH led to a slight increase in shear viscosity as increasing EPR-g-MAH content. The compatibilized blend fractured in a brittle manner. EPR-g-MAH led to more uniform in size and shape of PBS domains. Moreover, the ability to plastically flow of HDPE matrix was observable in the blend containing 6 and 8 phr EPR-g-MAH. Young's modulus, flexural modulus, and flexural strength of the blend decreased whereas tensile strength of the blend slightly increased with increasing EPR-g-MAH content. Elongation at break of the blend did not improve until 6 and 8 phr EPR-g-MAH were added. Impact strength of the blend greatly improved with increasing EPR-g-MAH content, especially at 6 and 8 phr EPR-g-MAH. Thermal stability of the blend improved when EPR-g-MAH was added. However, thermal stability of the blend was not much affect by EPR-g-MAH content. Adding EPR-g-MAH also resulted in heterogeneity of spherulitic structure of PBS observed from appearance of a small shoulder peak prior to the melting peak of PBS at high temperature. However, melting

temperature of PBS phase and melting temperature of HDPE phase was not insignificantly affected by the presence of EPR-g-MAH. In addition, water absorption of the blend slightly decreased whereas biodegradability increased with increasing EPR-g-MAH content. It could be concluded that EPR-g-MAH was not effective for improving tensile strength and Young's modulus of the blend but EPR-g-MAH was much effective for enhancement of toughness of the blend, especially at 6 and 8 phr EPR-g-MAH.

HDPE/PBS blend at 20, 30, 40 and 50 wt.% HDPE showed an increasing apparent shear viscosity as increasing HDPE content. Failure behavior of the blend containing 20 wt.% was a ductile failure whereas the blend at 30, 40 and 50 wt.% HDPE fractured in a brittle manner. The phase morphology of HDPE/PBS blend at 20 wt.% HDPE was a type of spherical domain dispersed in the PBS matrix. As increasing HDPE content to 30 wt.%, dispersed HDPE particles became larger and its shape turned into worm-like and elongated structure. In addition, at 40 wt.% HDPE, spheres, ovals and more elongation of dispersed HDPE was obtained. Co-continuous phase morphology of the blend was observable in the blend containing 50 wt.% HDPE. Young's modulus and flexural modulus of the blend increased with increasing HDPE content whereas yield strength, elongation at break, stress at break and flexural strength decreased. Impact strength of the blend decreased with more addition of HDPE content. In addition, adding HDPE insignificantly affected thermal stability, melting and crystallization behavior of the blend, as well. Water absorption and biodegradability of the blend decreased as increasing HDPE content.

As compatibilizing HDPE/PBS blend prepared at 30 wt.% HDPE with HDPE-g-MAH, viscosity of the blend slightly increased with increasing HDPE-g-MAH

content. Failure behavior of the blend at 2 and 4 phr HDPE-g-MAH was a brittle failure. However, the blend at 6 and 8 phr HDPE-g-MAH fractured in a ductile manner. Phase morphology of the compatibilized blend with 2 and 4 phr HDPE-g-MAH was more uniform and smaller in HDPE size. As increasing HDPE-g-MAH content to 6 and 8 phr, HDPE domain transformed to fibrillation phase morphology. Young's modulus, flexural modulus and flexural strength of the blend slightly decreased whereas tensile strength slightly increased with increasing HDPE-g-MAH content. Elongation at break and impact strength of the blend improved with increasing HDPE-g-MAH content. Adding HDPE-g-MAH slightly influenced thermal stability, and melting and crystallization behavior of the blend. In addition, water absorption and biodegradability of the blend decreased as increasing HDPE-g-MAH content. HDPE-g-MAH of 6 phr was the optimum content for effectively improving elongation at break, impact strength and stress at break of the blend without creating any significant change in tensile strength and Young's modulus.

As compatibilizing HDPE/PBS blend containing 30 wt.% HDPE with EPR-g-MAH, viscosity of the blend slightly increased with increasing EPR-g-MAH content. Failure behavior of the blend was still in a brittle manner. After compatibilized blend with EPR-g-MAH, phase morphology of the blend was a type of spherical HDPE domain dispersed in PBS matrix. However, the spherical HDPE domain get larger with adding EPR-g-MAH. Young's modulus and flexural modulus and flexural strength of the blend decreased whereas tensile strength and elongation at break of the blend insignificantly changed with increasing EPR-g-MAH content. However, adding EPR-g-MAH resulted in a great improved in impact strength of the blend. Thermal stability of the blend improved with adding 2 phr EPR-g-MAH but it did not further

improve with adding more EPR-g-MAH. In addition, adding EPR-g-MAH resulted in nonuniform spherulitic structure of PBS exhibiting as small shoulder of PBS melting peak at high temperature. However, melting temperature of PBS phase and melting temperature of HDPE phase was not insignificantly affected by the presence of EPR-g-MAH. In addition, water absorption of the blend decreased whereas biodegradability increased with increasing EPR-g-MAH content. In summary, EPR-g-MAH was ineffective for improving tensile strength and Young's modulus of the blend but it was much effective for enhancing toughness of the blend, particularly at EPR-g-MAH content higher than 2 phr.

REFERENCES

Abdul Razak, N.C., Inuwa, I.M., Hassan, A. and Samsudin, S.A. (2013). Effects of compatibilizers on mechanical properties of PET/PP blend. **Compos. Interfaces**. 20 (7): 507-515.

Ahmad, M., Uzir Wahit, M., Abdul-Kadir, M.R., and Mohd Dahlan, K.Z. (2012). Mechanical, rheological, and bioactivity properties of ultrahigh-molecular-weight polyethylene bioactive composites containing polyethylene glycol and hydroxyapatite. **ScientificWorldJournal**. 2012: 474851.

Ambrósio, J.D., and Junior, E.H. (2011). Effect of processing parameters on the mechanical properties of in situ compatibilized polybutylene terephthalate/acrylonitrile–butadiene–styrene blends. **J. Appl. Polym. Sci.** 124: 2753–2765.

Ao, Y.H., Sun, S.L., Tan, Z.Y., Zhou, C., Xu, N., Tang, K., Yang, H.D.,and Zhang, H.X. (2007). Polymer blends of PBT and PP compatibilized by epoxidized ethylene propylene diene rubber. **Polym. Bull.** 58: 447-455.

Arbelaiz, A., Fernández, B., Ramos, J.A., Retegi, A., Llano-Ponte, R., and Mondragon, I. (2005). Mechanical properties of short flax fiber bundle/polypropylene composites: Influence of matrix/fiber modification, fiber content, water uptake and recycling. **Comp. Sci. Tech.** 65: 1582-1592.

Bandyopadhyay, S., Iyer, R., Majumder, R., Satapathy, B., and Ghosh, A. K. (2013). Studies on wear properties of polystyrene in the presence of fibrillated network of polytetrafluoroethylene. **ISRN Polym. Sci.** 2013: 837952.

Bell, J.R. (2007). **Cocontinuous Polymer Blends: The Role of Block Copolymer in Blend Morphology Evolution**. Michigan: ProQuest Dissertations & Theses Global.

Boutevin, B., Lusinchi, J.M., Pietrasanta, Y., and Robin, J.J. (1996). Improving poly (ethylene terephthalate)/high-density polyethylene blends by using graft copolymers. **Polym. Eng. Sci.** 36 (6): 879–884.

Brough, I., Haward, R.N., Healey, G., Wood, A. (2004). Scanning electron micrographs of high density polyethylene fracture surfaces. **Polymer**. 45: 3115-3123.

Chanda, M., and Roy, S.K. (2006) **Plastics technology handbook**. United Kingdom: Taylor and Francis.

Chapleau, N., and Favis, B.D. (1995). Droplet/fibre transitions in immiscible polymer blends generated during melt processing. **J. Mater. Sci.** 30 (1): 142-150.

Chareunkvun, S. (2007). **A study of compatibilization and properties of recycled high density polyethylene (HDPE)/polyethylene terephthalate (PET)**. M. Eng. Thesis, Suranaree University of Technology, Thailand.

Chow, W.S., Bakar, A.A., Mohd Ishak, Z.A., Karger-Kocsis, J., and Ishiaku, U.S. (2005). Effect of maleic anhydride-grafted ethylene–propylene rubber on the mechanical, rheological and morphological properties of organoclay reinforced polyamide 6/polypropylene nanocomposites. **Eur. Polym. J.** 41: 687–696.

Dimitrova, T.L., La Mantia, F.P., Pilatib, F., Tosellic. M., Valenzad, A., and Viscod, A. (2000). On the compatibilization of PET/HDPE blends through a new class of copolyesters. **Polymer.** 41 (13), 4817–4824.

El Nashar, D.E., Maziad, N.A., and Sadek, E.M. (2008). Improving low-density polyethylene/poly (ethylene terephthalate) blends with graft copolymers. **J. Appl. Polym. Sci.** 110: 1929-1937.

Fasce, L., Seltzer, R., and Frontini, P. (2005). Mechanical and fracture characterization of 50:50 HDPE/PET blends presenting different phase morphologies. **Polym. Eng. Sci.** 45: 354-363.

Fujimaki, T. (1998). Processability and properties of aliphatic polyesters, 'BIONOLLE', synthesized by polycondensation reaction. **Polym. Degrad. Stabil.** 59: 209–214.

Groeninckx, G., Vanneste M., and Everaert V. (2003). Crystallization structure, Morphological structure, and melting of polymer. In Utracki, L.A. (ed.). **Polymer blends handbook**. (pp 203-294). Netherland: Academic.

Guerrero, C., Lozano, T., Gonzalez, V., and Arroyo, E. (2001). Properties and morphology of poly (ethylene terephthalate) and high-density polyethylene blends. **J. Appl. Polym. Sci.** 82: 1382-1390.

Harrats, C. (2009). **Multiphase Polymer- Based Materials: An Atlas of Phase Morphology at the Nano and Micro Scale**. Florida: CRC Press Taylor and Francis Group.

Harrats, C., Thomas, S., and Groeninckx, G. (2006). **Micro- and Nanostructured Multiphase Polymer Blend Systems: Phase Morphology and Interfaces**. Florida: CRC Press Taylor and Francis Group.

Headwaters Cooperative Recycling, Inc. **Recycling Facts.** Retrieved March 10, 2012 from http://www.naccc.org/CMSUploads/819_Recycling_Facts_for_%20.pdf.

Iniguez, C.G., Michel, E., Gonzalez-Romero, V.M., and Gonzalez-Nunez, R. (2000).

Morphological stability of postconsumer PET/HDPE blends. **Polym. Bul.** 45: 295-302.

Ito, K., and Guillet, J.E. (1979). Estimation of solubility parameters for some olefin polymers and copolymers by inverse gas chromatography. **Macromol.,** 12 (6): 1163–1167.

Jabarin, S.A. and Bhakkad, V.V. (1995). Morphology and properties of poly (ethylene blends: Effects of processing variables. In Rader, C.P., Baldwin, S.D., Cornell, D.D., Sadler, G.D., and Stockel, R.F. (ed.). **Plastics, rubber, and paper recycling** (pp. 113-138). Washington, DC: American Chemical Society.

Kang, T.K., Kim, Y., Lee, W.K., Park, H.D., Cho, W.J., and Ha, C.S. (1999). Properties of uncompatibilized and compatibilized poly (butylene terephthalate)–LLDPE blends. **J. Appl. Polym. Sci.** 72: 989-997.

Kalfoglou, N.K., Skafidas, D.S., and Kallitsis, J.K. (1995). Comparison of compatibilizer effectiveness for PET/HDPE blends. **Polym. J.** 36 (23): 4453-4462.

Khalf, A.I., El Nashar, D.E., and Maziad, N.A. (2010). Effect of grafting cellulose acetate and methylmethacrylate as compatibilizer onto NBR/SBR blends. **Mater. Des.** 31 (5): 2592–2598.

Kim, D.H., Park, K.Y., Kim, J.Y., and Suh, K.D. (2000). Improved compatibility of high-density polyethylene/poly(ethylene terephthalate) blend by the use of blocked isocyanate group. **J. Appl. Polym. Sci.** 78: 1017-102.

Kim, H.S., Yang, H.S., and Kim, H.J. (2005). Biodegradability and Mechanical Properties of Agro-Flour–Filled Polybutylene Succinate Biocomposites. **J. Appl. Polym. Sci.** 97: 1513–1521.

Kim, J., Kim, J.H., Shin. T.K., Choi, H.J., and Jhon, M.S. (2001). Miscibility and rheological characteristics of biodegradable aliphatic polyester and linear low density polyethylene blends. **Eur. Polym. J.** 37 (10): 2131–2139.

Kim, Y.J., and Park, O.O. (1999). Miscibility and biodegradability of poly (butylene succinate)/poly (butylene terephthalate) blends**. J. Envi. Polym. Degrad.** 7 (1): 53-66.

Łabużek, S., Nowak B., and Pająk, J. (2003). The susceptibility of polyethylene modified with Bionolle to biodegradation by Filamentous fungi. **Pol. J. Environ. Stud.** 13: 59-68.

Lafitte, G., Espuche, E., and Gerard, J.F. (2011). Polyamide 11/poly(hydroxy amino ether) blends: Influence of the blend composition and morphology on the barrier and mechanical properties. **Eur. Polym. J.** 47 (10): 1994–2002.

Laokijcharoen, P., and Coran, A.Y. (1998). The evolution of morphology in NR/HDPE blends. Part I. Microscopy for unvulcanized blends. **Rubber Chem. Technol.** 71 (5): 966-974.

Laurienzo, P., Immirzi, B., and Malinconico, M. (2001). A preliminary investigation on the use of poly[(ethylene terephthalate)-co-(ε-caprolactone)] copolymer as compatibiliser of HDPE/PET blends. **Macromol. Mater. Eng.** 286: 248–253.

Lee S., and Lee, J.W. (2005). Characterization and processing of Biodegradable polymer blends of poly (lactic acid) with poly (butylene succinate adipate). **Korea-Aust. Rheol. J.** 17 (2): 71-77.

Lei, Y., Wu, Q., Clemons, C.M., and Guo, W. (2009). Phase structure and properties of poly (ethylene terephthalate)/high-density polyethylene based on recycled materials. **J. Appl. Polym. Sci.** 113: 1710-1719.

Levitt, L. and Macosko, C.W. (1999). Shearing of Polymer Drops with Interface Modification**. Macromol.** 32: 6270-6277.

Liu, L., Yu, J., Cheng, L., and Qu, W. (2009). Mechanical properties of poly(butylene succinate) (PBS) biocomposites reinforced with surface modified jute fibre. **Compos. Part A-Appl.** 40: 669-674.

Liu, L., Yu, J., Cheng, L., and Yang, X. (2009). Biodegradability of poly (butylene succinate) (PBS) composite reinforced with jute fibre. **Polym. Degrad. Stab.** 94 (1): 90-94.

Liu, X., Li, C., Zhang, D., and Xiao, Y. (2006). Melting behaviors, crystallization kinetics, and spherulitic morphologies of poly (butylene succinate) and its copolyester modified with rosin maleopimaric acid anhydride. **J. Polym. Sci.: Part B: Polym. Phys.** 44: 900–913.

Lusinchi, J.M., Boutevin, B., Torres, N., and Robin, J.J. (2001). In situ compatibilization of HDPE/PET blends. **J. Appl. Polym. Sci.** 79: 874-880.

Maksimov, R.D., Meri, R.M., Kalnin, M., and Zicans, J. (2003). Mechanical properties of polyethylene and poly(ethylene terephthalate) blends. **Mech. Compos. Mater.** 39: 189- 196.

Martíne, J.G., Benavides, R., and Guerrero, C. (2007). Polyethylenes/PET blend compatibilization with maleic anhydride modified polyethylenes obtained by a UV preirradiation process. **J. Appl. Polym. Sci.** 104 (1): 560-567.

Mbarek, S., Jaziri, M., Chalamet, Y., and Carrot, C. (2010). Effect of the viscosity ratio on the morphology and properties of PET/HDPE blends with and without compatibilization. **J. Appl. Polym. Sci.** 117: 1683–1694.

Merdas, I., Thominette, F., Tcharkntchi., and Verdu, J. (2002). Factors governing water absorption by composite matrices. **Comp. Sci. Tech.** 62: 487-492.

Mitsubishi Chemical expands renewable chemical investments. **ICIS News online.** Retrieved August 29, 2011 from http://www.icis.com/Articles/2011/08/29/9488385/news-focus-mitsubishi-chemical-expands-renewable-chemical.html.

Moore, G. F., and Saunders, S.M. (1998). **Advances in Biodegradable** Polymers (p 19). Florida: CRC Press

Nalla, R.K., Kinney, J.H., and Ritchie, R.O. (2003). Effect of orientation on the in vitro fracture toughness of dentin: the role of toughening mechanisms. **Biomaterials**. 24: 3955–3968.

Nowak, B., Pająk, J., Bratkowicz, M.D., and Rymarz, G. (2011). Microorganisms participating in the biodegradation of modified polyethylene films in different soils under laboratory conditions. **Int. Biodeterior. Biodegrad.** 65: 757-767.

Okada, O., Keskkula, H., and Paul, D.R. (2001). Mechanical properties of blends of maleated ethylene-propylene rubber and nylon 6. **Polym. J.** 42: 8715-8725.

Pang, M.Z., Qiao, J.J., Jiao, J., Wang, S.J., Xiao, M., and Meng, Y.Z. (2008). Miscibility and Properties of Completely Biodegradable Blends of Poly (propylene carbonate) and Poly (butylene succinate). **J. Appl. Polym. Sci.** 107: 2854–2860.

Papadopoulou, C.P., Kalfoglou, N.K. (2000). Comparison of compatibilizer effectiveness for PET/PP blends: their mechanical, thermal and morphology characterization. **Polymer.** 41: 2543–2555.

Pawlak, A., Morawiec, J., Pazzagli, F., Pracella, M., and Galeski, A. (2002). Recycling of postconsumer poly (ethylene terephthalate)and high-density polyethylene by compatibilized blending. **J. Appl. Polym. Sci.** 86: 1473–1485.

Pietrasanta, Y., Robin J.J., Torres, N., and Boutevin, B. (1999). Reactive compatibilization of HDPE/PET blends by glycidyl methacrylate functionalized polyolefins. **Macromol. Chem. Phys.** 200: 142-149.

Polettoa, M., Zattera, A.J., Forte-Maria, M.C., Santana-Ruth, M.C. (2012). Thermal decomposition of wood: Influence of wood components and cellulose crystallite size. **Bioresour. Technol.** 109: 148–153.

Poly ethylene-high density (HDPE) Uses and Market Data**. ICIS News online.** Retrieved August 17, 2011 from http://www.icis.com/Articles/2007/11/06/9076152/ Polyethylene-high density (HDPE) Uses and Market Data .html.

Pracella, M., Pazzagli, F., and Galeski, A. (2002). Reactive compatibilization and properties of recycled poly (ethylene terephthalate)/polyethylene blends. **Polym. Bull.** 48: 67-74.

Pracella, M., Rolla, L., Chionna, D., and Galeski, A. (2002). Compatibilization and properties of poly (ethylene terephthalate)/polyethylene blends based on recycled materials. **Macromol. Chem. Phys.** 203: 1473–1485.

Puukilainen, E., Koponen, H.K., Xiao, Z., Suvanto, S., and Pakkanen, T.A. (2006). Nanostructured and chemically modified hydrophobic polyolefin surfaces. **Colloids Surf., A: Physicochem. Eng. Aspects.** 287 (2006) 175–181.

Qi, R., Nie, J., Zhou, C., Mao, D., and Zhang, B. (2006). Influence of high density polyethylene-g-maleic anhydride on compatibility and properties of poly (butylene terephthalate)/high density polyethylene blends. **J. Appl. Polym. Sci.** 102: 6081–6087.

Qiu, Z., Komura, M., Ikehara, T., and Nishi, T. (2003). DSC and TMDSC study of melting behavior of poly (butylene succinate) and poly(ethylene succinate). **Polymer.** 44: 7781–7785.

Rappaport, H. (2011). **Ethylene and Polyethylene Global Overview: SPI Film & Bag**. Retrieved June 1, 2014 from http://spi.files.cmsplus.com/about/fbf/H%20Rappaport%20SPI%20Film%20%26%20Bag%2005%2011.pdf

Seo, H.M., Park, J. H., Dao, T.D., and Jeong, H.M. (2013). Compatibility of functionalized graphene with polyethylene and its copolymers. **J. Nanomat.** DOI 10.1155/2013/805201.1-8.

Sewda, K., and Maiti, S.N. (2009). Mechanical properties of teak wood flour-reinforced HDPE composites. **J. Appl. Polym. Sci.,** 112: 1826-1834.

Shah, A.A., Hasan, F., Hameed, A., Ahmed, S. (2008). Biological degradation of plastics: a comprehensive review. **Biotechnol. Adv.** 26: 246–265.DOI

Singh, G., Bhunia, H., Rajor, A., and Choudhary, V. (2010). Thermal properties and degradation characteristics of polylactide, linear low density polyethylene, and their blends. **Polym. Bull**. 66: 939-953.

Song, Y.M., Chen, W.C., Yu, T. L., Linliu, K., and Tseng, Y. H. (1996). Effect of isocyanates on the crystallinity and thermal stability of polyurethanes. **J. Appl. Polym. Sci.** 62: 827-834.

Sung, J.H., Hyun, Y.H., Kwon, D.H., and Choi, H.J. (2002). Viscoelastic property of biodegradable polymer and polyethylene blends: effect of molecular weight of polyethylene. **J. Ind. Eng. Chem.** 8 (1): 28-33.

Torres, N., Robin, J.J., and Boutevin, B. (2001). Study of compatibilization of HDPE-PET blends by adding grafted or statistical copolymer. **J. Appl. Polym. Sci.** 81: 2377-2386.

Tsai, C.H., and Chang, F.C. (1996). Polymer blends of PBT and PP compatibilized by ethylene-co-glycidyl methacrylate copolymers. **J. Appl. Polym. Sci.** 61: 321-332.

Tsi, H.Y., Tsen, W.C., Shu, Y.C., Chuang, F.S., and Chen, C.C. (2009). Compatibility and characteristics of poly (butylene succinate) and propylene-co-ethylene copolymer blend. **Polym. Test.** 28: 875-885.

Wallheinke, K., Pötschke, P., Macosko, C. W., and Stutz, H. (1999). Coalescence in blends of thermoplastic polyurethane with polyolefins. **Polym. Eng. Sci.** 39 (6): 1022-1034.

Wang, X., Zhou, J., and Li, L. (2007). Multiple melting behavior of poly (butylene succinate). **Eur. Polym. J.** 43: 3163–3170.

Wang, Y., and Hillmyer, M.A. (2001). Polyethylene-poly(L-lactide) diblock copolymers: synthesis and compatibilization of poly (L-lactide)/polyethylene blends. **J. Polym. Sci.: Part A: Polym. Chem**. 39: 2755–2766.

Xu, J., and Guo, B.H. (2010). Microbial Succinic Acid, Its Polymer Poly(butylene succinate), and Applications. In Guo, G. and Chen, Q. (ed.). **Plastics from Bacteria: Natural Functions and Applications** (pp. 347-388). Berlin: Springer Berlin-Heidelberg.

Yasuniwa, M., Tsubakihara, S., Satou, T., and Iura, K. (2005). Multiple melting behavior of poly(butylene succinate). II. Thermal analysis of isothermal crystallization and melting process. **J. Polym. Sci.: Part B: Polym. Phys.** 43: 2039–2047.

Yoo, E.S., and Im, S.S. (1999). Melting Behavior of Poly (butylene succinate) during Heating Scan by DSC. **J. Appl. Polym. Sci. Part B: Polym. Phys.** 37: 1357–1366.

Zainuddin, Sudradjat, A., Razzak, M.T., Yoshii, F., and Makuuchi, K. (1999). Polyblend CPP and Bionolle with PP-g-MAH as compatibilizer: I. compatibility. **J. Appl. Polym. Sci.** 72: 1277–1282.

Zhao, J.H., Wang, X.Q., Zeng, J., Yang, G., Shi, F.H., and Yan, Q. (2005). Biodegradation of Poly(Butylene Succinate) in Compost. **J. Appl. Polym. Sci.** 97: 2273–2278

APPENDIX A

METHOD TO IDENTIFY THE NUMBER OF VIABLE MICRO-ORGANISMS IN SOIL

Mycology Laboratory
113 Thailand Science Park, Paholyothin Road,
Klong 1, Klong Luang, Pathumthani 12120, Thailand
Tel: +66-2-564-6700 ext 3202 Fax: +66-2-564-6707

BIOTEC
a member of NSTDA

รายงานผลการการตรวจสอบเชื้อราบนตัวอย่างทดสอบ

MY 05-04

ชื่อผู้ขอรับบริการ / Customer's name: น.ส.จิจฉราพร ธันที	เลขที่ / No. :
องค์กรและที่อยู่ / Institute and address: สำนักวิชาวิศวกรรมศาสตร์	วันที่ได้รับตัวอย่าง / Sample receive date : 22/04/2014
สาขาวิชาวิศวกรรมพอลิเมอร์ ม.เทคโนโลยีสุรนารี อาคารวิชาการ 1 เลขที่ 111	วันที่รายงานผล/ Report date: 16/06/2014
ถ.มหาวิทยาลัย อ.เมือง จ.นครราชสีมา 30000	

ตัวอย่าง	จำนวน	ผลการการตรวจสอบ	หมายเหตุ
SUT_SOIL	1	พบเชื้อรา *Aspergillus niger*	

โปรดทำเครื่องหมาย ✓ ในช่อง O ที่ต้องการ

เอกสารแนบ: ☑ วิธีการวิเคราะห์

ผู้ปฏิบัติงาน อัมพวา ปินเรือน
(นางสาวอัมพวา ปินเรือน)

ผู้รายงานและวิเคราะห์ผล อัมพวา ปินเรือน
(นางสาวอัมพวา ปินเรือน)

ผลการตรวจสอบเชื้อราบนตัวอย่างทดสอบ

ตัวอย่างทดสอบ: ดิน SUT_SOIL

วิธีการ

1.1 การแยกเชื้อรา

การแยกเชื้อราจากดินใช้วิธี dilution plate ดังนี้

1.1.1 ชั่งดินตัวอย่าง 10 กรัม ละลายในน้ำกลั่นที่ฆ่าเชื้อแล้ว 90 มล. จะได้สารละลายดินที่มีความเข้มข้น 10^{-1}

1.1.2 นำสารละลายที่ได้ไปเจือจางในน้ำให้ได้ความเข้มข้น 10^{-2},10^{-3} และ 10^{-4} ตามลำดับ

1.1.3 ใช้ปิเปตดูดสารละลายตัวอย่างใส่จานเลี้ยงเชื้อ ในแต่ละตัวอย่างและแต่ละความเข้มข้น ให้ดูดใส่จานละ 1 มล. ทำ 3 ซ้ำ

1.1.4 เทอาหาร Potato Dextrose Agar ครึ่งสูตร (1/2 PDA) ที่มีส่วนผสมของ Rose Bengal และ Streptomycin ลงในจานเลี้ยงเชื้อหมุนเบาๆ ให้สารละลายตัวอย่างกระจายทั่วจานเลี้ยงเชื้อ

1.1.5 นำจานเลี้ยงเชื้อไปบ่มไว้ที่อุณหภูมิห้อง

1.1.6 เมื่อเชื้อราเจริญขึ้นมา ใช้เข็มเขี่ยที่ฆ่าเชื้อแล้ว ย้ายโคโลนีเชื้อราแต่ละโคโลนีลงใน PDA

1.2 การจำแนกชนิดเชื้อรา

วิธีการจำแนกชนิดเชื้อราที่แยกได้ทำโดยสับเชื้อ (inoculate) ที่เลี้ยงไว้ในอาหารเลี้ยงเชื้อ PDA ลงบนอาหารเลี้ยงเชื้อที่เหมาะสมเป็น 3 จุด ให้แต่ละจุดมีระยะห่างจากขอบจานเลี้ยงเชื้อและจากจุดศูนย์กลางเท่าๆ กัน รวมถึงระยะห่างระหว่างจุดเท่ากันเพื่อเปรียบเทียบลักษณะของโคโลนี โดยหากพบเชื้อรา *Aspergillus* และ *Penicillium* จะเลี้ยงบนอาหาร CzA (Czapek's Solution Agar) และหากพบเชื้อรา *Rhizopus* จะเลี้ยงบนอาหาร PDA หลังจากสับเชื้อแล้วนำไปบ่มไว้ที่อุณหภูมิห้อง จนเชื้อรามีการเจริญเติบโตที่สามารถสังเกตลักษณะโคโลนีที่เด่นชัดและสร้าง spore จึงนำไปศึกษาลักษณะรูปร่างต่างๆ ของราอย่างละเอียด ภายใต้กล้องจุลทรรศน์แบบ Stereo และแบบ Compound เพื่อจำแนกชนิดรา

ผลการตรวจสอบ

พบเชื้อรา *Aspergillus niger* (รูปที่ 1) แต่ไม่พบเชื้อรา *Penicillium funiculosum* และ *Rhizopus niveus*

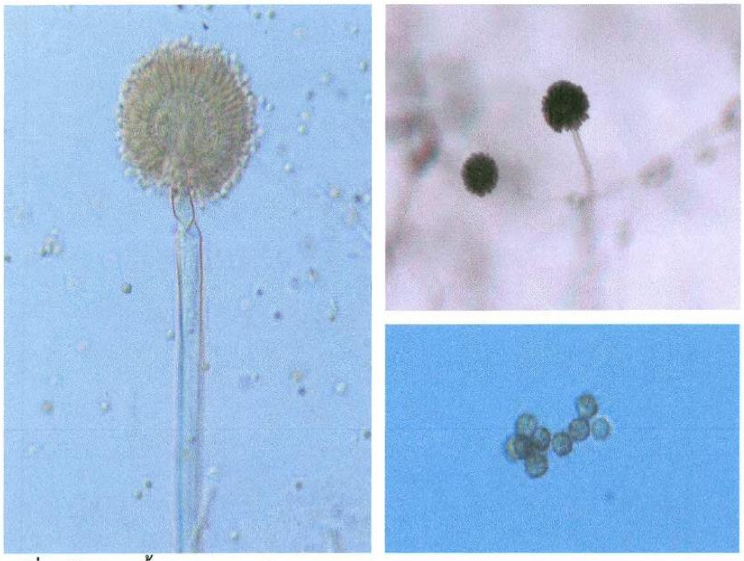

รูปที่ 1 ลักษณะเชื้อรา *Aspergillus niger*

APPENDIX B

LIST OF PUBLICATIONS

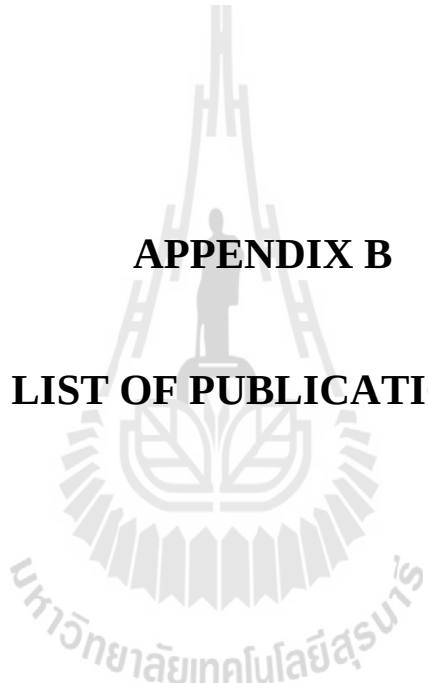

List of Publications

Parts of this conferences work were published and presented in the following journal;

Aontee, A., Sutapun, W., (2013). Mechanical properties of high density polyethylene and Poly (butylene succinate) blends. In Proceeding of **PACCON2013 (Pure and Applied Chemistry International Conference 2013)** (pp 611-614), Chonburi, Thailand.

Aontee, A., Sutapun, W., (2013). A study of compatibilization effect on physical properties of poly (Butylene Succinate) and high density polyethylene blend. **Adv. Mater. Res**.699 (2013) (pp 51-56).

Aontee, A., Sutapun, W., (2013). Effect of blend ratio on phase morphology and mechanical properties of high density polyethylene and poly (butylene succinate) blend. **Adv. Mater. Res**.747 (2013) (pp 555-559).

MECHANICAL PROPERTIES OF HIGH DENSITY POLYETHYLENE AND POLY (BUTYLENE SUCCINATE) BLENDS

Ajcharaporn Aontee[1], Wimonlak Sutapun[1]*

[1]School of Polymer Engineering, Suranaree University of Technology, Nakhon Ratchsima 30000, Thailand

*Author for correspondence; E-Mail: wimonlak@sut.ac.th, Tel. +66 44 224435, Fax. +66 44 224605

Abstract: In this work, the effect of PBS and HDPE blend ratio on mechanical properties of PBS/HDPE blend was investigated. PBS/HDPE blends were prepared at PBS content of 20, 30, and 40 wt.% via melt mixing process and molded using an injection machine. It was found that Young's modulus of PBS/HDPE blend gradually decreased with increasing PBS content along with considerable decrease of elongation at break. However, the yield strength did not much depend on PBS content but stress at break of PBS/HDPE blend increased with increasing PBS content. Flexural modulus of PBS/HDPE blend was lower than that of neat HDPE. On the other hand, flexural strength of the blend slightly increased with increasing PBS content. Unnotched impact strength of PBS/HDPE blend changed with PBS content. In addition, ultimate strain and impact strength of the blends were much lower than those of neat HDPE and decreased with more fraction of PBS. However, the ultimate strain and impact strength did improve when increased PBS content up to 40 wt.% due to fibrillation phase morphology of the PBS/HDPE blend. For phase morphology of PBS/HDPE blend, the blend containing 20 wt.% PBS exhibited phase morphology of dispersed in matrix. The HDPE blend with 30 wt.% PBS contained non-uniform phase morphology with spherical, elongated, and worm-like shape of PBS domain. Lastly, fibrillar phase morphology occurred when PBS content was 40 wt.%.

1. Introduction

With the increase in the global population, plastic materials have found wide applications in every aspect of life and industries. High Density Polyethylene (HDPE) is one of the most widely used plastics after PVC and PP [1]. Its applications including food and pharmaceutical packaging, potable water pipes, chemical containers, construction appliances and automotive parts. These widespread applications are due to its favourable mechanical and thermal properties [2, 3]. However, HDPE is a non-biodegradable plastic. The post consumer product of HDPE is end up with large quantities of plastic waste left in a landfill. In the next 5 year, approximately 10 million tons of HDPE waste will be gathered in nature causing much environmental pollution [4]. Therefore, the biodegradability of HDPE has to be enhanced in order to make it degradable in nature.

Poly (butylene succinate) (PBS) is a one type of biodegradable semi-crystalline polymers. PBS has a melting point close to that of LDPE, glass transition temperatures and tensile strength between those of PE and PP, and stiffness between that of LDPE and HDPE [1, 5]. In addition, it can be processed with the same processing machines and technique which were applied for those thermoplastics [6]. PBS has excellent biodegradability and is degraded in compost soil, fresh water and also in sea water [7]. It has been reported by Łabużek et al. [8] that the film of polyethylene blended with 60 wt.% PBS (Bionolle™) was degraded within 90 days by fungi which encountered in a dump. Therefore, it is expected that blending HDPE with PBS is not only able to improve biodegradability of consumer products derived from HDPE but also the preferred mechanical properties of the final product will be accessible.

However, the mechanical properties of PBS/HDPE blends strongly correlated with their phase morphology. The phase morphology of immiscible polymer blends depends on various parameters, e.g. blend ratio, mixing and processing condition, viscosity ratio and also interfacial force [9]. Material parameters as viscosity ratio and interfacial force are the significant parameters governing phase morphology of the immiscible blends. The equation for viscosity ratio is shown in Equation 1. The relationship between shear rate, a processing parameter, and interfacial force is expressed in the term of capillary number as shown below in Equation 2 [9, 10]:

$$\eta_r = \frac{\eta_d}{\eta_m} \quad (1)$$

$$Ca = \frac{\eta_m R\dot{\gamma}}{\Gamma} \quad (2)$$

Where η_d and η_m are the viscosity of dispersed phase and continuous phase, respectively, $\dot{\gamma}$ is the shear rate, R is the droplet diameter and Γ is the interfacial tension.

In this study, the effect of PBS content on mechanical properties and phase morphology of PBS/HDPE blend was investigated. the blends of HDPE were prepared with PBS content of 20-40 wt.%.

2. Materials and Methods

2.1 Materials

High density polyethylene (injection grade, EL-Lene™ H5814J) was purchased from SCG Chemicals Co., Ltd. It has a melt flow index (MFI) of 14 g/10 min (2.16 kg at 190ºC) and a melting temperature (T_m) of 131ºC.

Poly (butylene succinate) (GS Pla™, AZ91TN) was obtained from Mitsubishi Chemical Co., Ltd. Its melt flow index is 4 g/10 min (2.16 kg at 190ºC) and melting temperature (T_m) is 110ºC.

2.2 Preparation of PBS/HDPE Blends.

The pellets of neat PBS and neat HDPE were initially dried in an oven at 60ºC for 12 h. before preparing polymer blend. To prepare PBS/HDPE blends, PBS and HDPE were mixed at a weight ratio of 20:80, 30:70 and 40:60 in an internal mixer (HAAKE, Rheomix3000p). The mixing process was operated at 170°C under a rotor speed of 70 rpm and mixing time of 10 min. After that, the mixtures of PBS/HDPE were cooled down to room temperature and then grinded using a grinding machine. The specimens for tensile, flexural and impact test were molded by an injection machine (Chuan Lih Fa, CLF 80T). The injection molding process was carried out with a melting temperature of 180°C, a screw speed of 130 rpm, an injection speed of 47 mm/s, a holding pressure of 617 kg/cm^3 and a mold temperature of 30ºC.

2.3 Characterization of PBS/HDPE Blends.

Tensile properties including Young's modulus, yield strength, stress at break and elongation at break of PBS/HDPE blends were determined using a universal testing machine with a load cell of 5 kN (Instron, 5565), in accordance with ASTM D638. The tensile test was performed in uniaxial tension at a crosshead speed of 10 mm/min.

Flexural properties of PBS/HDPE blends were tested following ASTM D790 (procedure B) using a universal testing machine with a load cell of 5 kN (Instron, 5565) at a crosshead speed of 14 mm/min.

In addition, unnotched Izod impact strength following ASTM D 256 of the blends were evaluated, on an impact tester (Atlas, BPI), equipped with 5.4 J hammer.

The morphology of fracture surface obtained from chloroform etched specimens, using a scanning electron microscope (JEOL, JCM-5000 NeoScope) at 15kV. The specimens were coated with gold using an ion sputtering device for 9 min at a current of 10 mA.

3. Results and Discussion

3.1 Tensile properties

As observed in Figure 1, yield strength of PBS/HDPE blends was comparable to that of neat HDPE. It must be noted that neat HDPE did not break within an instrument limit. The addition of 20-40 wt.% PBS into HDPE matrix did not affect the yield strength of the blend. The stress at break of PBS/HDPE blend improved with 30 wt.% PBS, comparing to the blend with 20 wt.% PBS. However, adding PBS more than 30 wt.% did not create any more improvement of stress at break of the blends.

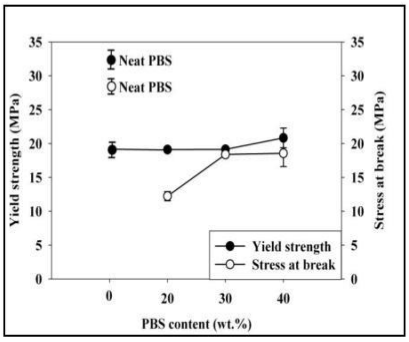

Figure 1. Plot of yield strength and stress at break of PBS/HDPE blends vs PBS content.

As presented in Figure 2, Young's modulus of neat HDPE blend was higher than that of neat PBS. Addition of PBS into HDPE matrix made a gradually decrease in Young's modulus of the blend. As mentioned previously, ultimate elongation of neat HDPE, under tensile test of a crosshead speed of 10 mm/min, was not obtained under an instrumentation limit. Addition of PBS content resulted in a decrease of elongation at break of the blends. The result corresponded well with the result obtained from unnotched impact strength of the blend. The similar result of decreasing in elongation at break of PET/HDPE blend was reported by Kim et al. [11] and Pietrasanta et al.[12]. They have found that blending HDPE with 10-40 wt.% PET (poly (ethylene terephthalate)) resulted in much decrease of elongation at break. The decreased elongation at break of the PBS/HDPE blend was a consequence of uncompatibility of polar PBS and non-polar HDPE. Under tensile loading, the interfacial voids led to a propagation of premature cracks by which the plastic flow of each phase was disrupted. Therefore, PBS/HDPE blend ruptured at lower ultimate strain with higher content of PBS. However, ultimate elongation of HDPE blend did not further decrease with 40 wt.% PBS due to the fibrillar phase morphology of PBS domain, as shown in Figure 5d.

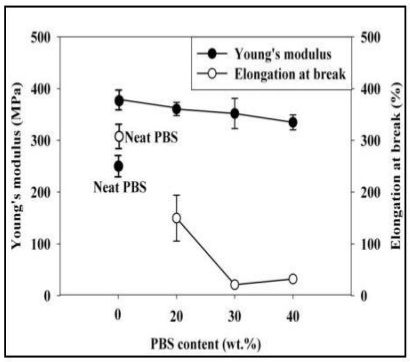

Figure 2. Plot of Young's modulus and elongation at break of PBS/HDPE blends vs PBS content.

3.2 Flexural properties

Flexural modulus and flexural strength of neat PBS, neat HDPE and PBS/HDPE blends at various contents of PBS were presented in Figure 3. Flexural modulus of neat HDPE was higher than that of neat PBS. PBS/HDPE blends had a flexural modulus between neat PBS and neat HDPE, and gradually decreased with increasing PBS content. On the other hand, flexural strength of neat PBS was higher than that of neat HDPE. Adding PBS into HDPE did insignificant influence flexural strength of the PBS/HDPE blends.

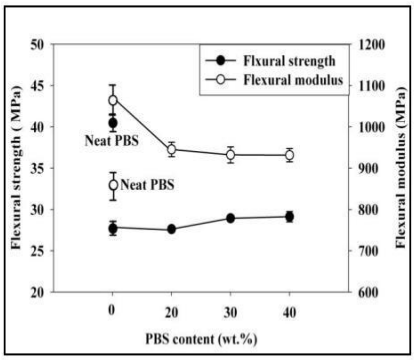

Figure 3. Plot of flexural modulus and flexural strength of PBS/HDPE blends vs PBS content.

3.3 Impact properties

It must be noted that unnotched impact strength of neat HDPE and neat PBS was not obtained; it was far beyond an instrumentation limit of a 135 kJ/m^2. As shown in Figure 4, unnotched impact strength of PBS/HDPE blends was much lower than that of neat HDPE and neat PBS because of high interfacial tension between PBS phase and HDPE matrix. With 30 wt.% PBS, impact strength of the blend continued to drop but with 40 wt.%, the impact strength of the

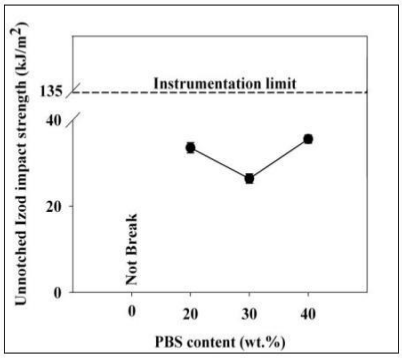

Figure 4. Plot of unnotched Izod impact strength of PBS/HDPE blends vs PBS content.

blend became higher than that of the blend with 30 wt.%.The result corresponded with elongation at break of the HDPE blends as discussed before. Fibrillar phase morphologyof the 40 wt.% PBS/HDPE blend, as depicted in Figure 5d, was a key factor for improving elongation at break and impact strength.

3.4 Fracture Surface Morphology

SEM micrographs of neat HDPE and HDPE blends at PBS content of 20, 30, and 40 wt.% were shown in Figure 5. Fracture surface morphology of HDPE, illustrated in Figure 5a, was rough with a blocky structure which was a characteristic of ductile polymer. However, the fine mesh of deformed polymer was not observed from the SEM of magnification at x1000[13]. Addition 20 wt.% PBS into HDPE gave rise to a heterogeneous phase morphology with spherical PBS domain dispersed in HDPE matrix according to high interfacial tension between PBS and HDPE phases. In addition, smoother surface of HDPE matrix was observed in Figure 5b. This was an indication of reduction in ductility of HDPE matrix. This phase morphology was responsible for decrease of ultimate elongation and impact strength comparing to those of neat HDPE. As increase PBS content to 30 wt.%, non-uniform size and shape, including spherical, elongated and worm-like, of dispersed phase were observed in Figure 5c. Phase morphology containing elongated and worm-like shape of dispersed PBS phase resulted in slight increase of ultimate stress but not yet ultimate strain and impact strength of the blend. In addition, the fibrillation of phase domain occurred at 40 wt.% PBS, as observed in Figure 5d. These results correlated with improved ultimate elongation and impact strength of the PBS/HDPE blend.

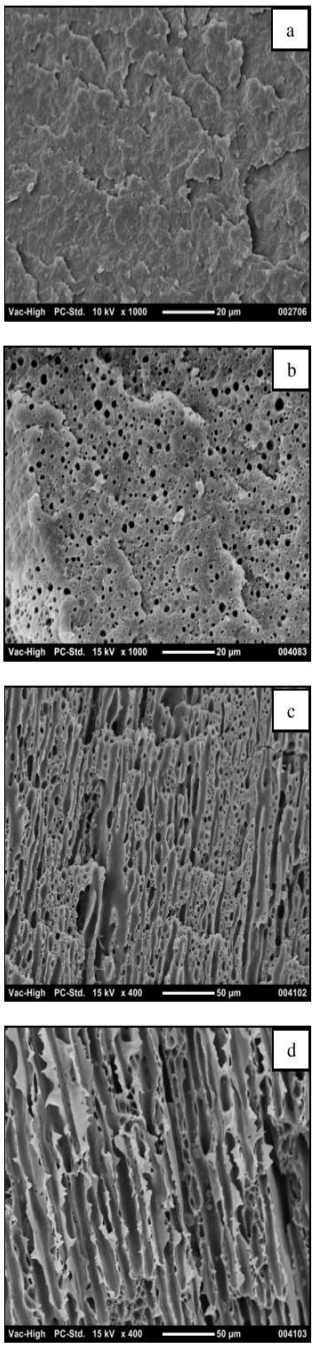

Figure 5. SEM micrographs of (a) HDPE (x1000), and PBS/HDPE of (b) 20 wt.% PBS (x1000), (c) 30 wt.% PBS (x400) and (d) 40 wt.% PBS (x400).

4. Conclusions

This research work revealed that PBS/HDPE blend was an immiscible blend with a type of dispersed in matrix morphology. In addition, phase morphology of the blend related with weight fraction of PBS dispersed phase. The blend morphologies were a spherical domain in a matrix at 20 wt.% PBS, a non-uniform shape of dispersed PBS at 30 wt.%, and fibrillar phase morphology at 40 wt.% PBS.

For tensile properties, yield strength did not change with higher composition of PBS. At higher than 20 wt.% PBS, stress at break of PBS/HDPE blend slightly increased with increasing PBS content. Young's modulus gradually decreased with adding more PBS content. In addition, ultimate strain and impact strength of the blends were much lower than those of neat HDPE and decreased with more fraction of PBS. However, the ultimate strain and impact strength did improve when increased PBS content up to 40 wt.% due to fibrillation phase morphology of the PBS/HDPE blend.

Flexural modulus of PBS/HDPE blends was in between flexural modulus of neat HDPE and neat PBS. However, PBS content did not significantly affect flexural strength of the PBS/HDPE blends.

Acknowledgements

The authors would like to thank Suranaree University of Technology for financial support.

References

[1] L. Liu, J. Yu, L. Cheng, W. Qu, Compos. Part A-Appl. , 40 (2009) 669-674.
[2] A. Arkatkar, J. Arutchelvi, M. Sudhakar, S. Bhaduri, P.V. Uppara, M. Doble, J. Environ. Eng., 2 (2009) 68-80.
[3] In: High density polyethylene (HDPE), Environmental Product Declarations of the European Plastics Manufacturers, Brussels, Belgium, 2008.
[4] S. Evans, in: GlobalData 2011, European plastics industry, 2012.
[5] Y. Shih, T. Wang, R. Jeng, J. Wu, C. Teng, J. Polym. Environ., 15 (2007) 151-158.
[6] S.K. Lim, S.G. Jang, S.I. Lee, K.H. Lee, a.I.-J. Chin, Macromol. Res., Vol. 16 (2008) 218-223.
[7] H.Y. Tsi, W.C. Tsen, Y.C. Shu, F.S. Chuang, C.C. Chen, Polym. Test., 28 (2009) 875-885.
[8] S. Łabużek, B. Nowak, J. Pająk, Pol. J. Environ. Stud. , 13 (2004) 59-68.
[9] L. Utracki, Polymer blends handbook, 1 (2003) 1-122.
[10] C. Tropea, A. Yarin, J.F. Foss, In: Springer Handbook of Experimental Fluid Mechanics, Berlin, 2007, pp. 714.
[11] D.H. Kim, K.Y. Park, J.Y. Kim, K.D. Suh, J. Appl. Polym. Sci., 78 (2000) 1017-1024.
[12] J.J. Robin. Y. Pietrasanta, N. Torres, B. Boutevin, Macromol.Chem.Phys., 200 (1999) 142-149.
[13] I. Brough, R.N. Haward, G. Healey, A. Wood, Polymer, 45 (2004) 3115-3123.

Advanced Materials Research Vol. 699 (2013) pp 51-56
© (2013) Trans Tech Publications, Switzerland
doi:10.4028/www.scientific.net/AMR.699.51

A Study of Compatibilization Effect on Physical Properties of Poly (Butylene Succinate) and High Density Polyethylene Blend

Ajcharaporn Aontee[1, a], Wimonlak Sutapun[1,b]

[1]School of Polymer Engineering, Suranaree University of Technology, Nakhorn Ratchsima 30000, Thailand

[a]ajcharaporn.sut@gmail.com, [b]wimonlak@sut.ac.th

Keywords: compatibilization, HDPE, PBS, PBS/HDPE Blends.

Abstract. The aim of this research is to improve compatibility of PBS/HDPE blend using HDPE-g-MAH as a compatibilizer. The effect of HDPE-g-MAH content on mechanical and thermal properties, and degree of crystallinity of PBS/HDPE/HDPE-g-MAH blend was investigated. The blends were prepared at PBS/HDPE weight ratio of 30/70 and HDPE-g-MAH was used at a content of 2, 4, 6 and 8 part per hundred of PBS and HDPE. The results showed that yield strength and stress at break of PBS/HDPE/HDPE-g-MAH blends insignificantly increased with adding HDPE-g-MAH more than 2 phr. In addition, addition of HDPE-g-MAH to the binary blends led to an increase of elongation at break while Young's modulus of blends exhibited an insignificant change. The addition of HDPE-g-MAH into PBS/HDPE blend did not affect both flexural modulus and flexural strength. In addition, unnotched impact strength of the blends greatly increased with increasing HDPE-g-MAH content and PBS/HDPE blend containing 8 phr of HDPE-g-MAH were not fractured within the instrument limit. For thermal properties, the presence of HDPE-g-MAH did not affect degradation temperature of PBS domain and HDPE matrix. HDPE-g-MAH of 8 phr markedly influenced the degree of crystallinity of the PBS and HDPE.

Introduction

High density polyethylene (HDPE) is a nonbiodegradable semicrystalline polymer with good mechanical properties and it is one of the most consumed plastics. Its consumption is about 24.4 million tons in 2011 [1] with an annual growth rate of 1.5 wt.% [2]. After it was consumed, enormous amount of the plastic waste was discared and cumulative in environment. Poly (butylene succinate) (PBS) is one of biodegradable semicrystalline polyesters of which some physical and mechanical properties are quite similar to those of HDPE, LDPE and PP [3]. Furthermore, it can be processed using the same processing machine and technique employed for those thermoplastics [4]. Therefore, it was expected that blending HDPE with PBS would improve biodegradability of consumer products derived from HDPE without deteriorating required mechanical properties.

In fact, HDPE is nonpolar but PBS is polar therefore the blend of HDPE and PBS is an immiscible blend. For immiscible polymer blend, the minor composition distribution is nonuniformly, the dispersed phase size is large with broad distribution, and interfacial adhesion is not good [5]. These are due to high interfacial tension of the blend system. As a result, mechanical properties of the blend especially tensile and impact strength become worsen. The technique for overcomming blend immiscibility and enhancing interfacial adhesion is to compatibilize the immiscible blend with a compatabilizer. For example, HDPE-g-MAH was used for the blend of HDPE and PET (Poly (ethylene terephthalate)), and PP-g-MAH (Polypropylene grafted with maleic anhydried) for the blend of CPP (Polypropylene-co-ethylene) and PBS. The compatibilizer will minimize interfacial tension between two phases of immiscible polymer blends [6-8]. It was reported by Boutevin *et al.* [9] that, the presence of HDPE-g-MAH resulted in increased tensile strength and elongation at break of PET/HDPE blend. Zainuddin *et al.* [10] have shown that the tensile strength and elongation at break of CPP/PBS blends was improved by adding PP-g-MAH.

In this study, HDPE was blended with 30 wt% PBS and the blend was compatiblized using various contents of HDPE-g-MAH. The effect of HDPE-g-MAH content on mechanical and thermal properties, and degree of crystallinity of PBS/HDPE blend was investigated.

Experimental

Materials. High density polyethylene (injection grade, EL-Lene™ H5814J) was purchased from SCG Chemicals Co., Ltd. It has a melt flow index (MFI) of 14 g/10 min (2.16 kg at 190ºC) and a melting temperature (T_m) of 131ºC. Poly (butylene succinate) (GS Pla, AZ91TN) was obtained from Mitsubishi Chemical Co., Ltd. Its melt flow index is 4 g/10 min (2.16 kg at 190ºC) and melting temperature is 110ºC. The high density polyethylene grafted with maleic anhydride (HDPE-g-MA) with 0.9 wt.% maleic anhydride (Fusabond® MB100D, Du Pont™) was kindly supplied by Chemical Innovation Co., Ltd. It has a MFI of 2 g/10 min (2.16 kg at 190°C), a density of 0.960 g/cm^3, and a melting temperature of 136°C.

Preparation of PBS/HDPE Blends. The pellets of PBS, HDPE and HDPE-g-MAH were initially dried in an oven at 60°C for 12 h. before polymer blend preparation. To prepare PBS/HDPE blend, PBS and HDPE were mixed at a weight ratio of 30:70 in an internal mixer (HAAKE, Rheomix3000p). For preparing compatibilized PBS/HDPE blend, PBS, HDPE, and HDPE-g-MAH were mixed in an internal mixer at HDPE-g-MAH content of 2, 4, 6 and 8 phr. The weight ratio of PBS and HDPE was kept at 30:70. The mixing process was operated at 170°C under a rotor speed of 70 rpm and a mixing time of 10 min. After that, the mixtures of PBS/HDPE and PBS/HDPE/HDPE-g-MAH were cooled down to room temperature and then grinded using a grinding machine. The specimens for tensile, flexural and impact test were molded by an injection machine (Chuan Lih Fa, CLF 80T). The injection molding process was carried out with a melting temperature of 180°C, a screw speed of 130 rpm, an injection speed of 47 mm/s, a holding pressure of 617 kg/cm^3 and a mold temperature of 30°C.

Characterization of PBS/HDPE Blends. Tensile properties including Young's modulus, yield strength, stress at break and elongation at break of PBS/HDPE blend and PBS/HDPE/HDPE-g-MAH blends were determined using a universal testing machine with a load cell of 5kN (Instron, 5565), in accordance with ASTM D638. The tensile test was performed in uniaxial tension at a crosshead speed of 10 mm/min. Flexural properties of PBS/HDPE blend and PBS/HDPE/HDPE-g-MAH blends were tested following ASTM D790 (procedure B) using a universal testing machine with a load cell of 5kN (Instron, 5565) at a crosshead speed of 14 mm/min. In addition, unnotched Izod impact strength of the blends was evaluated on an impact tester (Atlas, BPI), equipped with 5.4 J hammer following ASTM D 256.

Thermal decomposition of PBS/HDPE blend and PBS/HDPE/HDPE-g-MAH blends were investigated using a thermogravimetric analyzer (TA Instrument, SDT 2960) with a heating rate of 20ºC/min from 30ºC to 800ºC under a nitrogen atmosphere.

Melting temperature (T_m), crystallization temperature (T_c), and degree of crystallinity (X_c) of PBS/HDPE blend and PBS/HDPE/HDPE-g-MAH blends were determined using a differential scanning calorimetry, DSC, (Perkin Elmer, UNIX DSC-7). For DSC analysis, a sample was first heated to 200ºC, holded at 200ºC for 5 min, cooled to 30ºC and holded for 5 min, and then re-heated to 200ºC under a nitrogen atmosphere. The heating and cooling rate was 5ºC/min. Subsequently, T_m, T_c and X_c were determined according to ASTM D3417. Degree of crystallinity of HDPE and PBS was calculated using the equation shown below.

$$X_c(\%) = \frac{\Delta H_{f,sample} / \Delta H_{f,100\%crystalline}}{W_f} \times 100 \quad (1)$$

Where, $\Delta H_{f,sample}$ is the heat of fusion of sample (J/g), $\Delta H_{f,100\%crystalline}$ is the heat of fusion of 100% crystalline (J/g) and W_f is weight fraction of material; $\Delta H_{f,100\%crystalline}$ of PBS is 110.3 J/g [11] and $\Delta H_{f,100\%crystalline}$ of HDPE is 292.6 J/g [12].

Results and Discussion

Yield strength and stress at break of neat PBS, neat HDPE, PBS/HDPE blend and PBS/HDPE/HDPE-g-MAH blends are shown in Fig. 1a. It illustrates that yield strength and stress at break of neat PBS were higher than those of PBS/HDPE blend and PBS/HDPE/HDPE-g-MAH blends. It must be noted that neat HDPE specimens did not break within instrument limit. However, yield strength of the PBS/HDPE blend was close to that of neat HDPE. Addition of 2 phr HDPE-g-MAH resulted in a slight increase in yield strength and stress at break of the compatibilized PBS/HDPE blend. The improvement of yield strength and stress at break was a consequence of better interfacial adhesion between PBS domain and HDPE matrix. The better adhesion was promoted by physical or chemical interaction between maleic anhydride group of HDPE-g-MAH and ester groups of PBS [8,13] and also by physical entanglement of molecular chains between HDPE matrix and HDPE backbones of HDPE-g-MAH [14-16]. For the blends containing HDPE-g-MAH higher than 2 phr, yield strength and stress at break did not further improve.

As presented in Fig. 1b, Young's modulus of PBS/HDPE blend without HDPE-g-MAH was slightly lower than that of neat HDPE. Addition of HDPE-g-MAH into the binary blends of PBS and HDPE made a slight increase in Young's modulus. The increased Young's modulus was comparable to that of neat HDPE. However, there was almost no change in Young's modulus of the blends when HDPE-g-MAH was higher than 2 phr. These results corresponded well with the results of elongation at break. Nevertheless, the blends have much lower elongation at break than that of neat PBS and HDPE, adding HDPE-g-MAH more than 4 phr into the blend led to a significant increase of elongation at break which correlated well with the enhancement of impact strength of the blends shown in Fig. 2b. This might be an indication of better compatibility between PBS and HDPE phases, promoted by HDPE-g-MAH.

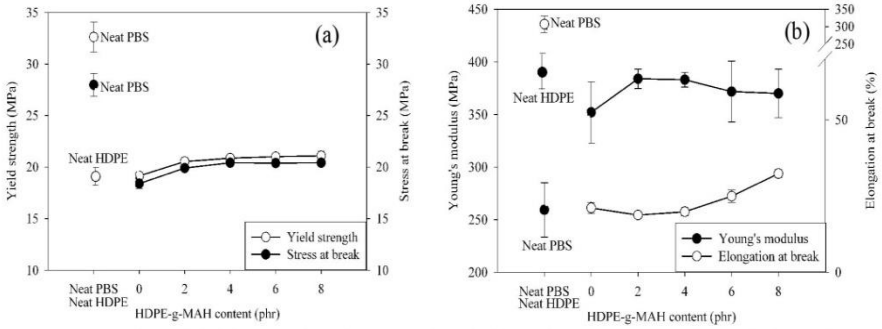

Figure 1. Plot of yield strength and stress at break (a), and Young's modulus and elongation at break (b) of PBS/HDPE blends vs HDPE-g-MAH content.

Flexural modulus and flexural strength of neat PBS, neat HDPE and PBS/HDPE blends at various content of HDPE-g-MAH were presented in Fig. 2a. Flexural strength of PBS/HDPE blend and PBS/HDPE/HDPE-g-MAH blends was comparable to that of neat HDPE. Addition of HDPE-g-MAH did not affect both flexural modulus and flexural strength of the compatibilized blends. The blend of HDPE and PBS without HDPE-g-MAH had impact strength much lower than that of neat PBS and HDPE, as shown in Fig. 2b. Compatibilizing PBS/HDPE blend with HDPE-g-MAH led to a great increase of unnotched impact strength and the impact strength increased with increasing HDPE-g-MAH content. At 8 phr HDPE-g-MAH, the impact strength of the blend was beyond the instrumentation limit (135 kJ/m^2). The much increase in ability to absorb impact energy prior to fracture was facilitated by improved PBS-HDPE compatibility.

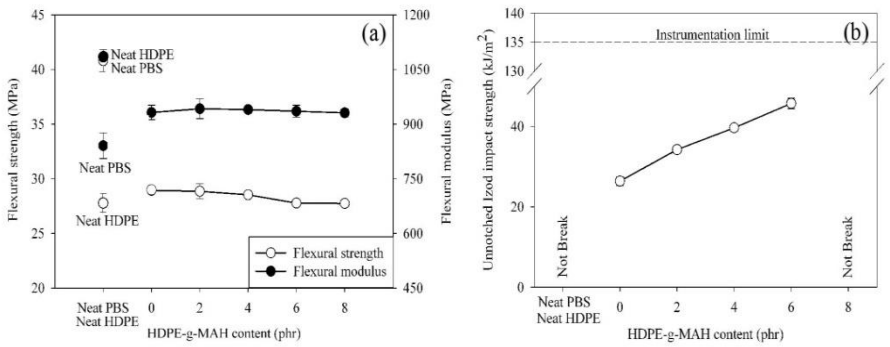

Figure 2. Plot of flexural modulus and strength (a), and impact strength (b) of PBS/HDPE blends vs HDPE-g-MAH content.

From thermogravimetric analysis, PBS/HDPE blend and PBS/HDPE/HDPE-g-MAH blends thermally decomposed into two steps, as shown in Fig. 3a. The first decomposition occurred at the temperature range of 360-420°C corresponding to the decomposition of PBS. The second decomposition occurred within a temperature range of 425-520°C, due to HDPE decomposition. For compatibilized blends having different composition of HDPE-g-MAH, their weight loss, due to thermal decomposition in each step, were slightly different. The degree of differences related to HDPE-g-MAH content included in the blends. From Fig. 3b with inserted table, thermal decomposition of PBS and HDPE of PBS/HDPE blends was not much affected by a presence of HDPE-g-MAH; PBS and HDPE phases of the uncompatibilized blend thermally decomposed at 407 and 488ºC, respectively.

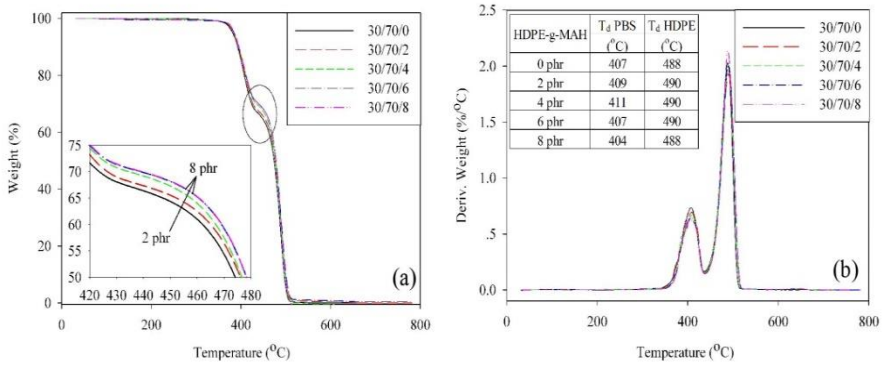

Figure 3. TGA (a) and DTGA curves (b) of PBS/HDPE blend at various HDPE-g-MAH contents.

DSC curves of PBS/HDPE blends at various contents of HDPE-g-MAH from the first cooling scan and the second heating scan were shown in Fig. 4a and Fig. 4b, respectively. The DSC curves of the heating scan show multiple melting peaks of PBS at a range of 99-100°C and at 108°C and a single melting peak of HDPE around 128-129°C, respectively. It was report by Xu *et al.* [17] that PBS had two spherulitic forms, α form and β form. The spherulite of α form melted at higher temperature than spherulite of β form. The melting endotherm of β spherulite might or might not be observed from a DSC thermogram depending on heating rate, cooling rate and thermal history. DSC curves in Fig. 4a and 4b illustrate that HDPE-g-MAH did not influence T_c and T_m of HDPE matrix and those of PBS domain, as well.

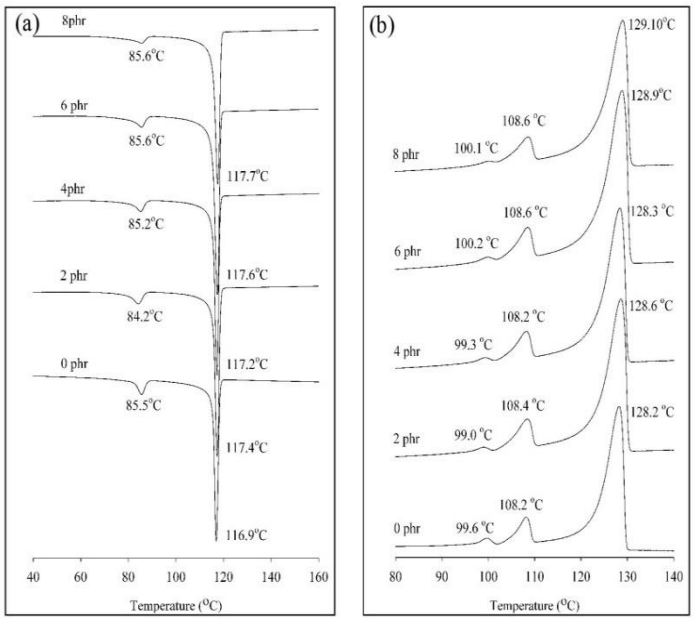

Figure 4. DSC curves from the first cooling scan (a) and the second heating scan (b) of PBS/HDPE blend at various HDPE-g-MAH contents.

Degree of crystallinity (X_c) of PBS/HDPE blend and PBS/HDPE/HDPE-g-MAH blends is comparatively shown in Table 1. It illustrates that at 2-6 phr, HDPE-g-MAH slightly affected crystallinity of HDPE matrix but made a significant increase in crystallinity of PBS phase comparing to crystallinity of those two phases of PBS/HDPE blend without the compatibilizer. However, the degree of crystallinity of HDPE in the blend containing HDPE-g-MAH of 8 phr was much lower than HDPE crystallinity of the blend containing HDPE-g-MAH lower than 8 phr. The decreased crystallinity of PBS domain of the 8 phr HDPE-g-MAH contained blend was also observed. These might be because at 8 phr HDPE-g-MAH, the compatibilized PBS/HDPE blend contained excessive HDPE-g-MAH. The excess composition located in proximity of PBS and HDPE interphase and affected HDPE crystallization, and also α form and β form crystallization of PBS.

Table 1. Degree of crystallinity (X_c) of PBS/HDPE blend at various HDPE-g-MAH contents.

Blend compositions PBS/HDPE/HDPE-g-MAH	X_c (%)	
	HDPE matrix	PBS domain
30/70/0	56%	47%
30/70/2	62%	54%
30/70/4	62%	52%
30/70/6	65%	51%
30/70/8	53%	38%

Summary
This research work revealed that HDPE-g-MAH was an effective compatibilizer for 30 wt% PBS/HDPE blend. HDPE-g-MAH of 2 phr was the optimum content for effectively improving yield stress and stress at break of the blend without creating any significant change in Young's modulus. In addition, impact strength greatly increased with increasing HDPE-g-MAH content. For thermal properties, decomposition, melting, and crystallizing temperature of the blend was not affected by a presence of HDPE-g-MAH. Degree of HDPE crystallinity was not much influenced by addition of HDPE except at 8 phr HDPE-g-MAH. HDPE crystallinity of PBS/HDPE/8 phr HDPE-g-MAH blend was lower than that of the blend without HDPE-g-MAH. The presence of HDPE-g-MAH resulted in increased PBS crystallinity except at 8 phr HDPE-g-MAH in which PBS crystallinity dramatically decreased.

Acknowledgement
The authors would like to thank Suranaree University of Technology for financial support and Chemical Innovation Co., Ltd. for supplying high density polyethylene grafted with maleic anhydride (HDPE-g-MAH).

References

[1] S. Evans, in: GlobalData 2011, European plastics industry, 2012.
[2] In: Renewable Energy Annual 2007, Energy Information Administration, Washington, DC, 2007, 2007, pp. 14.
[3] L. Liu, J. Yu, L. Cheng, W. Qu, Composites Part A, 40 (2009) 669-674.
[4] S. S. Ray, J. Bandyopadhyay, M. Bousmina, Macromol. Mater. Eng., 292 (2007) 729-747.
[5] S. Mbarek, M. Jaziri, Y. Chalamet, C. Carrot, J. Appl. Polym. Sci., 117 (2010) 1683-1694.
[6] D.-H. Kim, K.-Y. Park, J.-Y. Kim, K.-D. Suh, J. Appl. Polym. Sci., 78 (2000) 1017-1024.
[7] P. Laurienzo, B. Immirzi, M. Malinconico, Macromol. Mater. Eng., 286 (2001) 248-253.
[8] J.G. Martínez, R. Benavides, C. Guerrero, J. Appl. Polym. Sci., 104 (2007) 560-567.
[9] B. Boutevin, J. Lusinchi, Y. Pietrasanta, J. Robin, Polym. Eng. Sci. , 36 (1996) 879-884.
[10] Zainuddin, A. Sudradjat, M.T. Razzak, F. Yoshii, K. Makuuchi, J. Appl. Polym. Sci., 72 (1999) 1277-1282.
[11] Y. Phua, W. Chow, Z.A.M. Ishak, Express Polym. Lett., 5 (2011).
[12] S. Sahebian, S.M. Zebarjad, J.V. Khaki, S.A. Sajjadi, J. Mater. Process. Technol., 209 (2009) 1310-1317.
[13] J.M. Lusinchi, B. Boutevin, N. Torres, J.J. Robin, J. Appl. Polym. Sci., 79 (2001) 874-880.
[14] K. Sewda, S. Maiti, J. Appl. Polym. Sci., 112 (2009) 1826-1834.
[15] D.E. El-Nashar, N.A. Maziad, E.M. Sadek, J. Appl. Polym. Sci., 110 (2008) 1929-1937.
[16] H.-T. Chiu, Y.-K. Hsiao, J. Polym. Res., 13 (2006) 153-160.
[17] J. Xu, B.-H. Guo, in: Plastics from Bacteria, Springer Berlin Heidelberg, 2010, pp. 347-388.

Advanced Materials Research Vol. 747 (2013) pp 555-559
© (2013) Trans Tech Publications, Switzerland
doi:10.4028/www.scientific.net/AMR.747.555

Effect of Blend Ratio on Phase Morphology and Mechanical Properties of High Density Polyethylene and Poly (Butylene Succinate) Blend

Ajcharaporn Aontee[1, a], Wimonlak Sutapun[1,b]

[1] School of Polymer Engineering, Suranaree University of Technology, Nakhon Ratchsima 30000, Thailand

[a]ajcharaporn.sut@gmail.com, [b]wimonlak@sut.ac.th

Keywords: PBS, HDPE, HDPE/PBS Blends, Biodegradability.

Abstract. In this work, the effect of HDPE and PBS blend ratio on mechanical properties and phase morphology of the blend was investigated. HDPE/PBS blends were prepared at HDPE content of 20, 30, and 40 wt.% via melt mixing process and then molded using an injection machine. HDPE/PBS blend was an immiscible blend with a type of dispersed in matrix morphology and coalescence phase morphology depending on HDPE content. The blend morphology of 20 wt.% HDPE/PBS blend was a type of spherical domain dispersed in the PBS matrix. As increase HDPE content, the dispersed HDPE particles became larger and the shape turned into worm-like and elongated structure. In addition, at 40 wt.% HDPE, coalescence phase morphology was obtained. It was found that the PBS blends containing 30-40 wt.% HDPE did not show yield point; they exhibited brittle failure behavior. For tensile properties, yield strength and stress at break of HDPE/PBS blend gradually decreased with increasing HDPE content. However, addition of HDPE into PBS matrix resulted in an increase of Young's modulus of the PBS blend. Impact strength of the blends was much lower than that of neat PBS but the impact strength of the blend insignificant changed with 30-40 wt.% HDPE comparing to that with 20 wt.% HDPE.

Introduction

Biodegradable polymers have gained more attention from plastic industries due to their biodegradability and good excellent mechanical and thermal properties [1-3]. Poly (butylene succinate) (PBS) is one of biodegradable polymers aimed to soon replace non-biodegradable commodity plastics such as PE and PP [4]. The forecasting demand of PBS will grow to 50,000 ton/year in the next five years and up to 100,000 ton/year within 10 years [5].

However, PBS is much more expensive than conventional petroleum based thermoplastic such as HDPE and PP. Therefore, it is not economically feasible to be used alone without blending with cheaper plastics of similar required properties or compounding with low price functional fillers. High density polyethylene (HDPE) is a low cost commercial polymer. It has comparable mechanical properties to those of PBS including tensile strength, flexural strength and stiffness [6, 7]. Therefore, blending PBS with HDPE not only diluted the material cost but also acquires the preferred mechanical properties of the final product.

The parameters affecting final morphology and mechanical properties of immiscible blends include material and processing parameters. The materials properties are molecular weight, viscosity ratio, blend composition, elasticity and interface properties [8-10]. In addition, processing parameters, operating conditions for blend processing, are shear rate, barrel temperature, screw geometry, residence time of mixing and [11-13]. The mechanical properties of polymer blends strongly correlated with their blend composition and phase morphology. The relationship between viscosity of dispersed phase (η_d) and continuous phase (η_m) is expressed in the term of viscosity ratio (η_r) as shown below in Eq. 1.

$$\eta_r = \eta_d / \eta_m \quad (1)$$

In this study, the effect of HDPE content on mechanical properties and phase morphology of HDPE/PBS blend was investigated. The blends of PBS were prepared with HDPE content of 20-40 wt.%.

Experimental

Materials. High density polyethylene (injection grade, EL-LeneTM H5814J) was purchased from SCG Chemicals Co., Ltd. It has a melting temperature (T_m) of 131ºC. Poly (butylene succinate) (GS PlaTM, AZ91TN) was obtained from Mitsubishi Chemical Co., Ltd. Its melting temperature (Tm) was 110ºC. Viscosity (at 180ºC and shear rate of 1,000 s^{-1}) of HDPE and PBS was 151.2 Pa.s and 79.2 Pa.s, respectively.

Preparation of HDPE/PBS Blends. The pellets of neat HDPE and neat PBS were initially dried in an oven at 60ºC for 12 h. before preparing polymer blend. HDPE/PBS blends were prepared at a weight ratio of 20:80, 30:70 and 40:60 in an internal mixer (HAAKE, Rheomix3000p). The mixing process was operated at 170°C under a rotor speed of 70 rpm and a mixing time of 10 min. The blends of HDPE/PBS were cooled down to room temperature before ground by a grinding machine. After that, specimens for tensile, flexural and impact test were prepared using an injection machine (Chuan Lih Fa, CLF 80T). The injection molding was carried out with a melting temperature of 180°C, a screw speed of 130 rpm, an injection speed of 47 mm/s, a holding pressure of 617 kg/cm^3 and a mold temperature of 30ºC.

Characterization of HDPE/PBS Blends. The phase morphology of HDPE/PBS blends was investigated using a scanning electron microscope (JEOL, JCM-5000 NeoScope) at 15kV. The specimens were coated with gold using an ion sputtering device for 9 min at a current of 10 mA.

Tensile properties including Young's modulus, yield strength, stress at break and elongation at break of the blends were determined in accordance with ASTM D638 using a universal testing machine (Instron, 5565) equipped with 5 kN load cell. The tensile test was performed in uniaxial tension at a crosshead speed of 10 mm/min. In addition, unnotched Izod impact strength of the blends was evaluated, following ASTM D 256, on an impact tester (Atlas, BPI) equipped with 5.4 J hammer.

Results and Discussion

SEM micrographs of neat PBS and PBS blends at HDPE content of 20, 30, and 40 wt.% were shown in Fig. 1. Fracture surface of PBS, illustrated in Fig. 1a, was rough with a blocky structure which was a characteristic of ductile polymer [14]. The addition of 20 wt.% HDPE into PBS gave rise to an immiscible blend with a non-uniform size distribution of spherical HDPE domain according to high interfacial tension between PBS and HDPE phases. In addition, smooth surface of the spherical domain was also observed. This resulted in a decline of yield strength and ultimate strength of the blend as shown in Fig. 2b.

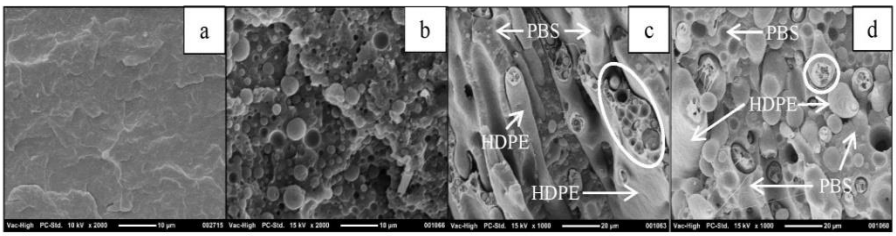

Figure 1. SEM micrographs of (a) neat PBS (x2000), and HDPE/PBS at (b) 20 wt.% HDPE (x2000), (c) 30 wt.% HDPE (x1000) and (d) 40 wt.% HDPE (x1000)

As increasing HDPE content, non-uniform size and shape, including spherical, elongated and worm-like, of HDPE dispersed phase were observed, as shown in Fig. 1c and 1d. This phase morphology resulted in a decrease of yield strength and stress at break. However, the worm-like and elongated shape of the dispersed HDPE helped maintain impact strength of the blend for not further declining. The similar result was observed by Kim *et al.*[15] for the blend system of 30 wt.% linear low density polyethylene (LLDPE) and 70 wt.% biodegradable aliphatic polyester (BDP).

Moreover, inclusion phase morphology of the blend at 30-40 wt.% HDPE was also observed. The fracture surface of the blend with 40 wt.% HDPE revealed coalescence phase morphology, as shown in Fig. 1d. As increasing more of higher viscosity composition of HDPE, the coalescence emerged in which the coalescence was in concurrence with flow-induced elongation of the dispersed HDPE.

Stress strain curves of neat PBS, neat HDPE and HDPE/PBS blends were shown in Fig. 2a. It illustrates that failure behavior of both neat PBS and neat HDPE was in a ductile manner as necking and then large strain deformation took place before fracture. Blending PBS with HDPE brought about brittle fracture behaviour of the blend. The blend lost ability to plastically flow and fracture occurred prior yielding. In addition, the brittle-ductile transition of the PBS blend was within HDPE content range of 20-30 wt.%.

Yield strength and stress at break of HDPE/PBS blends at HDPE content of 20, 30, and 40 wt.% are shown in Fig. 2b. It illustrates that yield strength of HDPE/PBS blends was lower than that of neat PBS. With increasing HDPE composition, yield strength and stress at break decreased. It must be noted that neat HDPE did not break within an instrument limit. The reduction of yield strength and stress at break was due to a non-uniform shape and size of the dispersed HDPE. The inclusion phase morphology created more incompatible HDPE-PBS interfacial contact by which the stress transfer across the interface was hardly possible. As a result the blend failure occurred at lower yield strength and stress at break.

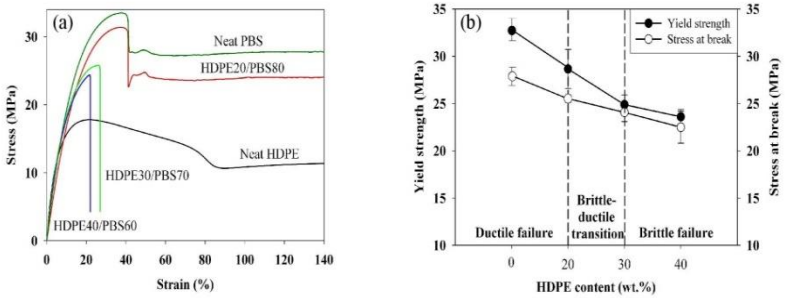

Figure 2. Plot of stress-strain curve (a), and yield strength and stress at break (b) of HDPE/PBS blends vs HDPE content

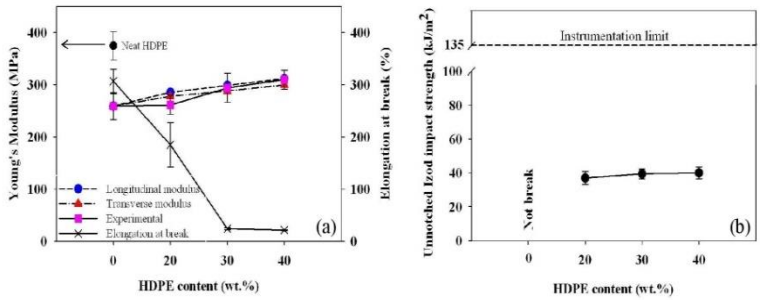

Figure 3. Plot of Young's modulus and elongation at break (a), and unnotched Izod impact strength (b) of HDPE/PBS blends vs HDPE content.

As presented in Fig. 3a, Young's modulus of neat HDPE was higher than that of neat PBS. The addition of HDPE into PBS matrix made a gradual increase in Young's modulus of the blend. In addition, Young's modulus of the blend obtained from the experimental data was close to the longitudinal and transverse modulus calculated through the equation of additivity law [16], except the blend with 20 wt.% HDPE, as shown in Fig. 3a. On the other hand, addition of HDPE at 20-30 wt.% resulted in large decrease of elongation at break of the blend. However, elongation at break of HDPE blend did not further decrease with adding 40 wt.% HDPE.

For impact property, it must be noted that unnotched impact strength of neat HDPE and neat PBS was not obtained; it was beyond an instrumentation limit of a 135 kJ/m^2. However, blending these two tough plastics gave rise to lower impact resistance material due to interfacial incompatibility of HDPE and PBS. For the blend containing 30 wt.% HDPE, impact strength of the blend slightly increased. However, impact strength of the blend did not further reduce with 40 wt.% HDPE due to coalescence phase morphology as shown in Fig.1d. Nevertheless, the much decrease of impact strength when 20 wt.% HDPE was added did not correspond well with the toughness observed from an area under the stress strain curve shown in Fig. 2a.

Summary

This research work revealed that HDPE/PBS blend was an immiscible blend with a type of dispersed in matrix morphology and coalescence phase morphology depending on HDPE content. The blend morphology of 20 wt.% HDPE/PBS blend was a type of spherical domain dispersed in the PBS matrix. As increase HDPE content, the dispersed HDPE particles became larger and the shape turned into worm-like and elongated structure. In addition, at 40 wt.% HDPE, coalescence phase morphology was obtained. It was found that the PBS blends containing 30-40 wt.% HDPE did not show yield point; they exhibited brittle failure behavior. For tensile properties, yield strength and stress at break of HDPE/PBS blend gradually decreased with increasing HDPE content. However, addition of HDPE into PBS matrix resulted in an increase of Young's modulus of the PBS blend. Impact strength of the blends was much lower than that of neat PBS but the impact strength of the blend insignificant changed with 30-40 wt.% HDPE comparing to that with 20 wt.% HDPE.

Acknowledgement

The authors would like to thank Suranaree University of Technology for financial support.

References

[1] H.S. Kim, H.J. Kim, J.W. Lee, I.G. Choi, Biodegradability of bio-flour filled biodegradable poly(butylene succinate) bio-composites in natural and compost soil, Polym. Degrad. Stab., 91 (2006) 1117-1127.

[2] C. Di Franco, V. Cyras, J. Busalmen, R. Ruseckaite, A. Vázquez, Degradation of polycaprolactone/starch blends and composites with sisal fibre, Polym. Degrad. Stab., 86 (2004) 95-103.

[3] M.N. Kim, A.R. Lee, J.S. Yoon, I.J. Chin, Biodegradation of poly (3-hydroxybutyrate), Sky-Green® and Mater-Bi® by fungi isolated from soils, Eur. Polym. J., 36 (2000) 1677-1685.

[4] E.H. Jeong, S.S. Im, J.H. Youk, Electrospinning and structural characterization of ultrafine poly (butylene succinate) fibers, Polymer, 46 (2005) 9538-9543.

[5] D.d. Guzman, in: ICIS Chemical Business online, 2011.

[6] L. Liu, J. Yu, L. Cheng, W. Qu, Mechanical properties of poly (butylene succinate)(PBS) biocomposites reinforced with surface modified jute fibre, Compos. Part A-Appl. , 40 (2009) 669-674.

[7] Y. Shih, T. Wang, R. Jeng, J. Wu, C. Teng, Biodegradable nanocomposites based on poly (butylene succinate)/organoclay, J. Polym. Environ., 15 (2007) 151-158.

[8] S.C. Jana, M. Sau, Effects of viscosity ratio and composition on development of morphology in chaotic mixing of polymers, Polym., 45 (2004) 1665-1678.

[9] C. Cramer, P. Fischer, E.J. Windhab, Drop formation in a co-flowing ambient fluid, Chem. Eng.Sci., 59 (2004) 3045-3058.

[10] V. Everaert, L. Aerts, G. Groeninckx, Phase morphology development in immiscible PP/(PS/PPE) blends influence of the melt-viscosity ratio and blend composition, Polymer, 40 (1999) 6627-6644.

[11] J.D. Ambrósio, E. Hage Junior, Effect of processing parameters on the mechanical properties of in situ compatibilized polybutylene terephthalate/acrylonitrile–butadiene–styrene blends, J. Appl. Polym. Sci., (2012).

[12] J. Cho, D. Paul, Nylon 6 nanocomposites by melt compounding, Polym., 42 (2001) 1083-1094.
[13] W. Lertwimolnun, B. Vergnes, Effect of processing conditions on the formation of polypropylene/organoclay nanocomposites in a twin screw extruder, Polym. Eng. Sci., 46 (2006) 314-323.
[14] I. Brough, R.N. Haward, G. Healey, Scanning electron micrographs of high density polyethylene fracture surfaces, A. Wood, Polymer, 45 (2004) 3115-3123.
[15] J. Kim, J.H. Kim, T. K. Shin, H.J. Choi, M. S. Jhon, Miscibility and rheological characteristics of biodegradable aliphatic polyester and linear low density polyethylene blends, Eur. Polym. J., 37 (2001) 2131-2139.
[16] R. Maksimov, R. Merii Meri, M. Kalnin, J. Zicans, Mech. Mechanical properties of polyethylene and poly (ethylene terephthalate) blends, Compos. Mater., 39 (2003) 189-196.

BIOGRAPHY

Miss Ajcharaporn Aontee was born on January 31, 1985 in Phetchabun, Thailand. She earned her Bachelor's Degree in Engineering in Petrochemical and polymeric materials from Silpakorn University in 2008. After graduation, she had worked in a position of R&D (flexible plastic packaging for cosmetic) for 2 years at S&J international enterprise Co., Ltd., in Bangkok. After that, she continued her Master's degree in Polymer Engineering at School of Polymer Engineering, Institute of Engineering, Suranaree University of Technology. During her master's degree study, she presented one oral presentation entitle: **"A Study of Compatibilization Effect on Physical Properties of Poly (Butylene Succinate) and High Density Polyethylene Blend"** at Materials Science and Chemical Engineering International Conference 2013 (MSCE 2013) in Singapore. She presented two poster presentations entitle: **"Mechanical Properties of High Density Polyethylene and Poly (Butylene Succinate) Blends**" at the Pure and Applied Chemistry International Conference 2013 (PACCON 2013) in Chonburi, Thailand and "**Effect of Blend Ratio on Phase Morphology and Mechanical Properties of High Density Polyethylene and Poly (Butylene Succinate) Blend"** at The 4th international conference on Multi-Functional Materials and Structures (MFMS 2013) in Bangkok, Thailand.